TISSUE FACTOR-RELATED MECHANISMS OF COAGULATION INITIATED ON THE VIRUS ENVELOPE

by

Huan-Jih Lin

B.Sc., The University of British Columbia, 2013

A THESIS SUBMITTED IN PARTIAL FULFILLMENT OF

THE REQUIREMENTS FOR THE DEGREE OF

DOCTOR OF PHILOSOPHY

in

THE FACULTY OF GRADUATE AND POSTDOCTORAL STUDIES

(Pathology and Laboratory Medicine)

THE UNIVERSITY OF BRITISH COLUMBIA

(Vancouver)

August 2019

[Committee page for doctoral committees with one supervisor. Select the correct committee page for your work, and delete unnecessary committee pages and this material in brackets, before submitting.]

The following individuals certify that they have read, and recommend to the Faculty of Graduate and Postdoctoral Studies for acceptance, the dissertation entitled:

Mechanisms of Coagulation Initiated on the Virus Envelope Related to Tissue Factor

submitted by HUAN-JIH LIN in partial fulfillment of the requirements for

the degree of Doctor of Philosophy

in Pathology and Laboratory Medicine

Examining Committee:

Ed LG Pryzdial, Pathology and Laboratory Medicine
Supervisor

William W-G Jia, Pathology and Laboratory Medicine
Departmental Committee Member

Jay N Kizhakkedathu, Pathology and Laboratory Medicine
Supervisory Committee Member

Ross TA MacGillivray, Biochemistry and Molecular Biology
University Examiner

Patricia C Liaw, McMaster University, Medicine
External Examiner

Additional Supervisory Committee Members:

Hélène C F Côté, Pathology and Laboratory Medicine
Supervisory Committee Member

Marc S Horwitz, Microbiology and Immunology
Supervisory Committee Member

Abstract

Infectious diseases do not always manifest in a predictable manner and may go undetected, especially in asymptomatic individuals. Here, virus infection as an underlying cause of vascular disease is investigated. When considered independently, both have major impacts on healthcare systems globally. However, a relatively unexplored area of investigation is that many virus types have been tied to cardiovascular and haemostatic diseases. The mechanisms by which viruses accomplish this is not understood. As a model, I have used herpes simplex virus type 1 (HSV1) to explore the concept that viruses that obtain an outer phospholipid bilayer membrane can acquire the main physiological initiator of coagulation, tissue factor (TF). The Pryzdial laboratory has previously shown that several herpesviruses, including HSV1, incorporate TF when they are propagated in TF-expressing cells. TF is involved in the activation of the coagulation pro-enzyme factor X through the enhancement of factor VIIa proteolytic activity. This was shown to enhance virus infectivity through coagulation protease-dependent activation of cell signaling. HSV1 also expresses its self-encoded membrane protein, glycoprotein C (gC), which is involved in cell adhesion and immune escape. As gC is also capable of binding factor X, I postulated that gC regulates factor X activation through TF on the virus surface. To study how gC affects TF function, protein interactions were followed via cross-linking, chromogenic activity assays and microscale thermophoresis. In this study, I discovered that gC interacted with factor VIIa and factor X, rather than with TF, to form a unique enzyme complex that activates factor X. Similar to TF and factor VIIa interaction, gC requires factor X to efficiently assemble with factor VIIa. This complex can directly activate factor X and induce fibrin formation in plasma. Although this pro-coagulant function of gC may be restricted to homologous gene products in all herpesvirus family members, I have demonstrated that other viruses can incorporate TF into their membranes. In addition to

purified viruses propagated in cell culture, I found that patient plasma-derived human immunodeficiency virus and hepatitis C virus can incorporate TF into their virus envelope. This could explain some of the haemostatic abnormalities associated with viral infection.

Lay Summary

Imbalances in blood clotting are leading causes of death worldwide. The reasons behind deadly blood clots are numerous. One of the possible links to blood clots that interest the Pryzdial laboratory is virus infection. My research focuses on how some viruses can promote clotting or clotting-related problems. Blood clotting is good when we want to stop bleeding. Yet, clotting can be bad when it is not needed or too much takes place. This can result in problems such as heart attacks and strokes. I have found that some viruses steal clotting factors from our cells. These factors may cause clotting and increase infection. Also, I have shown that the virus that causes oral herpes can make its own clotting factor. With this knowledge, we can be better prepared for fighting these viruses and their associated health problems. We can also learn how viral clotting factors work to improve our own.

Preface

The research question was originally proposed by my supervisor, Dr. Ed Pryzdial, Clinical Professor in the Department of Pathology and Laboratory Medicine, UBC. Herpesviruses were produced and purified by our laboratory Research Associate Dr. Michael Sutherland (Adjunct Professor, Department of Pathology and Laboratory Medicine, UBC). All experimental work presented in the dissertation was performed by me. Experimental work with human plasma was approved by the UBC Clinical Research Ethics Board (ethics certificate: H11-02845).

A version of Chapter 3 will be submitted for publication with the title: Coagulation factor X augments FVIIa binding to herpes simplex virus 1-encoded glycoprotein C forming an extrinsic tenase-like complex (by Bryan H. Lin, Michael R. Sutherland, Federico I. Rosell, James H. Morrissey, and Edward L.G. Pryzdial). The majority of experiments described in Chapter 3 were designed by me with the feedback from Dr. Michael Sutherland, our collaborator, Dr. James Morrissey (professor, departments of Biological Chemistry & Internal Medicine, University of Michigan Medical School) and thesis advisory committee members. I wrote the draft of the manuscript and revised the contents with my supervisor in addition to feedback from Drs. Sutherland and Morrissey.

The work presented in Chapter 4 was designed in large part by me with suggestions from Dr. Michael Sutherland and will be prepared in a manuscript in progress with the tentative title: Ubiquity of tissue factor on the surface of enveloped viruses (by Bryan H. Lin, Michael R. Sutherland, Guey-Chuen Perng, Ivan Sadowski, and Edward L.G. Pryzdial).

Parts of Chapter 3 and 4 were presented orally or in poster presentations at various local, national and international conferences, symposia and workshops. Microscale thermophoresis diagram and figure legend was obtained under a Creative Commons Attribution License (CC BY).

Table of Contents

List of Tables

List of Figures

List of Abbreviations

ADE, antibody-dependent enhancement

AIDS, acquired immunodeficiency syndrome

aPL, anionic phospholipid

APMSF, *p*-amidinophenylmethylsulfonyl fluoride

aPTT, activated partial thromboplastin time

ART, anti-retroviral treatment

BCA, bicinchoininic acid

Bmax, amount of ligand bound at receptor saturation

BSA, bovine serum albumin

CCR5, C-C motif chemokine receptor 5

CD4, cluster of differentiation

CI, confidence interval

CS, chondroitin sulfate

CTI, corn trypsin inhibitor

CXCR4, C-X-C chemokine receptor type 4

ddH2O, distilled and de-ionized water

DENV, dengue virus

DIC, disseminated intravascular coagulation

DMF, dimethylformamide

DMSO, dimethyl sulfoxide

DNA, deoxyribonucleic acid

DTSSP, 3,3'-dithiobis(sulfosuccinimidyl propionate

ECL, enhanced chemiluminescence reagent

EDTA, ethylenediamine tetraacetic acid

EGF, epidermal growth factor

EM, electron microscopy

EPCR, endothelial cell protein C receptor

F, factor

FII, prothrombin

FIIa, thrombin

FVII, factor VII

FVIIa, factor VIIa

FVIII, factor

FVIII/DP, factor VIII-deficient plasma

FX, factor X

FXa, factor Xa

GAG, glycosaminoglycan

gC, glycoprotein C

GdnHCl, guanidine hydrochloride

Gla, γ-carboxyglutamate

HA, hyaluronic acid

HBS, HEPES buffered saline

HCV, hepatitis C virus

His-tag, histidine tag

HIV, human immunodeficiency virus

HRP, horseradish peroxidase

HSPG, heparan sulfate proteoglycans

HSV1, herpes simplex virus type 1

HSV2, herpes simplex virus type 2

HVEM, herpesvirus entry mediator

IU, international units

K_d, equilibrium dissociation constant

K_m, Michaelis constant

LMWH, low molecular weight heparin

MAPK, mitogen-activated protein kinase

MARCO, macrophage receptor with collagenous structure

MST, microscale thermophoresis

NAPc2, nematode anticoagulant peptide c2

NHS, N-hydroxysuccinimide

DGS-NTA-Ni, the nickel salt of 1,2-dioleoyl-sn-glycero-3-[(N-(5-amino-1-carboxypentyl)iminodiacetic acid) succinyl

NP, normal human pooled plasma

OR, odds ratio

PAR, protease activated receptor

PC, phosphatidylcholine

PDB, protein data bank

PDI, protein disulfide isomerase

PI3K, phosphatidylinositol-3 kinase

PS, phosphatidylserine

PT, prothrombin time

PTA, phosphotungstic acid

RNA, ribonucleic acid

SD, standard deviation

SEM, standard error of the mean

sgC-His, soluble gC with His5 tag (gCΔ457t)

sTF-Cys, soluble tissue factor with N-terminal cysteine

sTF-His, soluble tissue factor with N-terminal His6 tag

TCS, Transitive Consistency Score

TF, tissue factor

TFPI, tissue factor pathway inhibitor

TNF, tissue necrosis factor

tPA, tissue plasminogen activator

UFH, unfractionated heparin

Vmax, maximal rate of reaction

vWF, von Willebrand Factor

Acknowledgements

I must give thanks to Ed, who will always remain a role model in his diligence towards good science, his patience towards my endless questions and ignorance, as well as his keenness in good communication skills. I owe thanks to Michael, whose questions, even the simplest, has guided me along my studies. I also can't argue that his favorite catchphrase "Stay positive, Unikitty©" has grown on me. Scott, thank you for your help and down-to-earth view on everything. To the current and previous members of the lab (Michael, Scott, Simon, Kat, Frank, Rolinda, Tseday, Ulli) that have supported me, much appreciation. Fred, I will not name my firstborn after you, but I give thanks for your advice and ideas. I would like to thank Val Smith of the Ross MacGillivray lab for her expertise with chromatography equipment during the early days of my protein purification woes . I also extend my thanks to Dr. James Morrissey who has graciously offered materials and knowledge that greatly helped my research. I greatly appreciate the time, effort and expertise my committee chair and members, Drs. Côté, Kizhakkedathu and Horwitz, have given me. Many thanks to the CBR office members, Hana and Anna, for making CBR a wonderful place to grow ourselves as scientists and people. I offer my enduring gratitude to the faculty, staff and my fellow students at UBC, who have inspired me to continue my work in this field. Special thanks to my mom, dad and brother, who have supported me throughout my years of education. To my family, I apologize for the rather haphazard schedule throughout my studies and have always appreciated the "free" bed, meals and rides. Shouts out to the de-stressing my good friend, Tony, has shared with me. And lastly, I would not have survived grad school without the support of my undergrad twin, Irene. Even though we are 4030 km away from each other, it is almost like we were working side-by-side to finish grad school. I'm always rooting for you too!

Dedication

I dedicate this dissertation to my family who have supported my journey into the great realm of science. Special dedication to my Taekwon-Do master, Benny Wong, who has inspired me to constantly improve not only for myself but for others and has taught me to maintain an indomitable spirit. The final dedication goes to Irene Lin, as your support has been instrumental in my pursuit of a career in science.

Chapter 1: Introduction

1.1 Thesis Rationale

Viral infections are major health problems worldwide. Furthermore, many viruses have been linked to cardiovascular diseases, including myocardial infarction, atherosclerosis, thrombosis and bleeding. This is important because the leading causes of death worldwide are cardiovascular diseases [1]. Considering the burden and ubiquity of viruses and cardiovascular diseases, extensive research has been invested in trying to understand their pathologies or pathophysiologies as well as to improve or discover treatments for these diseases. Viral infections are communicable; thus, the spread and impact of these diseases has been further accelerated by increased travel and migration of zoonotic reservoirs. This affects not only the immediate population but also blood banks where asymptomatic individuals who are unaware of their infection(s) and may spread pathogens through blood donations or donor-related products. Our work aims to address the issue of a lack of pan-specific antivirals by demonstrating that a common protein exists on a range of viruses and may be the basis of their links to cardiovascular diseases. This protein is tissue factor (TF), the main physiological initiator of coagulation. TF has been previously demonstrated to be involved in numerous disease states involving a haemostatic response and inflammation including virus infection, thrombosis and cancer. Studies from the Pryzdial laboratory have revealed the presence of TF on several herpesviruses [2]. Here, my thesis work focuses on virus-initiated coagulation and its relationship with TF.

1.2 Infectious diseases and coagulation

1.2.1 Thrombosis

Haemostasis is the physiological process of restoring or maintaining blood flow. This can be achieved by preventing blood loss from an injury through blood coagulation or restoring blood flow by dissolving a blood clot through fibrinolysis. When a blood clot is formed and hinders blood flow, this is known as thrombosis. This pathological condition can lead to poor oxygen and nutrient delivery to organs or tissues as well as inflammation. Thrombosis is divided into arterial and venous [3]. Arterial thrombi are typically formed by platelets and their interactions with abnormalities in the arterial walls (e.g. rupture of an atherosclerotic plaque). Arterial thromboses include ischemic heart disease (or coronary heart disease) and ischemic stroke. Venous thrombi, on the other hand, form in the veins and are mainly comprised of fibrin and red blood cells. Examples of venous pathology are deep-vein thrombosis and pulmonary embolism. Systematic analyses of global causes of death put thrombosis as the leading causing of death in 2010, accounting for 1 in 4 deaths worldwide, increasing from 1 in 5 since 1990 [1].

Well known risk factors associated with vascular disease are heredity, hypertension, obesity, diabetes, surgery and cancer [4–7]. Our work and others indicate that virus infection should also be on this list. Most risk factors are non-communicable, thus do not pose a threat to the public. However, infectious diseases are communicable and are major risks to the public and the healthcare system (e.g. blood donations and organ donations). Although blood transfusions and blood products are routinely screened for typical infectious diseases, the scope of detection is limited and may not detect all potential infectious agents [8].

1.2.2 Infectious diseases in inflammation

Infectious diseases, including viruses, bacteria, fungi and prions, affect us constantly. It is estimated that infectious diseases cause nine million deaths worldwide each year [9]. As for survivors, many are left with long-term disabilities. Most if not all virus-caused deaths are attributable to inflammation. Inflammation is a response by the body's immune system to specific stimuli, e.g. pathogens or injury, where the body attempts to restore homeostasis by healing tissues or removing pathogens. Inflammation was once thought to be separate from haemostasis. Yet, the two processes have similar activation stimuli as well as regulatory systems [10,11] and the multifunctional initiator of coagulation, tissue factor (TF), is the molecular bridge. Pathogens can induce vascular cells to initiate coagulation, which is quickly followed by local inflammation to recruit immune cells. The reverse scenario can also occur, where pathogens trigger immune cells to initiate coagulation. Increasing bodies of evidence intertwine inflammation and haemostasis, wherein more research is needed to understand the roles of specific pathogens in this interplay. Some pathogens such as herpesviruses establish a latent infection, with no displayed symptoms or a slow manifestation over the years. Thus, it is hard to gauge the burden of these diseases without first identifying the causative agents and understanding how they contribute to symptoms or other diseases. Our laboratory has demonstrated that herpes simplex virus type 1 takes advantage of the interplay between coagulation and inflammation to enhance infection [12,13]. This is achieved through clotting protease-mediated activation of cell receptors.

1.3 General coagulation overview

Blood clot formation may be activated by two pathways: extrinsic and intrinsic pathways (Figure 1). The induced availability of TF triggers clot formation via the extrinsic branch of the pathway. TF is a transmembrane protein that binds to the plasma protein factor (F) VIIa in the presence of anionic phospholipid (aPL) and Ca^{2+}. This TF/FVIIa/Ca^{2+}/aPL complex is known as the extrinsic tenase and is responsible for proteolytic activation of FX to FXa.

The intrinsic pathway is initiated by a negatively charged surface, such as aPL membranes, or collagen exposure that allows for a cascade of protease activation involving factors XIIa, XIa, IXa and VIIIa. Like the extrinsic tenase, FIXa/FVIIIa/Ca^{2+}/aPL is the intrinsic equivalent activator of FX to FXa. Although the extrinsic pathway is the physiological initiator of FX activation, the intrinsic pathway accelerates the accumulation of FXa. The extrinsic tenase can activate FIX to FIXa to amplify FX activation. FXa is capable of activating FVIII but only when in complex with the extrinsic tenase [14].

The convergence of the extrinsic and intrinsic pathways of physiological coagulation is referred to as the common pathway. FX activated by extrinsic and/or intrinsic pathways proceeds to cleave prothrombin (also known as FII) to the activated form, thrombin (or FIIa). FXa cleavage of prothrombin is greatly enhanced by its cofactor FVa. FV is cleaved to FVa by FXa and thrombin, with the former being critical for plasma clotting [15,16]. The resulting thrombin generation proceeds to activate fibrinogen to fibrin, which in turn is crosslinked by FXIIIa to stabilize the clot. To overcome the coagulation inhibitors intrinsic to plasma, feedback amplification is important. This is achieved through multiple mechanisms, including FXIa and FVa activation by thrombin [15,17].

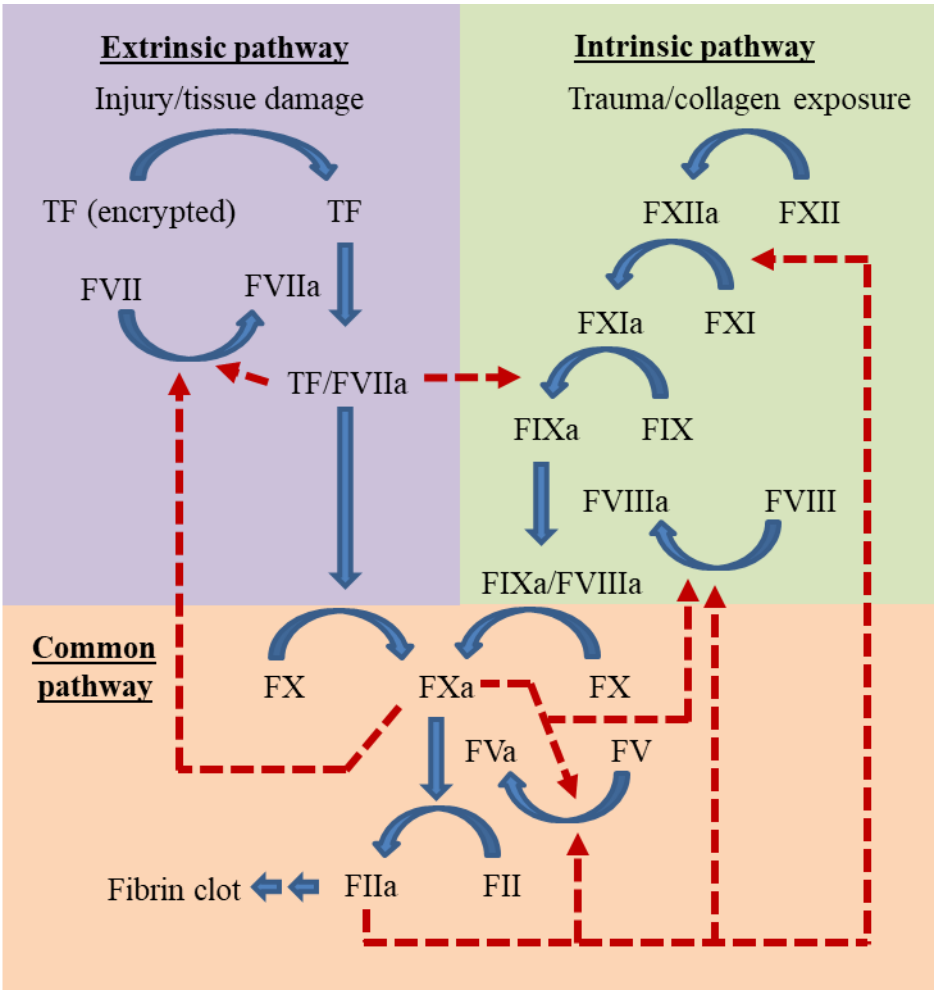

Figure 1. Coagulation pathway.

Coagulation is initiated by the extrinsic pathway and amplified by the intrinsic pathway. Through a series of interactions, the intrinsic tenase complex (FIXa/FVIIIa) or extrinsic tenase complex (TF/FVIIa) is formed. The tenases participate in the common pathway where FX is activated to FXa and subsequently activate prothrombin (FII) to thrombin (FIIa). A fibrin clot can then be formed. Red dashed arrows represent feedback or auxiliary mechanisms to amplify procoagulant proteases so that coagulation can occur.

Two clinical tests are typically performed to assess the function of the coagulation system in an individual. Prothrombin time (PT) measures the integrity of the extrinsic pathway and can determine if there are bleeding problems or if certain administered anticoagulants are effective. Activated partial thromboplastin time (aPTT) examines the intrinsic pathway and can also determine bleeding problems such as hemophilia and can be used to test if the anticoagulant, heparin, is working. These tests were derived from scientific methodologies and were used by the Pryzdial laboratory to investigate the interactions between viruses and coagulation. As previous work has shown, herpesviruses can initiate coagulation through both extrinsic and intrinsic pathways [2,18]. Our focus is on TF of the immediate extrinsic pathway.

1.3.1 Tissue Factor

1.3.1.1 Structure

Tissue factor (TF) is a 263 amino acid, 47 kDa transmembrane protein. Nemerson's group first isolated and purified the protein in 1981 [19]. This allowed for the cloning and gene sequencing of TF [20] with the first crystal structure of the soluble form (sTF) being solved 7 years later (Figure 2) [21]. TF is composed of three domains: cytoplasmic (residues 243-263), transmembrane (residues 220-242) and extracellular (residues 1-219) [20,22]. There are several crystal structures of TF and each structure can be obtained from the Research Collaboratory for Structural Bioinformatics protein data bank (PDB) e.g. PDB: 1DAN used in Figure 2.

The N-terminal extracellular domain contains two fibronectin type III domains linked by a single Pro102 to Asn107 linker, joined at an angle of 125° (Figure 2) [21]. These two domains both contain a three-stranded and a four-stranded anti-parallel sheet that are folded into a β-sandwich. The interface formed between the hydrophobic cores of the two fibronectin domains

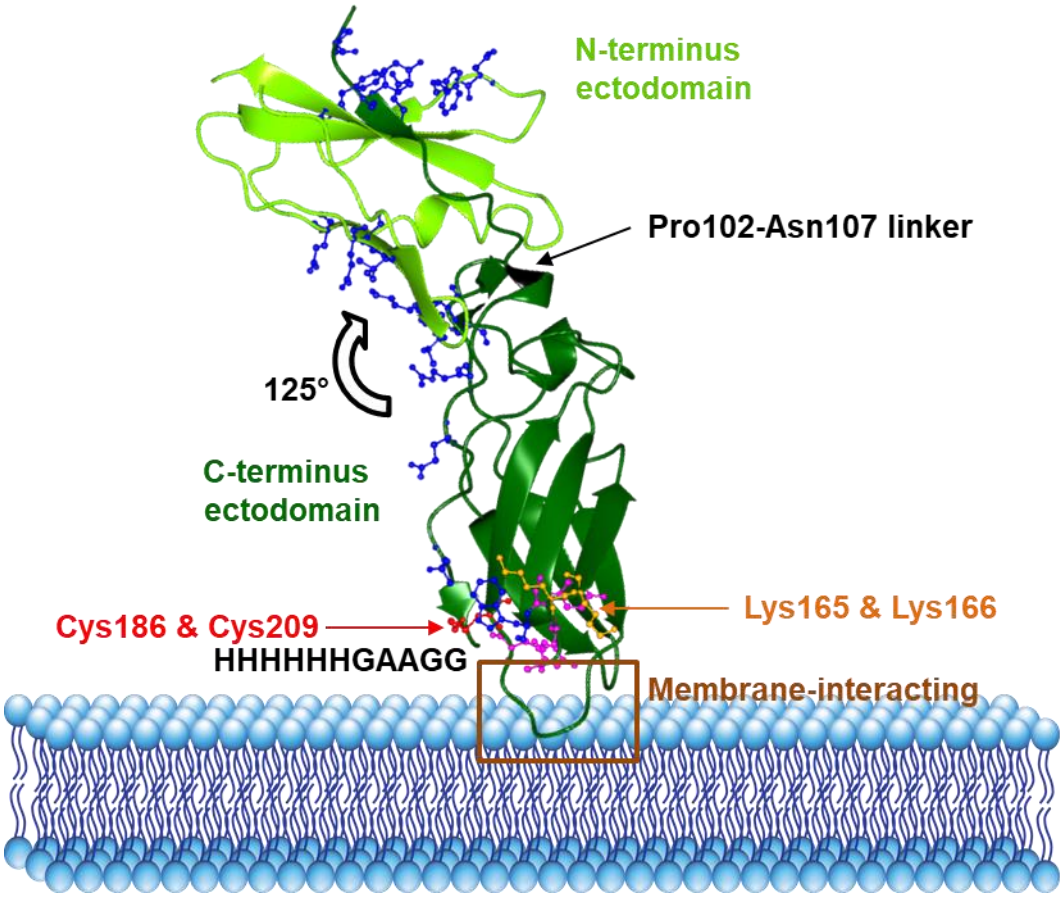

Figure 2. Crystal structure of sTF.

Solid ribbon representation of the sTF ectodomain with the two fibronectin domains connected by the Pro102-Asn107 linker to an angle of 125 degrees. Residues involved in TF/FVIIa interaction run along a strip on the entire TF molecule (blue ball and chains) as determined from the TF/FVIIa structure. The C-terminus contains multiple important residues for FVIIa substrates FX or FIX recognition (purple ball and chains). The Lys165 and Lys166 are also important in FVIIa substrate recognition and are susceptible to amine-reactive crosslinkers (orange ball and chains). The thioester bond between Cys186 and Cys209 control the encryption of TF function (red ball and chains). A form of soluble TF with a GGAAG spacer and a His_6 tag at the C-terminus was used in this study. A region with several putative membrane-interacting residues are found in the C-terminus ectodomain (brown box). The membrane-interacting site is theoretical as this structure was based on a solubilized form of recombinant TF lacking the transmembrane domain. The structure was obtained from the PDB code ID: 1DAN.

results in a large hydrophobic patch [23]. This patch contributes to a rigid structure for FVII or FVIIa binding (Figure 5). There are two disulfide bonds at Cys49-Cys57 and Cys186-Cys209, the latter being crucial for FVII binding [24].

TF displays high sequence similarity to the conserved class two of the cytokine receptor superfamily [25,26] for which structural comparisons describes immunoglobulin-like modules in a portion of the TF extracellular domain. Unlike the extracellular domain, the structure of the cytoplasmic domain is unknown as the crystal structure of full-length TF remains unresolved.

1.3.1.2 Function in haemostasis

TF is vital to life as shown by deletion mutants in mice resulting in death during embryonic development as a consequence of defective neoangiogenesis [27–29]. TF initiates coagulation by several mechanisms. The extracellular domain of TF binds to FVII and enhances its proteolytic auto-activation or activation by one of several other proteases. TF enhances the proteolytic activity of FVIIa towards FX and FIX [30]. Regions on TF interact with the phospholipid membrane [31,32] and conceivably affect function. The phospholipid-interacting domain is adjacent (or near) the FVIIa binding domain of TF. It was found that the lysine residues 165 and 166 are important in membrane, FVIIa and FX association. Crystal structure of soluble TF/FVIIa revealed 21 TF residues that interact with FVIIa [33]. Further mutagenesis studies have demonstrated the importance of Tyr157, Lys159, Ser163, Gly164 and Tyr185 on TF in FVIIa substrate recognition [34]. TF allosteric interaction with FVIIa results in an approximately million-fold increase in the rate of activation of FIX and FX [35], highlighting its importance in haemostasis.

TF also plays an important role in wound healing outside of the initial formation of a blood clot [36,37]. This was evident in mice models of diabetes mellitus, where wound healing is known

to be retarded, similar to that in humans with diabetes mellitus [38,39]. Deficiency in TF expression at the wound site in diabetic mice resulted in impaired healing processes and enhanced TF expression by gene transfer accelerated wound closure compared to non-treated diabetic mice [37]. Neoangiogenesis is also important in wound healing in which TF also plays a role [40]. This cell signaling-dependent process is regulated by both extracellular and intracellular domains of TF. While the extracellular domain of TF can mediate FVIIa-dependent activation of protease-activated receptor (PAR) signaling, the cytoplasmic domain of TF is involved in cell signaling [41–43]. A secreted form of the extracellular domain of TF, produced through alternative splicing, has also been demonstrated to connect integrins αvβ3 and α6β1 [44]. This resulted in the induction of cell signaling independent of PARs or the cytoplasmic domain of TF, leading to endothelial cell migration and blood capillary formation.

1.3.1.3 Protease-activated receptors and TF function

PARs are G protein-coupled receptors and activated by a variety of proteases including those involved in haemostasis. There are four known PARs, numbered from 1 through 4 [45,46]. These integral membrane proteins possess an activation peptide that upon cleavage, exposes a new N-terminal sequence that acts as a tethered ligand (Figure 3). The tethered ligand activates the PAR by binding unto itself. TF/FVIIa can activate PAR-2; FX can activate PAR-1 and PAR-2; and thrombin can activate PAR-1, PAR-3 and PAR-4.

Activation of PARs has a wide range of effects including inflammation, apoptosis and angiogenesis. TF/FVIIa-dependent activation of PAR-2 has been linked to angiogenesis and apoptosis [27,47–50]. Angiogenesis is stimulated through the increased production of pro-angiogenic factors such as vascular endothelial growth factor [51] and interleukin-8 [52]. PAR-2

phosphorylation downstream signaling includes phosphatidylinositol-3 kinase (PI3K) signaling and mitogen-activated protein kinase (MAPK) signaling pathways [53,54]. These pathways are pro-malignancy and stimulate oncogenic protein synthesis, thereby inhibiting apoptosis in cancer cells. TF/FVIIa-mediated activation of PAR-2 has been demonstrated to enhance virus infectivity [12,13]. Furthermore, PAR-2 activation can result in phosphorylation of TF cytoplasmic domain residue Ser253 by protein kinase C and subsequently allows phosphorylation of Ser258 [41,43]. Ser253 phosphorylation and PAR2 signaling are more efficient when TF is bound to β1-integrins [55]. Ser253 phosphorylation is involved in triggering TF incorporation into microvesicles and their release [41]. This could explain why cancer patients have increased TF-expressing microparticles and increased associated risk of venous thromboembolism [56]. TF/FVIIa-mediated PAR-2 activation also contributes to tumor angiogenesis and growth in breast cancer development [57,58].

1.3.1.4 Function(s) in non-haemostatic settings

Besides the well-established role of TF in haemostasis, TF has been implicated in inflammation. Mice expressing TF mutants with defunct cytoplasmic tail domains displayed reduced severity of arthritis, reduced synovial cytokine mRNA expression and impaired adaptive immune responses [59]. TF expression is also elevated in other inflammatory diseases such as ulcerative colitis [60] and multiple sclerosis [61], further stressing the importance of TF in inflammation.

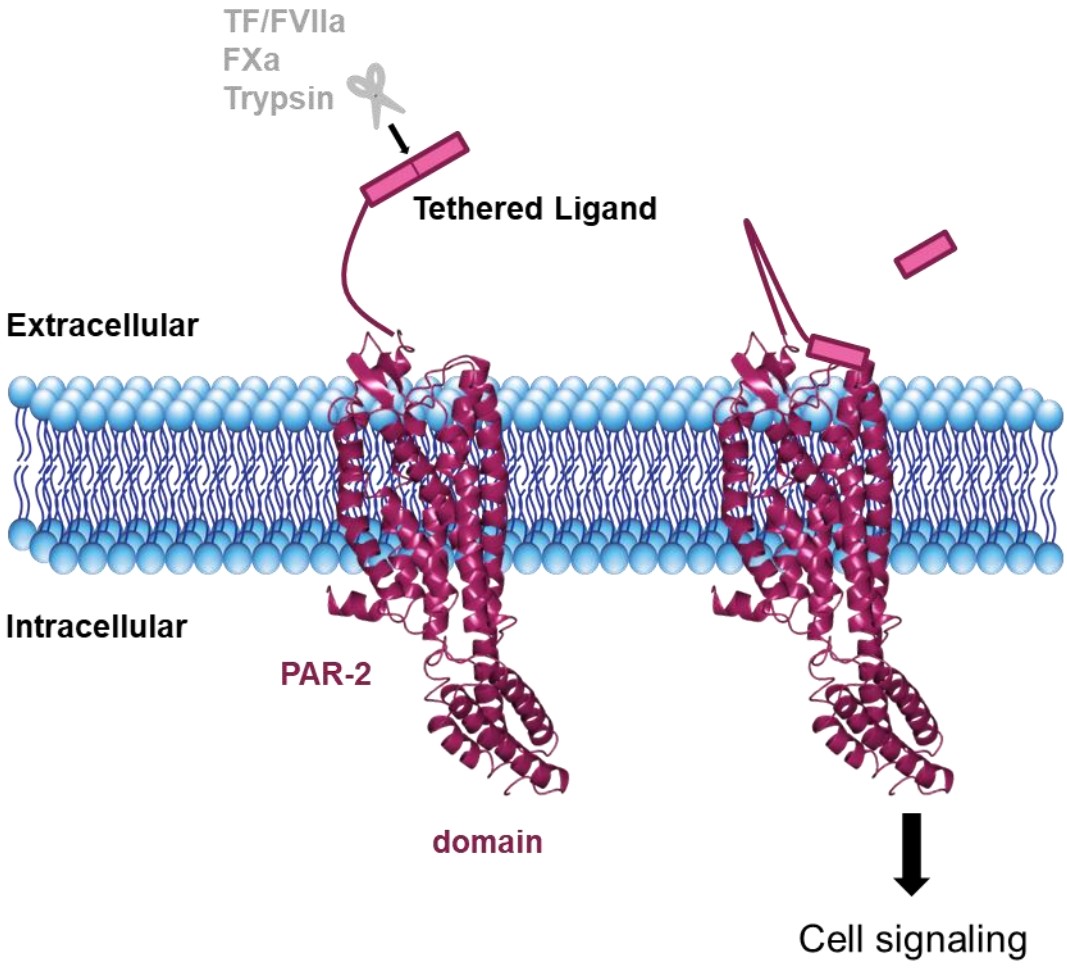

Figure 3. Protease-activated receptor activation by clotting proteases.

PARs are activated via cleavage of the extracellular tethered ligand by multiple serine proteases. PAR-2, depicted here from PDB code 5NJ6, is activatable by TF/FVIIa complex and FXa. The newly exposed N-terminus tethered ligand can bind to the core of the PAR, resulting in activation and cell signaling through G-protein coupled signaling.

1.3.1.5 Regulation of TF function

TF expression can be found in a wide range of cells, including vascular smooth muscle cells, pericytes, monocytes, astrocytes and cardiomyocytes (partially listed in) [62–65]. Yet, its procoagulant activity is not always present. The finding that surface exposed TF in dermal vessels was bound to FVII in the absence of injury, suggested that TF function exists in an "encrypted" form [66]. TF has a disulfide bond at Cys186-Cys209 within the C-terminal domain (Figure 2) that exists in an allosteric configuration. Allosteric disulfide bonds have been demonstrated to be involved in controlling protein function via redox state changes of the cysteine residues [67]. Since TF binding to FVIIa and subsequent FX activation is compromised when the disulfide bond at Cys186-Cys209 was reduced, the hypothesis was that the redox state of Cys186-Cys209 governs TF function on the cell surface [68]. The importance of Cys186-Cys209 led to the investigation of protein disulfide isomerase (PDI), a subcellular protein that catalyzes the formation of disulfide bonds between cysteine residues on proteins. While the role of PDI is still debated, most recent studies observe PDI expression enhancing TF-dependent thrombin generation [69]. However, alterations in membrane phospholipid asymmetry have also been implicated in the description of TF function.

Further regulatory mechanisms of TF function include tissue factor pathway inhibitor (TFPI). TFPI blocks TF/FVIIa function when bound to FXa, thereby stopping the initiating pathway [70]. This occurs in two steps: 1) TFPI binds to and inhibits FXa via its Kunitz-type homology domain 2; and 2) TFPI/FXa binds to and inhibits TF/FVIIa via the Kunitz domain 1 [71,72]. Inhibition of TF/FVIIa by TFPI is not calcium-dependent but is most efficient when TFPI-FXa is in complex with FV, calcium and aPL [70].

Proinflammatory cytokines, such as interleukin-1β and TNF-α, can increase TF expression on endothelial cells and/or monocytes *in vitro* [73,74]. Inflammatory reactants (proteins or markers that increase or decrease following an inflammatory response), such as C-reactive protein, can induce TF expression on human peripheral blood monocytes but not human umbilical vein endothelial cells [75]. This suggests that TF expression can be regulated by different stimuli depending on the cell type. In cancer biology, several defined pathways have been implicated in upregulating TF expression [76]. Some examples include epidermal-to-mesenchymal transformation and transforming growth factor-β signaling [77,78]; hypoxia-induced signaling of early growth response protein-1 [79]; and constitutive activation of PI3K and MAPK signaling [53,54].

1.3.2 Factor VIIa

1.3.2.1 Structure

Factor VII (FVII) is a serine protease zymogen synthesized in the liver and circulates in the plasma. The zymogen circulates the plasma at 10 nM, whereas its activated form FVIIa circulates at 0.1 nM. FXa is the most potent activator for FVII but it can also be activated by FVIIa, FVII-activating protein and other proteases [80–83]. Cleavage at Arg212 exposes the protease domain upon a conformational change with the activating peptide remaining bound by a single disulfide chain. However, FVIIa specific activity is considerably low and has been described as zymogen-like in solution [84]. The light chain, comprised of a γ-carboxyglutamate (Gla)-rich domain and two epidermal growth factor (EGF) homology domains, is covalently linked to the heavy chain which contains a single protease domain (Figure 4).

The Gla domain is a membrane binding motif with many Gla residues, where the synthesis is dependent on the γ-carboxylase cofactor, vitamin K, for the post-translational conversion of Glu to Gla. Proteins containing this modification are collectively known as vitamin K-dependent proteins. Membrane interaction occurs with aPL such as phosphatidylserine and phosphatidylethanolamine. For FVII, these interactions are of weak affinity compared to other vitamin-K-dependent proteins in coagulation, FIX, FX and prothrombin. Rather, FVII preferentially binds to phosphatidic acid [85]. At supraphysiological concentrations of calcium (>2.5 mM), 7 calcium ions bind to the Gla domain of FVIIa, resulting in a conformational change of the Gla domain [33]. However, in plasma, free calcium (1.25 mM) and magnesium (0.6 mM) occupy the Gla domain of FVIIa (4 and 3 divalent cations, respectively) [86]. Although the conformational change induced by the two metal ion occupancies are dissimilar, the proteolytic function of the two are identical.

Two EGF domains, EGF1 and EGF2, serve to tether the protease domain of FVII to an appropriate phospholipid surface via the Gla domain. The EGF domains are tethered by a single stabilizing hydrogen bond between the main-chain carbonyl of Lys143 on EGF1 and the main-chain amino group (Nδ2) of Asn153 on EGF2 [87]. EGF1 contains a calcium binding site at the N-terminal end. In the protease domain there is a calcium binding site which is essential for amidolytic activity. The protease domain of FVIIa shares structural homology with trypsin, similar to other coagulation serine proteases, including FX, FIXa, and thrombin, as well as the anticoagulant serine protease, activated protein C [88].

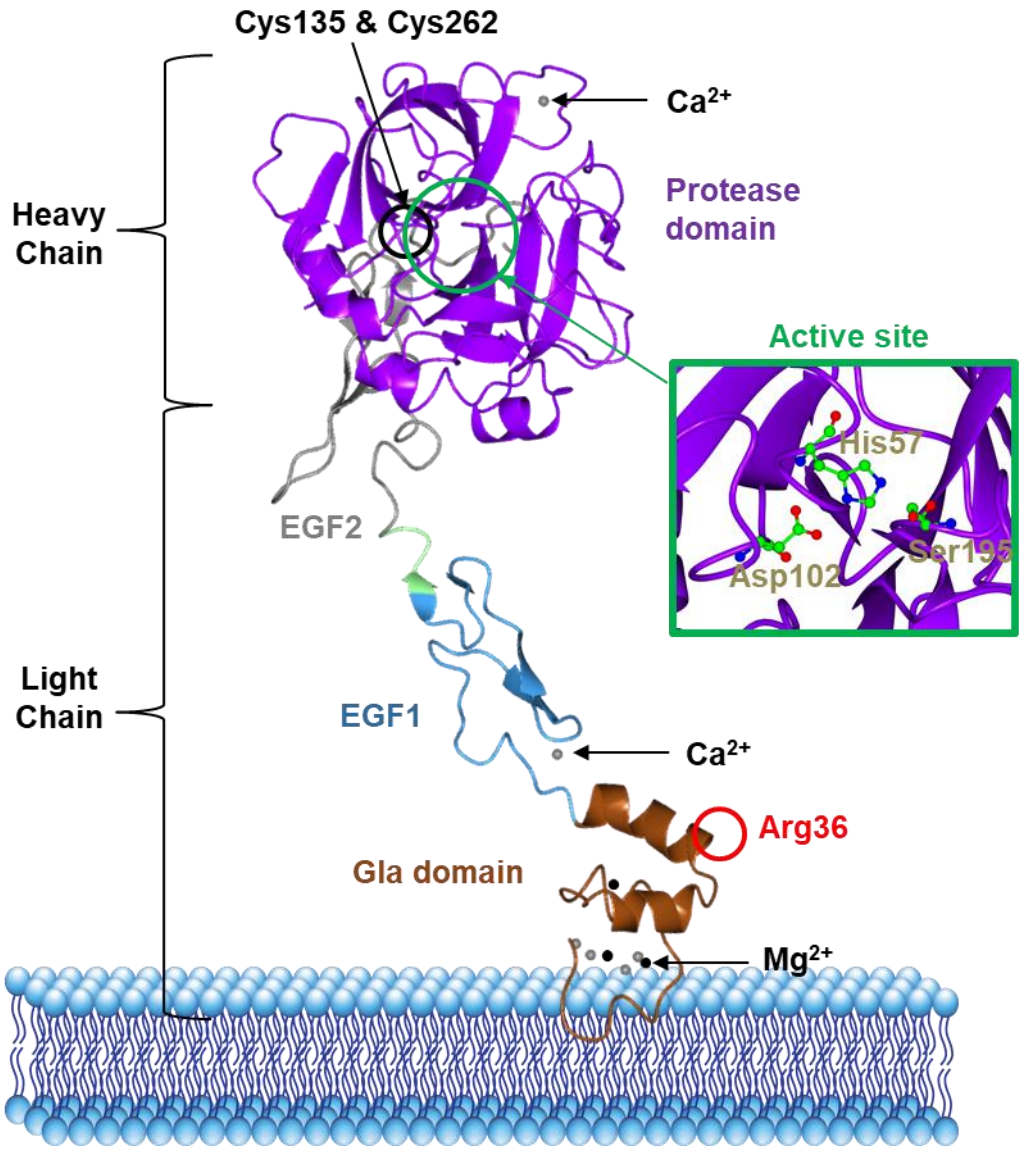

Figure 4. Crystal structure of FVIIa.

The heavy chain of FVIIa, consisting the protease domain (purple), is connected to the light chain comprising the EGF2 (gray), EGF1 (blue) and Gla (brown) domains. Several divalent cation binding (gray spheres for calcium and black spheres for calcium/magnesium) sites are depicted: one in the protease domain, one in the EGF1 domain and seven in the Gla domain. The active site contains the catalytic triad: His57, Asp102 and Ser195 (green circle and inset). Arg212 cleavage of FVII results in a single Cys135-Cys262 thioester bond joining the heavy and light chain (posterior, black circle). The EGF2 and EGF1 domains are connected by a single stabilizing hydrogen bond (light green chain). Arg36 is highlighted for its importance in FX and TFPI recognition. Structure derived from PDB code 1DAN. Magnesium binding sites derived from PDB code 2A2Q.

1.3.2.2 Function

Although humans can live with low levels of FVII [89], complete absence of FVII, as described in mutant mice, results in hemorrhagic lethality in the perinatal period [90,91]. This highlights the importance of FVIIa in haemostasis. The primary function of FVIIa is the catalytic conversion of FX to FXa. FVIIa binding to TF increases the catalytic efficiency of FX activation. This is achieved by structural rearrangement of FVIIa, allowing for optimal substrate binding to exosites on TF and/or FVIIa. Although TF can bind FVII and FVIIa (Figure 5), only when FVIIa has its Arg212-Ile213 scissile bond broken and subsequently the Ile213 allowed to form a salt bridge with Asp244, can TF induce FVIIa rearrangement [84]. Interestingly, TF binding does not cause the catalytic oxyanion hole to form but rather, FX binding to the exosite [92,93] results in the formation of the oxyanion hole [86]. The Gla domain of FVIIa has been shown to be dispensable for its amidolytic activity [94] but is important for FX activation [32,94]. Arg36 of FVIIa Gla domain connects with TF residues 159 to 164 with an extensive network of hydrogen bonds [95]. Arg36, along with TF residues 165 and 166, were proposed to be important in FX substrate as well as TFPI recognition [96], though some opposing evidence or inconsistencies have been noted [95].

In addition to a procoagulant role, TF/FVIIa also is also important in cell signaling (Chapter 1.3.1.3). FVIIa can also participate in cell signaling in the absence of TF through interactions with endothelial cell Protein C receptor (EPCR) [97]. Activation of PAR-1 signaling by EPCR/FVIIa resulted in suppression of tissue necrosis factor (TNF)-α-induced inflammation and LPS-induced endothelial activation and inflammation. The precise mechanism is not yet understood but evidence pointed to an early step in TNF receptor 1-mediated signaling [97].

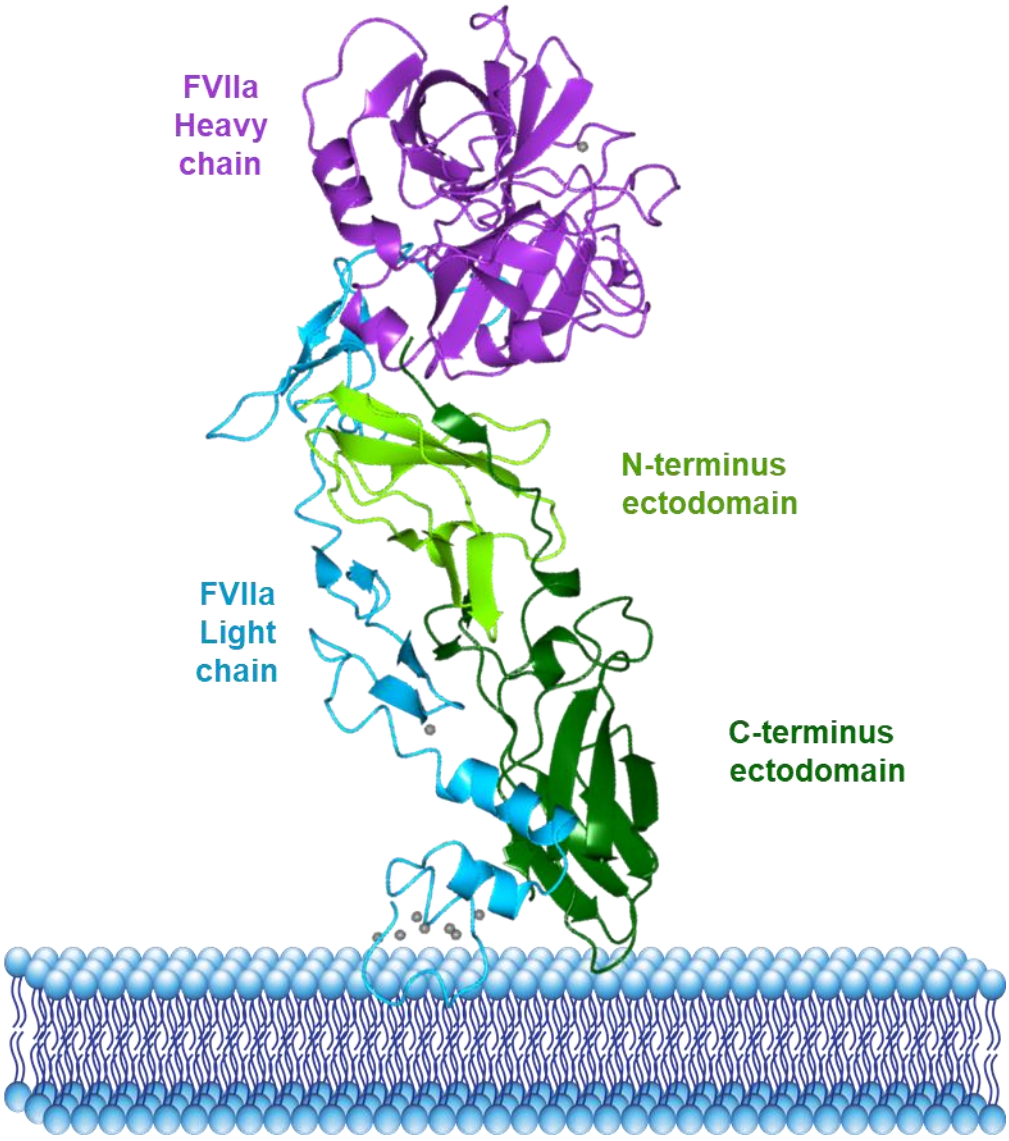

Figure 5. Soluble TF/FVIIa crystal structure.

FVIIa heavy chain (purple) connected to light chain (blue) is bound to soluble TF, comprised of the N-terminus and C-terminus ectodomains (light green and dark green, respectively). Calcium binding is depicted as gray spheres. A phospholipid membrane is shown as a reference to orientation on a membrane. Structure is derived from PDB code 1DAN.

The importance of FVIIa is further accentuated by its use as a therapeutic for treating hemophiliacs with FVIII inhibitors and other coagulation disorders (e.g. acquired hemophilia, and congenital FVII deficiency). Its indisputable coagulation ability has also warranted its use in off-label situations such as surgery and critical care management of bleeding [98,99].

1.3.2.3 Regulation of FVIIa expression and function

FVII circulates the plasma at ~0.5 µg/mL or ~10 nM whereas its activated form exists at less than 1% of total FVII(a) at ~0.1 nM [100]. FVII has a shorter half-life than any other clotting factor, of ~5 hours [101,102]. Interestingly, other clotting proteases tend to be cleared very quickly upon activation (~3 min). In contrast, the half-life of FVIIa is 2 to 4 hours [103,104]. This would suggest that the clearance of FVII/FVIIa is due to a specialized mechanism by the liver. However, studies suggest high membrane turnover on primary liver cells and yet unknown factors contribute to the slower clearance rate of FVIIa to other activated clotting proteases [105]. Freely circulating plasma FVIIa is inhibited by antithrombin III in the presence of heparin at a slower rate than the TF/FVIIa complex [106]. As described in Chapter 1.3.1.5, FVIIa activity is inhibited by TFPI.

1.3.3 Factor X

1.3.3.1 Structure

Like FVII, FX is a serine protease zymogen that is synthesized in the liver. The protein consists of a 139 amino acid residue light chain and a 306 amino acid residue heavy chain linked through a single disulfide bond (59 kDa). The light chain is distinguished by three structural domains: A N-terminal Gla domain, a short hydrophobic domain, and similar to FVII, two EGF-homology domains (EGF1 and EGF2). The heavy chain is comprised of a single protease domain.

There are no crystal structures of the zymogen form, but inhibited FXa has several crystal structures available (Figure 6, PDB code 1XKA) [107,108].

Prior to FX secretion into circulation, the Arg140-Lys141-Arg142 tripeptide in the heavy chain is excised [109]. The mature FX consists of an activation peptide (Ser143-Arg194) [110] at the N-terminus of the protease domain, which is irreversibly connected to the light chain by a single disulfide bond between Cys132 and Cys302 [111]. Similar to FVII and FIX, the protease and EGF1 domains have a single calcium binding site [107]. The Gla domain of FX is linked to the EGF domains through several aromatic residues and contains 11 Gla residues. FX binds to aPL via the Gla domain at nM affinity, in contrast to FVIIa (~0.2 μM and 15 μM, respectively) [112]. In models of sTF/FVIIa/FXa, the Gla domain of FX is depicted as interacting with both FVIIa Gla domain and TF domain [113–115]. 8 calcium ions are coordinated by the Gla residues although Asp residues may also participate (Figure 6, PDB code 1IOD) [116].

1.3.3.2 Function

Activation of FX by the extrinsic or intrinsic tenase through cleavage of Arg194-Ile195 releases the 52-residue activation peptide [117]. FXa can then assemble with FVa, calcium and aPL to form the prothrombinase complex, resulting in an ~278,000-fold increase in FXa-mediated prothrombin activation rate [96]. Prothrombin is activated by FXa-mediated cleavages at both Arg271 and Arg320 (Figure 8) [92]. FXa/calcium/aPL predominantly cleaves Arg271 to form prethrombin before cleaving Arg320. FXa/FVa/calcium/aPL, on the other hand, first cleaves Arg320 to form meizothrombin followed by Arg271 cleavage to form fully active thrombin (α-thrombin). Although both cleavage sites are accessible [118], the presence of a cofactor shifts bond cleavage preference.

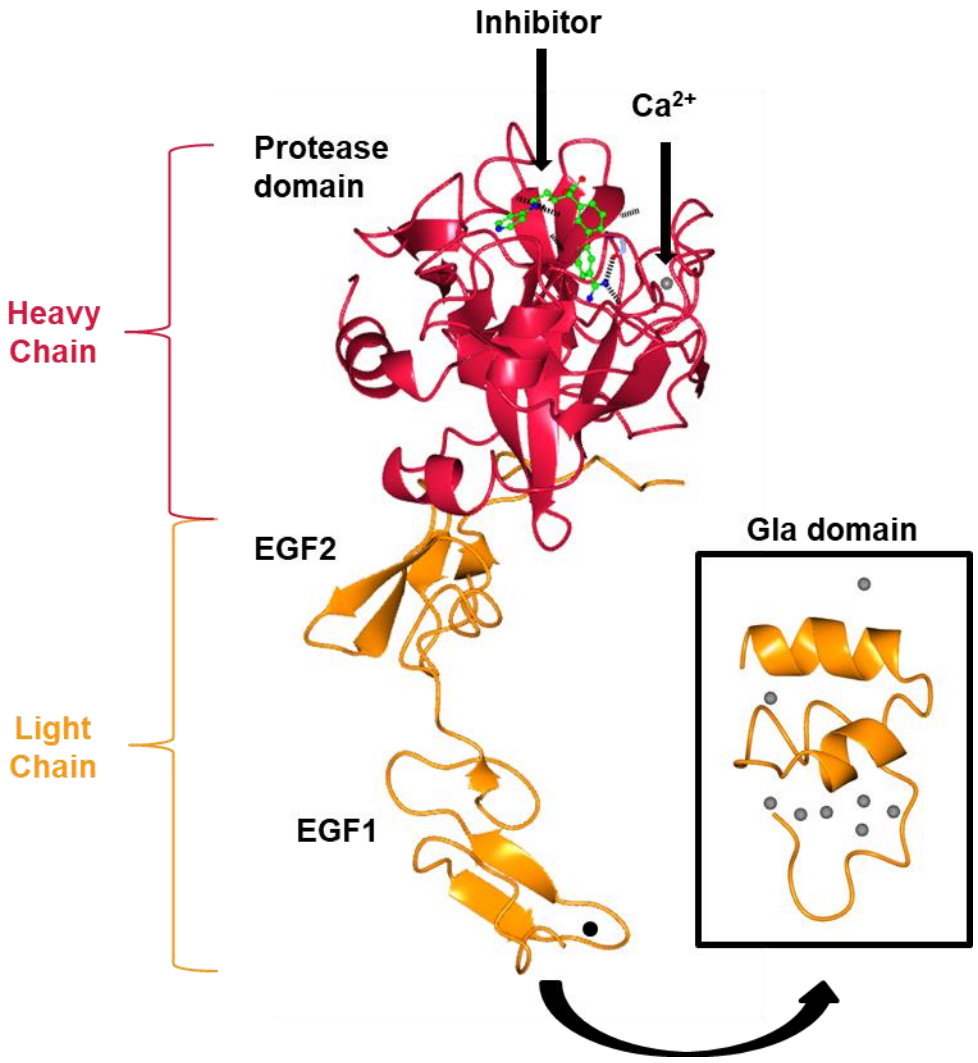

Figure 6. Crystal structure of FXa in complex with an inhibitor, FX-2212.

FXa inhibited with an active site inhibitor, FX-2212, in the presence of calcium (PDB code IXKA). The heavy chain (red) has the protease domain sitting on top of the light chain (orange) consisting of EGF2, EGF1 and Gla domain. A single calcium ion is bound in the protease domain. Similar to FVIIa, a calcium binding site is found in the EGF1 domain (black dot, inserted from PDB code 1XKB). The Gla domain is missing from the structure and is depicted separately in the black box with calcium ions depicted in gray (PDB code 1IOD).

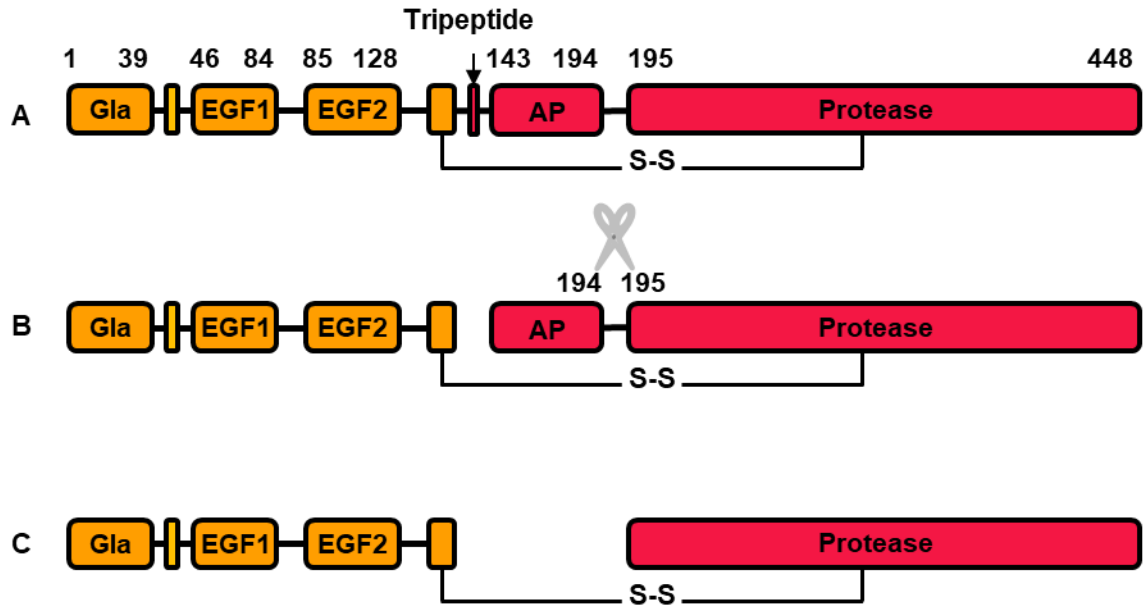

Figure 7. Schematic representation of FX and FXa.

(A) Premature form of FX includes a tripeptide linking the activation peptide (AP) to the light chain. The light chain is also linked to the heavy chain via a single disulfide bridge between Cys132 and Cys302. (B) During or after secretion into blood plasma, the tripeptide is cleaved to form mature FX. This results in the AP being linked to the heavy chain by a single Arg194-Ile195 bond. Proteolytic cleavage of this bond by tenases results in (C) the active form, FXa.

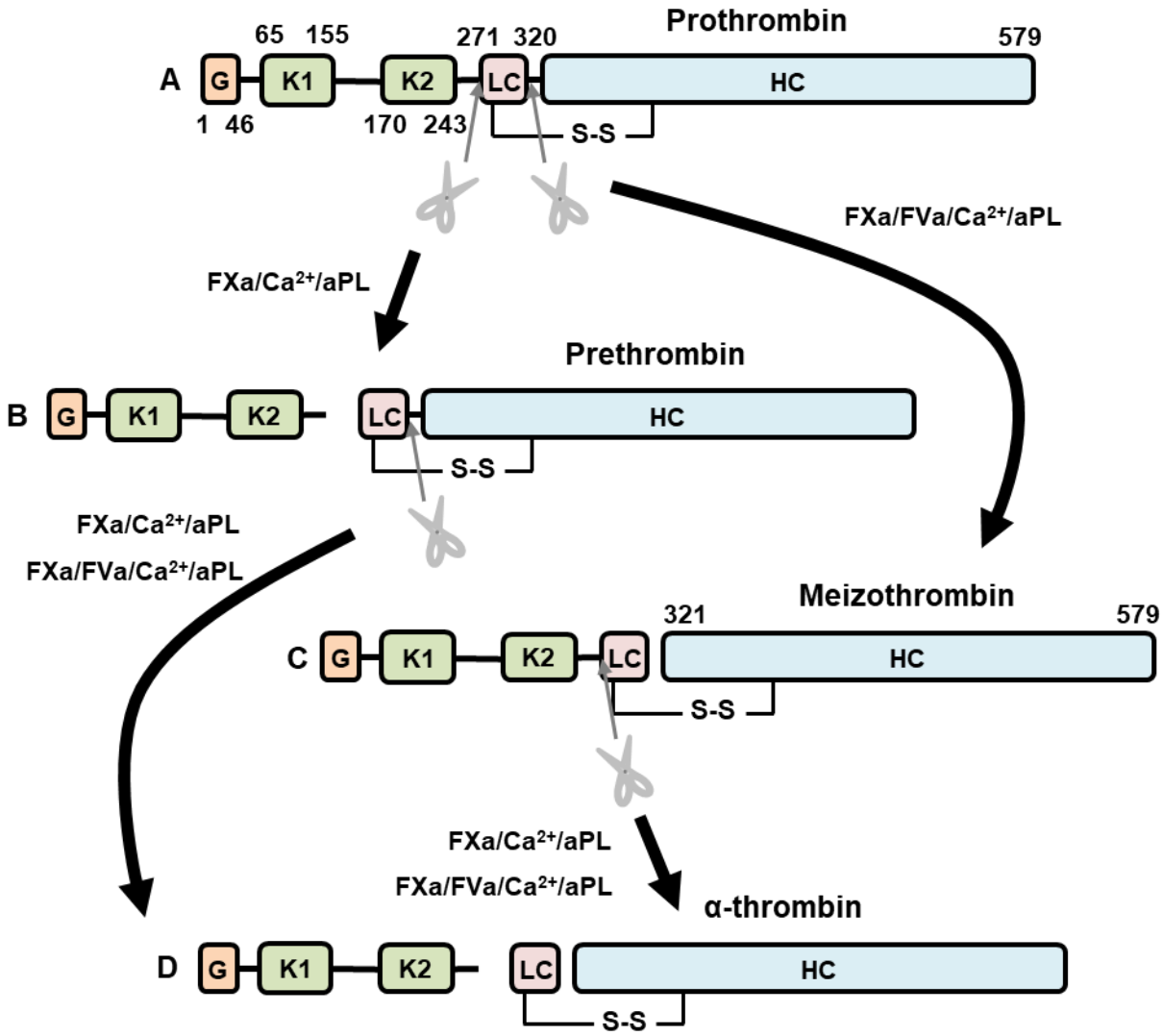

Figure 8. Prothrombin conversion to thrombin by FXa.

(A) Prothrombin consists of a Gla domain (G), two kringle domains (K1 and K2), and a trypsin-like serine protease domain that contains a light chain (LC) and a heavy chain (HC). Two different cleavage scenarios can occur depending on whether or not FXa/Ca^{2+}/aPL is in complex with the cofactor FVa. (B) In the absence of FVa, Arg271 is predominantly cleaved, releasing the G, K1 and K2 domains, to form prothrombin. (C) In the presence of FVa, Arg320 is predominantly cleaved to form meizothrombin, where the LC remains anchored to the G, K1 and K2 domains. (D) The final cleavage of the non-cleaved Arg271 or Arg320 results in the fully active form, thrombin or α-thrombin. The LC and HC are held together by a single disulfide bond.

FXa is also involved in amplification of its own zymogen activation through FVII [119] and FVIII activation [120]. FV can be activated by FXa to increase FXa-mediated production of thrombin [120]. Furthermore, FX switches from a procoagulant state to an anticoagulant state through plasmin cleavage into FXa33/13 when bound to aPL resulting in fragments with C-terminal lysines [121–123]. C-terminal lysines are important in the degradation of the clot (fibrinolysis) as cofactor binding sites for tissue plasminogen activator and plasminogen. The former cleaves plasminogen into plasmin, the physiological protease responsible for fibrinolysis.

PAR-1 [124] and PAR-2 [125] are activated by FXa to participate in cell signaling [125]. FXa-mediated PAR-1 and -2 signaling can result in enhanced cell proliferation and migration in fibroblasts and smooth muscle cells, increased pro-fibrotic and pro-inflammatory cytokine production and secretion [126–129]. EPCR interaction with TF/FVIIa/FXa was shown to enhance PAR-1 and PAR-2 activation [130].

1.3.3.3 Regulation of expression and function

FX activation is tightly regulated to prevent aberrant coagulation. The activation is localized to areas of vascular damage and is restricted to a phospholipid membrane. TFPI is the physiological inhibitor of coagulation, inhibiting FXa and subsequently inhibiting TF/FVIIa many fold efficient than TFPI alone. Antithrombin is the main serine protease inhibitor of the intrinsic pathway [111]. This serpin forms a 1:1 covalent complex with FXa, thrombin, FIXa, FXIa, and FXIIa. The rate of complex formation is greatly enhanced when bound by heparin [131]. These rates differ depending on the substrate, e.g. FXa inhibition is accelerated by ~1000 fold compared to ~4000 fold for thrombin inhibition [132]. Once FXa is inhibited, it is rapidly cleared from the

body within minutes via degradation in the liver [133,134]. FXa activity is also indirectly regulated by activated protein C-mediated proteolysis of FVa [135].

1.3.4 Anticoagulation and fibrinolysis

The main topic of the studies presented here is coagulation. It is, however, important to understand that anticoagulant and profibrinolytic factors are working against coagulation. As noted, anticoagulant factors include TFPI, antithrombin and activated protein C. Thrombin generated by FXa can bind to an endothelial cell integral membrane protein known as thrombomodulin [136]. This shifts thrombin from a procoagulant state to an anticoagulant state. The thrombin/thrombomodulin complex activates protein C into activated protein C. Activation of protein C is markedly enhanced when bound to EPCR found on the endothelial cell surface. Once released from EPCR, activated protein C proteolytically inactivates FVa and FVIIIa. The former decreases FXa/FVa prothrombinase assembly and the latter decreases FIXa/FVIIIa tenase assembly. Therefore, FXa activity and FX activation are inhibited, respectively.

Fibrinolysis is the degradation of a blood clot. The process involves tissue plasminogen activator (tPA) and plasminogen binding to C-terminal lysines found on the fibrin clot. tPA then cleaves plasminogen to plasmin and the plasmin cleaves the fibrin clot [121]. Cleavages at lysine residues by plasmin can result in additional C-terminal lysines. This allows additional tPA and plasminogen binding, resulting in amplified plasmin generation. Much like coagulation, there are antifibrinolytic factors such as plasminogen activator inhibitor-1 and thrombin-activatable fibrinolysis inhibitor [137]. Thus, it is important for sufficient plasmin to be formed to overcome the antifibrinolytic factors and allow complete clot dissolution.

1.4 Enveloped viruses

Viruses are obligate parasites that require a host to replicate and sustain itself. Although they fit under this basic requirement, the methods by which a virus achieves this can be very different. As such, virus classification systems were established to categorize viruses to better organize and identify them. The Baltimore classification system is based on the genetic material (DNA or RNA), sense (positive or negative), strandedness (single or double) and replication strategy. The viruses can then be further separated into orders and families depending on their structure, ancestry and target organisms, although this classification is still incomplete.

All viruses have genomic material encased within a protein cage, the capsid. This basic form of a virus is known as a naked or non-enveloped virus. Some viruses are further encased by an outer phospholipid bilayer membrane structure termed envelope. This envelope is derived from the host cell during egress, though how the different viruses obtain their envelope can differ. Enveloped viruses are more prone to degradation compared to non-enveloped viruses, through desiccation and chemical inactivation. However, the envelope imparts the advantage of immune evasion to the virus. Glycoproteins encoded by the virus or host and found on the viral envelope can prevent immune recognition and/or aid in cell recognition and entry. Herpesviruses are a prime example of a large enveloped virus that has evolved several mechanisms on its envelope structure to enhance its survivability. I am most interested in enveloped viruses involved in haemostatic abnormalities and can be replicated in TF-expressing cells. A summary of TF-expressing cells and evidence of *in vivo* and/or *in vitro* replication of herpes simplex virus type 1, dengue virus, human immunodeficiency virus and hepatitis C virus is found in Table 1.

Table 1. Enveloped viruses and TF-expressing cell tropism.

Tissue factor expressing cells	Virus replication
Astrocytes [65]	HSV1 [138] DENV [139] HIV [140]
Dendritic cells [141]	HSV1 [142] DENV [143–145] HIV [146–148] HCV [149–151]
Epithelial cells [152,153]	HSV1 [154,155] DENV [156] HIV [146–148,157] HCV [158–160]
Endothelial cells [161–164]	HSV1 [165–169] DENV [170–172] HIV [173,174] HCV [175]
Hepatocytes [176,177]	HSV1 [178,179] DENV [180,181] HIV [182] HCV [183]
Megakaryocytes [184]	HSV1 [185] DENV [186–189] HIV [190,191] HCV [192]
Monocytes/macrophages [161,193]	HSV1 [194–196] DENV [170,172,197] HIV [198] HCV [199–201]
T lymphocytes [202]	HSV1 [203–205] DENV [206] HIV [207–209] HCV [210–212]

HSV1, herpes simplex virus type 1; DENV, dengue virus; HIV; human immunodeficiency virus; HCV, hepatitis C virus

1.4.1 Herpesviridae

The family of viruses, *Herpesviridae*, consists of double-stranded linear DNA viruses that causes diseases in humans as well as other animals. Of the over a hundred known herpesviruses [213], only eight are known to affect humans. Herpesviruses share common traits; they have an envelope, their large genome (>80 genes) is packed into a icosahedral (T=16) capsid and their capsid is tethered to their envelope by a matrix of proteins and mRNA known as the tegument (Figure 9) [213].

When herpesviruses enter a cell, their genome is inserted into the nucleus wherein the linear DNA circularizes into an episome. At this stage, the virus can either cause a productive infection or remain dormant in a latent state [214]. For some viruses such as Epstein-Barr virus and human herpesvirus 6, latency can be achieved through integration of their genetic material into the host genome [213]. The ability of herpesviruses to establish dormancy in humans allows the viruses to establish lifelong infections.

Reactivation of the virus can result in symptoms similar to the initial infection or different disease sequelae. For example, reactivation of Varicella-Zoster virus (chickenpox virus) results in shingles, a painful rash that can cause neural pain more severe than the primary infection of chickenpox.

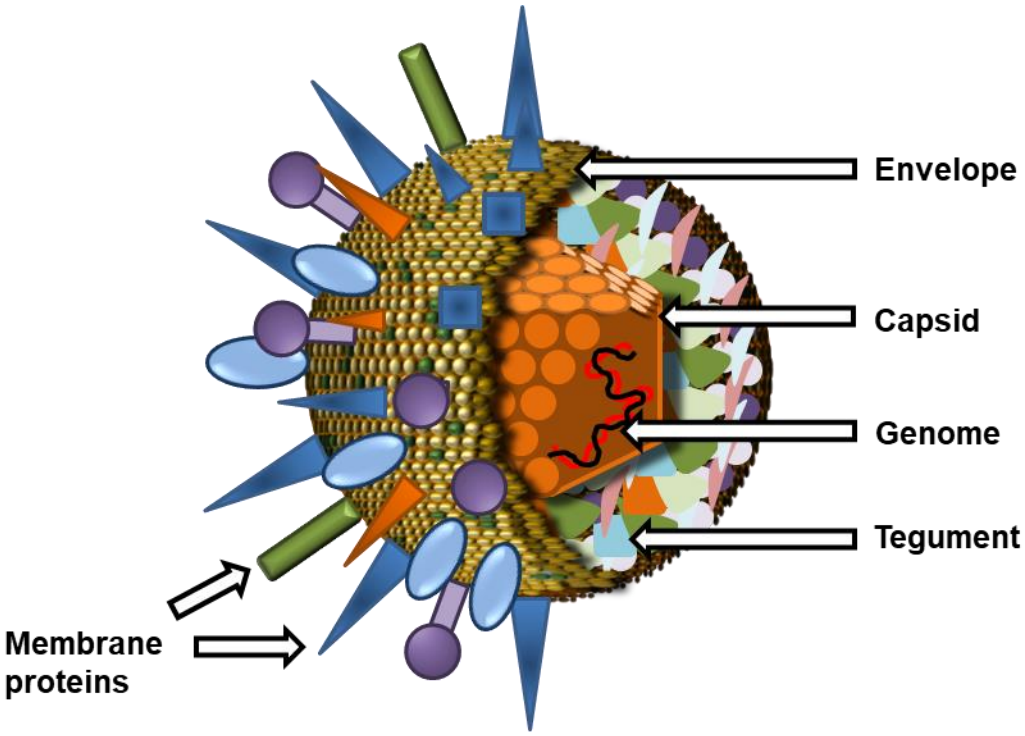

Figure 9. Structural diagram of a basic herpesvirus.

Members of the *Herpesviridae* family share the same basic structure. A bilayer phospholipid membrane, known as the envelope, stores the capsid that is protecting the viral dsDNA genome. There are numerous host- and virus-encoded membrane proteins present on the envelope. A cluster of proteins fills the space between the capsid and the envelope, this viral matrix is known as the tegument.

1.4.1.1 HSV1

HSV type 1 (HSV1) or human herpesvirus 1 is of the genus *Simplexvirus*, along with HSV type 2 (HSV2). HSV1 causes cold sores for which it has developed the moniker, cold sore virus. However, HSV1 can also cause genital herpes, a disease that was once predominantly caused by HSV2 [215]. Other important diseases caused by HSV1 include infectious blindness through keratitis [216], neonatal herpes [217], and encephalitis [218]. According to the WHO, in 2012, HSV1 was estimated to affect 3.7 billion people under the age of 50, representing 67% of the world's population. A more recent study in 2015–2016 of the United States' population, observed a prevalence of 47.8% of people aged 14-49. The prevalence increased with age and was more prevalent in females.

Primary infection by HSV1 typically begins with attachment to epithelial cells via viral glycoproteins gB and gC binding to heparan sulfate proteoglycans (HSPG). Entry occurs by membrane fusion involving gB, gD, gH and gL with entry receptors: herpesvirus entry mediator (HVEM), Nectin-1 and/or 3-O-sulfated HSPG [154,219,220]. However, depending on the cell type, receptor-mediated endocytosis is preferred [221,222]. In both scenarios, the viral capsid is eventually released into the cytoplasm where it travels to the nucleus for unloading of viral genome and subsequent replication processes. In addition to cell lysis promoting HSV1 spread, HSV1 has developed multiple modes of cell-to-cell spread. Some of these infection modes are not well understood, but include cell-to-cell fusion [223] and tight junction transfer [224]. Eventually, HSV1 infects and lays dormant as an episome in sensory neurons [214].

HSV1 has a slew of virulence factors that contribute to its potent infectivity and extremely wide cell tropism [219,225]. These include multifunctional glycoprotein for attachment and entry, ubiquitously expressed entry receptors, multiple entry mechanisms and diverse spread strategies.

As a consequence, HSV1 envelopes have the potential to obtain a wide breadth of host-derived proteins and incorporate them on its envelope [226]. Previous work in the Pryzdial laboratory have identified TF and aPL on HSV1, HSV2 and cytomegalovirus [2], as evidence of direct links to thrombotic pathologies.

1.4.1.1.1 Implications in cardiovascular/haemostatic abnormalities

HSV1 involvement in cardiovascular abnormalities was postulated upon discovery of HSV antigen/genetic material in atherosclerotic plaque [227]. Herpesviruses persist as lifelong infections, with frequent reactivation promoting leukocyte and platelet adhesion to the vascular wall, lipid accumulation in smooth muscle cells and thrombin deposition in the periphery. These effects contribute to vascular pathologies [165,228–231]. This led to studies looking into HSV1 prevalence and risk factors [232,233]. The first meta-analysis of 17 studies evaluating the risk of atherosclerosis associated with HSV1 found that there is an increased risk of developing atherosclerosis (OR = 1.77; 95% CI: 1.40–2.23; $P < 0.001$) in HSV1-positive patients [234]. While these examples provide a retrospective clinical correlation, causal evidence was reported using HSV1 as a targeted cytolytic therapeutic for melanoma cells, which resulted in a high propensity for deep vein thrombosis [235]. Case reports have also detailed the presence of thrombi [236,237] and/or bleeding [238,239] in patients with HSV1 encephalitis. In one study examining predictors of outcome in HSV1 encephalitis, half of patients experienced acute thrombocytopenia and a few cases of hemorrhage in the brain (5%) [238].

1.4.1.2 Glycoprotein C

HSV1 encodes multiple glycoproteins on its envelope surface: gB, gC, gD, gE, gG, gH, gI, gJ, gL, gK, and gM. These glycoproteins aid in its virulence. Of these glycoproteins, gC is of utmost interest to me because of its ability to bind and affect FX activation [12,240,241].

1.4.1.2.1 Structure

gC is a highly glycosylated transmembrane protein, with molecular weights ranging from 55 kDa in its non-glycosylated form to 130 kDa when fully glycosylated. The extracellular domain of gC contains nine consensus sites for N-glycosyl oligosaccharides and predicted to be 7 to 13 sites for O-glycosyl oligosaccharide [242]. Due to the variability in extent of post-translational modification, gC exists in different functional forms [243]. The mucin-like region of gC comprises the majority of glycosylation sites. This heterogeneity and high glycosylation pose problems for protein crystallization, hence there still lacks a 3-dimensonal gC structure. Nonetheless, a predicted folded structure of gC was proposed based on the derivation of disulfide bond arrangement (Cys127-Cys144, Cys286-Cys347, Cys386-Cys442, and Cys390-Cys419), homologous regions and molecular binding sites and inferred discontinuous antigen folding (Figure 10) [244,245]. These binding sites include heparan binding and C3b binding, important in its function.

1.4.1.2.2 Function

gC is a multifunctional transmembrane glycoprotein that is expressed on the virus surface and docks the virus to host cellular sulfated glycosaminoglycans (GAGs), such as heparan sulfate (Figure 11A) and chondroitin sulfate [246–248]. The mucin-like region of gC is important for

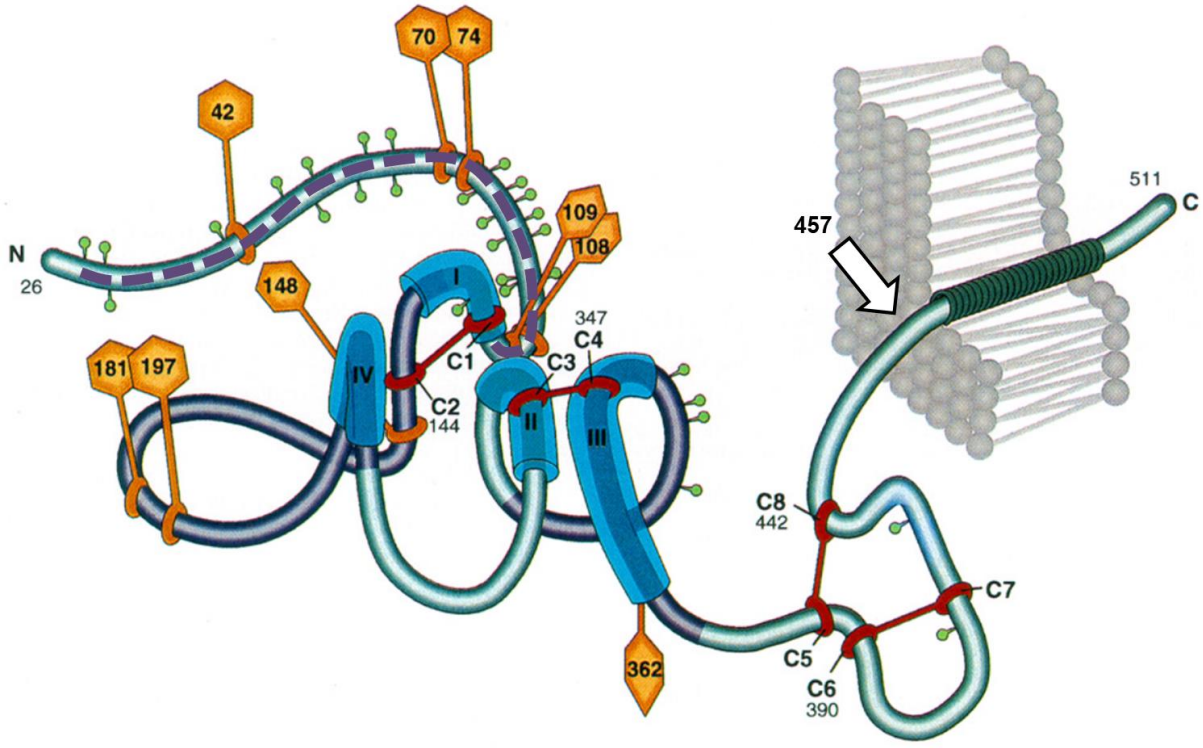

Figure 10. Schematic illustration of HSV1 gC.

Hypothesized structural model of gC based on its disulfide bond arrangements, homologous regions and molecular binding site. N-CHO glycosylation modifications (orange hexagons) and O-CHO glycosylation modifications (small green circles) are predicted at the stated amino acids. The purple dashed region denotes a highly glycosylated mucin-like region. The blue regions numbered I, II, III, and IV represent the important regions for C3b binding. Antigenic sites are shown in dark blue. gCΔ457t (sgC-His) is truncated at the C-terminal amino acid 457 (white arrow). Image from Rux *et al.* (1996) J Virol. [245].

GAG binding, with the deletion mutant (Δ33–123) exhibiting lower affinity to immobilized heparin and heparan sulfate (purple-dashed line, Figure 10) [246].Mutational studies of gC and subsequent binding to isolated heparan sulfate chains had shown that heparan sulfate binding required a cluster of arginine residues surrounding the Cys127–Cys144 disulfide bridge with Ile142 substantially supporting the binding [249]. This region is well-conserved among mammalian herpesviruses, further adding to the importance of this region towards its function as a cell adhesion molecule [242]. A synthetic peptide mimicking the amino acid residues 137 to 151 of gC has been demonstrated to compete with HSV1 binding to GAGs, thereby inhibiting infection [250].

Recently, gC has been discovered to bind with <1 pM affinity to a cell surface scavenger receptor known as macrophage receptor with collagenous structure (MARCO) on keratinocytes [251]. Overexpression of MARCO in keratinocytes resulted in enhanced HSV1 skin infection whereas $MARCO^{-/-}$ mice were less susceptible. Even though the role of gC has been downplayed as non-essential for viral entry [219], removal of gC results in ~10-fold reduction in infectivity *in vitro* [252] and ~100-fold reduction *in vivo* [253].

The reduction in infectivity of gC knockout mutants of HSV1 *in vivo* can be partly attributed to its role in the evasion of host innate immunity and phagocytosis (Figure 11B) [254,255]. Complement protein C3b can bind to the virus and allow for the binding of properdin to stabilize the alternate pathway C3 convertase (C3b and factor Bb) (Figure 11B) [256]. The C5 convertase cleaves complement protein C5 to C5a and C5b, the latter being involved in the formation of the membrane attack complex (MAC). C3b can also serve to opsonize the pathogen, targeting the virus for destruction by phagocytes via recognition by C3b receptor (Figure 11C). gC interrupts these complement functions by binding to C3b via residues 124 to 366 [255], thereby

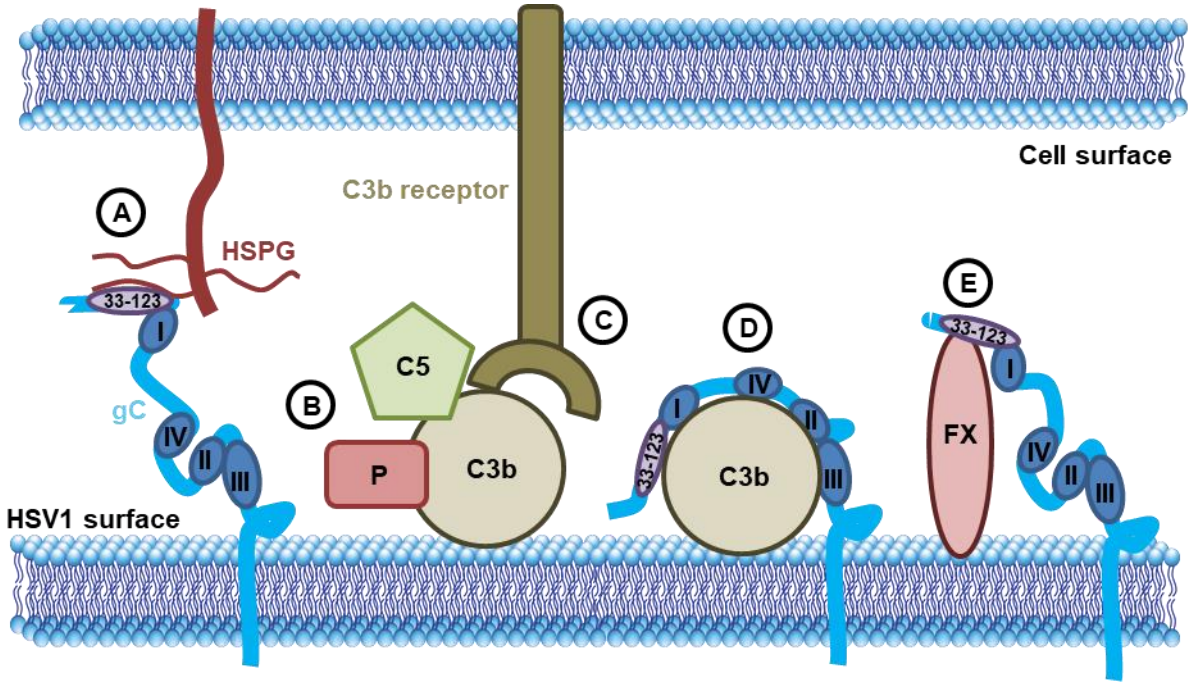

Figure 11. Multiple functions of HSV1 gC.

(A) gC is known to bind to heparan sulfate proteoglycans (HSPG) on target cells as the primary step of infection. The mucin-like domain of gC (33-123) is known to be important in this interaction. (B) Complement protein C3b binding to the virus allows the binding of properdin (P) which stabilizes the C5 convertase (C3b and Factor Bb (not shown)). This allows the binding of C5 which is important for the formation of the membrane attack complex (MAC). (C) C3b can also serve to opsonize the pathogen, targeting the virus for destruction by phagocytes via recognition by C3b receptor. (D) gC binding of C3b prevents binding of C5a and properdin to C3b. (E) gC can also bind the coagulation zymogen FX and affect its activation. Diagram of gC binding to C3b was adapted from Lubinski *et al.* (1999) J Exp Med. [257].

blocking C5 binding (Figure 11D). The mucin-like region of gC, residues 33 to 123, blocks properdin from binding [255]. This results in an accelerated decay of the alternate pathway C3 convertase.

As a possible contributor to vascular lesion development, gC has been linked to monocyte adhesion to HSV1-infected endothelial cells [240]. This effect was dependent on thrombin generation, alluding to a role for gC in coagulation protease activation. Using transgenic expression of gC in murine L cells, FX binding to cell-surface gC was observed (Figure 11E) [240]. Since gC is found on the virus envelope, I investigated FX binding to purified HSV1 and showed that the presence of viral gC created FX binding sites [241]. The mucin-like region of gC was demonstrated to be important for FX binding. Viral gC was also shown to enhance FVIIa-dependent FX activation. Although the Pryzdial laboratory reported that a soluble form of gC (gCΔ457t or sgC, Figure 10) contributes to FX activation without being membrane-tethered, the activity was ~1000-fold higher when combined with the virus [258].

1.4.2 Flaviviridae

Members of the *Flaviviridae* family of viruses are small (~40-60 nm), enveloped, single stranded positive-sense RNA viruses. Their genomes are ~11 kb in size and encode a single long open reading frame that is flanked by a 5' and 3' highly structured untranslated region [88]. As such, translation of the viral genome results in a single large polyprotein that is cleaved into mature proteins by host and virus proteases. As the virus genome is positive-sense RNA, the virus encodes its own RNA-dependent RNA polymerase to replicate its genome. The *Flavivirus* genus consists of many arthropod-borne viruses, important human pathogens include dengue virus, West Nile

virus, yellow fever virus, Japanese encephalitis virus, and Saint Luis encephalitis virus. Another important human bloodborne pathogen is hepatitis C virus of the *Hepacivirus* genus.

1.4.2.1 Dengue virus

Dengue virus (DENV) is a bloodborne virus and is the causative agent of dengue break-bone fever, dengue hemorrhagic fever and dengue shock syndrome. The virus is transmitted to humans via *Aedes* mosquitos, mainly *Aedes aegypti*. This species of mosquito is prevalent in tropical and subtropical areas, with their habitats growing due to urbanization, global warming and mosquito adaptation. There is an estimated 390 million infections and 24,000 deaths each year and half the world's population are at risk of infection [259]. Until recently, there were four known serotypes of DENV, aptly named DENV-1, DENV-2, DENV-3 and DENV-4. DENV-5 is a new variant of DENV that was first isolated in the fall of 2013 [260] but as yet known to infect only non-human primates. Similar to influenza, different serotypes are a problem in vaccine development as the main antigen on the virus surface, the envelope protein (E protein), is antigenically distinct on each serotype. Infection with one serotype confers life-long immunity to only that specific serotype. Partial immunity is obtained to some of the other serotypes. Antibodies are directed towards E protein, which shares structural homology between serotypes as well as the other members of the *Flavivirus* genus, West Nile virus, Zika virus and Japanese Encephalitis virus [261,262]. A secondary infection of a different serotype can culminate into a more severe form of dengue infection due to antibody-dependent enhancement (ADE). ADE of dengue infection occurs when pre-existing antibodies cannot neutralize the virus but instead, enhance monocyte infection via Fc receptor-mediated entry [263,264]. This phenomenon poses a crucial problem in vaccine development.

1.4.2.1.1 Implications on cardiovascular/haemostatic abnormalities

Thrombocytopenia has been observed in dengue fever and is always seen in dengue hemorrhagic fever [265,266]. Disseminated intravascular coagulation (DIC), a phenomenon wherein small blood clots are formed throughout the body resulting in depletion of platelets and coagulation factors, have been noted in dengue hemorrhagic patients [266–268]. Minor hemorrhagic manifestations of dengue fever may occur in the form of petechiae, epistaxis, and gingival bleeding [265]. Increased vascular permeability and the resulting diapedesis (migration of blood cells through the vasculature) is also seen in dengue fever and more severe forms of dengue infection. Although bleeding is more commonly reported, DENV-associated thrombosis (e.g. deep vein thrombosis) may be under-reported [269–273]. DENV activation of endothelium can result in vascular leakage and TF expression [274–276]. For TF to induce vascular leakage, FVIII has to be depleted, hinting to additional mechanisms in DENV-induced haemorrhage [277,278].

1.4.2.2 Hepatitis C virus

Hepatitis C virus (HCV) is the leading cause of liver transplants, hepatocellular carcinoma and liver-related deaths worldwide [279–282]. As HCV can persist in the blood due to several virulence factors and reservoirs (Table 1), this leads to chronic HCV infection. Continued liver damage eventually results in fibrosis, scarring, loss of liver function (cirrhosis) and carcinoma [283]. HCV is transmitted human-to-human through the parenteral route, with humans and chimpanzees being the only known hosts [283]. HCV circulates the blood as free particles or coated by host low-density lipoproteins. Blood donations are routinely tested for HCV, a major concern that had plagued the North American blood system in the 20th century. No vaccine is

available for HCV. However, direct acting antivirals are now available with some treatments reaching over 90% cure rate of HCV infected patients [284]. However, treatment is still costly, up to 150,000 USD. Other complications of HCV infection include cardiovascular/haemostatic abnormalities which can persist even after antiviral treatment of HCV [285].

1.4.2.2.1 Implications in cardiovascular/haemostatic abnormalities

HCV infections result in liver damage and impaired function. As most coagulation factors are synthesized in the liver, there is a decrease in vital coagulation factors e.g. FX, FVII, FIX, and prothrombin [286,287]. Although lower levels of coagulation factors would indicate hypocoagulability, anticoagulant proteins Protein C, Protein S and antithrombin [285] are also decreased. There is also an increase in FVIII levels in these patients [288]. This could be due to increased von Willebrand Factor (vWF) expression and decreased clearance of vWF [289,290]. The rise in vWF results in lower clearance of FVIII from the blood, which is typically high if not in complex with vWF. High FVIII levels has been associated with increased thrombosis [291]. Interestingly, there have been several case reports of acquired FVIII autoantibodies in patients with HCV [292–296]. Following treatment with directly acting antivirals in patients with hepatitis C virus related cirrhosis, procoagulant and anticoagulant proteins are gradually restored. Yet, patients treated for HCV and had achieved a sustained virologic response (defined as being clear of HCV in the blood at 24 weeks post-treatment) still exhibited impaired platelet aggregation [285]. As disease progresses, viral liver cirrhosis results in hypercoagulability in patients [288,297–299] with HCV patients being up to 1.9 times more likely to suffer from venous thromboembolism than the healthy human population [300]. Liver cirrhosis caused by HCV has also been linked to enhanced expression of monocyte TF [301].

1.4.3 Retroviridae

Measuring around 90-140 nm in diameter, retroviruses house double-stranded RNA genomes of about 7-12 kb [302]. These viruses encode reverse transcriptases to convert their RNA genome into a DNA intermediate which is incorporated into the host genome. Around 8% of the human genome is made up of sequences from viruses of the *Retroviridae* family of enveloped viruses [303]. The genome integrating capability of retroviruses allows the inserted genomic material to be passed on to daughter cells, making their use as vectors for gene delivery very attractive [304]. Retroviruses have two main assembly mechanisms: Type B and Type C [302]. Type B retroviruses assemble their capsids in the cytoplasm and obtain their envelope via budding at the plasma membrane. Type C differs in that the capsid is formed at the plasma membrane. One of the most prominent examples of Type C retroviruses is human immunodeficiency virus.

1.4.3.1 Human immunodeficiency virus

Human immunodeficiency virus (HIV) is a bloodborne virus that continues to plague the global population. Transmission occurs human-to-human through sexual intercourse, by contaminated blood and blood products, by needle-sharing, or by vertical transmission (mother-to-child). HIV primarily binds to cluster of differentiation 4 (CD4) antigen via the envelope protein subunit gp120 [305,306]. This initial binding step causes a structural change in gp120, allowing for binding to a secondary receptor (C-C motif chemokine receptor, CCR5, and/or C-X-C chemokine receptor type 4, CXCR4) to enable membrane fusion. The genomic material is inserted into the cell and reverse transcribed prior to nuclear import of the genome. The complimentary DNA viral genome is then integrated into the host genome. HIV infection eventually manifests as acquired immunodeficiency syndrome (AIDS) [307]. This is caused by the infection and

destruction of CD4+ T helper cells, a key player in the adaptive immune system. The weakened immune system is unable to fight off other infections, known as opportunistic infections. Anti-retroviral treatment (ART) goals include minimizing viral load in the plasma, increasing patient CD4+ T cell count, and preventing transmission.

1.4.3.1.1 Implications in cardiovascular/haemostatic abnormalities

Although ART has successful prolonged survival times, HIV-infected individuals are suffering from non-AIDS complications. Many of which are ageing-related diseases such as cardiovascular disease, hypertension, diabetes mellitus, bone fracture and renal failure [308]. The risk of venous thromboembolism in HIV-infected individuals is up to ten-fold higher than the general population [309]. HIV-infected individuals have a heightened expression of TF in their monocyte populations [310,311]. ART treatment decreased circulating TF-containing microparticles and TF activity in the blood [312]. Many studies have explored the coagulant phenotype of HIV-infected individuals, many of which have demonstrated significant prolongation of PT and aPTT [313–315]. aPTT showed an inverse relationship with patient CD4+ cell count, suggesting the use of aPTT as a clinical marker for HIV severity/status in areas where CD4 tests are not readily available [315].

1.5 Hypotheses

Considering that FX activation is affected by the presence of gC and that TF is functionally present on HSV1, my hypothesis is that gC aids FX activation through enhancing TF function (Figure 12). I hypothesize that *Herpesviridae* is not the only family of enveloped virus that

incorporates TF into its viral envelope and that other blood-relevant enveloped viruses can incorporate TF so long as it infects and propagates in a TF-expressing cell.

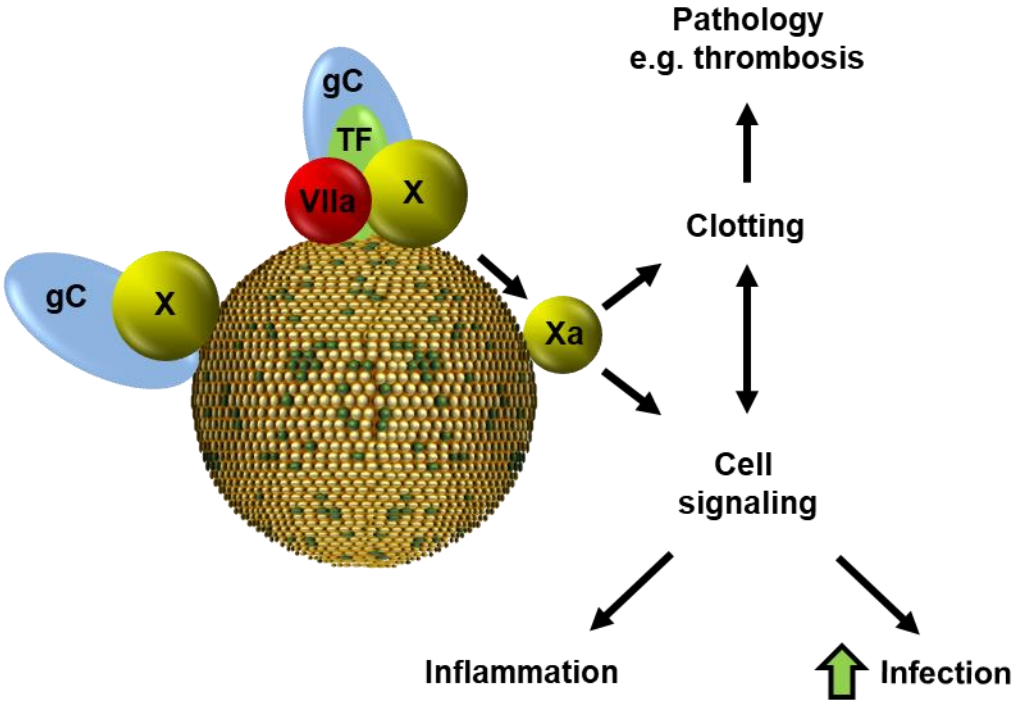

Figure 12. Hypothesized model of gC-TF interaction.

The known gC/FX interaction may aid in TF/FVIIa-mediated activation of FX on the virus surface. These clotting proteases are involved in cell signaling and inflammation. HSV1 has been demonstrated to make use of cell signaling to increase infection. As a side-effect of clotting protease activation, clots are formed which may lead to pathologies such as thrombosis.

Chapter 2: Material and Methods

2.1 Proteins and reagents.

Dry dimethylformamide (DMF), 4-(2-hydroxyethyl)-1-piperazineethanesulfonic acid (HEPES), acetone, dry dimethyl sulfoxide (DMSO), dithiothreitol (DTT), and cyanogen bromide (CNBr) were purchased from Sigma-Aldrich Inc. (St. Louis, MO, USA). Calcium chloride dihydrate (EMD Chemicals, Inc. Greenwich Township, NJ, USA). Tetrasodium ethylenediaminetetraacetic acid (EDTA) and 3,3'-dithiobis(sulfosuccinimidyl propionate) (DTSSP) were purchased from Thermo Fisher Scientific (Waltham, MA, USA). SeaPlaque™ agarose was purchased from Lonza (Basel, Switzerland). Paraformaldehyde (32% in methanol free solution) was purchased from Electron Microscopy Sciences (Hatfield, PA, USA).

Purified human plasma-derived factor VIIa (FVIIa), factor X (FX), factor Xa (FXa) and corn trypsin inhibitor (CTI) were purchased from Haematologic Technologies (Essex Junction, VT, USA). Recombinant human FVIIa was gratefully obtained from Novo Nordisk (NovoSeven®) through a research grant. Innovin (Siemens Healthcare Diagnostic Inc., Delaware, USA) was used as a source of purified recombinant human TF inserted into liposomes. In-house purified FX from normal human pooled plasma (NP) was also used [316,317]. Plasmids for the expression of soluble TF (sTF-His), where the transmembrane and cytoplasmic domains were substituted for His_6 and a 5-amino acid spacer restoring full cofactor activity [318], were obtained through my collaboration with Dr. James Morrissey (University of Michigan Med. School, Ann Arbor, MI, USA). Baculovirus engineered to express a soluble form of gC where the membrane-spanning domain was substituted with His_5 (gCΔ457t, referred to as sgC-His) [319,320] was a kind gift from Dr. Gary Cohen and Dr. Roselyn Eisenberg (University of Pennsylvania, Philadelphia, PA, USA). Frozen NP and congenital factor VIII (FVIII)-deficient plasma

(FVIII/DP) were obtained from George King Bio-Medical (Overland Park, KS, USA). NP was also purchased from Affinity Biologicals Inc. (Hamilton, ON, Canada). L-α-phosphatidylserine (Brain, Porcine, PS), L-α-phosphatidylcholine (Egg, Chicken, PC) and the nickel salt of 1,2-dioleoyl-sn-glycero-3-[(N-(5-amino-1-carboxypentyl)iminodiacetic acid) succinyl] (DGS-NTA-Ni) were purchased from Avanti Polar Lipids, Inc. (Alabaster, AL, USA). FXa-specific chromogenic substrate Z-D-Arg-Gly-Arg-pNA (S-2765) and broad-spectrum chromogenic substrate H-D-lle-Pro-Arg-pNA (S-2288) were purchased from Chromogenix (Milano, Italy). Fluorophores Alexa Fluor 647 succinimydl ester and Alexa Fluor 647 maleimide were purchased from Invitrogen (Carlesbad, CA, USA). His-Tag Labeling Kit RED-tris-NTA, Protein Labeling Kit RED-NHS, and NT.115 Standard and Premium Capillaries for microscale thermophoresis (MST) were from NanoTemper Technologies GmbH (Munich, Germany).

2.1.1 Antibodies and probes

Mouse anti-TF (TF9-9B4) monoclonal antibody was obtained from Dr. James Morrissey [321]. Mouse anti-TF (TF8-5G9) monoclonal antibody was obtained from Dr. Wolfram Ruf (Scripps Research Institute, La Jolla, CA, USA) [322]. Rabbit anti-sgC-His polyclonal antibody (R118) was a kind gift from Dr. Gary Cohen and Dr. Roselyn Eisenberg. Mouse anti-HSV1 major capsid protein monoclonal (MCP, Biodesign International, Saco, ME, USA), mouse anti-TF monoclonal (4503, American Diagnostica, Stamford, CT, USA), rabbit anti-TF polyclonal (ab48647, Abcam, Cambridge, UK), Mouse anti-flavivirus E-glycoprotein monoclonal antibody (ab155882, Abcam), and Anti-6X His tag® antibody (horseradish peroxidase, HRP) (ab1187, Abcam), mouse anti-gC monoclonal (P1104, EastCoast Bio), HRP-conjugated goat anti-mouse IgG (115-035-146, Jackson Immunological, West Grove, PA, USA) and HRP-conjugated goat

anti-rabbit IgG antibodies (115-035-003, Jackson Immunological) were purchased. Biotin annexin V was purchased from BioLegend (San Diego, CA, USA). Goat anti-mouse IgG Fc pre-adsorbed with 6 nm gold particles (ab105285) and goat anti-rabbit IgG H&L pre-adsorbed with 15 nm gold particles (ab27236) were purchased from Abcam and goat anti-biotin pre-adsorbed with 10 nm gold particles were purchased from BBI Solutions (Crumlin, UK). Acetylated BSA and Aurion gold sol (6 nm and 15 nm) were commercially obtained (Aurion; Wageningen, The Netherlands). Goat anti-HCV E2 polyclonal antibody (PA1-73105) was purchased from Invitrogen, Thermo Fisher Scientific. Mouse anti-HIV gp120 monoclonal antibody (clone 55-36) was purchased from Bio X Cell (West Lebanon, NH, USA).

2.1.2 Preparation of gold-conjugated primary antibodies

Gold conjugation was performed as per supplier instructions (Aurion) [323]. Briefly, antibodies were buffer exchanged with 5 mM $NaHCO_3$, pH 8.5 or 9.0 using Amicon® 10 kDa centrifugal filter or Slide-A-Lyzer™ MINI Dialysis Device, 10K MWCO (Thermo Scientific). Mouse monoclonal antibodies were conjugated using 5 mM $NaHCO_3$ at pH 8.5 whereas rabbit monoclonal antibodies used pH 9.0. Prior to conjugation, the antibodies were tested for the minimal protecting amount of protein for gold conjugation. In the case of low quantities of antibody, only the appropriate isotype was tested for the minimal protecting amount of protein.

2.1.3 Viruses

HSV1 NS strain, a low passage clinical isolate that expresses gC (gC^+), and ns-1 strain, a mutant lacking expression of gC on its envelope (gC^-), were kind gifts from Dr. Harvey Friedman (University of Pennsylvania, Pittsburgh, PA, USA). Initial virus stocks were passaged in African

green monkey kidney cells (Vero CCL-81; ATCC). To obtain viruses expressing surface gC and/or TF, gC^+ and gC^- viruses were propagated through a TF-deficient human melanoma cell line, A7, and an engineered TF^+ derivative cell line, A7/TF, as previously described [12]. Virus purity was assessed by negative-staining transmission electron microscopy (EM) and was confirmed to contain only enveloped particles. Quantification of virus particles was performed using known concentrations of latex spheres. Western blot analysis was performed to validate the presence of desired antigen(s) and their molecular weight in each purified virus sample (Figure 13).

2.1.3.1 Characterizing antigens in HSV1 panel

The presence or absence of gC and TF was confirmed by Western Blot analysis following sodium dodecyl sulfate polyacrylamide gel electrophoresis (SDS-PAGE) of purified virus (1 x 10^{11} virus particles, vp) using a 5-15% gradient acrylamide gel. Samples were reduced with 80 mM DTT. The proteins were transferred to a polyvinylidene difluoride (PVDF) membrane and blocked with 2% skim milk in TBST for 1 h at room temperature. The membrane was then probed for 1 h at room temperature with the primary antibodies anti-gC (P1104, 2 µg/mL), anti-TF (4503, 1.5 µg/mL) and anti-HSV1 MCP (1 µg/mL) diluted in TBST/2% skim milk. MCP was used as a loading control as there is a specific amount of MCP per virus. After three quick washes with TBST, the membranes were washed thrice with TBST for 5 min each. Secondary antibody treatment was performed using horseradish peroxidase-conjugated goat anti-mouse IgG (1:20,000) in TBST for 1 h at room temperature. Following the previous washing step, reactive bands were visualized using enhanced chemiluminescent substrate (Pierce, Ontario, Canada) as per supplier instructions. The concentration of virus TF was determined by comparison to a purified sTF standard curve.

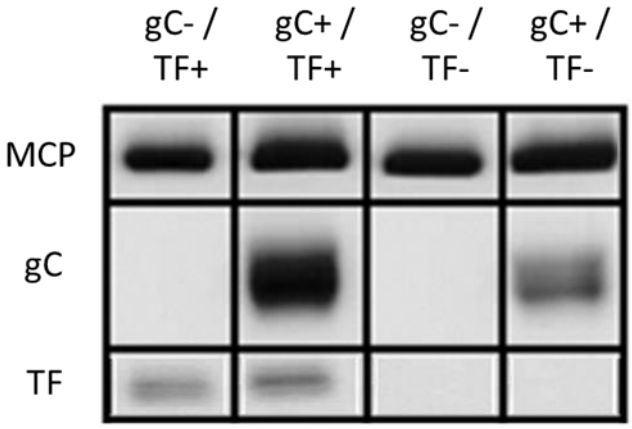

Figure 13. Characterization of antigens on HSV1.

Western blot analysis of panel of HSV1 used in this study confirming the presence of gC and/or TF in the virus samples. Major capsid protein (MCP) was used as a loading control due to its defined stoichiometry per virus. 10^{10} HSV1 particles were run on a reducing 5-15% polyacrylamide gel. MCP, gC and TF migrated at 150 kDa, 90 kDa and 47 kDa, respectively.

2.1.4 Small unilamellar vesicles

Compositions of small unilamellar vesicles (SUVs) were as follows (mole percent): PCPS (20% PS and 80% PC); NiPC (15% DGS-NTA-Ni and 85% PC); and NiPCPS (15% DGS-NTA-Ni, 65% PC and 20% PS) [318]. SUVs were prepared by sonication and differential centrifugation with modifications from previously established protocols [324]. Briefly, lipids dissolved in chloroform were mixed and dried under nitrogen gas. Following resuspension in 0.22 µM filtered HBS (20 mM HEPES, 150 mM NaCl, pH 7.4) and incubation for 10 min on ice, the lipids were treated with a direct sonication probe (Misonix microtip #419, 1/8") at an amplitude of 70 for 5 min using 10 s on/off cycles to prevent overheating the suspension (Misonix sonicator S-4000). The vesicles were transferred to 1.5 mL ultracentrifuge tubes and centrifuged at 114,600 x g for 3.5 h at 20 °C in a TLA-55 rotor using a Beckman Optima Refrigerated Benchtop Ultracentrifuge. The upper 65% was collected and stored under argon gas at 4 °C. The concentration of PC was determined using the mole percent of PC to derive the total concentration of lipid after enzymatic hydrolysis with a Phospholipids C kit (Wako, Mountain View, CA, US). Quantified SUVs were sized by dynamic light scattering with a Beckman Coulter N4 PLUS Particle Size Analyzer or the Malvern Panalytical ZetaSizer Nano ZS and fell in the 41 ± 15 nm average diameter range.

2.1.5 Protein expression and generation

Two proteins were recombinantly expressed for the study of gC and TF interactions in Chapter 3, sgC-His and sTF-His. Both proteins possess His-tags that facilitate purification as well as docking onto a nickel-chelating surface, e.g. small unilamellar vesicles synthetically produced in Chapter 2.1.4. A graphical representation of this is shown in Figure 14.

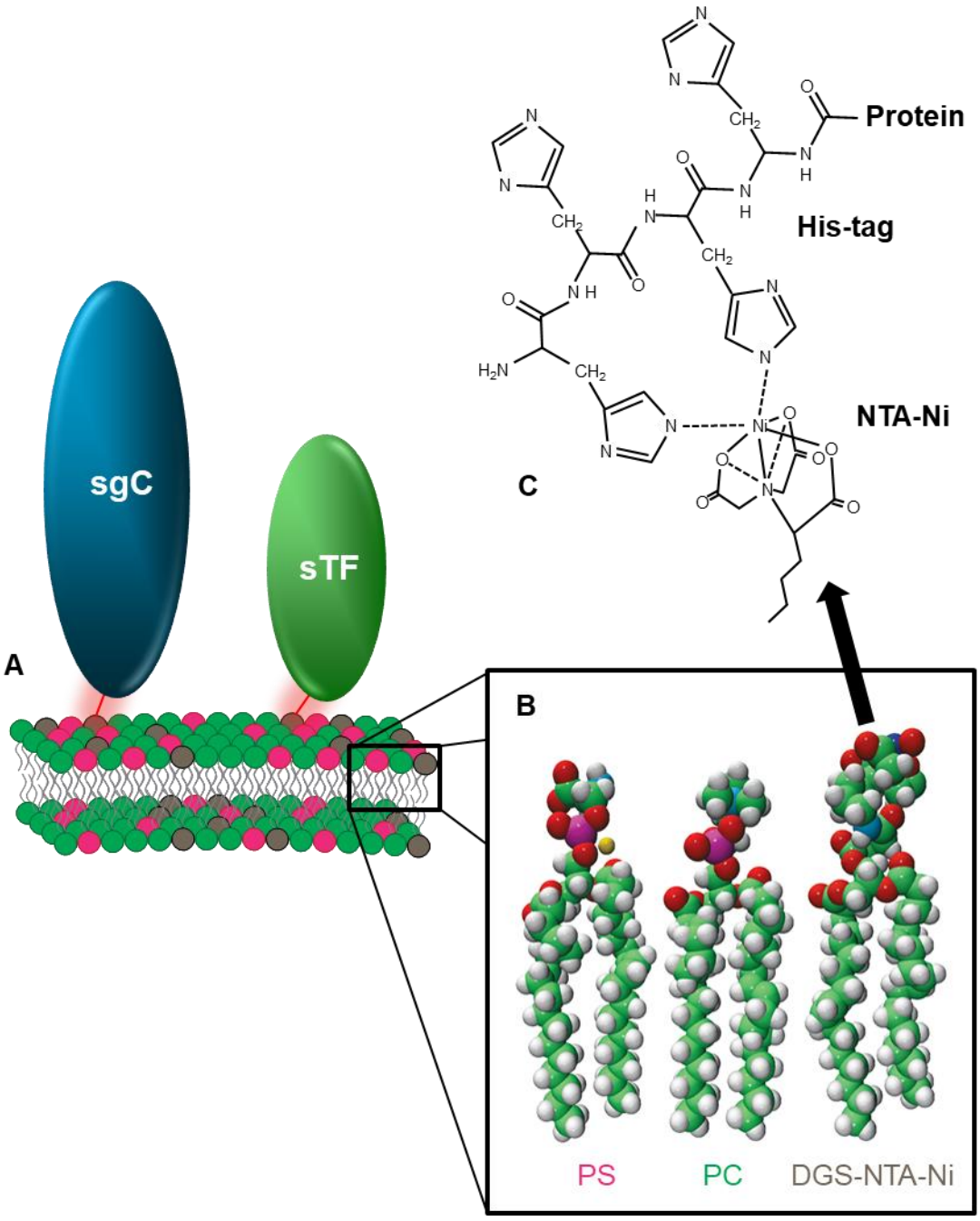

Figure 14. Recombinantly expressed sgC-His and sTF-His interaction with a Ni-chelating membrane.

(A) A NiPCPS membrane is depicted with sgC-His and sTF-His bound to the membrane via their His-tags (red glowing lines). (B) Phosphatidylserine (PS, magenta), phosphatidylcholine (PC, green) and DGS-NTA-Ni (gray) are depicted. Lipid images originated from the product website (https://avantilipids.com/). (C) The NTA-Ni headgroup coordinates with two histidine residues from a His-tagged protein.

2.1.5.1 gCΔ457t/sgC-His

A baculovirus expression system was used to enable production of large amounts of glycosylated secreted sgC-His. *Spodoptera frugiperda* cells (Sf9) were chosen based on a previously described protocol [319]. sgC-His has a portion of the extracellular domain removed along with the transmembrane domain and cytoplasmic tail (Figure 10) and three additional histidine tags were engineered into the C-terminal at residue 457. Due to the heterogeneity of the recombinant protein generated based on previous protocols (Figure 15A), several modifications were made to improve homogeneity of the sgC-His (Figure 15B). Sf9 cells were grown to confluence in T-175 cm^2 tissue culture flasks and were then seeded into 500 mL Celstir flasks containing no more than 400 mL of serum-free Sf900IIM. Cells were maintained at no more than 4 x 10^6 cells/mL and >95% viability as determined by trypan blue exclusion. For expansion of P1 and P2 stocks of baculovirus, 400 mL of 2 x 10^6 cells/mL were infected with a multiplicity of infection (MOI) of 0.5. Fetal bovine serum (FBS) was added to the media at 10% as a stabilizer if the stocks were to be kept for longer than 1 year at -80 °C (typically for P1 and P2 stocks). The inclusion of FBS lowered the efficiency of downstream purification of proteins and thus, P3 stocks were made serum-free. For protein expression, a MOI of 4 was used when the cells reached 4 x 10^6 cells/mL in 4-5 separate flasks of 400 mL. After 4 days, the media was collected and centrifuged at 2,000 x g for 20 min at 4 °C to remove cells and cell debris. Viral stocks were frozen at -80 °C and the viral titer was determined as detailed in 2.1.5.1.2.

2.1.5.1.1 Protein purification

The supernatant was filtered through a 0.45 µM filter and precipitated with ammonium sulfate in two steps. The first precipitation step was 20% ammonium sulfate (fine powder) slowly

added with stirring on ice over 30 min. After centrifugation at 12,900 x g for 30 min, the supernatant was transferred to a new beaker. The second precipitation step required 70% ammonium sulfate, added slowly over 1.5 h then left undisturbed at 4 °C for 1 h. The media was centrifuged at 12,900 x g for 35 min and the supernatant removed. The floating lipid material in the supernatant was discarded. The pellet was drained before resuspending in 30-40 mL of Cohen's PBS (20 mM sodium phosphate, 150 mM NaCl, pH 7.3). The resuspended pellet was then dialyzed at 4 °C against Cohen's PBS thrice (3 L) using a 3.5 kDa membrane (SpectraPor).

The dialysate was centrifuged at 100,000 x g for 1 hr at 4 °C prior to loading the supernatant onto a heparin Sepharose column. The heparin Sepharose CL-6B (GE Healthcare) was packed and equilibrated with Cohen's PBS (Buffer A) in a XK16 column as per supplier's instruction, with a column volume of approximately 24 mL. The filtered dialysate was added at a flow rate of 1 mL/min. At this point, the resin was tinted brown due to the color of the dialysate. After washing with 5 column volumes of Buffer A, the proteins were eluted and collected in 1 mL fractions with 0-60% Buffer B (20 mM sodium phosphate, 2 M NaCl, pH 7.3) over 75 min, 60-100% Buffer B over 10 min and 100% Buffer B for 5 min. Fractions were analyzed by Western blot to determine sgC-His-containing fractions. The majority of sgC-His was found in fractions 53 to 75 and was pooled together before dialyzing at 4 °C against Cohen's PBS twice using a 3.5 kDa membrane (SpectraPor) to a final dilution of 6,000.

The dialyzed pooled fractions were centrifuged at 25,000 x g for 15 min at 4 °C. The supernatant was added to 3 mL of 50% Ni-NTA resin in Buffer A (20 mM sodium phosphate, 500 mM NaCl, pH 7.5) and incubated for 3 h with shaking at 4 °C. The resin and media were transferred to a 5 mL column and the resin was washed with 100 mL of Buffer A followed by 100 mL of 10 mM imidazole in Buffer A. Elution was performed using a step gradient as previously described

[319]. sgC-His containing fractions were pooled together, concentrated and buffer-exchanged in an Amicon® Ultra 15mL 10K molecular weight cut-off centrifugal filter (Millipore) at 4 °C.

The final step of the purification involves size exclusion chromatography using a Sephacryl S-200 column. The column (Pharmacia 10/200) was packed as per supplier's instruction manual. The sgC-His-containing sample was run through the Sephacryl S-200 column with a flow rate of 1 mL/min in HBS at 4 °C, whilst collecting 1 mL fractions. Fractions with the least amount of large molecular weight species (>150 kDa, as compared to 75-90 kDa sgC-His, as determined by Western blot) were pooled together and concentrated using an Amicon® Ultra 15 mL 10K molecular weight cut-off centrifugal filter. The sample was aliquoted, flash frozen in LiN_2 and stored at -80 °C. Protein concentrations were measured using the bicinchoninic acid assay and UV-Vis method (A_{280} with A_{320} correction).

2.1.5.1.2 Determination of baculovirus titer

Sf9 cells (1×10^6) were seeded into 6-well Corning® Costar® tissue culture-treated plates (Sigma-Aldrich) and grown at 28 °C, 0% CO_2. At ~85% confluency, the cells were infected with 1 mL of titrated baculovirus-infected supernatant for 1 h at 28 °C, 0% CO_2. The baculovirus-infected supernatant was aspirated and 3 mL of 1X Grace's Insect Medium with 1.5% SeaPlaque™ agarose were overlaid onto the cell monolayer. After 5 days of incubation at 28 °C, 0% CO_2, plates were stained with 1 mL of 0.22 µm-filtered 0.02% neutral red in PBS for 2 h at 28 °C. The remaining dye was removed, and the plates are returned to the incubator at 28 °C until plaques are visible. Neutral red is a vital dye that is taken up by live cells, the absence of red denotes a plaque. Plaques are counted and multiplied by the dilution factor to obtain the plaque forming units (pfu), a unit of virus infectivity.

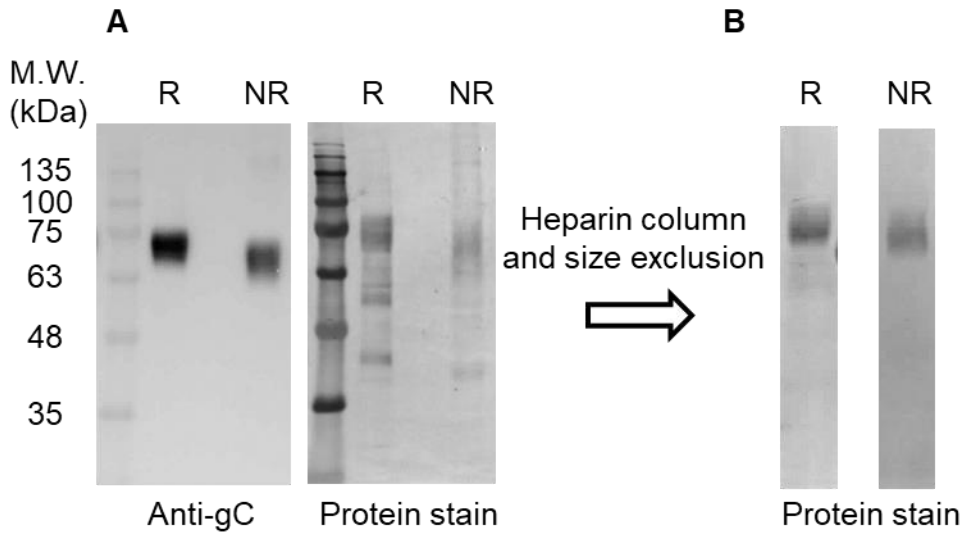

Figure 15. Recombinant sgC-His antigen confirmation by protein stain and Western blot.

(A) sgC-His was purified with a nickel metal-ion affinity chromatography and samples were reduced (R, 12 mM DTT) or non-reduced (NR) when loaded into a 5-20% gradient polyacrylamide gel. Anti-gC (anti-gC (2 µg/mL, P1104) was used as the primary antibody with goat anti-mouse HRP (1:10,000) as the secondary antibody. Protein staining was achieved by using Coomassie R-250 protein stain. (B) Improvements to previous protocols included heparin column prior to metal-ion affinity and size exclusion post-metal-ion affinity chromatography and resulted in a cleaner preparation. Molecular weight (M.W.) determined using BLUeye Prestained Protein ladder.

2.1.5.2 sTF-His

Expression and purification of sTF-His was performed using an *Escherichia coli* expression system that was previously established by my collaborator (Morrissey) [318]. sTF-His is a soluble form of TF (sTF) that lacks the transmembrane and cytosolic domains, and contains a sequence encoding a dodecapeptide epitope for the calcium-dependent monoclonal antibody HPC4, as well as a hexa-histidine tag (His-tag), and a spacer sequence at amino acid 219 before the His-tag (depicted in Figure 2). The spacer sequence was included to help orient the protein when bound to an appropriate membrane surface. Briefly, *E. coli* strain BL21 (DE3) was transfected with pJH776 (sTF with a spacer before the N-terminal His-tag). Transformants were selected with kanamycin and were grown in a 16x150 mm test tube containing 1.5 mL MDG (non-inducing minimal medium) for 7 h at 37 °C (300 rpm shaking). This culture was expanded into 500 mL of MDG medium and grown overnight at 37 °C (300 rpm shaking). The bacteria were pelleted and the MDG medium was replaced with 1 L Terrific Broth medium with 0.1% glucose and 20 µM IPTG to a final A600 absorbance unit reading of 3.0.

Following IPTG induction and overnight incubation at room temperature (300 rpm shaking), the media was collected and centrifuged to remove cells and cell debris. Osmotic shock was performed on the pelleted cells to release sTF stuck in the periplasmic space of the bacteria [325]. The supernatant and the osmotic shock sample were precipitated using 70% ammonium sulfate. Following dialysis of the precipitate, the protein solution was batch-treated with Q Sepharose. The unbound solution contained sTF-His and was applied to an immobilized nickel ion affinity resin. sTF-His bound to the resin was eluted, fractions were pooled and buffer-exchanged to HBS. The purified protein was aliquoted, flash frozen and stored at -80 °C until use.

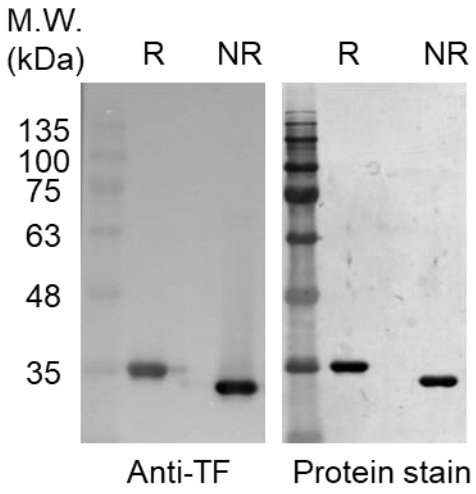

Figure 16. Recombinant sTF-His antigen confirmation by protein stain and Western blot.

sTF-His under reducing (R, 12 mM DTT) or non-reducing (NR) conditions was loaded into a 5-15% gradient polyacrylamide gel. Anti-TF (1:750, ab48647) was used as the primary antibody with goat anti-rabbit HRP (1:10,000) as the secondary antibody. Protein staining was achieved by using Coomassie R-250 protein stain. Molecular weight (M.W.) determined using BLUeye Prestained Protein ladder.

2.2 Detection of specific antigens on the virus envelope

2.2.1 Immunogold electron microscopy

The standard for characterizing virus surface antigens on membranes is immunogold EM. This method relies on antibody recognition of an antigen with visualization of these antigens via dense colloidal gold. Colloidal gold appears as dark dots by EM and can be generated in different sizes. Conjugation of gold colloidal to antibodies (either primary or secondary) can be easily achieved through passive adsorption or covalent chemistry. For my cell-cultured virus studies, gold visualization was performed using commercial secondary antibodies conjugated to gold particles of varying diameters (6 nm, 10 nm and 15 nm). For patient-derived virus studies, in-house conjugation of primary antibodies was performed. This was important due to the lack of host selection of antibodies against virus proteins which would complicate simultaneous labeling of antigens on the virus surface.

There are two main methods of loading samples onto an EM grid: drop-on-grid and grid-on-drop (Figure 17A and Figure 17B, respectively). As the names imply, drop-on-grid involves securing a grid with the shiny film side up, typically with forceps, and applying a drop of sample on top of the grid. Grid-on-drop method places the grid on top of a droplet of sample. The former method allows for larger particles to sediment onto the grid and is superior for large viruses such as poxviruses [326]. The benefit of using the latter method is the ability to handle multiple samples easily. Although both methods were tested for HSV1 samples, the grid-on-drop was predominantly used and then further adapted to a pseudo-drop-on-grid method (Figure 17C). This method entailed applying grids with the shiny side onto 20-30 µL of sample deposited in the wells of a Terasaki 60-well microtest plate (Sarstedt). The entire plate was then inverted such that the shiny sides of the grids were facing upward. This technique allowed for gravity to pull down virus particles onto

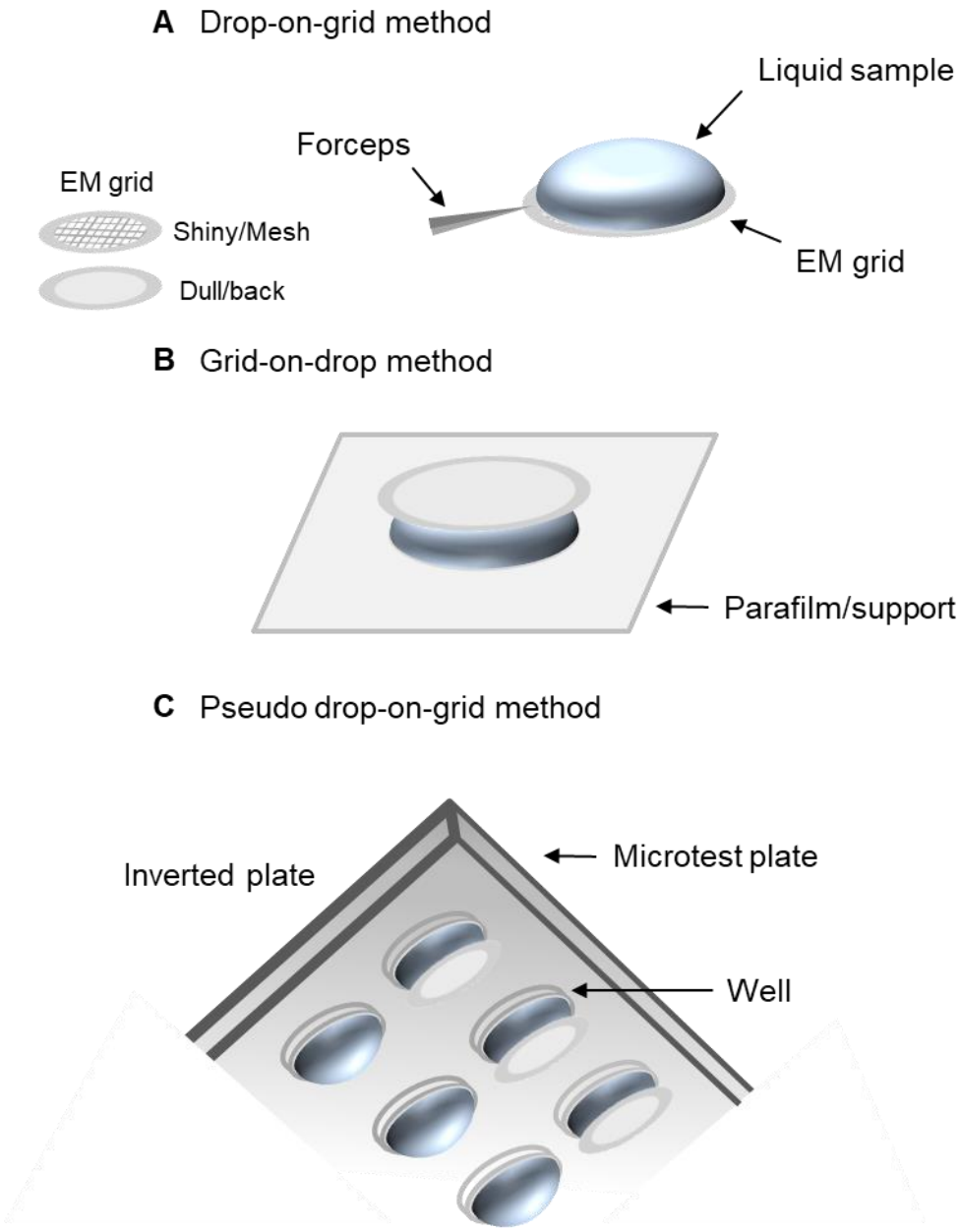

Figure 17. Sample adsorption to grids for EM.

Three methods for sample adsorption: (A) Drop-on-grid, an EM grid is secured with the shiny side upward using forceps and the sample is placed on top of the grid; (B) Grid-on-drop, the sample is placed on a parafilm/support and the shiny side of the grid is placed on top of the sample; and (C) Pseudo drop-on-grid method, the sample is placed within a well (e.g. Terasaki microtest plate) with the EM grid sitting on top of the sample and the entire plate is inverted to mimic a drop-on-grid.

the grid whilst retaining the easy manipulation advantage of the grid-on-drop method. For samples less than 20 µL, parafilm was first fitted onto the wells of the microtest plate, thereby creating a shallower well to hold smaller volumes.

All virus EM work were performed in a BSL2+ facility using sterile equipment and solutions. Formvar® carbon-coated nickel 400-mesh grids (EMS, Hatfield, PA, USA) were used in lieu of the more common copper grids as copper can become oxidized by gold nanoparticle antibody solutions. As nickel grids are magnetic, non-magnetic forceps were used when handling the grids for staining.

2.2.2 Purified cell culture-derived HSV1 particles

Using the grid-on-drop method, nickel grids were floated on a 10 µL drop of HSV1 (1 x 10^{10} vp) diluted in low salt HBS (20 mM HEPES, 75 mM NaCl, pH 7.4). After 15 min of adsorption at room temperature, the grids were transferred to a 30 µL drop of low salt HBS. The grids were then placed on a drop of filter-sterilized blocking buffer consisting of 5% BSA, 5% goat serum (or 100 µg/mL goat IgG) and 0.1% cold water fish scale gelatin in low salt HBS for 1 h at room temperature. The grids were washed by transferring the grids to 30-40 µL drops of low salt HBS for 4 min and repeated four times. The grids were then incubated with primary antibodies in low salt HBS and 0.1% acetylated BSA (acBSA). Antibody concentrations were as follows: 5 or 10 µg/mL tissue factor antibody (rabbit or mouse, respectively); 10 µg/mL (or 1:100 for rabbit serum) anti-gC antibody; and/or 10 µg/mL biotinylated-Annexin V. Matching isotype/host controls for each of the antibodies were used to test for specificity. In the case of Annexin V, the negative controls included no calcium added or EDTA treatment. In experiments probing for aPL, 5 mM $CaCl_2$ was added to all buffers to allow for calcium-dependent binding of Annexin V to

aPL. After 1 h of incubation, the grids were washed five times. Secondary antibodies at 1:40 dilutions of goat anti-mouse IgG conjugated to 6 nm beads, goat anti-biotin conjugated to 10 nm and goat anti-rabbit IgG conjugated to 15 nm beads was incubated for 1 h. Following five washes, the grids were negatively stained on 10 µL drops of 2% phosphotungstic acid (PTA), pH 6.5 for 1 min. PTA is electron dense and is a commonly used negative stain for visualization of viruses. The negative stain was removed by wicking with filter paper and the grids were air-dried in a container for EM grids. PTA can potentially degrade viral membranes; therefore, the grids were viewed within a day of preparing them. Viruses were inactivated by UV light after negative staining or by fixation with 2% paraformaldehyde before negative staining.

2.2.3 Purified cell culture-derived DENV particles

Due to the relatively small size of DENV (>3 fold smaller than HSV1 in diameter), an extra measure was taken to improve detection of the virus. Glow discharge can be used to deposit positive ions onto the EM grid, which in turn increases negatively charged virus particle adsorption[318]. After glow discharge (PELCO easiGlow™ 91000, 120 s at 0.2 mbar and 15 mA), 5 µL of DENV sample was adsorbed onto the grid. Then the same protocol as in HSV1 (Section 2.2.2) was followed but using 10 µg/mL mouse anti-DENV and 10 µg/mL rabbit anti-TF antibodies for the primary antibody incubation.

2.2.4 Patient plasma-derived virus particles

Virus concentrations in patient plasma can vary depending on the type of virus and the severity of the disease. From purified virus titrations, it was determined that at least 1 x 10^6 vp/mL is needed to visualize ~10 vp/square in a 400-mesh EM grid. High titer samples that meet this

minimum requirement are easier to come by in HCV and HIV. DENV viremia results in at least 10 to 100-fold lower titres compared to HCV or HIV and is difficult to obtain peak titers. Furthermore, there is only one example in the literature successfully extracting and visualizing DENV from patient plasma [327]. In anticipation of the difficulties in detecting virus particles, two methods were developed to concentrate viruses from patient plasma: centrifugation and immunocapture.

2.2.4.1 Centrifugation method

The following protocol was based on the ability of gold-conjugated antibodies to pellet using speeds much lower than those required for smaller viruses such as dengue virus. For this purpose, 15 nm gold beads were chosen as they pellet at 12,000 x g_{av}. Viremic patient plasma was pre-spun at 15,000 x g for 5 min to remove large aggregates or debris. Gold-conjugated primary antibodies were incubated with the plasma in solution for 2 h at 37 °C with 0.1% acBSA. Antibody dilutions were dependent on the OD_{520}: mouse anti-HIV gp120 (1:80), mouse anti-flavivirus E protein (1:160), goat anti-HCV E2 (1:80), and mouse anti-human TF (1:100). The plasma was then centrifuged at 8,000 x g for 20-30 min at 4 °C. The pellet was washed with HBS/0.1% acBSA (HBS/acBSA) and pelleted as above. The virus pellet was resuspended in 5-20 µL low salt HBS, loaded directly onto a nickel grid and allowed to adsorb for 5 min at room temperature. The virus was then fixed with 2% paraformaldehyde for 30 min prior to negative staining with 2% PTA, pH 6.5 for 1 min. The grids were then dried and visualized.

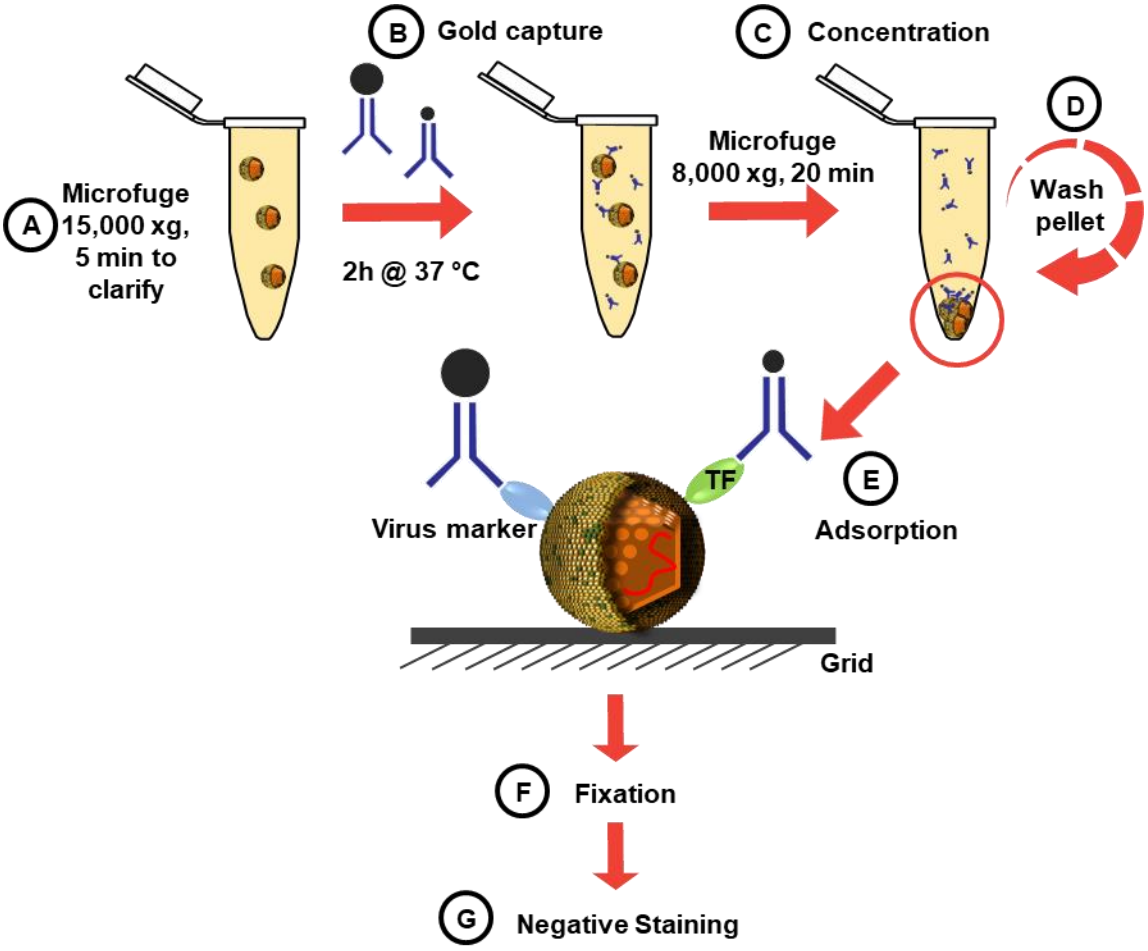

Figure 18. Centrifugation method for capturing and concentrating viruses in plasma.

(A) Viremic plasma was clarified by centrifugation at 15,000 x g. (B) Viruses were incubated with 15 nm gold-conjugated virus-specific antibodies and 6 nm gold-conjugated anti-TF antibodies. (C) The 15 nm gold beads allowed for centrifugation at 8,000 x g to pellet the gold/antibody/virus complexes. (D) The pellet was washed before resuspending the pellet in a smaller volume. (E) The virus pellet was transferred to an EM grid for adsorption. (F) The virus was fixed with 2% paraformaldehyde. (G) After fixation, the grids were negatively stained with 2% phosphotungstic acid.

2.2.4.2 Immunocapture method

This method involves capturing viruses onto an EM grid using virus-specific antibodies. Nickel grids are incubated with 10-100 µg/mL virus-specific antibodies for 20 min at room temperature. After two 4-min washes in low salt HBS, the grids are blocked with Block buffer for 20 min at room temperature. The grids are washed twice with low salt HBS. 20 µL of patient plasma are added to wells of a Terasaki 60-well Microtest plate. The pseudo-drop-on-grid method was employed. After incubating the grid with patient plasma for 15 min at room temperature, another 20 µL of sample are added to new wells and grid incubation was repeated. Following the incubation, the grids were washed five times with low salt HBS/acBSA for 4 min each. Grids were transferred to gold-conjugated antibody solutions in low salt HBS/acBSA for 1 h at room temperature. Antibody dilutions were dependent on the optical density at 520 nm: mouse anti-HIV gp120 (1:80), mouse anti-flavivirus E protein (1:100), goat anti-HCV E2 (1:80), and mouse anti-human TF (1:40). Grids were washed five times with low salt HBS for 4 min each before fixing with 30 µL 2% paraformaldehyde in low salt HBS for 30 min at room temperature. The grids were washed twice briefly with low salt HBS before negative staining with 2% PTA. Samples were visualized shortly after drying.

Alternatively, a primary and secondary antibody labeling technique as performed for HSV1 was used for detecting DENV due to the low virus titers and overall difficulty in detecting DENV particles. The primary antibodies were used at 10 µg/mL and were a mixture of anti-flavivirus E protein and anti-DENV E protein (Abcam) to increase sensitivity.

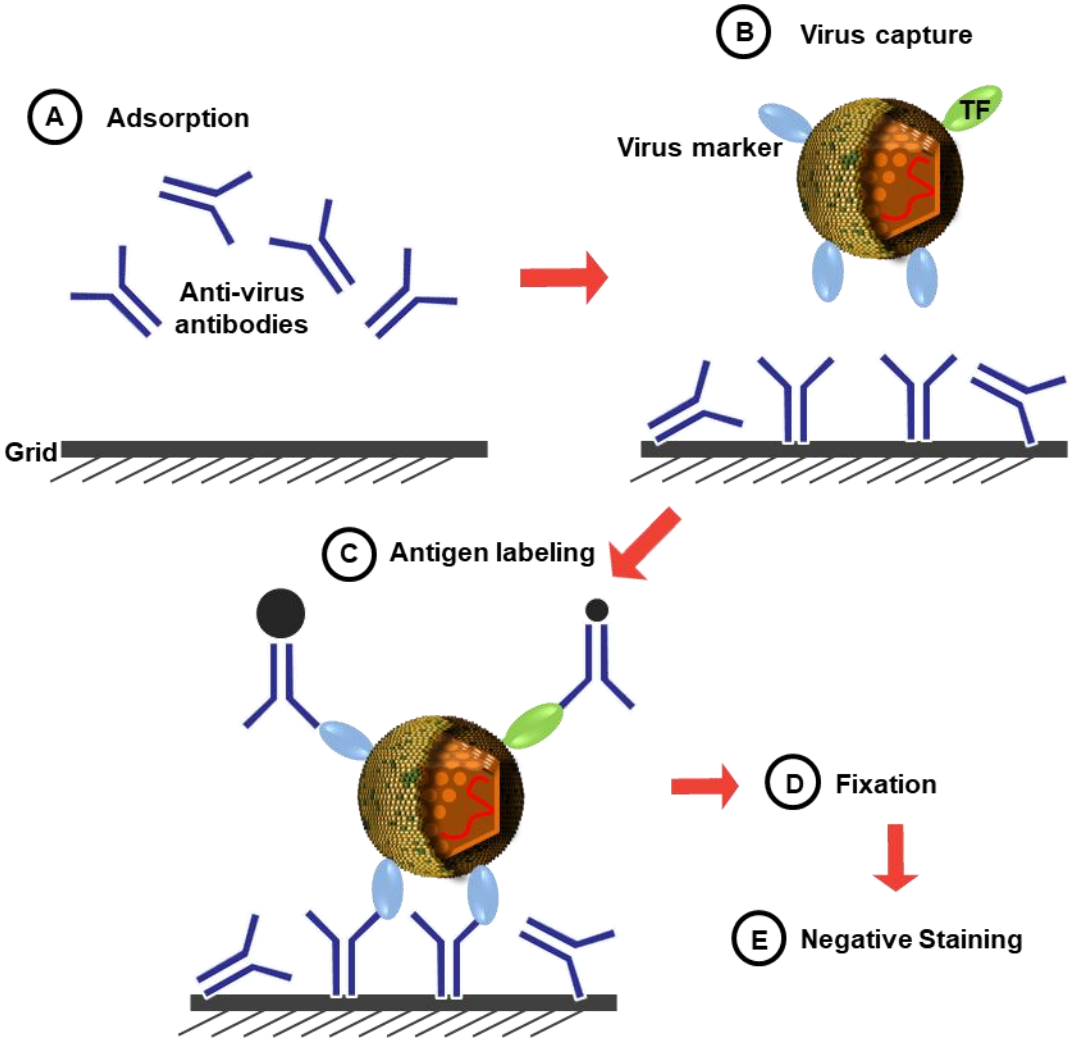

Figure 19. Immunogold capture of viruses from plasma for EM.

(A) Virus-specific antibodies are adsorbed to an EM grid. (B) Viremic plasma was incubated on immune-EM grids. (C) Grids are incubated with 15 nm gold-conjugated virus-specific antibodies and 6 nm gold-conjugated anti-TF antibodies. (D) The virus was fixed with 2% paraformaldehyde. (E) After fixation, the grids were negatively stained with 2% phosphotungstic acid.

2.3 Assessing the function of procoagulant factors.

2.3.1 Virus-mediated FX activation

All experiments used HBS/BSA as a stabilizer unless otherwise stated. In a final reaction volume of 20 µL, virus was first mixed with 100 nM FX and 1 nM FVIIa in 15 µL. After 5 min at room temperature, 5 µL of 20 mM $CaCl_2$ was added to start the reaction. After 20 min at 37 °C with shaking every 5 min, 10 µL was transferred to a 96-well plate and 90 µL of 200 µM S-2765 and 12 mM EDTA. The amount of FXa generated was then monitored at 405 nm at room temperature using a Vmax or Spectramax multiwell plate spectrophotometer (Molecular Devices, Sunnyvale, CA, USA). The amount of FX activation was derived from a standard curve using purified FXa.

For dengue virus experiments, inhibitors of the TF-FVIIa complex were used to determine if the sole contributor to enhanced FVIIa activity was TF. The nematode anticoagulant protein c2 (NAPc2) and human TF-specific monoclonal mouse antibody TF8-5G9 were pre-incubated with the virus at 50 nM and 100 µg/mL, respectively, for 5 min at 37 °C before addition of other coagulation factors.

2.3.2 Analysis of FX activation in purified systems

Initial rates of FX activation were measured with a two-step discontinuous chromogenic assay as previously described [328] with modifications. This assay involves activating FX, stopping the reaction at various times and measuring the FXa generated at each time point. Reaction mixtures in HBS contained 5 mM $CaCl_2$, 500 pM FVIIa, and either 10 pM sTF-His or 10 nM sgC-His with 100 µM NiPCPS. Varying concentrations of FX were added to initiate the reaction at 37 °C. Over the course of 10 min, 20 µL aliquots of the reaction mixture were added to

50 µL stop buffer (40 mM Mes-NaOH (pH 5.8), 12 mM EDTA, 50 mM NaCl and 0.25% Triton X-100) at 4 °C. After 10 min, the stopped reactions were then warmed to room temperature and neutralized with 0.6 M Tricine-NaOH (pH 8.4). Immediately following, the amount of FXa generation was detected by the addition of 0.6 mM S-2765 and 5 mM $CaCl_2$. A SpectraMax was used to follow FX activation at OD_{405} over 10 min, 15 s intervals with 3 s shaking between reads at 25 °C.

2.3.2.1 Deriving FX activation kinetics parameters

The 2-step chromogenic assay raw data values are converted to nM FXa with a standard curve using purified FXa. The data are fitted to a 2nd order polynomial curve ($Y = A + BX + CX^2$). As this equation described the amount of FX activation (Y) as a function of time (T), the derivative of this equation was the rate of FX activation. Thus, the rate of FX activation was equal to B + CX. The initial rate of reaction, V_0, was the B value, when T = 0. The V_0 values are plotted as a function of [FX]. Using the Michaelis-Menten equation, $Y = \frac{V_{max}[FX]}{K_m+[FX]}$, the K_m value can be derived. Subsequently, k_{cat} was determined from V_{max} (B_{max} on GraphPad) and known [FVIIa/cofactor] using $k_{cat} = \frac{Vmax}{[FVIIa/cofactor]}$. The presence of nickel-chelating lipid influenced the His-tagged protein cofactor tethering and orientation. This subsequently affected the availability of the protein cofactor for FVIIa binding. Thus, the binding affinity of protein cofactor to lipid cofactor ($K_{d,C}$), as described in Figure 20, was determined to assess the amount of available protein cofactor that complexes with FVIIa. This was simplified with the assumption that the dissociation value of cofactor to FVIIa is much larger than that of cofactor/lipid to FVIIa.

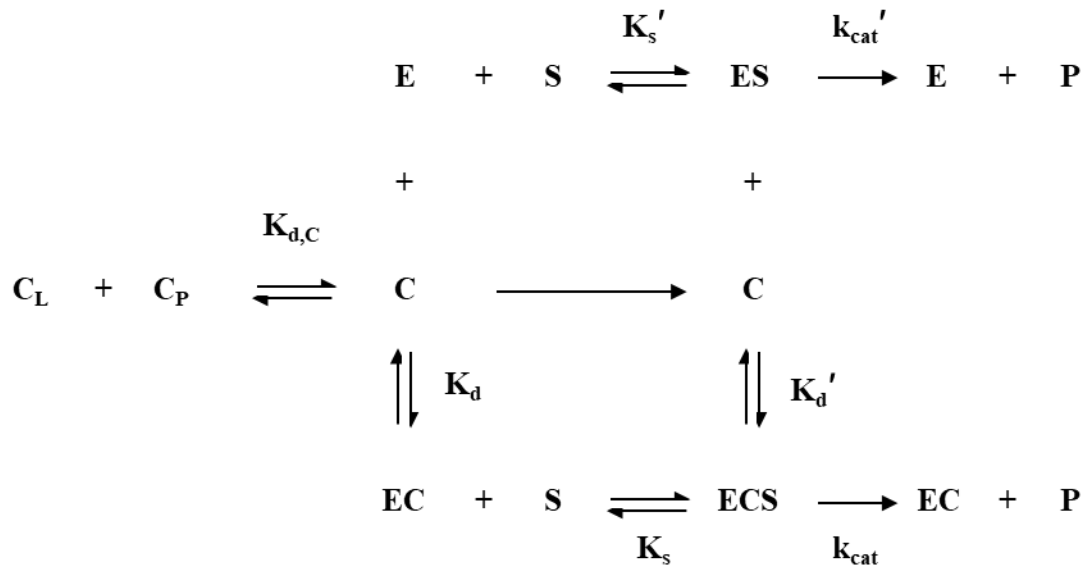

Figure 20. Schematic of non-enzymatic and enzymatic reactions involved in FVIIa-mediated FX activation.

Enzyme (E, FVIIa) activation of the product (P, FX) is influenced by several factors. As the protein cofactor (C_P), sTF-His or sgC-His, can bind to Ni-chelating lipids (C_L), this equilibrium is described by $K_{d,C}$. This protein/lipid cofactor (C) can bind to E, with the equilibrium denoted by K_d. E can bind to S in the absence or presence of cofactors ((binding affinity K_s' and K_s, respectively). K_d' describes the equilibrium of ECS to ES and C. The conversion of S to P by either ES or ECS is represented by k_{cat}' and k_{cat}, respectively. This schematic was modified from Neuenschwander *et al.* (1994) [94].

2.3.2.2 Nickel binding of purified proteins

sTF-His and sgC-His binding to NiPC and NiPCPS was determined by a continuous chromogenic assay linked to FVIIa-mediated FX activation. Varying concentration of NiPCPS were mixed with 5 mM $CaCl_2$, 1 nM FVIIa, 0.2 mM S-2765 and either 20 pM sTF-His or 1 nM sgC-His. FX was added to initiate the reaction at a final concentration of 100 nM. FXa generation was immediately followed at room temperature over 20 min, with a data acquisition interval of 15 s preceded by a 3-second shake at each read. The initial rate of FX activation was determined by fitting the activity data to a second-order polynomial [94]. Typically, to determine the dissociation constant, the initial rate of FX activation is converted to [enzyme/cofactor] and plotted against the titrating [cofactor]. However, the effect of free FVIIa may need to be accounted for. This is assessed by the following summation: $v_{obs} = \alpha[FVIIa] + \beta[FVIIa/cofactor]$ [94], where v_{obs} is the measured activity of FXa (initial rate of FX activation in mol/L per unit time). Values of α and β were experimentally determined using no cofactor and saturating amounts of cofactor, respectively. No measurable activity was measurable with up to 10 nM FVIIa (100-1000 fold more than was used in binding experiments), revealing that $\alpha << \beta$ similar to other studies [329]. Thus, the equation was simplified to $v_{obs} \approx \beta[FVIIa/cofactor]$. The typical values for β were 4.4 x 10^{-2} mol FXa/s/mol sgC-His/FVIIa/NiPCPS; 4.3 x 10^{-2} mol FXa/s/mol sTF-His/FVIIa/NiPCPS; 1.8 x 10^{-3} mol FXa/s/mol sgC-His/FVIIa/NiPC; and 2.7 x 10^{-3} mol FXa/s/mol sTF-His/FVIIa/NiPC. The dissociation constant was determined by plotting the converted [FVIIa/cofactor] versus [cofactor]. The data was fit to the following quadratic equation:

$$v = \frac{V_{max} \cdot S}{2 \cdot E_0(K_s + S)}\left(E_0 + C_0 + K_{d,app} \pm \sqrt{\left(E_0 + C_0 + K_{d,app}\right)^2 - 4 \cdot E_0 \cdot C_0}\right)$$

Where, S is [FX] (30 nM), E_0 is the initial [FVIIa] (0.1 nM), C_0 is the titrating [cofactor]. K_S describes the dissociation value of the FVIIa/cofactor and FX (Figure 20). The assumption that $K_m \approx K_s$ (values from Table 3) was made in order to fit the data using the above quadratic binding isotherm. $K_{d,app}$ is the apparent dissociation value of cofactor and FVIIa. It represents the true K_d only when the substrate concentration is limiting relative to the K_s for substrate binding and is described by $K_{d,app} = K_d \frac{K_s + K_S \cdot S/K_s'}{K_s + S}$. If $K_s = K_s'$, then $K_{d,app} = K_d$. Derivation of all formulae is found in the appendix (A.1).

2.3.2.3 FVIIa binding to lipid/protein cofactors

Binding of sTF-His or sgC-His to either FVIIa was assessed using continuous chromogenic assays monitoring FXa generation. sTF-His or sgC-His was titrated in HBS with 5 mM $CaCl_2$, 10 pM FVIIa and 100 µM SUVs. After 10 min of pre-incubation at room temperature to allow equilibration, 30 nM FX and 0.2 mM S-2765 was added to start the reaction. As with Chapter 2.3.2.2, FXa generation was followed at room temperature over 20 min. $K_{d,app}$ was determined by fitting the data using C_0 as the titrating , E_0 = 0.01 nM FVIIa, S = 30 nM FX, $K_s = K_m$ (values from Table 3) with the equation:

$$v = \frac{V_{max} \cdot S}{2 \cdot E_0 (K_s + S)} \left(E_0 + C_0 + K_{d,app} \pm \sqrt{\left(E_0 + C_0 + K_{d,app}\right)^2 - 4 \cdot E_0 \cdot C_0} \right).$$

2.3.3 Plasma clotting

Virus-induced coagulation was monitored using an ST4 coagulation analyzer (Diagnostica Stago). Briefly, a magnetic bead was added to the bottom of a cuvette which oscillates freely in solution. Frozen plasma was defrosted at 37 °C for 5 min then set on ice until use (as per product

specifications). In a final reaction volume of 75 µL, 12.5 µL of virus and 12.5 µL of HBS was added to 37.5 µL of plasma. Pre-warmed magnetic beads were added to the cuvette and incubated for 1 min at 37 °C. To start the clotting and timing, 12.5 µL of 60 mM $CaCl_2$ was injected into each cuvette. The machine then counted the time (s) it took for the magnetic bead to stop moving in the cuvette due to clot formation. For inhibition of the intrinsic pathway, CTI was pre-incubated with NPP for 5 min at 37 °C. CTI inhibits FXIIa and is used to assess TF-dependent coagulation [330,331]. Similarly, for TF inhibition, NAPc2 or TF8-5G9 was pre-incubated with virus at 50 nM and 100 µg/mL, respectively.

2.4 Determining binding partners

To determine which factors in virus-mediated FX activation are interacting with one another, several techniques were employed: crosslinking, enzyme-linked assays and microscale thermophoresis.

2.4.1 Crosslinking

To investigate protein interactions between gC and TF, crosslinking was performed. 3,3'-dithiobis(sulfosuccinimidyl propionate) (DTSSP) is a 12 Å water-soluble crosslinker containing an amine-reactive N-hydroxysulfosuccinimide (sulfo-NHS) ester at both ends of the spacer. Sulfo-NHS esters react with primary amines at pH 7-9 to form stable amide bonds. DTSSP also features a single disulfide bond in the middle of the spacer which can be reduced to release crosslinked adducts. In addition, DTSSP is membrane-impermeable, making it ideal for investigating only protein interactions on the virus surface [332].

HSV1/TF+/gC+, HSV1/TF+/gC-, HSV1/TF-/gC+, and HSV1/TF-/gC- (2 x 10^{10} vp) was incubated with 2.5 mM DTSSP for 15 min on ice. The reaction was then quenched with 1 M Tris-glycine (pH 7.0) to a final concentration of 50 mM. A control reaction where Tris-glycine (pH 7.5) was added prior to the cross-linker was also performed. For purified proteins, 12 µM sTF-His and/or 2.5 µM sgC-His was mixed with 50 µM NiPCPS and 5 mM Ca^{2+}. DTSSP (500 µM) was incubated with the protein mixture for 24 h at 4° C with agitation.

The samples were run on a 5-15% polyacrylamide gradient gel under non-reducing or reducing conditions with 80 mM DTT. Western blot analysis was performed using polyclonal antibodies against TF (Abcam, 1:1500) and gC (R118, 1:1000) as primary antibodies and goat anti-rabbit (HRP) (Jackson, 1:10000) as the secondary antibody.

2.4.2 ELISA-based chromogenic assay

Relipidated TF (Innovin) at 1:100 dilution was coated onto a 96-well plate in 50 µL 100 mM bicarbonate/carbonate coating buffer pH 9.6 overnight at 4 °C. Wells were washed twice with 200 µL HBS. Wells were blocked with 200 µL 2% BSA in HBS for 2 h at room temperature. After two washes with HBS, 40 µL of sgC-His at varying titrations from 0 to 1 µM was incubated for 1 h at room temperature. Following several HBS washes, two different detection methods were used: enzyme-linked immunoassay and enzyme-linked functional assay.

The former method requires a primary antibody incubation step with 10 µg/mL mouse anti-gC monoclonal antibodies for 2 h at room temperature. After several washes, the secondary antibody step consists of 1:10000 HRP-conjugated goat anti-mouse antibodies incubation for 2 h at room temperature. Detection of bound sgC-His was determined through 3,3',5,5'-tetramethylbenzidine (TMB) conversion to a diamine form, causing the solution to turn blue. A

sulfuric acid solution was added to stop the reaction, resulting in a yellow solution which can be spectrophotometrically read at 450 nm. Purified sgC-His was used as a loading control and for the creation of a standard curve.

The latter method depends on FX activation by FVIIa. TF and sgC-His cofactor activity were expected to enhance FVIIa-mediated FX activation. Similar to the assays described in section 2.3.1, 20 µL final volume consisting of 100 nM FX, 5 mM $CaCl_2$ and 1 nM FVIIa was added to each well and incubated for 20 min at room temperature. 80 µL of 200 µM S-2765 and 12 mM EDTA was added to each well. The plate was then immediately read at 405 nm, reading samples every 12 s for 5 min. Enhancement was determined against a no added sgC-His control.

2.4.3 Microscale thermophoresis

MST is used for determining binding parameters of proteins or small molecules in solution based on thermodiffusion. All molecules move away from a temperature gradient and this effect is altered for individual molecules when they associate. Although this principle was described in 1856, the theory is incomplete. The speed at which a molecule diffuses is dependent on its size, charge and hydration shell. When molecules interact, at least one parameter changes, thereby altering the way the complex moves through the temperature gradient. MST devices use infrared lasers to induce a temperature gradient in a capillary tube containing the samples (Figure 21). The device uses an excitation laser to track the movement of fluorescent molecules. Therefore, a fluorescence label is required for one of the molecules. As with other protein-interaction investigation approaches that involve labeling, there is the inherent disadvantage of affecting the target molecule's behavior(s). Thus, controls must be performed to ensure that target binding or function is not affected. Non-labeled proteins can be followed with the shift of intrinsic tryptophan

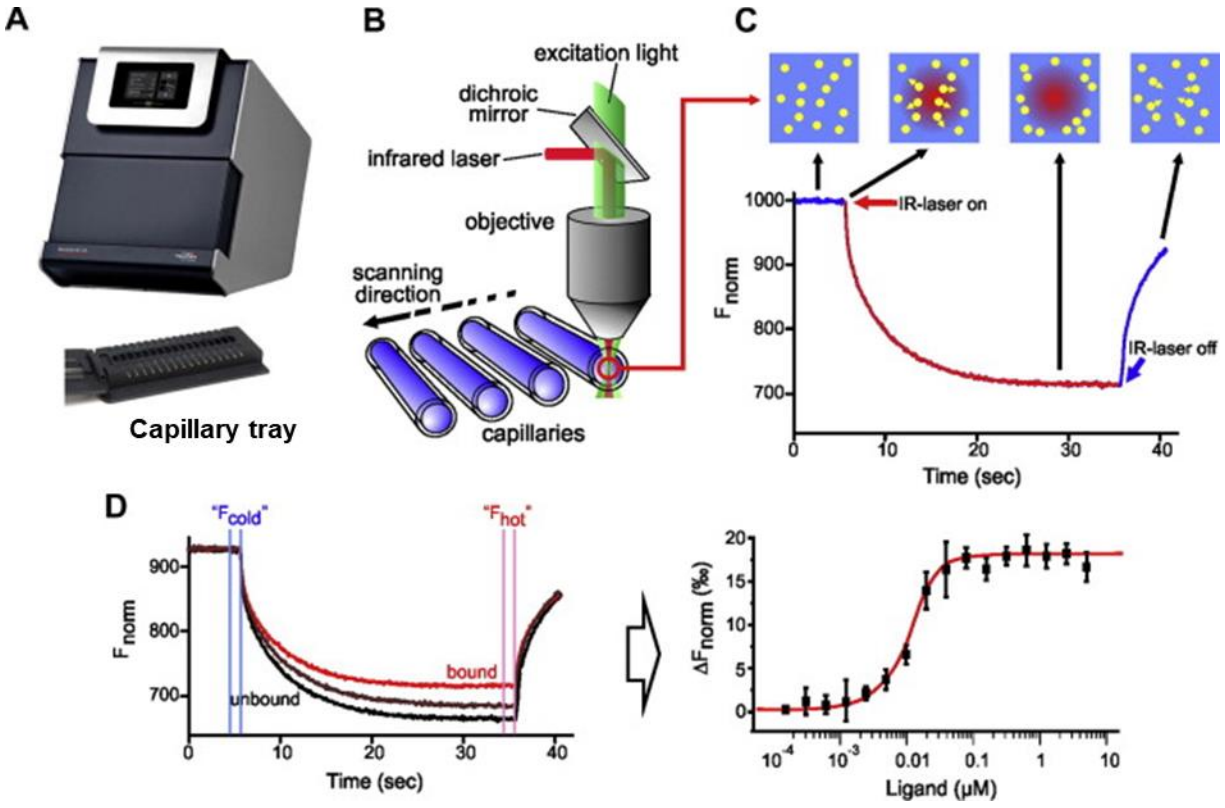

Figure 21. MST basic theory and set-up.

(A) The Monolith NT.115 from NanoTemper Technologies GmbH. Up to 16 capillaries can be loaded onto a capillary tray. (B) Schematic representation of MST optics. The fluorescence within the capillary (~4 µL volume) is excited and detected through the same objective. A focused IR-Laser locally heats a defined sample volume. Thermophoresis of fluorescent molecules through the temperature gradient is detected (C) Example of MST experiment. Initially, the molecules are homogeneously distributed and a constant "initial fluorescence" is detected. Once the IR laser is activated, a temperature jump (T-Jump), corresponding to a rapid change in fluorophore properties due to the fast temperature change, is observed. Subsequently, thermophoretic movement of the fluorescently labeled molecules out of the heated sample volume can be detected and is measured over a defined length of time. Deactivation of the IR-Laser results in an inverse T-Jump occurs, followed by the "back diffusion" of molecules, which is solely driven by mass diffusion. (D) Typical binding experiment. The thermophoretic movement of a fluorescent molecule (black trace; "unbound") changes upon binding to a non-fluorescent ligand (red trace; "bound"), resulting in different traces. For analysis, the change in thermophoresis is expressed as the change in the normalized fluorescence (ΔF_{norm}), which is defined as F_{hot}/F_{cold} (F-values correspond to average fluorescence values between defined areas marked by the red and blue cursors, respectively). Titration of the non-fluorescent ligand results in a gradual change in thermophoresis, which is plotted as ΔFnorm to yield a binding curve, which can be fitted to derive binding constants. Figure and legend obtained under a Creative Commons license with minor modifications [333].

fluorescence at emission wavelengths of 330 nm and 350 nm. This non-labeling approach is typically only feasible when the titrating ligand does not absorb at those wavelengths (e.g. small peptides, small molecules). The main advantage of MST is the ability to work with samples in different types of solvent in solution (e.g. in plasma). Furthermore, the sample requirements are very low, using less than 10 µL of sample for a complete binding isotherm.

2.4.3.1 Experimental conditions

MST was performed at 25 °C with medium MST power and varying LED power to ensure the minimum amount of fluorescence counts are met. As a cost-saving measure, capillaries were split into two using a zirconium blade and nitrogen gas was passed through the capillaries to remove resulting glass dust. Controls were performed using uncut vs cut capillaries to ensure reproducibility. Two types of capillaries were used: Standard Treated and Premium Coated. Unlike the Standard Treated capillaries, Premium Coated have a hydrophobic polymer coating in the capillary tubes that prevent adsorption of molecules to the capillary walls. This is particularly important for proteins or molecules that display strong adsorption to the walls, thereby giving rise to a non-uniform signal. Other methods to prevent adsorption include the use of a carrier e.g. BSA or detergents e.g. Tween-20. Premium Coated capillaries were only used when significant adsorption to the capillary walls was noted (as flagged by the MST software).

MST samples were read three times as technical replicates. The readings were performed at different sections of the capillary to prevent photobleaching and fluorescence exhaustion. Binding isotherms are derived from at least 12 different concentrations and were performed in at least three independent replicates. The F_{hot} values (Figure 21D) used were typically between 5 to

10s and data analyses used the same F_{hot} value for each specific binding interaction. Curve fitting was tested with two equations:

(1) Simple binding curve: A single interaction between two molecules is characterized by $Kd = \frac{[A]\cdot[T]}{[AT]}$, where A is the protein being monitored (e.g. fluorescent), T is the titrant, and AT is the resulting complex. Where A_0 and T_0 are the initial concentrations added and A and T are the free/unbound concentration, the law of conservation of mass dictates

$[A_0] = [A] + [AT]$ and $[T_0] = [T] + [AT]$. These are used to derive the quadratic equation:

$$[AT] = \frac{1}{2}\left([A_0] + [T_0] + K_d \pm \sqrt{([A_0] + [T_0] + K_d)^2 - 4 \cdot [A_0] \cdot [T_0]}\right).$$

To convert Fnorm to [AT], the following equation was used:

$$F_{norm} = \left(\frac{[A]}{[A_0]} \cdot F_{norm,A}\right) + \left(\frac{[AT]}{[A_0]} \cdot F_{norm,AT}\right)$$

$F_{norm,A}$ is the normalized fluorescence signal when A is not bound to T. Conversely, $F_{norm,AT}$ is the corresponding signal when A is bound to T.

(2) Hill equation: This equation describes binding events where ligand binding shows cooperativity or are not simple 1:1 binding,

$$F_{norm}(c) = Unbound + \frac{Bound - Unbound}{1 + 10^{Hill \cdot \log(EC50 - c)}}.$$

The concentration of titrant (c) was subject to $\log_{10}$ transformation. “Unbound” is the F_{norm} signal of the non-complexed protein whereas “Bound” is the F_{norm} signal of the complex. EC_{50} is the half-maximal effective concentration and “Hill” is the Hill coefficient of cooperativity.

2.4.3.2 Protein labeling with fluorophores.

MST requires one of the target proteins to be fluorescently labeled. There were two labeling strategies used for this project: amine-reactive crosslinking and His-tag affinity labeling. All fluorophores (Alexa Fluor 647 and NanoTemper RED 2nd generation dye) absorb strongly at the infrared range with an approximate excitation max of 650 nm and emission max of 670 nm.

2.4.3.3 Amine-reactive crosslinker reactive groups

Linkage of the fluorophore through N-hydroxysuccinimide (NHS) ester chemistry is dependent on the availability of free primary amines, particularly lysine residues on proteins. As such, the conjugation is also pH-dependent as at low pH, the primary amine is protonated and cannot react with the NHS ester. The optimal pH is 8.3-8.5 in a primary amine-free (e.g. carbonate-bicarbonate or HEPES) buffer. Typically, NHS esters are dissolved in an anhydrous DMSO or DMF as NHS esters hydrolyze quickly to an inactivated form in water. As a small amount of fluorophore-NHS ester is needed, the powder was dissolved in acetone and small aliquots were made before drying under a vacuum with a Speed-vac (Savant, Thermo Scientific). The aliquots were stored at -20 °C and used fresh each time.

Both the NanoTemper and ThermoFisher kits follow a similar protocol involving buffer exchange of protein, conjugation of dye to protein and separation of unconjugated from conjugated dye. For consistency, the proteins were buffer-exchanged to an appropriate buffer at pH 8.5. Conjugation of freshly prepared Alexa Fluor 647 dye took place in the dark at room temperature with a final dye:protein molar ratio of 10:1, achieved through three 15-min steps of 3.33:1. For the NanoTemper RED-NHS 2nd generation dye, conjugation took place in the dark at room temperature with a ratio of 2.5:1 for 30 min, following the manufacturer's instructions. The 2nd

generation dye has improved amplitudes and signal to noise ratios compared to 1st generation. To remove non-conjugated dye and non-labeled protein, the conjugation samples were eluted through a Sephadex G-25 PD-10 column (for Alexa Fluor 647) or through the kit-supplied gel filtration column (NanoTemper).

2.4.3.4 Histidine tag affinity labeling

A non-covalent fluorophore that is attached to tris-nitrilotriacetic acid (tris-NTA) was used to investigate protein interactions in solution since sTF-His and sgC-His contain His-tags. This nickel-chelating group allows the fluorophore to bind to the His-tag in solution and would have a lesser potential of an impact on the protein function. The unbound fluorophore also does not have to be removed during application. A downside to this application is the need for high nanomolar concentrations of protein to maintain binding the tris-NTA fluorophore. Furthermore, it prevented the use of nickel-chelating liposomes to facilitate membrane-protein complex assembly. Nonetheless, I used this tris-NTA fluorophore to probe for interactions in solution.

The tris-NTA-linked fluorophore is water-soluble and was maintained at -20 °C after rehydration in water or a buffer of choice. To allow time for the tris-NTA to bind to the His-tag, the fluorophore was incubated with the target protein for 1 h at room temperature. For sTF-His binding, a 4X stock of 400 nM sTF-His and 14 nM of tris-NTA linked fluorophore was prepared. At 1X, this allowed for ~11000 fluorescent counts (arbitrary units) with 20% LED power. For sgC-His, a 4X of 800 nM sgC-His and 14 nM of tris-NTA linked fluorophore was prepared. Standard treated cut capillaries (NanoTemper) were used with 0.1% BSA as a carrier. However, there was significant adsorption to the capillary walls. This was resolved with the inclusion of 0.01% Pluronic F-127, an inert non-ionic surfactant, as suggested by the manufacturer (NanoTemper).

2.4.3.5 Determining protein concentration and degree of labeling

The degree of labeling (ratio of dye to protein) was measured spectroscopically by measuring absorbances at 280 nm and 650 nm. Formulae for calculating protein concentration and protein to dye ratio is as follows:

$$protein\ concentration\ (M) = \frac{[A_{280} - (A_{650} \times CF_{280})] \times dilution\ factor}{\varepsilon_{protein}(cm^{-1}M^{-1})}$$

$$degree\ of\ labeling = \frac{A_{650} \times dilution\ factor}{\varepsilon_{dye} \times protein\ concentration\ (M)}$$

where,

CF_{280} is the correction factor for the dye's absorbance at 280 nm.

$\boldsymbol{\varepsilon}_{dye}$ is the extinction coefficient in cm^{-1} M^{-1}.

Alexa Fluor 647 has a CF_{280} of 0.03 and an $\boldsymbol{\varepsilon}_{dye}$ of 239,000 cm^{-1} M^{-1}.

NanoTemper RED (2^{nd} generation dye) has a CF_{280} of 0.04 and $\boldsymbol{\varepsilon}_{dye}$ of 195,000 cm^{-1} M^{-1}.

To further assess purity, the proteins were subject to SDS-PAGE and the protein bands were visualized by infrared illumination using the LI-COR Odyssey Imaging System. Alexa Fluor 647 labeled sgC-His, Alexa Fluor 647 labeled sTF-His, and NanoTemper RED labeled FVIIa had degrees of labeling of 1.4, 2.1, and 0.9, respectively.

2.4.4 Removal of His-tag on sTF-His by cyanogen bromide (CNBr) cleavage.

Cleavage protocol was adapted as previously described [334]. Briefly, protein solution was buffer-exchanged with 20 mM sodium phosphate buffer, 150 mM NaCl, pH 7.5 using an Amicon® 0.5 mL 10K molecular weight cut-off centrifugal filter. HCl and CNBr (dissolved in acetonitrile) was added to 100 µM sTF-His to a final concentration of 0.1 M HCl and 10 mM CNBr. Ratio of

methionine residues to CNBr was 100:1. After 24 h of cleavage in the dark at room temperature, a SpeedVac was used to dry and stop the reaction. The solid was resuspended in HBS and 2.5 M Guanidine-HCl (GdnHCl) [335]. Cleaved sTF (sTF-Cys) was retrieved in the flow-through following Ni-NTA metal affinity chromatography. HBS was added slowly to the flow-through with mixing until 0.25 M GdnHCl was obtained. Samples were spun at 15,000 x g for 30 min prior to concentrating and buffer-exchange in a Microcon®. Western blot analysis of sTF-Cys using an anti-His-tag antibody (1:665) revealed that the His-tag was removed (Figure 22). In addition, sTF-Cys function was tested using chromogenic functional assays and sTF-Cys binding to FVIIa was confirmed by MST (not shown).

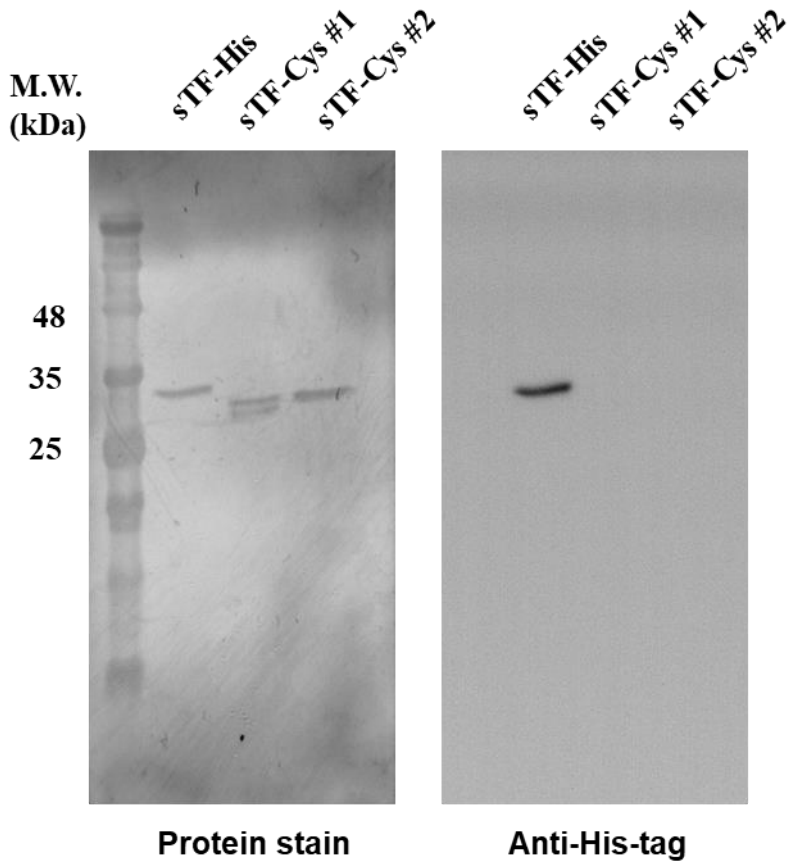

Figure 22. sTF-His cleavage by CNBr removes the C-terminus His-tag.

sTF samples (0.25 µg) were run in a non-reducing 10% polyacrylamide gel. sTF-Cys lacks the His-tag as revealed by Western blot using an HRP-conjugated anti-His-tag antibody (1:665). sTF-Cys #1 was re-folded after a GdnHCl denaturing nickel affinity column by 10 slow step-wise dilutions of HBS to a final [GdnHCl] of 0.25 M (1:1.25 dilution each step). sTF-Cys #2 was diluted with 5 step-wise dilutions (1:2 dilution each step) to the same final [GdnHCl].

Chapter 3: HSV1 glycoprotein C and its effect on TF/FVIIa complex

In this chapter, I will be addressing my hypothesis that gC aids in FX activation through enhancing TF function. This will be accomplished by first demonstrating TF presence and function on the virus surface. Following this, variations of HSV1 with or without gC and/or TF will be used to establish the effect of gC on TF-mediated FX activation on the virus surface. gC function was then pursued under purified, virus-free systems whereby binding partners can be determined and their direct effects on overall FX activation attained in the absence of additional contributing envelope constituents.

3.1 TF function on the virus surface

Previous work from the Pryzdial laboratory demonstrated that procoagulant phospholipids existed on several herpesviruses and could support prothrombinase complex formation [2,336]. Further investigation revealed that herpesviruses grown in TF-bearing cells could express envelope TF [2]. This was shown by flow cytometry as well as single immunogold EM. As it had been demonstrated that the virus envelope protein gC was involved in TF-mediated FX activation, single virus particles were probed for the simultaneous availability of TF, gC and aPL on their surface.

3.2 Procoagulant factors on the virus surface

Immunogold EM analysis of wildtype HSV1 was used to demonstrate that the host procoagulant factors, TF and aPL, as well as the viral procoagulant factor gC are on the same virus surface. A multiple labeling strategy involving the use of different sized gold beads to differentiate antigens was successfully employed to simultaneously detect all procoagulant factors on a single

virus particle (Figure 23). This technique would also be translated to my second hypothesis as it confirms the identity of virus particles containing procoagulant factor(s). HSV1 antigen expression levels appeared varied as seen in the single labeling controls compared to the triple labeling (Figure 23). However, stoichiometry cannot be inferred from immunogold EM as antibody or probe access to antigens can be limited by several factors. Nonetheless, HSV1 incorporated TF, aPL as well as gC on the same envelope, thereby supporting a gC/TF interaction.

An important technical EM observation made for HSV1 was that it readily aggregated. This technical issue was addressed by pre-treating the EM grids with 10 µg/mL anti-HSV1-positive human IgG. Antibody-mediated retention of the virus on the grid served to prevent the virus from repositioning during the labeling procedure. The purified human IgG1 was derived from NP and was tested positive for reactivity to HSV1, the importance of this will be alluded to in plasma clotting studies (Section 3.7.1).

Initial labeling strategy consisted of a rabbit antibody against TF; however, the relatively low amounts of TF compared to other virus antigens required the use of high concentrations of TF antibody. This resulted in high background when an isotype control was used. HSV1 encodes the transmembrane glycoproteins gE and gI, which form a heterodimer on the virus surface as well as the infected cell surface that can bind to Fc regions of antibodies [338,339]. The gE-gI Fc receptor binds more avidly to rabbit IgG than other species' [340]. This could explain why the rabbit IgG isotype control displayed high background compared to the near-zero background in mouse or goat isotype controls at similar concentrations. Thus, the TF and gC reporting antibodies were switched such that the TF antibody was of mouse origin and the gC antibody was of rabbit origin. gC is more abundant on the virus compared to TF as determined by western blot (Figure 13) and as observed in the initial labeling strategy using the mouse antibody. This allowed us to eliminate

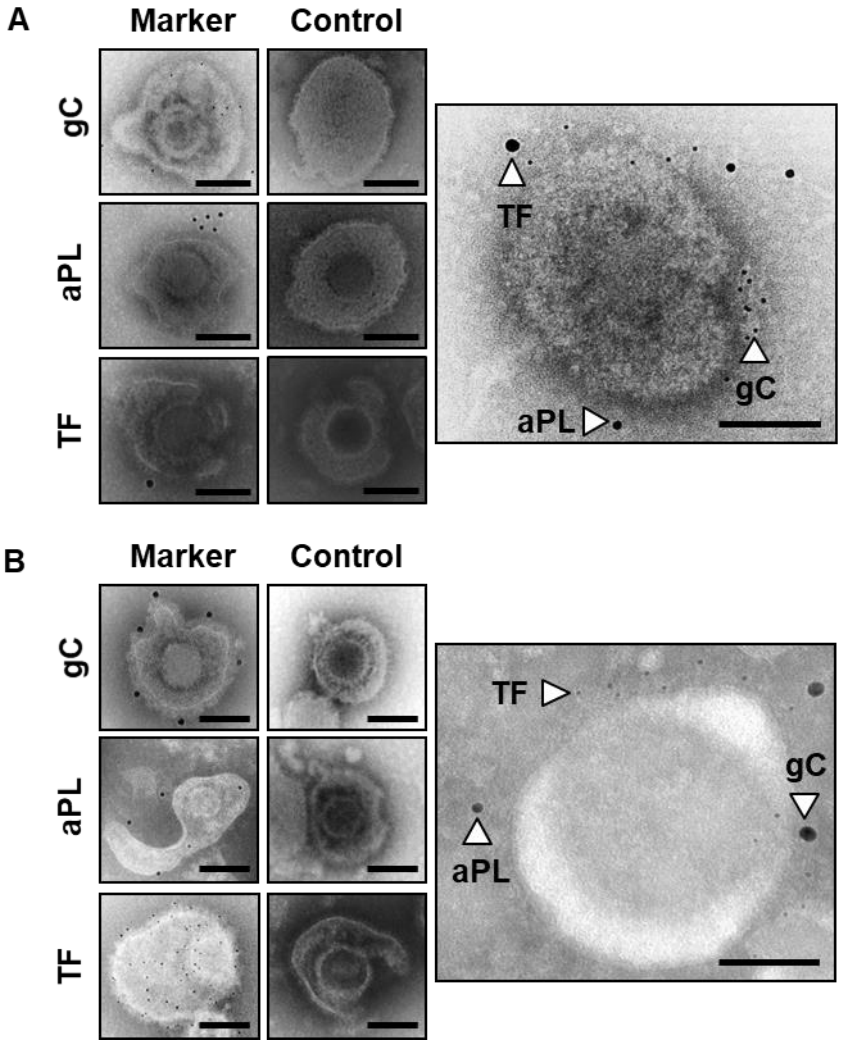

Figure 23. Initiators of coagulation found on the virus surface.

Immunogold electron microscopy on HSV1. HSV1 was confirmed by presence of gC, size and morphology. TF and aPL are found on the surface of HSV1. Two different labeling strategies were used. (A) mouse anti-gC: 6 nm gold-conjugated goat anti-mouse; aPL probe (annexin V): 10 nm gold-conjugated goat anti-biotin; rabbit anti-TF: 15 nm gold-conjugated goat anti-rabbit. (B) rabbit anti-gC: 15 nm gold-conjugated goat anti-rabbit; aPL: 10 nm gold; mouse anti-TF, 9B4: 6 nm gold-conjugated goat-anti-mouse. Controls used were isotype controls for gC/TF and inclusion of EDTA for aPL probe. Scale bar: 100 nm.

rabbit IgG background by lowering the antibody concentration while still facilitating gC detection. In addition, the TF antibody concentration could be increased to better detect for the less abundant protein. These modifications revealed that HSV1 particles incorporated the host procoagulant factors TF and aPL into the same envelope as well as the virus procoagulant factor, gC. However, the presence of these markers does not demonstrate functionality but confirms the possibility.

3.2.1 Effect of gC on TF function

The presence of TF procoagulant function on HSV1 was previously tested through inhibition assays [258]. TF-specific inhibitory antibodies resulted in ~90% inhibition of FX activation by FVIIa on HSV1/TF+/gC- (~90%). However, in these earlier studies only 40% inhibition was achieved on HSV1/TF+/gC+, suggesting that both TF and gC are involved in FXa generation on the virus. To quantify the individual contributions of TF and gC on the virus surface, I used HSV1/gC+ or HSV1/gC- propagated in TF-inducible human carcinoma cells to produce HSV1/TF+/gC+, HSV1/TF+/gC-, HSV1/TF-/gC+, and HSV1/TF-/gC-.

HSV1/TF-/gC+ displayed <2% FVIIa-mediated FX activation compared to HSV1/TF+/gC+ (Figure 24A). The presence of gC enabled approximately 3-fold enhancement of FVIIa-mediated FX activation by TF-competent virus, as compared to HSV1/TF+/gC-. This contrasts with TF-deficient virus, where gC had no noticeable impact on the amount of FX activation under these conditions (Figure 24B). Thus, viral gC enhancement of FVIIa activity is appreciable only in the presence of TF on the virus surface.

The viruses were grown in sister cells to minimize variability in protein expression during infection. Interestingly, western blot and densitometry analyses of equal virus particle numbers displayed differences in TF protein expression per virus (Figure 25A). For this virus preparation,

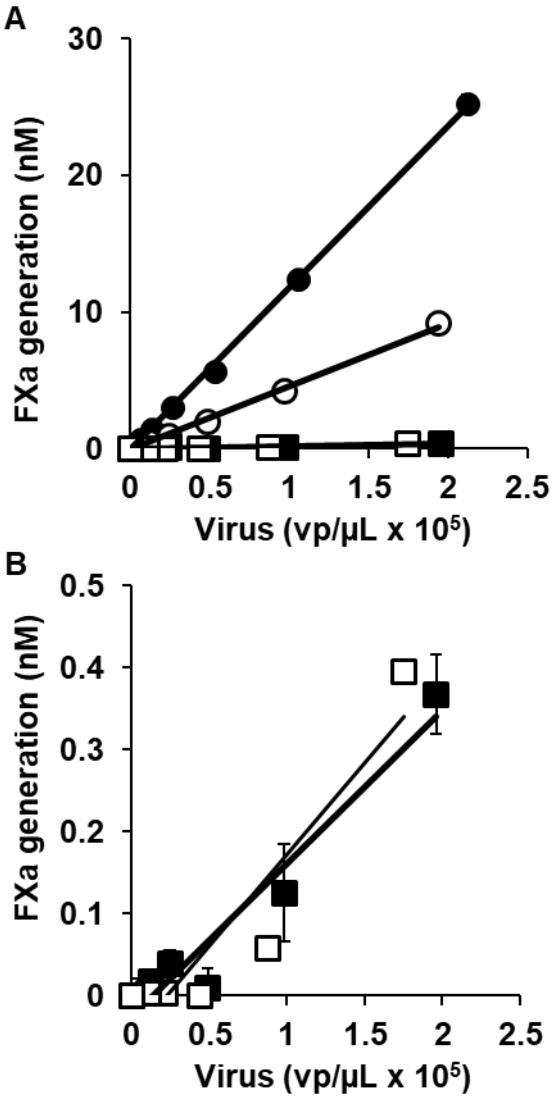

Figure 24. gC enhances TF-dependent FX activation on the virus envelope.

(A) FX activation was followed using the panel of HSV1: TF+/gC+ (●), TF+/gC- (○), TF-/gC+ (■), and TF-/gC- (□) viruses. (B) Magnification of TF-/gC+ and TF-/gC-. 100 nM FX and 1 nM FVIIa was mixed with HSV1 prior to the addition of 5 mM Ca^{2+} to initiate the reaction. After 20 min at 37 °C, the samples were stopped with EDTA and chromogenic substance S-2765 was added to determine the generation of FXa spectrophotometrically. N = 4 independent replicates; Error bars: standard error of the mean (SEM).

HSV1/TF+/gC+ had an average of 3300 ± 520 molecules of TF/vp whereas HSV1/TF+/gC- had 2600 ± 410 molecules of TF/vp (Figure 25B, N = 4, p = 0.03, Student's t-test). The major capsid protein (MCP) was used to compare the amount of capsid-containing virus particles, because MCP comprises the viral capsid and its content is constant due to specific capsid architecture. Of note, there was a two-fold decrease in the total MCP when gC was absent with the same amount of virus particles loaded. Even when factoring in the 30% difference in TF, the amount of FX activation generated by HSV1/TF+/gC+ was more than 2-fold greater than HSV1/TF+/gC- (Figure 25C).

3.2.2 Effect of soluble gC to viral TF

It was previously demonstrated that a transmembrane domain-truncated form of gC (sgC-His) enhanced FVIIa-mediated FX activation on the virus surface [258]. Here, sgC-His was incrementally added to the purified HSV1 variants to determine if sgC-His binding to virus was dependent on TF. FX activation was increased ~2-fold by the addition of sgC-His due to the presence of TF on the virus (Figure 26A). Addition of sgC-His to TF-deficient virus had a relatively small effect on FX activation (Figure 26B). The effect of sgC-His on FXa generation was greatest in the following order: HSV1/TF+/gC+ > HSV1/TF+/gC- >> HSV1/TF-/gC+ > HSV1/TF-/gC- (Figure 26C and D). Since sgC-His enhanced HSV1/TF+/gC+ more than HSV1/TF+/gC- suggests that another factor besides gC and TF could be affecting sgC-His-mediated enhancement of FXa production.

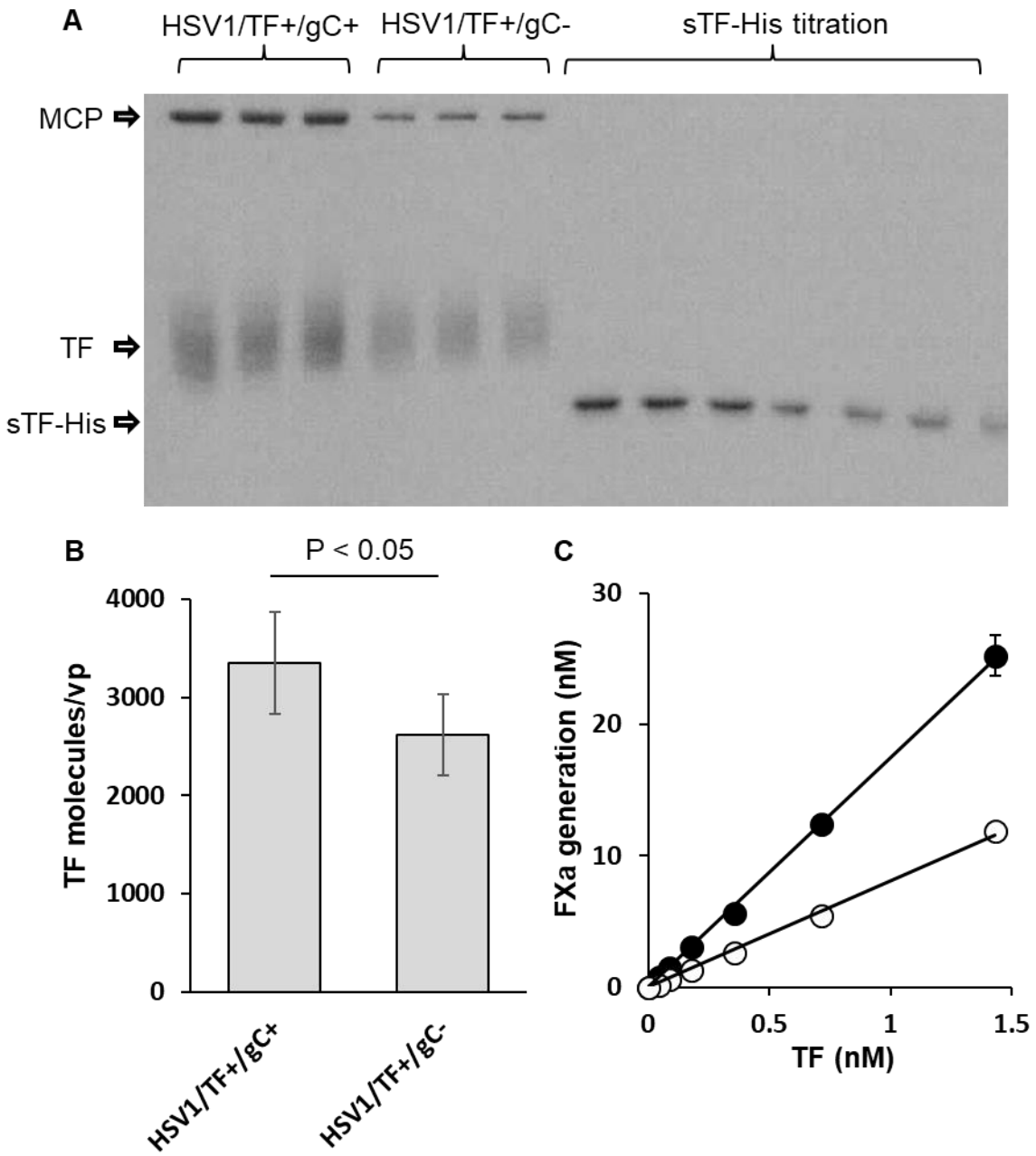

Figure 25. Difference in viral TF expression does not explain gC-mediated FX activation.

(A) Western blot of 10^9 virus particles of HSV1/TF+/gC+ or HSV1/TF+/gC- loaded on a reducing 5-15% polyacrylamide gel. TF and MCP were probed simultaneously with mouse monoclonal antibodies that were demonstrated to have zero cross-reactivity. Purified sTF-His was titrated as a standard curve for quantitatively determining [TF] of each virus by densitometry. N = 4 independent replicates; Error bars: SEM. (B) Densitometry-derived concentrations of TF were converted to number of TF molecules per virus particle (vp) for each virus. (C) By converting the vp concentration to [TF], the effect of gC on FVIIa-mediated FXa generation by HSV1/TF+/gC+ (●) and HSV1/TF+/gC- (○) was assessed as a function of [TF].

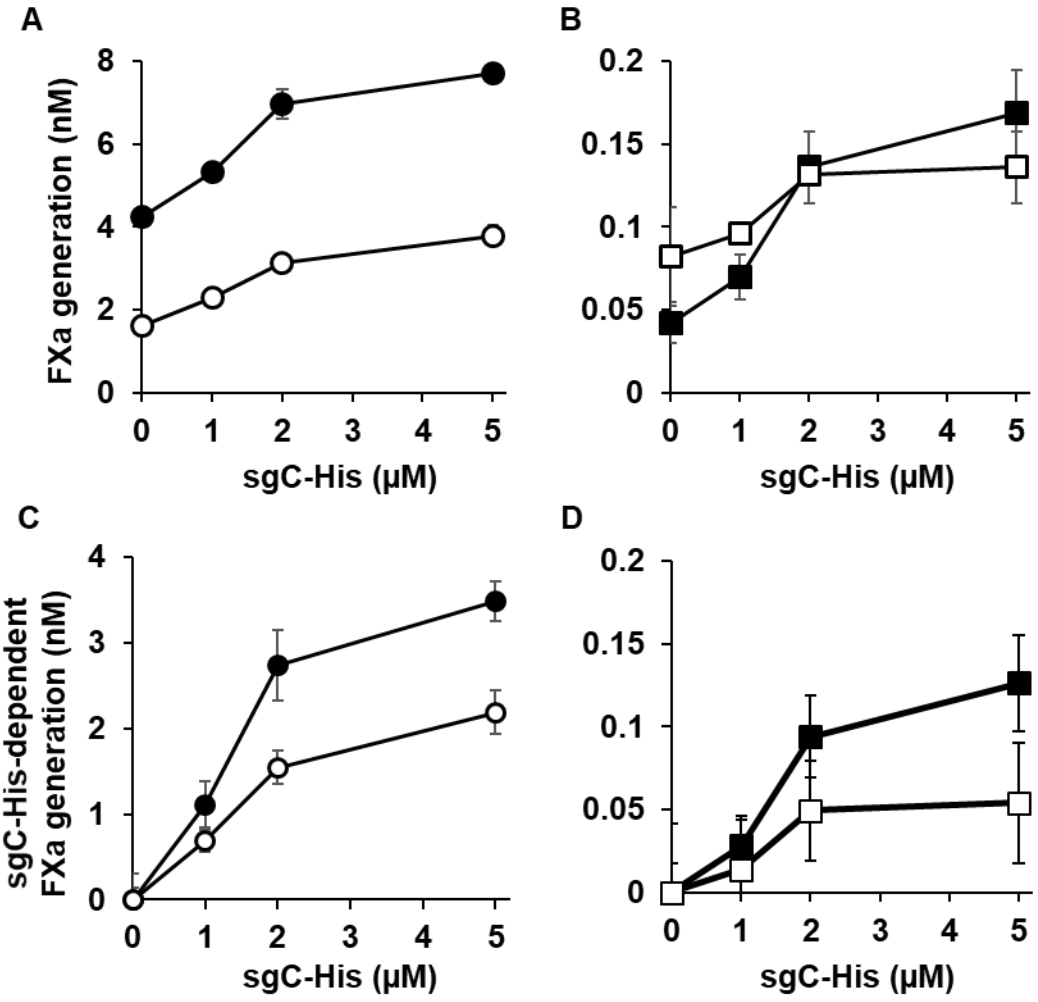

Figure 26. Addition of sgC-His to HSV1 enhances FVIIa-mediated FX activation.

Purified sgC-His (titration), FX (100 nM) and FVIIa (1 nM) were combined with purified HSV1 variants: (A) HSV1/TF+/gC+ (●) or HSV1/TF+/gC- (○) and (B) HSV1/TF-/gC+ (■) or HSV1/TF-/gC- (□) viruses in the presence of $CaCl_2$ (5 mM) and FXa generation was followed using the chromogenic substrate S-2765. (C and D) sgC-His-dependent FXa generation was determined by subtracting baseline virus-mediated FX activation. N > 3 independent replicates; Error bars: SEM.

3.2.3 Effect of soluble gC to relipidated TF

To exclude other virus- or host-encoded factors associated with the envelope of purified HSV1, sgC-His was added to Innovin as a source of relipidated full-length TF and aPL. Enhancement of FVIIa-dependent activation of FX by sgC-His was demonstrated. The activity of FVIIa was saturable, indicating occupancy of a cofactor(s) (Figure 27A). FX (Figure 27B), the reaction substrate, also reached saturation, which is consistent with either a FVIIa cofactor that docks the substrate or maximal FVIIa-binding. The addition of 2 μM sgC-His increased maximal activation by ~2-fold. However, the inability to vary the specific components of Innovin prevented detailed assessments of TF and/or aPL contribution(s) to the gC/TF/FVIIa interaction. Furthermore, it is uncertain whether gC requires membrane-association for full functionality. Hence, a defined and versatile system was required to ascertain the importance of each component in FX activation.

3.3 gC function in a divisible system

The function and manner by which gC affects FX activation is not clear. Especially in the case of sgC-His, its ability to enhance FX activation is FX- and FVIIa-dependent but is relatively weak in solution and in the absence of relipidated TF. Membrane association is important for TF cofactor function. Hence, sgC-His function may also be restricted from a lack of membrane association/interaction. Soluble TF can enhance FVIIa-dependent FX activation in the presence of aPL and Ca^{2+} [328]. Yet, its cofactor activity is 1000-fold less than its native membrane-bound form. sTF-His is known to optimally enhance FX activation by FVIIa when DGS-NTA-Ni is incorporated into an aPL-containing membrane [318]. The DGS-NTA-Ni enables membrane-binding of sTF-His and the aPL enables Ca^{2+}-dependent membrane-binding of FVIIa and FX.

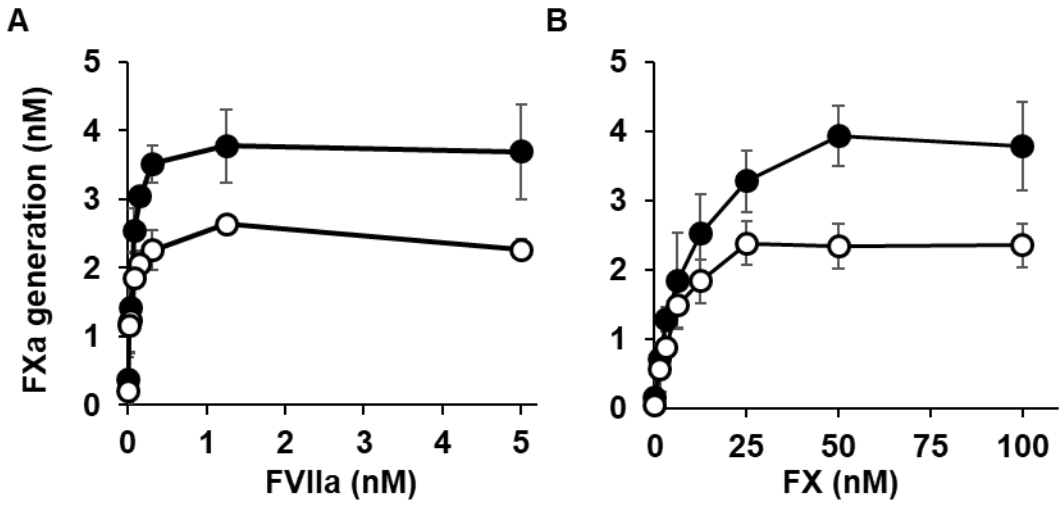

Figure 27. sgC-His effect on FX activation by relipidated TF.

The effect of sgC-His on FX activation by relipidated full-length TF (1:3000, Innovin) was assessed chromogenically using S2765 in the presence (●) or absence (○) of sgC-His (2 μM) at constant FX (100 nM, A) or FVIIa (10 nM, B). N = 3 independent replicates; Error bars: SEM.

Thus, suggesting orientation and membrane association is important for TF biological activity. This approach was adapted for investigating sgC-His function as the protein also carries a C-terminal His-tag.

3.4 Effect of sgC-His on TF function in a purified and defined system

The respective contributions of cofactors were evaluated by comparing vesicles toward increasing the activity of FVIIa by sgC-His. As negative controls, none of the various lipid compositions yielded appreciable FX activation by FVIIa in the absence of sTF-His or sgC-His (Figure 28A, lanes 1-3). This low activity persisted when the essential components, Ca^{2+}, FX or FVIIa, were omitted in the presence of sgC-His (Figure 28A, lanes 4-6). As a positive control for the anticipated activity of the three vesicle compositions, FX activation was shown to be enhanced by sTF-His in the following order PCPS << NiPC < NiPCPS (Figure 28A, lanes 7-9). Interestingly, a cofactor effect on FVIIa was similarly observed for sgC-His (Figure 28A, lanes 10-12). Based on previous findings, I expected minute FX activation (pM) [258]. However, there was 100-fold higher activity and furthermore, required 1000-fold lower concentration of sgC-His. Exclusion of phosphatidylserine (PS) from the Ni-chelating vesicles resulted in a 4-fold decrease in FX activation by sgC-His.

To ensure no contaminating proteases were found in the sgC-His preparation, sgC-His was pre-treated with the protease inhibitor *p*-amidinophenylmethylsulfonylfluoride (APMSF). APMSF is an irreversible inhibitor of trypsin-like serine proteases and quickly hydrolyzes into an inactive form in aqueous solution. No effect of APMSF was observed on the activation of FX catalyzed by sgC-His nor did high concentrations of sgC-His (5 μM) in the absence of FVIIa result in any FX activation (data not shown).

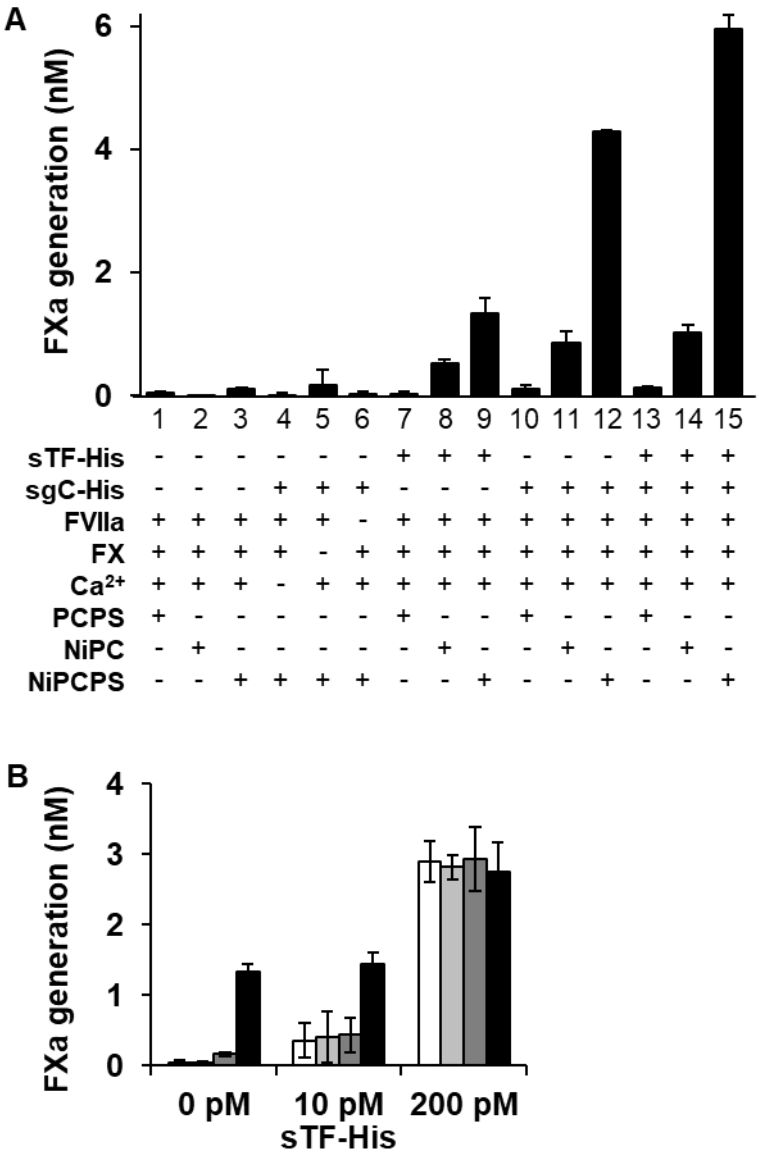

Figure 28. Ni-chelating lipids enhance sgC-His and sTF-His cofactor function.

(A) FX activation was monitored by variably assembling tenase constituents on 50 μM PCPS, NiPC or NiPCPS in the presence or absence of 1 pM sTF, 1.2 nM sgC-His, 1 nM FVIIa, 100 nM FX, 5 mM Ca^{2+}. (B) FXa generation by 0, 1, 10 or 100 nM sgC-His (from white to dark bars) in the presence of 0, 10 or 200 pM sTF-His was investigated for synergy with 100 nM FX, 5 mM Ca^{2+} and limiting concentration of FVIIa (10 pM). N = 3 independent replicates; Error bars: SEM.

To explore the apparent synergistic effect of gC and TF on the virus (Figure 27), sTF-His was combined with sgC-His. Unlike, the HSV1 variant experiments, the effect of sgC-His on sTF-His was additive in these purified protein experiments (Figure 28A, lanes 13-15). As this was performed with non-saturating amounts of sTF-His (relative to the concentration of FVIIa), it was postulated that perhaps sgC-His favored binding to unbound FVIIa in the presence of sTF-His. And so, the experiment was set-up to have a limiting concentration of FVIIa, for which sTF-His and sgC-His would either compete or interact simultaneously with FVIIa (Figure 28B). In this scenario, I found that sgC-His did not have any enhancing effect on sTF-His/FVIIa beyond sTF-His saturation of FVIIa cofactor activity. This would suggest that sTF-His competes with sgC-His for binding to FVIIa. Surface plasmon resonance studies by another group on relipidated TF binding to FVIIa revealed that TF/FVIIa does not dissociate easily as the k_{off} was immeasurable under their conditions [341]. Nonetheless, the ability of sgC-His to enhance FX activation in the absence of TF prompted further investigation.

3.4.1 FX activation kinetics by sgC-His/FVIIa

To assess whether sgC-His behaves differently to sTF-His in its ability to enhance FX activation, the kinetics of FX activation was followed with FX chromogenic assays. To determine this, the affinity of cofactor to NiPCPS and NiPC was quantified by FX chromogenic assays. As PCPS with sgC-His did not show appreciable amounts of FX activation unless at µM concentrations and the cofactors lack any known membrane-tethering domains without Ni-chelating groups, PCPS affinity was not determined. When titrating NiPCPS or NiPC, the maximal rate of FX activation was higher for sTF-His than sgC-His (Figure 29A and B). This is explained by the difference in affinity of cofactor to FVIIa and the sensitivity of the assay. At lower than 100

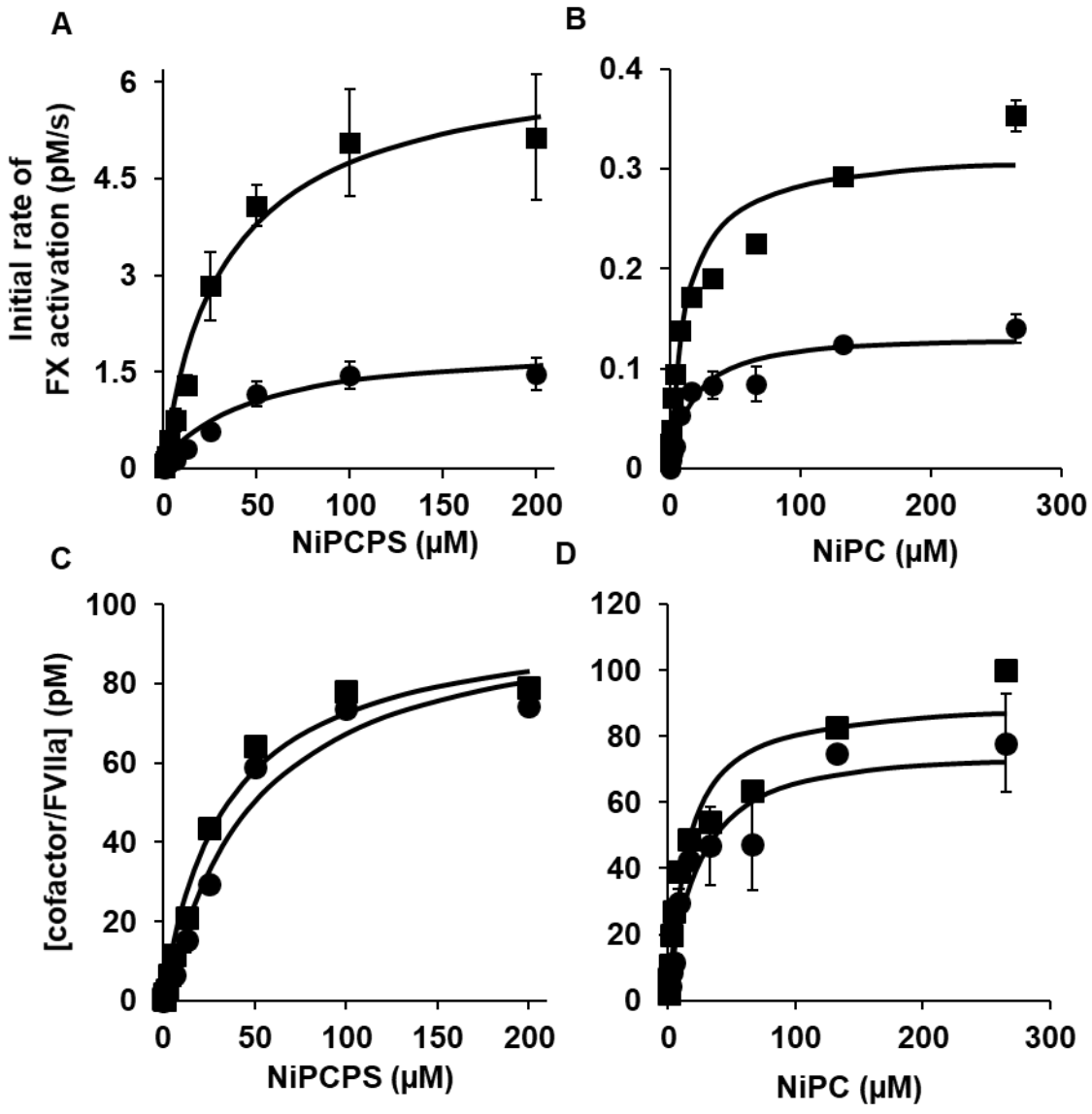

Figure 29. sgC-His and sTF-His binding to NiPCPS or NiPC vesicles.

Binding of cofactors to (A) NiPCPS or (B) NiPC was assessed by following continuous FX activation by the assembled cofactor/FVIIa complex. NiPCPS and NiPC SUVs were titrated with either 120 nM sgC-His (●) or 100 pM sTF-His (■) in a mixture containing final concentrations of 100 pM FVIIa and 5 mM Ca^{2+}. 30 nM FX and 0.2 mM S-2765 was added to initiate the reaction. FX activation was followed over time to determine the initial rate of FX activation. This rate was converted to concentration of cofactor/FVIIa complex to determine the apparent dissociation constants for sgC-His or sTF-His to NiPCPS or NiPC (C and D, respectively). N = 3 independent replicates; Error bars: SEM.

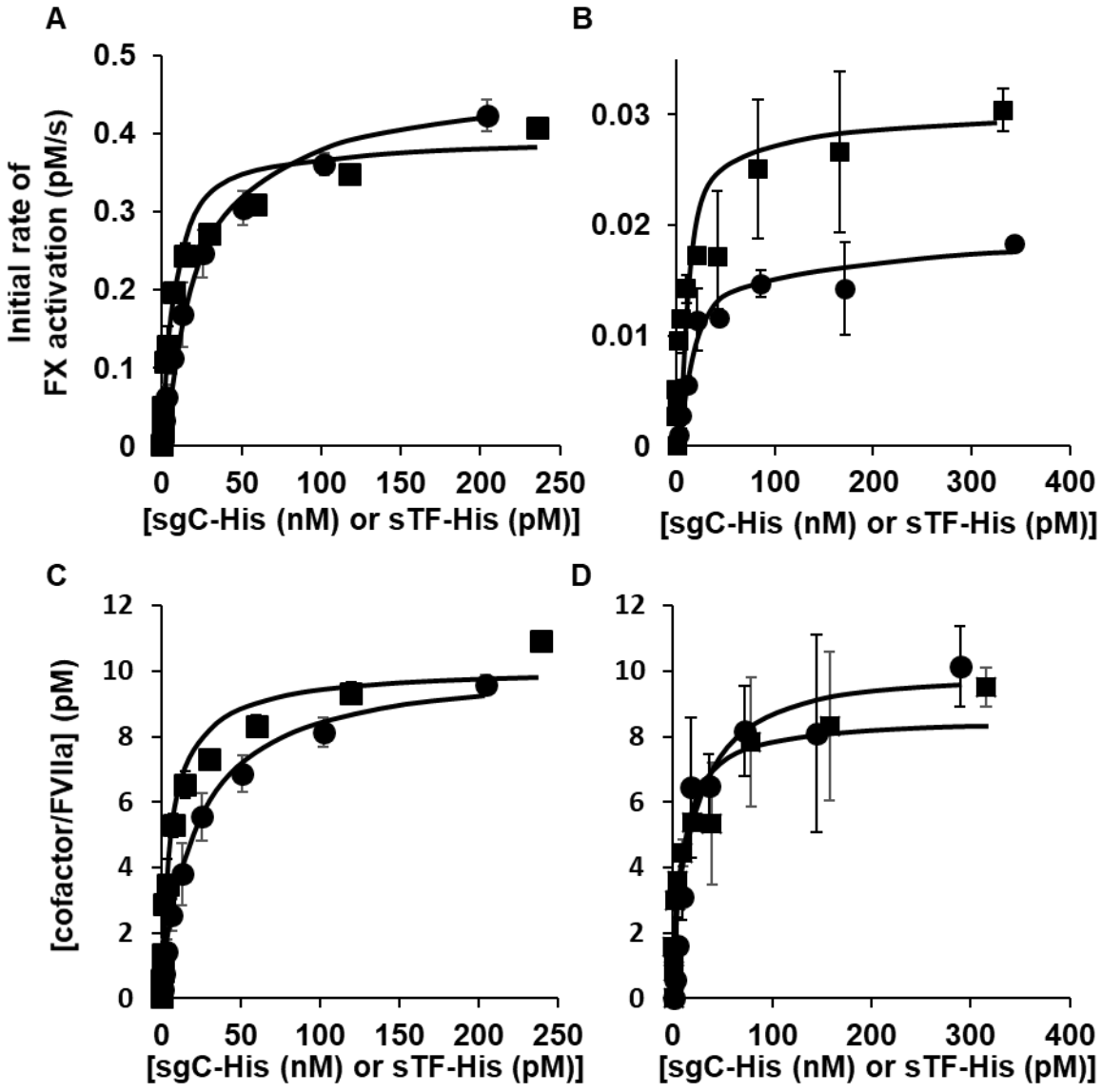

Figure 30. Binding of sgC-His or sTF-His to FVIIa in the presence of NiPCPS or NiPC.

Binding of sgC-His and sTF-His to FVIIa was determined by continuous FX chromogenic assays in the presence of (A) NiPCPS or (B) NiPC. sgC-His (●) or sTF-His (■) was titrated in a mixture with 100 µM NiPCPS or NiPC, 10 pM FVIIa and 5 mM Ca^{2+}. 30 nM FX and 0.2 mM S-2765 was added to initiate the reaction. FX activation was followed over time to determine the initial rate of FX activation. This rate was converted to concentration of cofactor/FVIIa complex to determine the apparent dissociation constants for sgC-His or sTF-His to FVIIa (C and D, respectively). N = 3 independent replicates; Error bars: SEM.

Table 2. Binding affinities of sTF-His and sgC-His as derived from linked enzyme kinetics.

		Nickel binding	FVIIa binding
Ligand	**Lipid**	**$K_{d,app}$ (μM) (95% CI)**	**$K_{d,app}$ (nM) (95% CI)**
sTF-His	NiPCPS	33.8 (23.0 – 44.4)	7.0×10^{-3} (4.4×10^{-3} – 9.6×10^{-3})
sTF-His	NiPC	13.4 (5.6 – 21.2)	8.9×10^{-3} (2.9×10^{-3} – 1.5×10^{-4})
sgC-His	NiPCPS	48.0 (26.0 – 70.0)	21.5 (18.3 – 24.7)
sgC-His	NiPC	19.1 (7.4 – 30.7)	18.0 (8.7 – 27.3)

Table 3. Kinetics of FX activation as derived from linked enzyme kinetics.

Cofactor	Lipid	K_m (μM)	k_{cat} (s^{-1})	k_{cat}/K_m (μM^{-1} s^{-1})
sTF-His	NiPCPS	0.16 ± 0.02	3.8 ± 0.5	23.6 ± 1.4
sgC-His	NiPCPS	0.14 ± 0.02	2.5 ± 0.3	16.6 ± 1.0

pM FVIIa, titrating phospholipid resulted in immeasurable FX activation (not shown). Nonetheless, transformation of the initial rate of FX activation to concentration of cofactor/FVIIa complex (Figure 29C and D) revealed that sTF-His and sgC-His have similar affinities for NiPCPS and NiPC, as summarized in Table 2. Contrary to my expectations, the hexa-His-tag sTF-His did not have a tighter affinity than the penta-His-tag sgC-His. It is interesting to note that NiPC appeared to have a higher affinity for the cofactors than NiPCPS.

3.4.2 sgC-His-induced plasma clotting

When 1 µM sgC-His was added to NP, no clotting was observed in the presence of 50 µM PCPS vesicles after recalcification with 10 mM $CaCl_2$ for over 15 min (Figure 31). With the substitution of PCPS with NiPCPS, clot formation time was 136 s ± 11 s. Of note, the batches of NP used contained antibodies against HSV1, including gC (Figure 32), accredited to the prevalence of HSV1 within the adult population. The presence of inhibitory antibodies could explain the high concentration of gC required to initiate clotting.

3.5 Interactions between TF and gC

3.5.1 Cross-linking on the virus surface

As HSV1/TF+/gC+ has enhanced TF/FVIIa activity compared to gC-deficient, it was speculated that an interaction between TF and gC existed. Crosslinking experiments of TF+/- and gC+/- HSV1 using the thiol-reduceable DTSSP did not reveal any detectable TF-gC interaction (Figure 33). There was, however, more monomeric TF in HSV1/TF+/gC+ compared to the HSV1/TF+/gC-. Of note, gC appeared as two distinct bands of similar quantity under low exposure in the HSV1/TF+/gC+. HSV1/TF-/gC+ only had the larger form of gC (Figure 33B, lane 2/8).

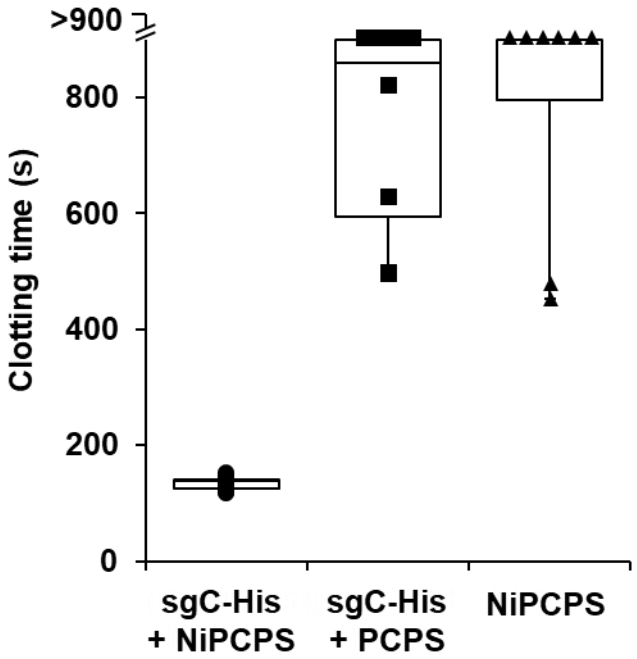

Figure 31. sgC-His-induced plasma clotting.

Normal pooled human plasma clotting was initiated by the inclusion of sgC-His (1 µM), 50 µM PCPS or NiPCPS, and 10 mM Ca^{2+}. Clotting was followed for up to 900 s. N > 5 independent replicates; box plot.

Since the virus contains other gC crosslinking partners, the proportion of gC interacting with TF may be low and undetectable in the purified virus setting. To address this, a recombinant form of gC lacking its transmembrane domain (sgC-His) was produced to probe for TF interactions in a more controlled setting without extraneous virus- or host-derived factors. This form of gC retains its complement inhibiting and heparin binding functions as well as conformation [320].

3.5.2 Cross-linking of purified proteins

gC forms complexes with other viral glycoproteins, thus perhaps only a small proportion of membrane gC is bound to TF. To increase the interaction between TF and gC, purified sTF-His and sgC-His were incubated with Ni-chelating membranes (NiPCPS, 50 μM) to mimic a virus membrane-bound TF and gC. However, DTSSP crosslinking of sTF-His to sgC-His did not result in any sTF-His/sgC-His adducts (Figure 34). Poor or a lack of crosslinking is not dismissive given that TF has been previously shown to be unable to crosslink with FVIIa using DTSSP [334].

3.5.3 ELISA-modified approach

An ELISA-based approach was employed to determine sgC-His/TF interactions. Full-length relipidated TF (Innovin) was adsorbed to the bottom of the wells, and sgC-His was incubated at varying concentrations. After thorough washing, the amount of bound sgC-His was determined by antibodies. No sgC-His was found to be bound to the wells. With the opposite approach using adsorbed sgC-His, no TF was bound. To enhance detection, a chromogenic assay was employed and monitored the assembly of TF/FVIIa and subsequent FX activation. However, sgC-His did not retain TF nor was TF enhanced by sgC-His in either adsorption scenarios. sgC-His may have a low affinity for TF or the complex is not stable when gC is not membrane-bound.

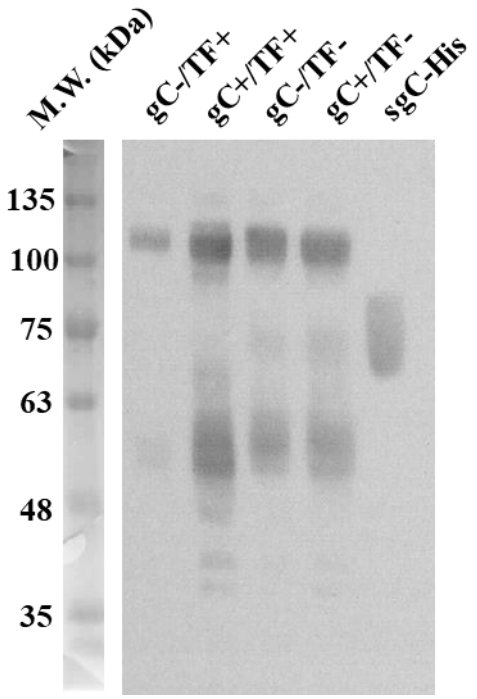

Figure 32. Antibodies against HSV1 exist in normal human pooled plasma-derived IgG.

Human IgG purified from NP by Protein G agarose chromatography was used as a primary antibody to detect for virus proteins from different forms of HSV1 (HSV1/TF+/gC+, HSV1/TF+/gC-, HSV1/TF-/gC+, and HSV1/TF-/gC-) that were separated by SDS-PAGE (1×10^{10} virus particles). gC is highly antigenic and sgC-His was detected (100 ng).

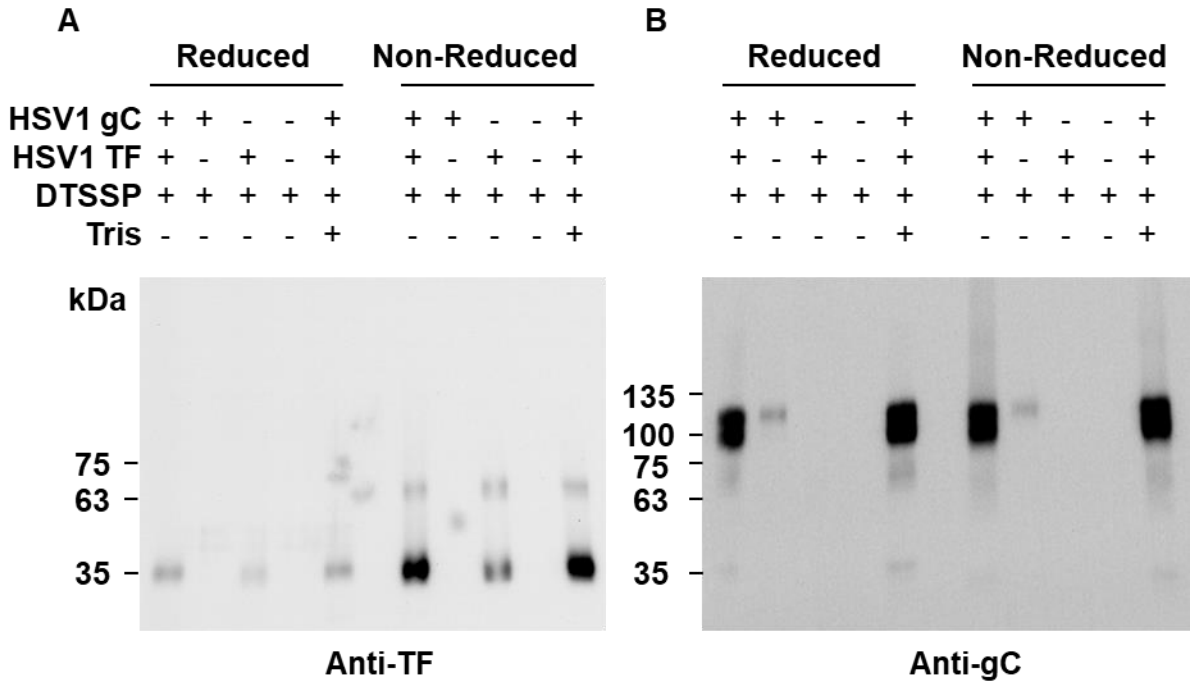

Figure 33. Crosslinking of proteins on HSV1 surface by DTSSP.

HSV1 panel (2 x 10^{10} vp each virus) was subjected to the 2.5 mM DTSSP crosslinker for 15 min on ice. The reaction was then quenched with 1 M Tris-glycine (pH 7.0). A negative control reaction where Tris-glycine (pH 7.5) was added prior to the cross-linker was also performed. Reduced and non-reduced samples were loaded on a 5-15% gradient gel and detected by Western blot using polyclonal antibodies against TF and gC.

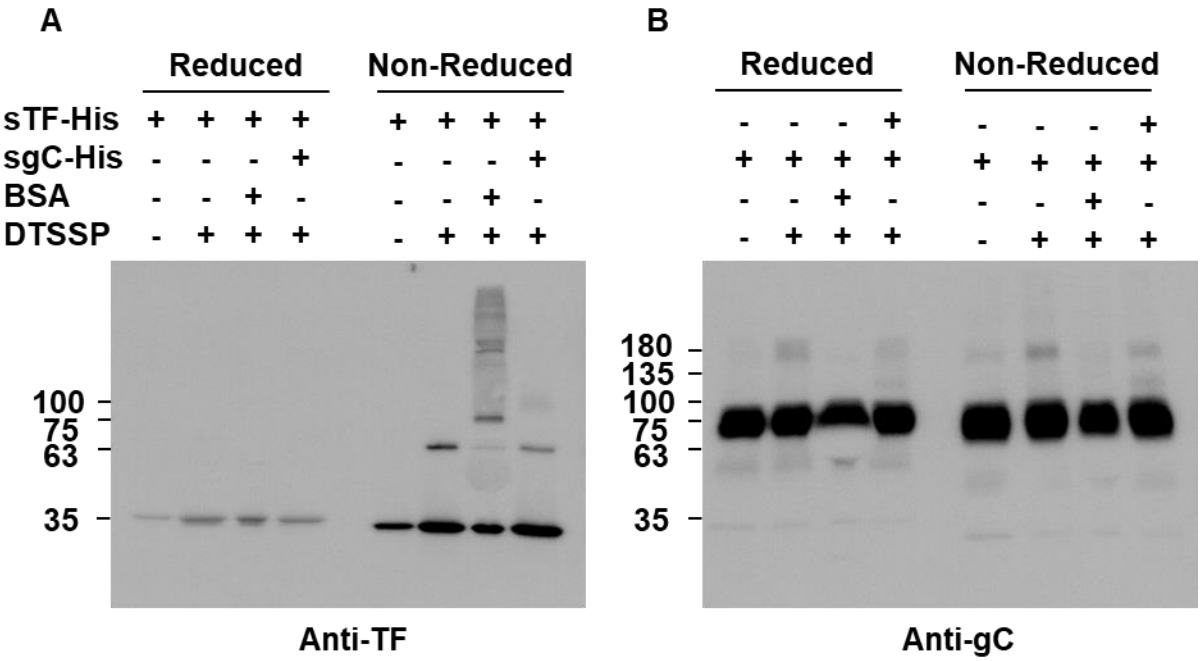

Figure 34. Crosslinking of purified sgC-His and sTF-His on NiPCPS vesicles.

12 µM sTF-His was mixed with 2.5 µM sgC-His, 50 µM NiPCPS and 5 mM Ca^{2+}. DTSSP (500 µM) was incubated with the protein mixture for 24 h at 4 °C with agitation. Reduced and non-reduced samples were loaded on a 5-15% gradient gel and detected by Western blot using polyclonal antibodies against TF and gC.

3.5.4 Microscale thermophoresis

As an alternative approach to searching for sTF-His/sgC-His interactions, microscale thermophoresis (MST) was employed. The main advantage of this technique is that it can follow interactions of molecules in solution without tethering one of the binding partners onto a surface. In addition, miniscule amounts of reagent are required to derive an entire binding isotherm (<12 μL). To monitor an interaction, one of the ligands must be fluorescently labeled through amine-reactive probes, thiol-reactive probes, or non-covalent affinity probes (e.g. His-tag probes).

3.5.4.1 Fluorophore labeling of sTF-His

There are two important lysines in the FVIIa-interacting domain of TF [31]; thus labeling of sTF-His using amine-reactive probes could pose a problem. It was shown that these lysines are required for membrane-associated enhancement of FVIIa activity. As expected, amine-labeled sTF-His loss the ability to further enhance FVIIa activity in the presence of NiPCPS. This initial labeling strategy resulted in FVIIa-dependent quenching of amine-labeled sTF-His fluorescence by MST, which was used to derive a binding affinity that was comparable to FVIIa binding to sTF-His in solution (data not shown). No sgC-His direct interaction with amine-labeled sTF-His could be demonstrated. However, initial MST results revealed that the binding affinity of amine-labeled sTF-His to FVIIa in solution is decreased upon the addition of sgC-His. This would hint towards an interaction between sgC-His and FVIIa.

3.5.4.2 Fluorophore labeling of sgC-His

As amine-labeled sgC-His did not appear to bind to sTF-His in solution. This would suggest that sgC-His displaced labeled sTF-His from FVIIa in solution based on the initial MST results with sTF-His-R. However, amine-labeled sgC-His also did not appear to directly bind to FVIIa or FX in solution. FX binding to gC is known thus amine-labeling may have affected its function. The thermophoresis profile of amine-labeled sgC-His displayed slow/minimal movement. Furthermore, heparin binding to labeled sgC-His resulted in a large increase in mobility of the complex. Taken together, amine-labeled sgC-His was most likely aggregated but was stabilized into monomers by heparin.

An alternate labeling approach consisted of a fluorophore conjugated to a hist-tag probe (tris-NTA-RED). As sgC-His and sTF-His can both bind to tris-NTA-RED, a His-tag needed to be removed from one of the proteins. sTF-His has a single methionine residue located at 9 amino acids upstream the His-tag (and spacer). Thus, cyanogen bromide specific cleavage of methionine was used to cleave off the His-tag. Functional studies confirmed the absence of the His-tag while retaining FVIIa cofactor activity in solution. Yet, no sTF-Cys/sgC-His interaction was measurable (Figure 35).

3.6 Interactions between gC and FVIIa

3.6.1 sgC-His binding interactions in solution-phase

sgC-His conjugated to fluorescent RED-tris-NTA via the His-tag (sgC-His-R) was followed by MST for interactions with FVIIa or FX in the absence of vesicles (Figure 36). Indicative of a relatively weak association between sgC-His and FVIIa or FX, the binding isotherms did not approach saturation at the highest available concentration of either ligand and

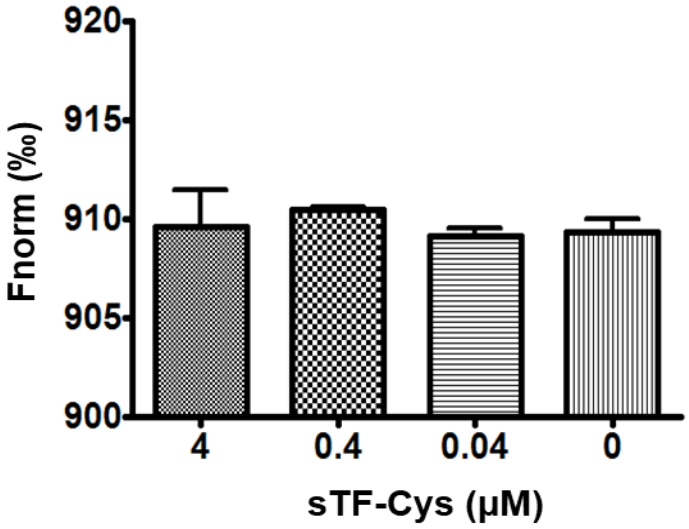

Figure 35. Interaction between sgC-His-R and sTF-Cys was probed using MST.

sgC-His interaction with sTF-His was probed by MST. The His-tag of sTF-His was removed by CNBr cleavage, resulting in sTF-Cys. sgC-His (200 nM) was mixed with the RED-tris-NTA fluorescent probe (3.5 nM) for 30 min at room temperature before the addition of sTF-Cys in HBS/0.05% BSA/0.05% Tween-20/5 mM Ca^{2+}. MST power was set at medium with 10% excitation power. Samples were equilibrated at 25 °C prior to instrument reading. N = 2 independent replicates, technical triplicates; Error bars: SD from pooled technical replicates.

could not be fit to a binding model. While the solution-phase enhancement of FVIIa activity was independent of sgC-His-R labelling (not shown), RED-tris-NTA prevents NiPCPS-binding. Therefore, I pursued amine-labeling of FVIIa (FVIIa-R) given its newly discovered intrinsic interaction with sgC-His (Figure 36). FVIIa-R retained 62% and 85% function in FX chromogenic assays in the presence of sTF-His or sgC-His, respectively (Appendix A.2). As a positive control, sTF-His binding to FVIIa-R was measured by MST. In the presence of NiPCPS, sTF-His binding to FVIIa had a binding affinity of 1 nM (Figure 37A). This was higher than expected as FX chromogenic assays demonstrated a K_d in the low pM range as well as previous reports (~10 pM) when determined by a linked enzyme chromogenic assay [318]. To reconcile this discrepancy, FX was included to best mimic the conditions of the assay, with the protease inhibitor, benzamidine, to ensure no FX cleavage occurred. MST analysis revealed that FX enhanced sTF-His binding to FVIIa-R on NiPCPS by 30-fold to 30 pM (Figure 37B), which was consistent with the previously reported value.

3.6.2 sgC-His binding interactions on membranes

In comparison to vesicles without DGS-NTA-Ni, the ability for sgC-His assembled onto a membrane displayed higher affinity for FVIIa-R (

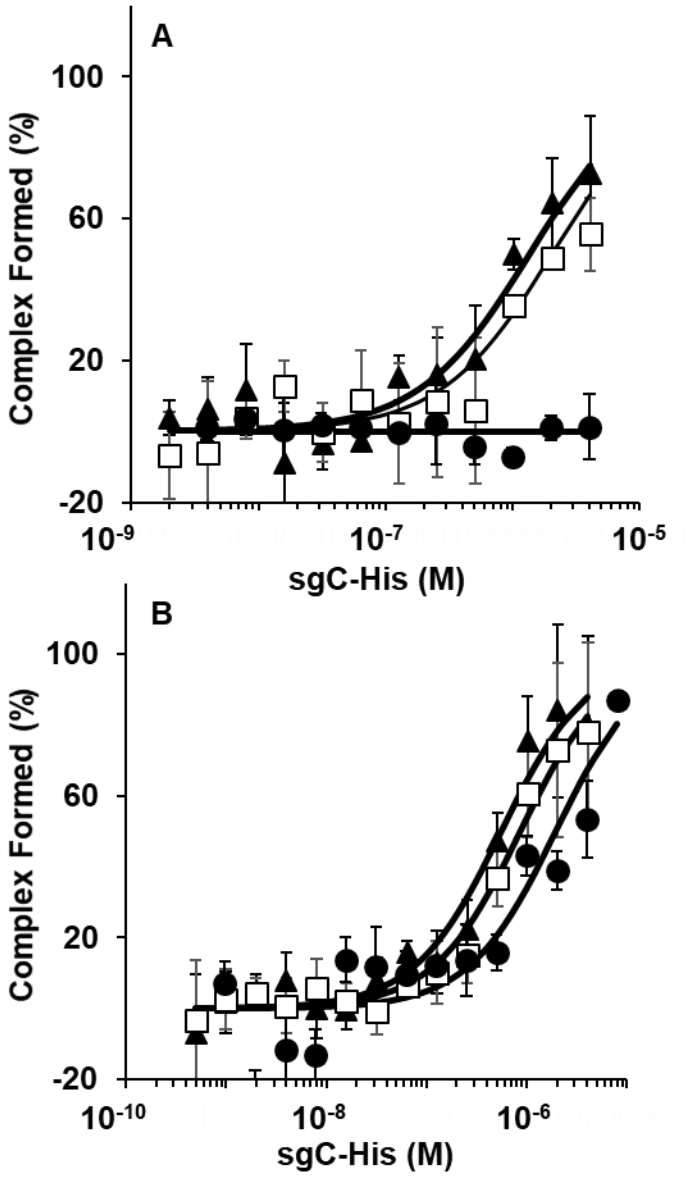

Figure 38A). This was independent of the presence of aPL, implying that a FVIIa-R-membrane interaction was not required. When sgC-His binding to Ni-chelating liposomes was facilitated (NiPC or NiPCPS), the K_d for FVIIa-R was 2.0 and 1.3 μM (Table 1). In the presence of PCPS without DGS-NTA-Ni, binding of sgC-His to FVIIa was weaker and not quantifiable. This was consistent with the solution-phase interaction in the absence of vesicles (Figure 36). The

addition of FX further increased the binding affinity of sgC-His for FVIIa-R to NiPC and NiPCPS (K_d; 0.9 and 0.6 µM, respectively) (

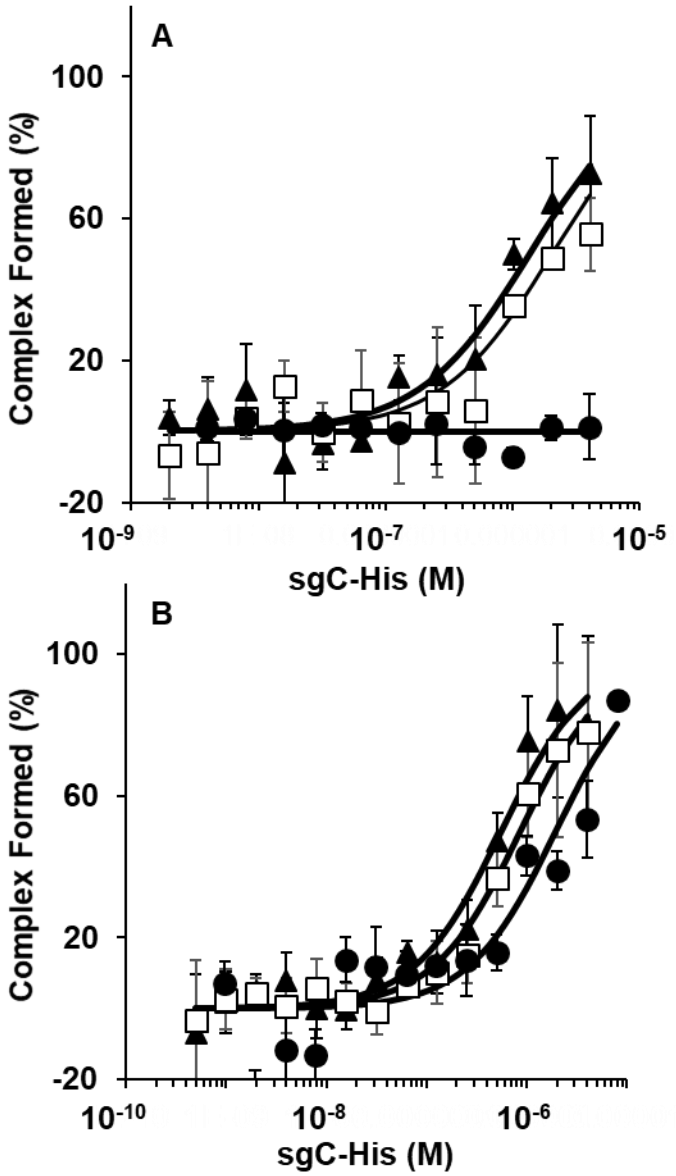

Figure 38B).

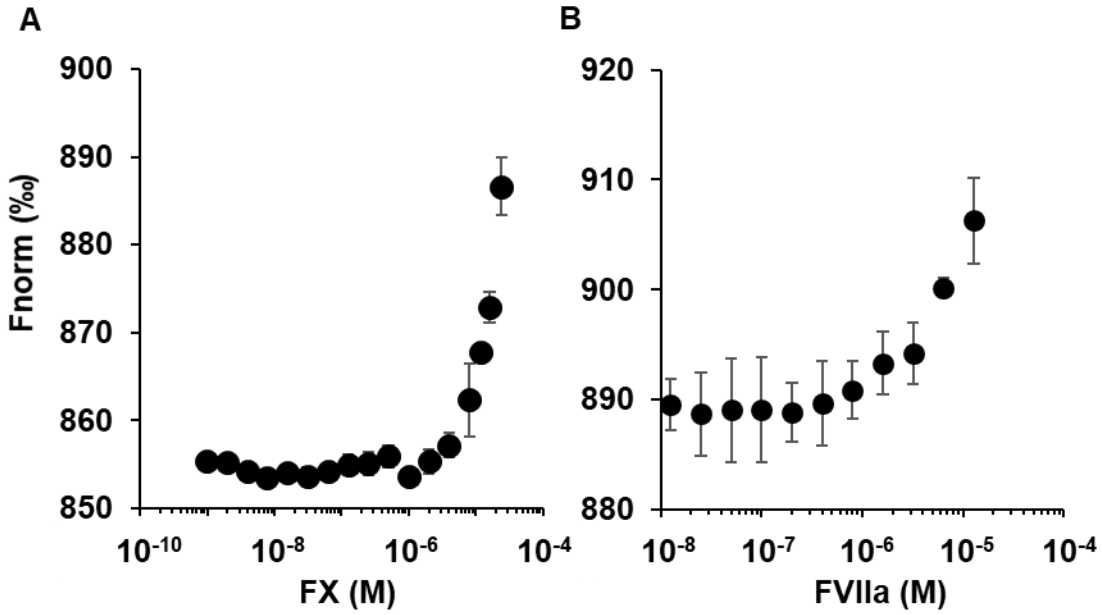

Figure 36. sgC-His can bind to FVIIa in addition to FX.

MST was used to follow the interaction between sgC-His and (A) FX or (B) FVIIa. sgC-His (200 nM) was mixed with the RED-tris-NTA fluorescent probe (3.5 nM) for 30 min at room temperature before the addition of FX or FVIIa in HBS/0.05% BSA/0.05% Tween-20/5 mM Ca^{2+}. MST power was set at medium with 10% excitation power. Samples were equilibrated at 25 °C prior to instrument reading. N = 3 independent replicates; Error bars: SEM.

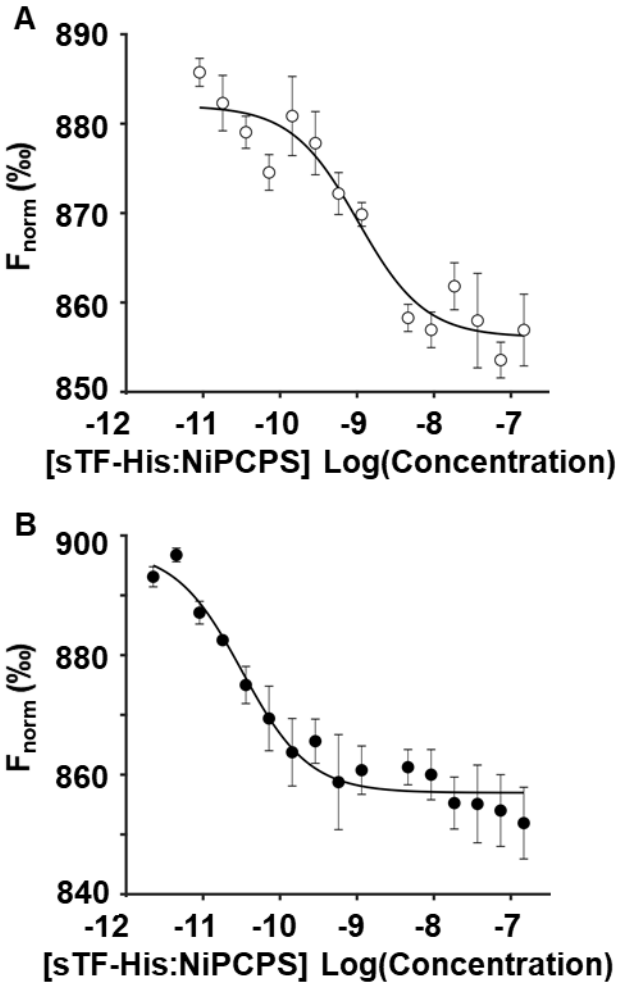

Figure 37. sTF-His binding to FVIIa-R is enhanced by FX.

MST following the interaction between FVIIa-R (1 nM) and sTF-His on NiPCPS membranes (50 µM) with $CaCl_2$ (5 mM) and benzamidine (2 mM) in the absence or presence of 30 nM FX (A and B, respectively). Concentration is in M units. N = 3 independent replicates; Error bars: SEM.

Omission of DGS-NTA-Ni from the aPL-containing vesicles reduced the overall affinity (K_d; 2.7 μM). This suggests that sgC-His-FVIIa complex formation is only enhanced by PS in the presence of FX when DGS-NTA-Ni is absent. This is consistent with the observation by others that the affinity of the Gla-domain of FX is greater than FVIIa (approximately 0.2 μM and 15 μM, respectively). In the current system, FVIIa binding to PCPS was ~65 μM as measured by MST (not shown). The Hill equation fit produced similar K_d values to the simple binding curve fit but with a better fit (as determined by r^2 value, Appendix A.3). Although the r^2 value for the latter generally indicated a superior fit, the respective K_d and half-maximal effective concentration of titrant (EC_{50}) were similar between data-fit methods. The parameters affecting binding were consequently considered based on the simplest model.

3.6.3 sgC-His/FVIIa amidolytic activity

Given the importance of FX in gC-FVIIa binding, the ability of sgC-His to enhance FVIIa activity was further investigated by following FVIIa amidolytic activity by cleavage of the chromogenic substrate S-2288 in the presence of sTF-His or sgC-His and nickel-chelating lipids (Figure 39). Consistent with the MST-derived lower K_d of sTF-His or sgC-His to FVIIa, there was no saturation of enhancement of S-2288 cleavage rate at the concentration used. sTF-His/FVIIa K_d was 1 nM (Table 4) and at 1 nM sTF-His, FVIIa amidolytic activity was not saturated. S-2288 cleavage by sgC-His/FVIIa was 3-fold less than sTF-His/FVIIa at the highest concentrations used (Figure 39B). The presence of aPL did not benefit FVIIa amidolytic activity, as was previously described [35,94].

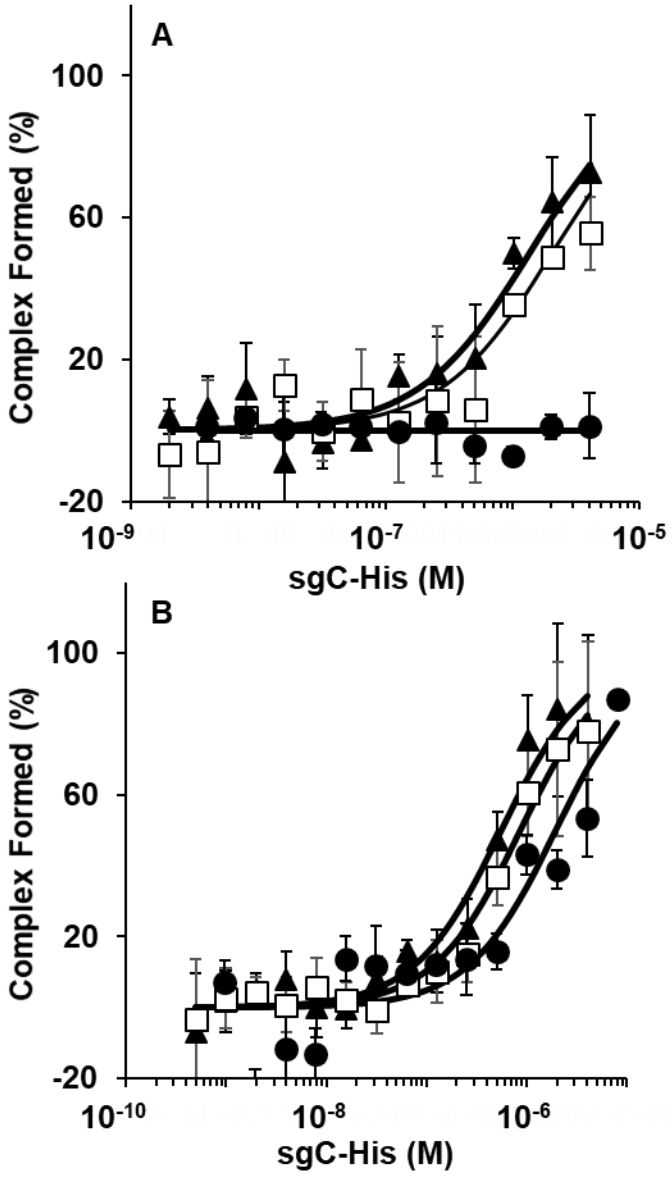

Figure 38. sgC-His interacts with FVIIa with enhancement by FX.

(A) MST was used to follow sgC-His binding to fluorescently labeled FVIIa in the presence of 50 µM PCPS (●), NiPC (□) or NiPCPS (▲). (B) Similar to (A) but with the inclusion of 30 nM FX and 2 mM benzamidine to inhibit FVIIa. N ≥ 3; Error bars: SEM.

Table 4. FVIIa-R binding affinities as determined by MST.

		No FX	With FX
Ligand	**Lipid**	**K_d (μM) (95% CI)**	**K_d (μM) (95% CI)**
sTF-His	NiPCPS	8.2×10^{-4} (8.6×10^{-5} – 1.5×10^{-3})	3.0×10^{-5} (8.0×10^{-6} – 5.2×10^{-5})
sgC-His	NiPC	2.0 (1.3 – 2.8)	0.9 (0.7 – 1.0)
sgC-His	NiPCPS	1.3 (0.8 – 1.7)	0.6 (0.2 – 0.9)
sgC-His	PCPS	>13.0	2.2 (0.9 – 3.5)
sgC-His	None	>12.0	2.9 (1.5 – 4.2)

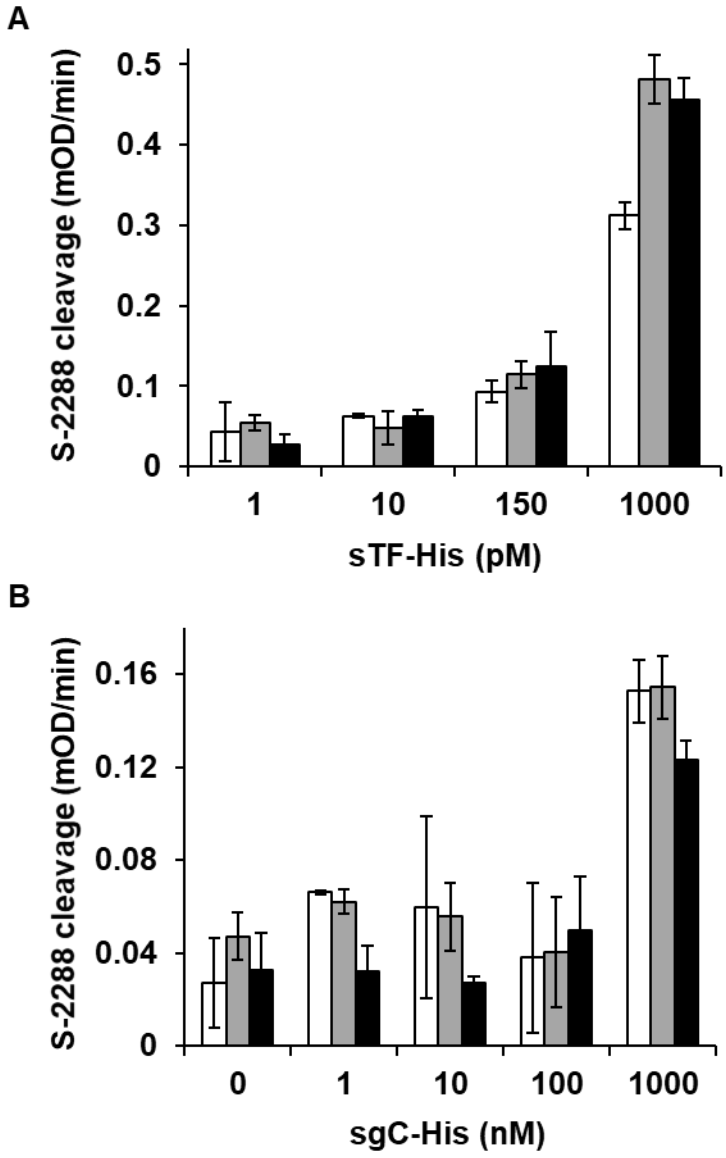

Figure 39. sTF-His and sgC-His enhancement of FVIIa amidolytic activity.

FVIIa catalytic activity was assessed by following FVIIa cleavage of the chromogenic substrate S-2288 in the presence of sTF-His or sgC-His, 5 mM Ca^{2+}, and 50 μM PCPS (white bars), NiPC (grey bars) or NiPCPS (black bars). N = 3 independent replicates; Error bars: SEM.

3.7 Coagulation initiated by HSV1

3.7.1 HSV1-mediated plasma clotting

To better understand the importance of gC and TF in the context of coagulation, plasma clotting assays were performed. The extrinsic pathway is the major initiator of clotting on TF-containing viruses as those that lack TF require at least 100-fold more virus to achieve similar clotting times in NP (Figure 40A). From my FX chromogenic assays (section 3.2.1), gC was expected to enhance TF-induced clotting in NP but no enhancement was observed (Figure 40A). However, upon removing the analogous FX activating pathway mediated by FVIII using FVIII/DP, the effect of gC in accelerating TF-mediated clotting was observable (Figure 40B). HSV1/TF-/gC- appeared to have faster clotting times in FVIII/DP than HSV1/TF-/gC+. The gC enhancing effect on TF-bearing virus was not observed in FXII-deficient plasma, suggesting that FVIII compensates for the lack of gC-mediated enhancement (Figure 40C).

3.8 Effect of glycosaminoglycans on gC

gC has been shown to bind to several sulfated GAGs. Given that the heparin-binding site deletion mutant of gC does not bind FX [241], I expected that blocking of the site would lead to decreased FX activation. Contrary to my expectations, sulfated GAGs in the presence of either sTF-His or sgC-His resulted in enhanced FVIIa-mediated FX activation (Figure 41). Unfractionated heparin (UFH) and chondroitin sulfate (CS) enhanced sTF-His/FVIIa-mediated FX activation to an identical degree, whereas low molecular weight heparin (LMWH) enhanced the most. However, this difference may be a concentration effect. The average weight of UFH and CS from commercial sources is 15 kDa whereas LMWH was 6 kDa. Taken this 2.5-fold difference into account and assuming FXa generation is not saturated, the GAGs would be identical in terms

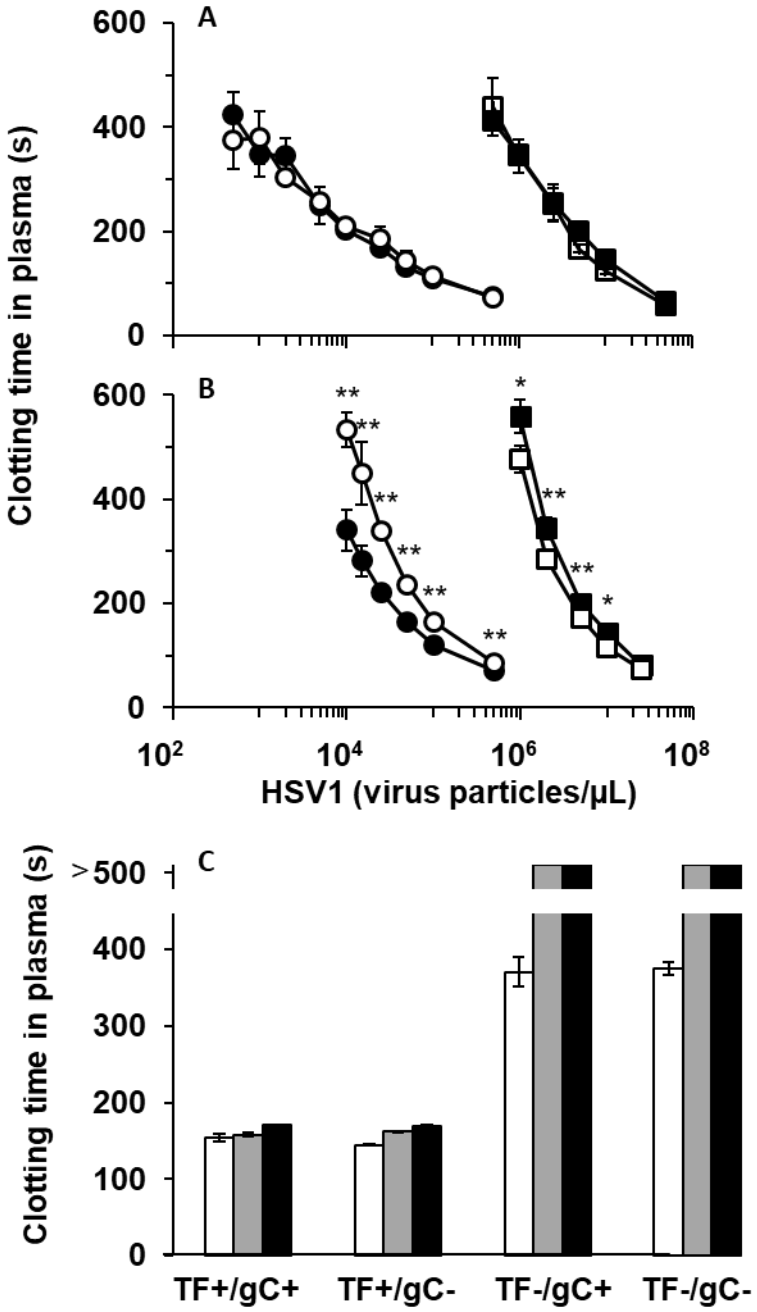

Figure 40. Plasma coagulation by HSV1 is TF-dependent.

HSV1/TF+/gC+ (closed circle); HSV1/TF+/gC- (open circle); HSV1/TF-/gC+ (closed square); and HSV1/TF-/gC- (open square) were added to either (A) NP or (B) FVIII/DP. Clotting was initiated with 5 mM $CaCl_2$. N = 4 independent replicates; Error bars: SEM; * $p < 0.05$; ** $p < 0.01$. (C) HSV1-induced clotting in NP treated with the FXII inhibitor, CTI. NP was pre-treated with 0, 50, 200 µg/mL CTI before the addition of virus (white, gray and black bars, respectively). N = 2 independent replicates, technical triplicates; Error bars: SD from pooled technical replicates.

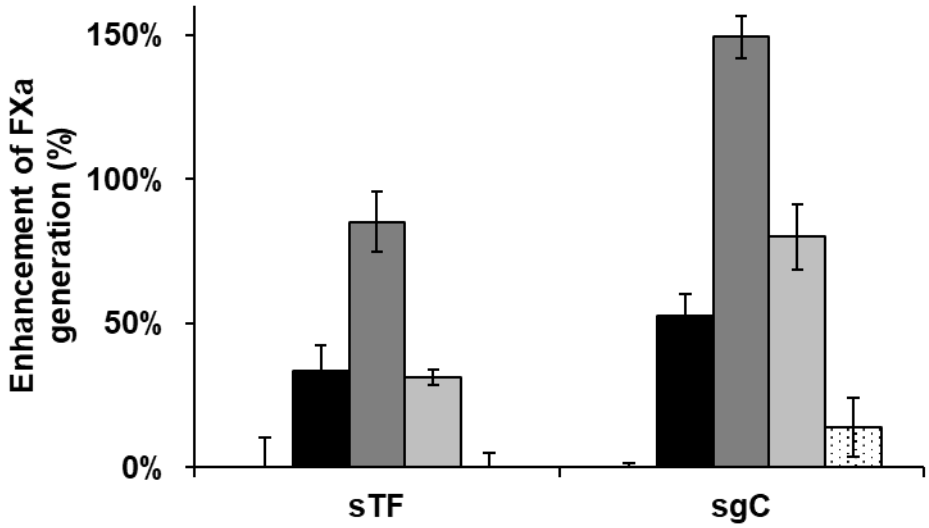

Figure 41. GAGs are procoagulant in FX chromogenic assay.

sTF-His or sgC-His with NiPCPS was pre-incubated with buffer control, 50 µg/mL unfractionated heparin (black bar), 50 µg/mL low molecular weight heparin (dark gray bar), 50 µg/mL chondroitin sulfate (gray bar) or 50 µg/mL hyaluronic acid (dotted bar) prior to the addition of FVIIa (1 nM) and Ca^{2+} (5 mM). FX (100 nM) was added to initiate the reaction. After 20 min, the reaction was stopped with EDTA. The amount of FXa formed was followed by the addition of 0.2 mM S-2765. N = 2 independent replicates, technical triplicates; Error bars: SD from pooled technical replicates.

of specific activity in the enhancement of FX activation with sTF-His. This is not true for sgC-His, where CS enhanced FX activation more than UFH ($p < 0.01$) and LMWH enhanced FX activation greater than 2.5-fold compared to UFH. Hyaluronic acid is non-sulfated and was not expected to bind or affect sgC-His function. Neither sTF-His/FVIIa or sgC-His/FVIIa-mediated FX activation was significantly affected by hyaluronic acid ($p = 0.8$ and $p = 0.08$, respectively).

3.9 Discussion

In the present study, I explored the effect of gC on TF function on the virus surface as well as in a purified, virus-free system. TF, gC and aPL were all found on a single virus particle by immunogold EM, suggesting that the three factors could work together to enhance FVIIa activity. TF was required for virus-bound gC to enhance FVIIa-dependent FX activation. Due to the minimal contribution of gC to FX activation in the absence of TF on the virus, it was speculated that gC interacted with TF to synergistically enhance FVIIa activity. However, attempts at teasing out a TF/gC direct interaction was not fruitful.

3.9.1 Interactions between TF and gC

Neither crosslinking, ELISA nor MST experiments revealed an association between purified sTF-His and sgC-His or the full-length gC and TF embedded in the virus. This suggests that another constituent on the virus surface is contributing to the enhancement of TF function by gC. Considering that gC may interact with other virus surface proteins (e.g. gB, gD, gE), several options are possible, but not detected by crosslinking. The availability of gC in concert with one of these may contribute to its ability to enhance FX activation [332]. Co-immunoprecipitation may provide novel information on a gC/TF interaction or on common binding partners of gC and TF.

gC is known to have several forms during infection. The mucin-like domain of gC contains multiple predicted O-linked glycosylation sites [246]. This domain mediates gC-GAG interaction but undergoes heterogenous post-translational modification that alters the affinity of gC to different GAGs [246,342]. TF has three glycosylated asparagine residues in its extracellular domain but these asparagine residues do not affect its function in FVIIa-dependent FX activation or protease activated receptor signaling [343,344]. It should be noted that the *E. coli* produced recombinant sTF-His does not contain any glycosylation. The lack of glycosylation may affect sTF-His interaction with sgC-His. However, our crosslinking experiments using viruses containing full-length (and presumably glycosylated) TF did not demonstrate gC interactions. Perhaps the choice of a shorter or a more flexible crosslinker may reveal missed interactions.

A small subset of gC could interact with TF through their N-linked glycans via the mucin-like region of gC to affect TF/FVIIa function. The use of Sf9 insect cells may result in a different glycosylation to that of human origin, even though this recombinant expression system was developed because of high yield and similarity to human glycosylation patterns. Furthermore, conformational antibodies confirmed proper gC conformation, implying there is no effect conferred by altered glycosylation compared to the human protein [320]. Nevertheless, this putative difference in carbohydrate may affect the coagulation cofactor function of gC expressed on the purified virus produced in mammalian cells, versus that generated in insect cells. There is no evidence in the literature that suggests TF can bind to GAGs. If a TF-GAG interaction existed, GAGs could mediate an interaction indirectly between TF and gC. The preliminary evidence from section 3.8**Error! Reference source not found.** indirectly implies a potential mechanism.

Heparin is well known in antithrombin-mediated inactivation of clotting proteases but in the absence of antithrombin, heparin is procoagulant [345]. As sulfated GAGs are highly

negatively-charged, they can bind to numerous molecules (e.g. antithrombin, selectins, fibronectin) [346]. The size of the sulfated GAGs may act as a scaffold for which FVIIa [347] and FX can bind [348]. Like many GAG-interacting proteins, gC does not bind to the non-sulfated GAGs such as hyaluronic acid [246]. The lack of FXa generation enhancement by hyaluronic acid supported the importance of sulfate groups and the notion of a protein-GAG scaffold. In the current work, GAGs increased the cofactor activity of sgC-His more than sTF-His, this would suggest that GAGs bridge sgC-His to FVIIa/FX. But, a quaternary complex of gC/FVIIa/FXa/heparin and the effect of heparin-dependent inhibitors such as antithrombin in plasma may be interesting to explore.

3.9.2 Nickel-chelating lipids as a tool for discovery

The ability of sgC-His to enhance FVIIa-mediated FX activation in the absence of TF was demonstrated through FX chromogenic assays as well as plasma clotting assays. The use of nickel-chelating lipids provided a method of studying sgC-His function. The advantages over full-length expression is that soluble proteins require less manipulation of the protein (e.g. denaturation and refolding) and the purification process is simpler as they are secreted. One downside to this approach is the added complexity of the binding interaction between the histidine-tagged protein and the nickel-chelating lipid results. The head group of the DGS-NTA-Ni is slightly elongated compared to that of PS and PC (Figure 14), and only carries a single nickel ion resulting in a micromolar binding affinity. A single DGS-NTA-Ni can coordinate with two histidine residues. The lack of difference between sTF-His (His_6) and sgC-His (His_5) binding to phospholipid (Table 2) would suggest that the same ratio of DGS-NTA-Ni is coordinated with the His-tag. As the affinity of sTF-His or sgC-His (~5-7 μM for DGS-NTA-Ni) is similar to that of His_6 tags to NTA-

Ni (10 μM) [349], it is most probable that both sTF-His or sgC-His are bound to the same ratio of DGS-NTA-Ni. Another factor to consider is the distribution of DGS-NTA-Ni on the vesicle membrane. Gla domain-binding to PS can result in an umbrella covering of DGS-NTA-Ni. The Gla domain of FVIIa occupies approximately six phospholipid molecules but when complexed with TF, the total area the complex envelops expands to 23-26 phospholipid molecules [297]. DGS-NTA-Ni made up 15% of the vesicles, giving ~4 DGS-NTA-Ni per TF/FVIIa surface area. For multiple Ni^{2+} ions to co-ordinate with a single His-tag, the lipids need to be within proximity of one another. Other laboratories have used Tris-NTA derivatives, that chelate three nickel ions. This increases His-tag affinity to a K_d in the nanomolar-picomolar range with the caveat of a bulkier head group [247]. This larger head group could potentially impact protein-membrane interactions but would otherwise ease the difficulties of easily dissociable low affinity nickel-histidine interactions.

3.9.3 Microscale thermophoresis

The use of MST allowed for better understanding of complex formation(s). The non-covalent histidine-tag fluorophores provided information on the binding partners for sgC-His. This technique allowed the first demonstration that sgC-His interacts directly with FVIIa. The low cost and low reagent use, as well as the flexibility of manipulating components (e.g. inclusion of anti-adsorptive materials or splitting of capillary tubes) made MST an attractive tool for investigating protein interactions.

3.9.4 gC interaction with FVIIa

FVIIa/sgC-His complex formation as determined by MST is ~10-fold weaker than determined by chromogenic assay. Labeled FVIIa retained most of its activity and the degree of labeling suggested that only one lysine was labeled. It is, however, unknown whether the same lysine residue was labeled. Benzamidine was added to prevent cleavage of FX and did not affect sgC-His binding to FVIIa in the absence of FX as measured by MST (data not shown). Binding experiments by laboratories using other methods had difficulty corroborating demonstrating affinity in the pM Kd range due to the limited sensitivity of their nM experimental approaches [341]. One group used surface plasmon resonance (SPR) with relipidated TF and measured a pM K_d [341] that was very similar to that obtained by enzymatic assays or fluorescence anisotropy [94,350,351]. However, the TF/FVIIa/aPL complex did not dissociate significantly over the course of the measurement. This causes concern into how an accurate K_d could be derived, which was recognized by the authors. In the current study, the binding affinity of sTF/labeled-FVIIa/FX on a NiPCPS membrane measured by MST approached values (K_d = 32 pM) determined by enzymatic assays.

FVIIa/sgC-His complex formation was greatly enhanced in the presence of FX in the absence or presence of PCPS, suggesting that PS was not required for forming the FVIIa/sgC-His/FX complex. The inclusion of a Ni tether for sgC-His was essential for detectable FVIIa/sgC-His formation in the absence of FX. FX could compensate for a lack of Ni-mediated sgC-His membrane binding. This is consistent with the observation by others that the affinity of the Gla-domain of FX is greater than FVIIa (approximately 0.2 µM and 15 µM, respectively) [29,30]. This suggests that PS contribution to the overall complex is predominantly attributed to the FX Gla-domain interaction.

A discrepancy was observed here between MST-derived binding of sgC-His to FVIIa/FX in the absence of DGS-NTA-Ni compared to linked-enzyme derived values. The addition of DGS-NTA-Ni to PC or PCPS increased binding affinity by 2.7- and 7-fold, respectively. Yet, enzymatic activity increased 8- and 40-fold, respectively (Figure 28). While the qualitative enhancement is consistent between techniques, a possible explanation for quantitative discrepancy is the difference in experimental temperature, 25 °C vs 37 °C for MST and enzymatic, respectively. Lower temperatures can affect TF/FVIIa function, with a 60% decrease in FXa generation at 24 °C compared to 37 °C [352]. Furthermore, FVIIa-R retained 85% of its FX activating ability with sgC-His. The remaining difference in sgC-His/FVIIa-R/FX binding versus activation on NiPCPS suggests PS could play a larger role in substrate recognition and proteolytic cleavage by sgC-His/FVIIa than MST binding experiments can distinguish.

The ability of sTF-His to substantially enhance S-2288 cleavage by FVIIa unlike sgC-His suggests the latter requires FX binding to affect FVIIa function. This phenomenon is similar to tPA cleavage of plasminogen [353]. The cofactor, C-terminal lysines on fibrin, allows for the substrate (plasminogen) to bind along with the enzyme (tPA). sgC-His binding to the substrate, FX, improves the interaction of sgC-His with FVIIa. This could be due to conformational changes in sgC-His upon FX binding that allow for a tighter sgC-His/FVIIa interaction, sgC-His better presenting FX as a substrate for FVIIa, or FX providing a binding site for FVIIa enhancing the apparent affinity by avidity effects. The latter seems unlikely as I would have expected sgC-His to act in concert with TF to enhance FX activation. In addition, sgC-His/FVIIa can support FX activation to a similar catalytic efficiency as TF/FVIIa when tethered to NiPCPS. This suggests that sgC-His, like sTF-His, can stabilize FVIIa in its active configuration [35,354,355].

These data could steer new forms of procoagulant drugs for the treatment of hemophiliacs or to combat bleeds in a controlled manner. To accomplish this, a structure of gC, which has remained elusive, would be instrumental to designing a mimetic. A crystal structure with FVIIa and/or FX may stabilize gC and allow for a solvable structure, similar to that which has been done with sTF/FVIIa.

3.9.5 gC procoagulant activity in infection

During the later stages of HSV-1 infection of cells, gC can be efficiently secreted from the cell due to intron splicing within the transmembrane domain of gC [356]. This soluble form of gC could play a role in haemostasis similar to sgC-His. For sgC-His to effectively function, it would require either high local concentrations or a surface to tether and orient itself. Our findings that the addition of sgC-His to HSV1 enhanced its FVIIa-dependent FX activation, suggests that sgC-His is capable of binding to the virus envelope. The partner of this interaction is still unknown although I initially speculated that this may be TF. Coagulation induced by sgC-His in plasma was achievable when NiPCPS was present. This phenomenon required high concentrations of sgC-His which is much greater than expected, as determined by FX chromogenic assays. As most adults in the human population have HSV1, I tested whether antibodies against gC existed in the plasma samples. Indeed, the plasma samples used in the experiments contained anti-HSV1 antibodies that could recognize sgC-His. The presence of these antibodies may explain the need for high amounts of sgC-His to initiate coagulation in these purified experiments.

Human endothelial cells increase TF expression on their surface during viral stimulation. HSV1 is known for its wide cell tropism. But in cells that lack inducible TF expression, could gC replace the procoagulant function of TF? gC was shown to be expressed on the cell surface during

infection and could bind to FX [240], suggesting that gC plays a role in protease activation on the cell surface. PAR activation could contribute to virus propagation. PAR activation can promote Rab5a expression [357]. Rab5a has been positively linked to HSV1 envelopment and subsequent virus production and secretion [358,359].

3.9.6 Coagulation initiated by HSV1

Enhancement of plasma clotting was evident when TF was present on the virus. Though the role of gC was not discernible in NP, gC enhancement was demonstrated in FVIII/DP. This could suggest a mechanism in HSV1/TF+/gC- that makes use of the amplifying pathway. What was not considered in the experiment was the presence of antibodies against HSV1. Antibodies against HSV1 could result in antibody-mediated complement activation or crowding of antibodies/complement on the virus surface. Complement complexes are large and may prevent clotting protease assembly on the virus surface. As gC inhibits complement protein C3b, it is expected that steric factors due to complement protein assembly would not occur. Thus, gC+ viruses should clot faster than gC-deficient viruses. HSV1/TF-/gC- virus clotted faster than HSV1/TF-/gC+, this has implications.

The putative antibody-mediated complement activation or crowding did not cause a decrease in clotting protease complex formation. The gC- virus is a selective mutant that does not express gC on the infected cell surface and lacked the ability to inhibit complement activation on the virus surface. The faster clotting in FVIII/DP with the mutant strain compared to wildtype could suggest that gC binding to C3b prevents FX interaction on the virus surface. However, if this were true, I would expect the same effect in NP which was not the case. Rather, crowding of proteins on the limited virus surface may play a bigger part in this discrepancy. Experiments using

HSV1 seronegative plasma are required to conclude the role of antibodies and complement on HSV1-mediated clot formation. gC could be playing another role in haemostasis. It is also possible that gC affects coagulation downstream of FX activation. Evidence that FXa remained bound to gC after activation was presented in previous work from the Pryzdial laboratory [241]. It is unknown whether gC prevents FVa association with FXa, thereby interfering with thrombin generation. This could also explain why HSV1/TF+/gC+ does not have faster clot formation than HSV1/TF+/gC- in NP. In this manner, the virus can "escape" being bound by a clot and perhaps make use of the PAR activation ability of FXa and/or FVIIa, rather than thrombin.

An unexpected result was that the HSV1/TF+/gC+ was different to HSV1/TF+/gC- in terms of TF and MCP expression per virus particle. The difference could imply that the virus replicates differently, even though the viruses were grown in the same cell. The gC mutant produces a truncated form of gC that is not expressed on the infected cell surface or virus surface and does not exhibit C3b inhibition [360,361]. Although the structure of the gC mutant has not been elucidated, it was speculated that the mutant gC left a "stub" that occupies transmembrane space in the virus envelope, helping to maintain a virus particle surface configuration similar to wild-type virus. Whether this mutant gC affects cellular processes (e.g. envelope formation or TF expression) during infection is not known. Nonetheless, TF on the virus was the main initiator of clot formation and gC enhanced this function.

Chapter 4: Tissue factor on enveloped viruses

To expand the Pryzdial model of TF on enveloped viruses from the *Herpesviridae* family to a more general model encompassing many enveloped viruses, I investigated DENV and HCV of the *Flaviviridae* family of viruses, as well as HIV of the *Retroviridae* family of viruses. These each pose a significant threat to healthcare and blood transfusion systems around the world. Although DENV affects more than half the world's population and is a large healthcare burden, DENV is not endemic to Canada. However, parts of the Eastern US were predicted to be suitable habitats for *Aedes aegypti* and *Aedes albopictus*, two major mosquito vectors for DENV [362]. *Aedes albopictus* in particular was estimated to be capable of establishing near Southern Canada. The vector was rarely spotted in Southern Ontario [363] until the past few years where sightings have grown [364,365]. Furthermore, the close relative and arbovirus, West Nile virus (WNV), has been found in many mosquito vectors endemic to Canada [363,366,367]. WNV is an immediate threat, having resulted in over 5000 confirmed cases and 243 deaths in Canada [367,368]. WNV is classified as a Containment Level 3 pathogen whereas DENV is a Containment Level 2 pathogen in Canada. Thus, DENV is highly relevant to Canada and WNV work, less restrictive to work with, and an appropriate *in vitro* model before investigating other enveloped viruses.

The aims of this study are: a) to determine the presence of TF on purified cell culture-derived DENV; b) to establish TF function on purified cell culture-derived DENV; and c) to investigate whether TF is found on patient-derived viruses.

4.1 Tissue factor presence on purified dengue virus

It was expected that cultured DENV could obtain TF from their cell source, Vero kidney epithelial cells, similar to herpesviruses [2,258]. Picomolar amounts of TF can support enhancement of FVIIa activity, as demonstrated in section 3.4 and by others [32,94,318]. Furthermore, femtomolar amounts of TF can accelerate clotting in plasma [369]. Thus, two methods were used to determine if TF was present in the purified DENV samples: FX chromogenic assay and plasma clotting assay.

4.1.1 FVIIa-mediated FX activation

TF activity on purified DENV was investigated by enhancement of FVIIa-mediated FX activation in a chromogenic assay. DENV2 was chosen in all experiments as this serotype is the most common [370–372]. FVIIa-mediated FX activation was enhanced in a concentration-dependent manner by DENV. To demonstrate that TF on the virus is contributing to this effect, a TF/FVIIa-specific inhibitor, NAPc2, was used. NAPc2 binds FX at an exosite as a scaffold to bind TF/FVIIa, thereby preventing FX activation but having a minimal effect on FXa amidolytic activity [373]. NAPc2 completely inhibited FXa generation by DENV. In addition, the inhibitory TF antibody, TF8-5G9 [322], resulted in a >90% decrease in TF activity.

4.1.2 TF-mediated plasma clotting

To further support the presence and function of TF on purified DENV, a plasma clotting assay was carried out. Here, the virus concentration-dependent increase in FX activation observed in the chromogenic assay resulted in decreased clotting times in NP (Figure 43). Either NAPc2 (10 nM) or TF8-5G9 (100 µg/mL) significantly reduced plasma clotting. It should be noted that

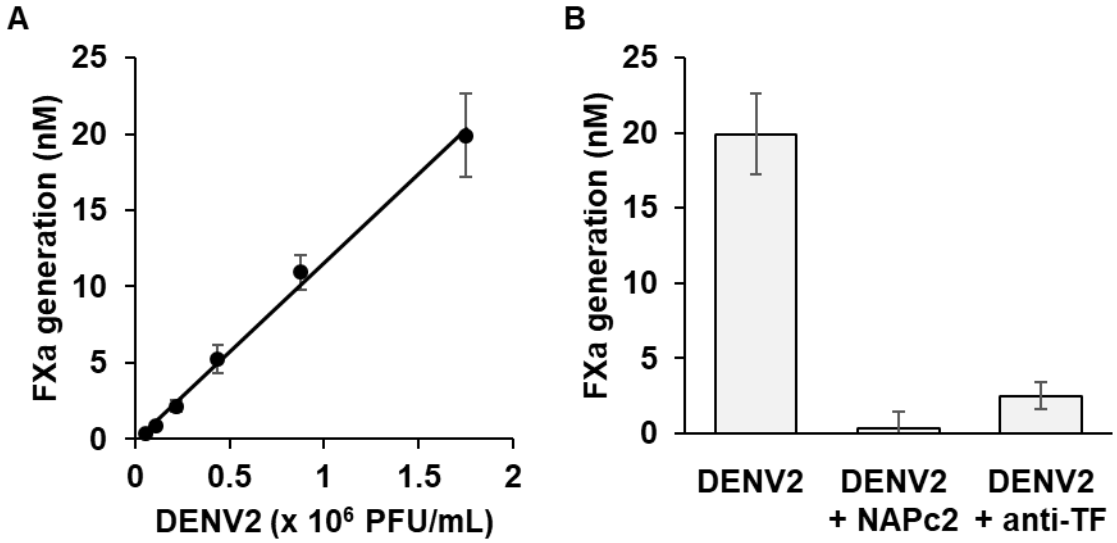

Figure 42. TF on DENV enhances FVIIa-mediated FX activation.

(A) FXa generation by FVIIa was followed in the presence of TF-bearing DENV2. (B) 2 x 10^6 PFU/mL DENV was pre-treated with or without the TF/FVIIa inhibitors, NAPc2 and inhibitory antibody 5G9 (anti-TF). FVIIa (1 nM) was added with $CaCl_2$ (5 mM) and the reaction was initiated with the addition of FX (100 nM) at 37 °C. N = 3 independent replicates. Error bars: SEM.

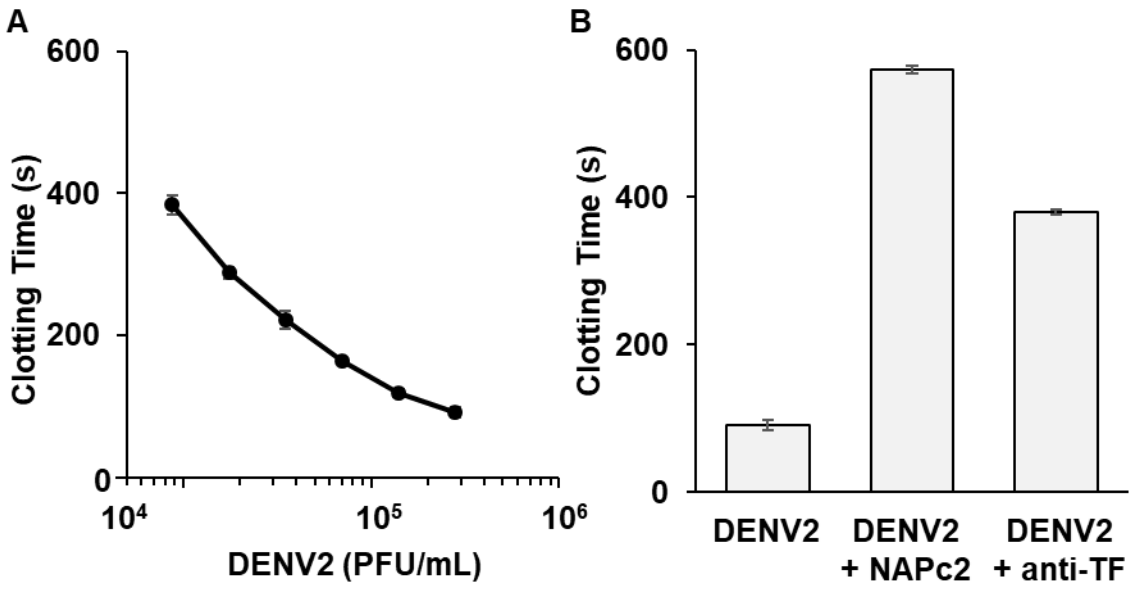

Figure 43. DENV-initiated coagulation is TF-dependent.

(A) Clotting was initiated by DENV in NP. (B) The TF/FVIIa inhibitor NAPc2 (50 nM) or TF8-5G9 anti-TF (100 µg/mL) was pre-incubated with DENV2 prior to the addition of NP. 5 mM $CaCl_2$ was added to initiate clotting. N = 4 independent replicates. Error bars: SEM.

TF8-5G9 was selected due to its ability to immediately inhibit TF/FVIIa complexes without the need of pre-incubation in plasma [322]. The presence of TF in purified DENV preparations was attempted to be confirmed through Western blot. However, possibly due to the low titres of DENV or conversely, low TF abundance, a conclusive TF band could not be demonstrated. Still, more sensitive assays unequivocally supported the presence of TF function in the purified DENV preparations. However, this does not confirm that TF is found directly on the DENV surface.

4.1.3 Immunogold EM

As in section 3.2, I used immunogold EM to determine if a virus particle contains TF. aPL was initially investigated; however, the size of virus particles (~50 nm) was anticipated to be prohibitive towards effective triple labeling strategies due to steric limitations caused by primary and secondary probes. Furthermore, the literature supports phosphatidylserine presence on dengue virus [374] and HIV [375]. HCV contains less than 1% PS [376] but may interact differently with coagulation factors or other aPL-binding proteins [377]. Thus, TF presence on these viruses was the primary investigation as they constitute novel knowledge.

Immunogold EM was performed to determine the presence of TF on purified DENV (Figure 44). TF was indeed identified. The isotype controls displayed inconsequential non-specific binding of the antibodies or probes. aPL was also confirmed to be present on the virus envelope. DENV possessed accessible aPL as the absence of calcium failed to show any calcium-independent binding of annexin V to DENV. TF and accessible aPL on the envelope are important for the function of TF-initiated FX activation. Even though triple-labeling precluded positive results (not shown), TF and aPL were most likely present on the same virus particle as both are required for the FVIIa-dependent activation of FX.

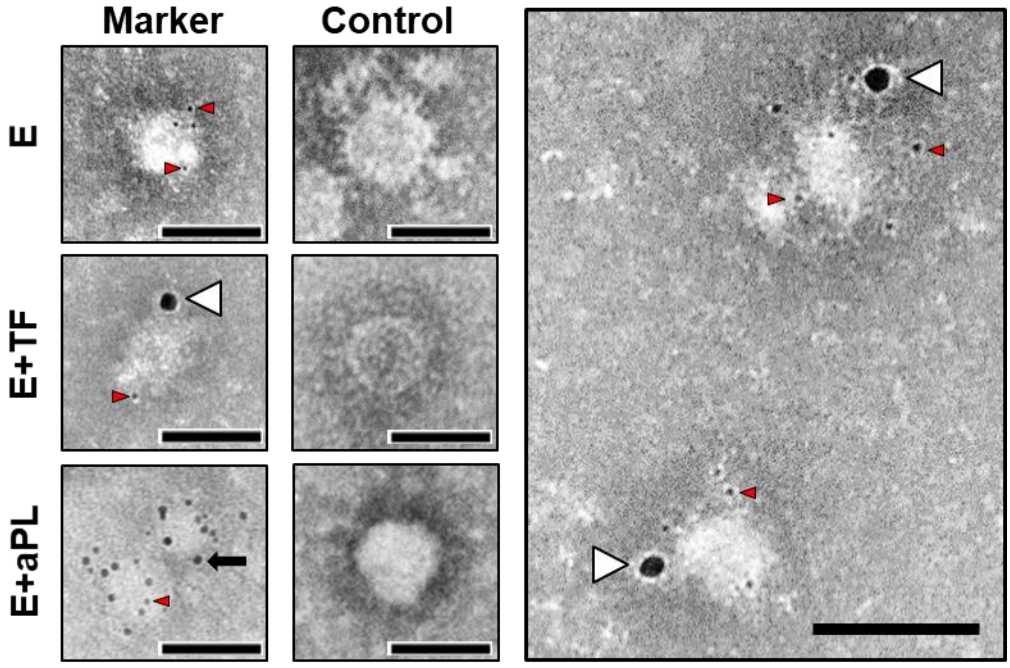

Figure 44. TF and aPL are found on DENV.

Differential immunogold EM showing DENV labeled with biotinylated-annexin V (aPL marker) and anti-TF. Specific virus-encoded proteins were detected with anti-DENV E-protein. To differentiate molecules, 6, 10 or 15 nm gold-conjugated 2º antibodies were used to label for E protein (red arrowheads), aPL (black arrow) and TF (white arrow heads), respectively. Grids were negatively stained with 2% phosphotungstic acid. Scale bar = 50 nm.

4.2 Prevalence of tissue factor on patient-derived viruses

To confirm the findings of TF on cell culture-derived viruses is applicable to a clinical scenario, viremic plasma specimen were evaluated for TF using immunogold EM. For this study HIV and HCV were selected as they are more easily obtainable in comparison to dengue due to their ability to establish chronic infections and their incidence in our local community. These two viruses are also very important blood-borne pathogens that affect our healthcare, blood supply and blood products. In addition, their links to thrombotic diseases hint at a possible dysregulation of TF activity [301,310,311].

The initial technique employed was the centrifugation method (section 2.2.4.1). The advantage of this technique was the formation of a pellet that could be resuspended in any volume to load onto an EM grid. This technique showed promise in cell culture-derived HSV1 with controls showing little to no background (Appendix A.4). However, in cell culture-derived DENV and in patient-derived HCV, there was overwhelming background (not shown). This was most likely due to excessive unbound gold-labeled antibodies that prohibited distinct immune-pelleting. This did not occur for HSV1, because the virus is much larger, facilitating differential centrifugation due to more copies of antigen per virus. Rather, the immunocapture technique was used as it overcame the issue with excessive non-specific binding of antibodies to the grid.

4.2.1 HIV and TF

HIV from viremic patient plasma was immunocaptured onto a virus antibody-coated EM grid and probed for TF and the virus-specific gp120. Anti-HIV gp120 antibodies were adsorbed onto the EM grid as capture antibodies for HIV. Gold particles directly conjugated to antibodies recognizing TF and gp120 were used as the detecting antibodies. gp120 was chosen due to its

relative exposure on the viral envelope compared to the gp41 transmembrane protein that anchors gp120. HIV was detected by EM and was demonstrated to possess TF on its surface (Figure 45A). The negative controls did not demonstrate any binding of the antibodies to virus-like-particles (VLPs) (Figure 45B). Of note, patient plasma contained a wide range of VLPs of sizes 30 nm to 200 nm, some of which labeled positive for TF and/or gp120. Thus, the size and the number of TF and/or gp120-containing vesicles were counted in randomly selected EM fields to quantitatively describe the population of these VLPs. Purified HIV diameter varies greatly in the literature, ranging from 90 to 200 nm [378–380]. Sizes 90 to 160 nm were chosen to represent HIV particles [378] and the upper limit was lowered to narrow the wide size range and segregate VLPs into different populations to facilitate quantification. Examples of the three populations: 30 nm to 90 nm, 90 nm to 160 nm, and larger than 160 nm are depicted in Figure 45.

Approximately 40%, 50% and 10% of VLPs were not labeled with either gp120 or TF (30 nm to 90 nm, 90 nm to 160 nm, and larger than 160 nm, respectively) (Figure 46). Approximately half of the VLPs expressed only gp120, with <15% expressing only TF. Of all HIV1 particles (gp120-labeled and within 90 to 160 nm), 10% were positive for both TF and gp120. ~20% of gp120-labeled VLPs expressed TF. Interestingly, this percentage remained approximately constant in all populations of VLPs.

4.2.2 HCV and TF

HCV patient plasma was probed for TF and the virus marker E2 protein. HCV encodes E1 and E2 envelope proteins that form a heterodimer on its surface [381]. E2 is twice the molecular weight of E1 (70 vs 35 kDa) [382,383] and therefore likely occupies a larger space on the virus envelope. Thus, E2 was chosen as a virus marker in patient plasma.

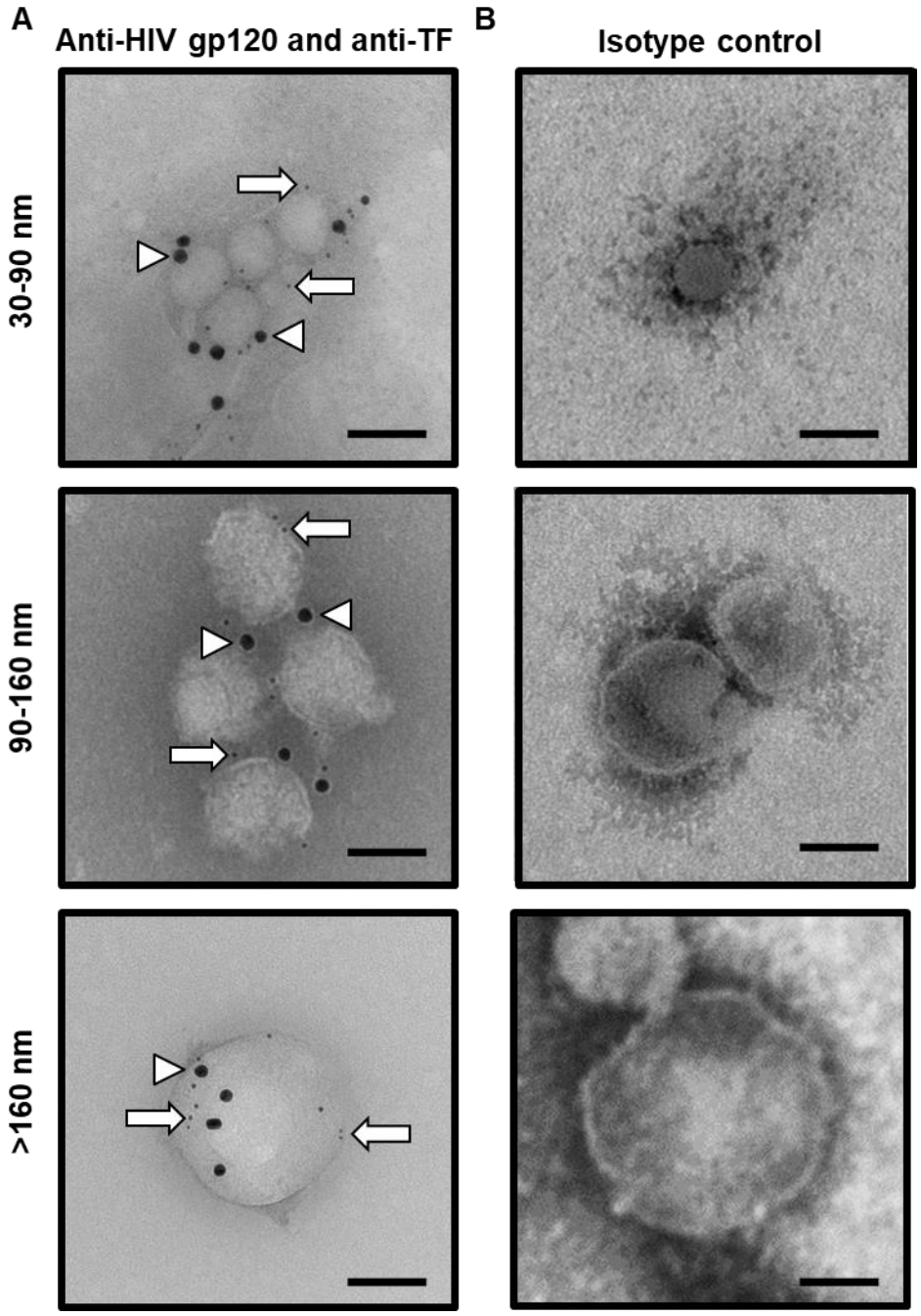

Figure 45. HIV harbors TF on its viral envelope.

Immunogold EM of HIV in patient plasma. HIV was captured onto EM grids with anti-gp120 antibodies and subsequently probed for TF (arrows; 6 nm gold bead) and gp120 (arrowhead; 15 nm gold bead). Isotype antibodies were used as a negative control. Scale bar: 100 nm.

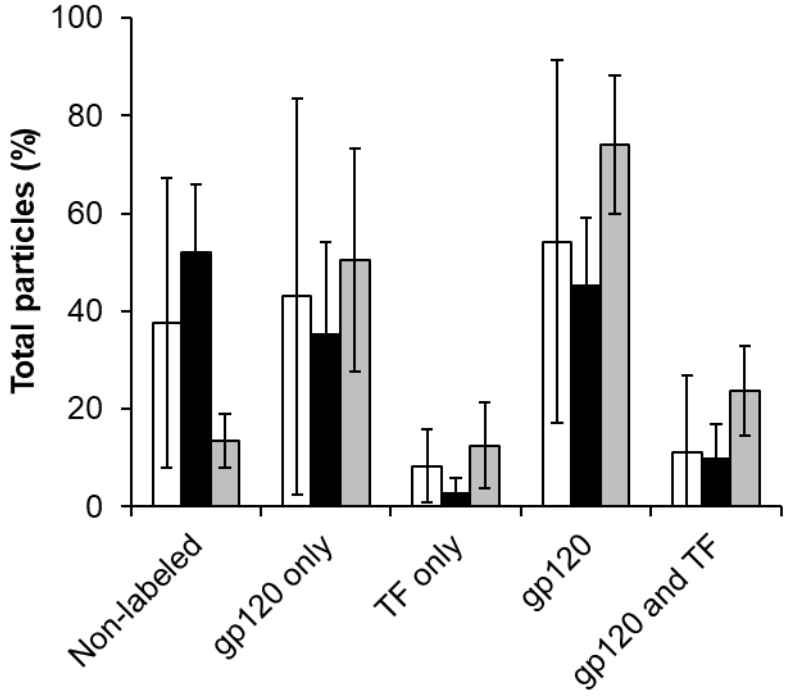

Figure 46. Patient-derived HIV displays a heterogenous phenotype.

Different sizes of VLPs were characterized as being labeled with or without HIV gp120 and/or TF. The three sizes were: 30 to 90 nm (empty bars); 90 to 160 nm (black bars); and larger than 160 nm (gray bars). N = 3 independent replicates. Error bars: SEM.

HCV particles were separated into two populations, 30 to 80 nm and 80 to 200 nm. The former was defined in previous literature as purified HCV [384] and the latter encompassed a larger range as described in patient-derived VLPs [385]. Both populations of HCV particles were shown to harbor TF on their envelope surface (Figure 47A and B). Isotype controls displayed inconsequential non-specific binding (Figure 47C). Interestingly, there was a population of particles, presumably low-density lipoprotein (LDL)-associated HCV [385], that were resistant to antibody labeling (Figure 47D). The morphology of these LDL-associated HCV are consistent with those seen in other patient-derived HCV [385].

Approximately 30% and 40% of VLPs were labeled with E2 (30 to 80 nm and 80 to 200 nm, respectively, Figure 48). Of those E2-expressing populations, ~10% and ~20% also express TF, respectively. Unlike HIV, the increase in HCV VLP size resulted in an increased proportion of TF expressing VLPs.

4.3 Discussion

As with my work on herpesviruses, TF presence on cell culture-derived DENV confirmed the ability of enveloped viruses to obtain transmembrane coagulation proteins. Even though cellular TF function is restricted by encryption and accessibility to plasma proteins, here TF on the DENV envelope was functionally active in both FVIIa-mediated FX activation and in extrinsic pathway initiation of coagulation. These results supported the endeavor of searching for TF on patient-derived viruses.

The findings that HIV as well as HCV incorporate TF onto their envelope are exciting and could explain their contribution to hypercoagulability [300,310,311]. Approximately 20% of discernible HIV and HCV particles expressed TF. Since not all particles expressed TF, this may

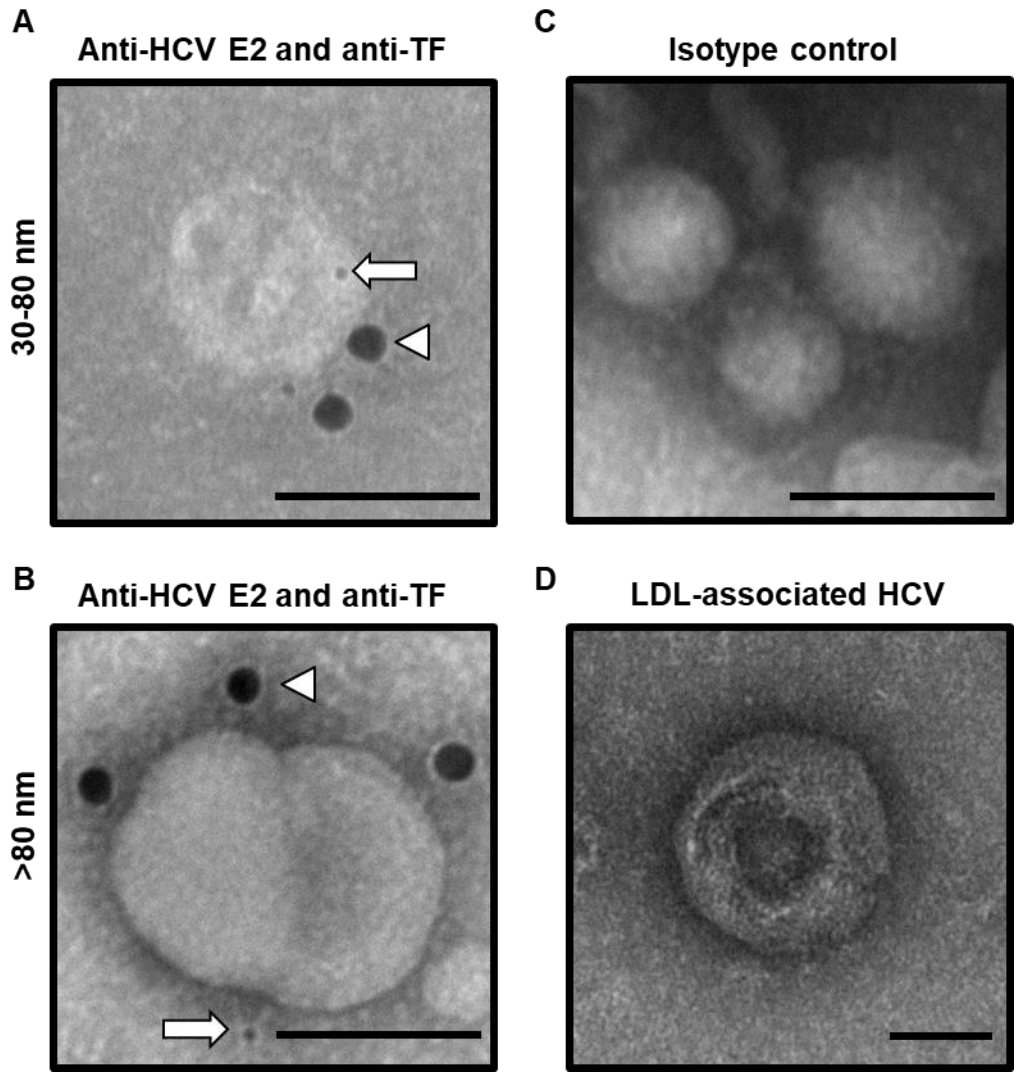

Figure 47. Patient-derived HCV expresses TF on its surface.

Immunogold EM of HCV in patient plasma. HCV was captured onto EM grids using anti-E2 antibodies and subsequently probed for TF (arrows; 6 nm gold bead) and E2 (arrowhead; 15 nm gold bead). Isotype antibodies were used as a negative control. Low-density lipoprotein (LDL)-associated HCV is also depicted. Scale bar: 100 nm.

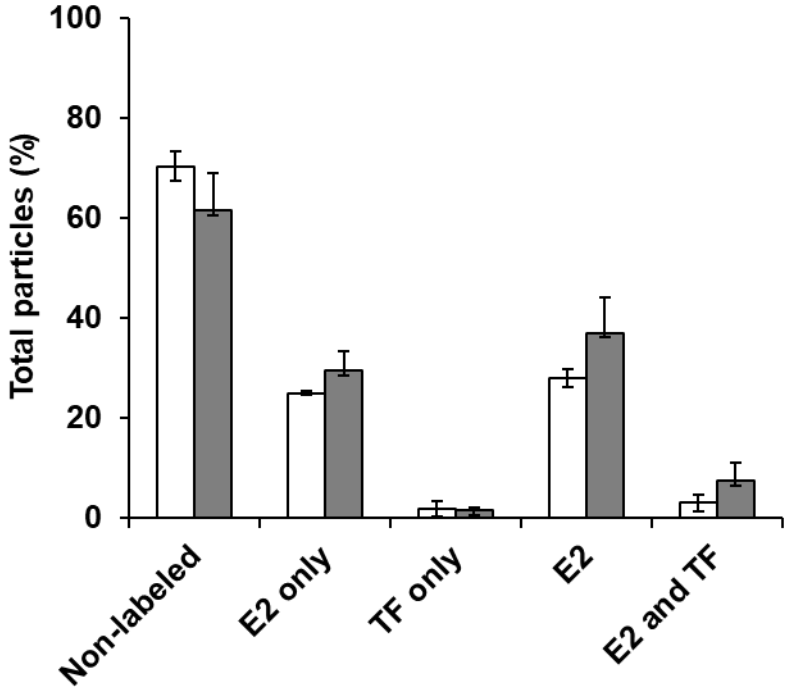

Figure 48. Phenotypes of HCV particle population.

Different sizes of VLPs were characterized as being labeled with or without HCV E2 and/or TF. The two sizes were: 30 to 80 nm (empty bars); and 80 to 200 nm (gray bars). N = 3 independent replicates. Error bars: SEM.

suggest that the viruses are antigenically heterogenous in patients and perhaps derived from several sources of infected cells, some of which express TF and others may not. Another explanation could be TFPI inhibition of TF/FVIIa on the virus, thereby masking recognition of TF by the antibody. TF function was not assessed, however, one study demonstrated that untreated HIV-positive individuals have higher TF-expressing microparticle procoagulant activity than treated HIV-positive individuals [312]. They speculated that these TF-expressing microparticles originate from monocytes. Monocytes are known to be infectible by HIV [198]. As microparticles range in sizes of 100 to 1000 nm in diameter [386] and HIV particles range in sizes of 90-200 nm in diameter [378–380], it may be possible that HIV co-exists with, masquerades as or is mistaken for a microparticle.

As DENV was demonstrated to possess TF in cell culture, there were attempts at probing viremic DENV individuals for TF expression. The prior immune-depletion strategies were not successful. However, there were small non-labeled VLPs of ~50 nm, consistent with the size of DENV in cell culture. Other modifications to the protocol included the use of heparan sulfate [387] or concanavalin A [388] layer onto the EM grid to capture DENV. Concanavalin A resulted in enhanced adsorption of cell culture-derived DENV to the EM grid but in plasma samples, resulted in an excess of plasma protein binding, a known phenomenon [389]. This resulted in a dark film of protein that obstructed the view by EM. As some of the patients had detectable IgG and/or IgM to DENV, dissociation of the antibodies using low pH glycine was attempted [390]. The difficulty in detecting even DENV-encoded antigen may be attributed to the storage and processing of the patient plasma used in this study. The only recorded successful attempt at identifying the virus by EM was performed with freshly prepared plasma [327]. The same group discovered that plasma-isolated infectious DENV vesicles were dominantly derived from CD61+ expressing

megakaryocytes lineage cells. Megakaryocytes are known to express TF [184], so it is reasonable to expect the presence of TF to be on patient-derived DENV particles.

One of the limitations of immunogold EM is that antigen detection may not be saturated, due to affinity, steric hindrance or balancing the concentration to avoid non-specific binding. Thus, the true proportion of TF-expressing particles may be under-reported. Also, only viruses that have adsorbed to the grid are detected. In the case of HCV, lipid-associated HCV particles may not have been captured by the antibodies as the E2 protein may have been masked. Although EM remains the gold standard for sizing and identification of viruses, newer technologies for the characterization of virus particles in the nanometer range have been improving. High throughput and rapid antigen identification could be achieved through flow virometry [391], an adaptive form of using flow cytometry to characterize small virus particles.

Chapter 5: Summary

5.1 HSV1 gC has evolved to affect FVIIa function

The ability of sgC-His to independently enhance FVIIa activity through viral tenase assembly with FX (sgC-His/FVIIa/FX) on a purified, virus-free membrane differs from that on the virus membrane (as modeled in Figure 49). A lack of synergism in the purified system would suggest that in the particular system, sgC-His competes with sTF-His binding to FVIIa. Both cofactors appeared to stabilize FVIIa and enable efficient FX activation as their catalytic efficiencies were similar. Viral membrane gC enhancement of TF function on the virus towards FX activation may be aided by an unknown factor (Figure 49E). Nonetheless, the work presented here adds further evidence that HSV1 has evolved to affect the haemostatic system. Subsequently, activation of clotting proteases provides a link to cardiovascular diseases such as thrombosis and atherosclerosis. The dependence of gC on FX to mediate FVIIa cofactor function may guide therapeutic development.

The evolutionary advantage of an evolved viral coagulation factor could be enhanced infectivity via the activation of clotting protease-mediated cell signaling. gC and TF was previously shown by the Pryzdial laboratory *in vitro* to achieve enhanced infectivity via PAR-2 activation [12]. Subsequent *in vivo* work further supported the TF-mediated infection, demonstrating that envelope TF was critical for infection of BALB/c mice and also enhanced infection in C57BL/6J mice [13]. It is, however, unknown how gC affects TF-mediated infectivity *in vivo*.

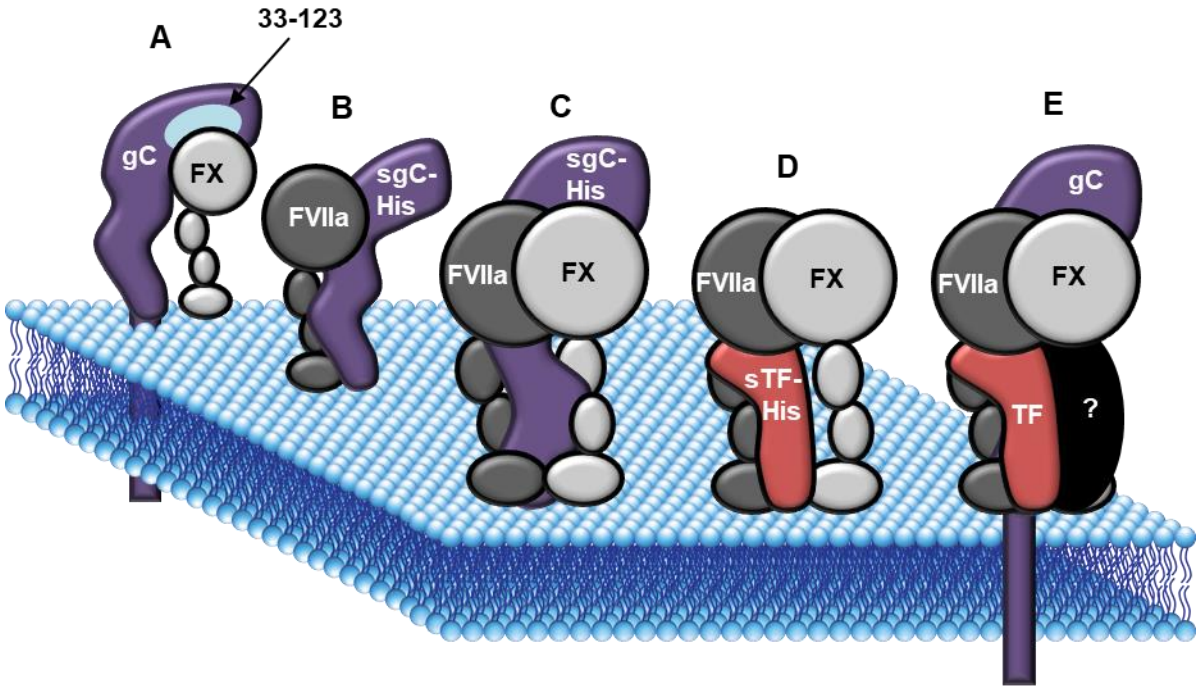

Figure 49. Working model of gC interaction with FVIIa/FX.

(A) gC speculated binding to FX as the 33-123 amino acid residue region near the C-terminal end has been implicated. (B) sgC-His binding to FVIIa is enhanced upon membrane binding. (C) sgC-His binding to FVIIa is increased by FX binding. This viral tenase can work independently from (D) the extrinsic tenase, depicted as a speculated interaction with FX. (E) On the virus surface, gC enhancement of TF function is aided by an unknown factor (?). aPL is not required for the interactions between gC and FVIIa or FX but contributes to the proteolytic activity of the tenase.

5.1.1 gC mimetics

No other herpesvirus has been investigated for FX or FVII-modulating function. HSV1 gC is homologous to HSV2 gF (gC-2) [392] and shares the ability to bind to heparan sulfate [320] and inhibit complement [393], albeit in a different manner. Marek's disease virus (MDV), another member of *Herpesviridae* family, causes a severe disease in chickens and has a large impact on the poultry industry. MDV gC shares some homology with HSV1 gC such as the conserved cysteine residues that confer the complement-inhibiting ability to HSV1 gC [394]. It would be interesting to determine if these or other virus proteins interact with FX and/or FVIIa in a similar manner to gC.

One non-herpesvirus has been shown to interact with coagulation factors. Human adenovirus is capable of binding several vitamin K-dependent coagulation factors, including FX, FVII and FIX with high affinity (via their Gla domains) to enhance liver transduction [395,396]. The Thr423-Glu424-Thr425 of human adenovirus serotype 5 (HAdv5) hexon protein was demonstrated to be crucial for FX binding [397]. Preliminary sequence alignment of the HAdv5 hexon protein with HSV1 gC was performed using T-Coffee, an internet protein comparison algorithm [398]. Sequence alignment showed 21% identical sequence with areas of similar properties within a 76 amino acid immediate region containing the Thr423-Glu424-Thr425 amino acid motif (Figure 50). The gC segment aligning with this region is near the IV C3b binding region (Figure 10). The FX and/or FVIIa interacting regions of gC have not been elucidated, however the 33-123 region is known to be important in FX binding [241].

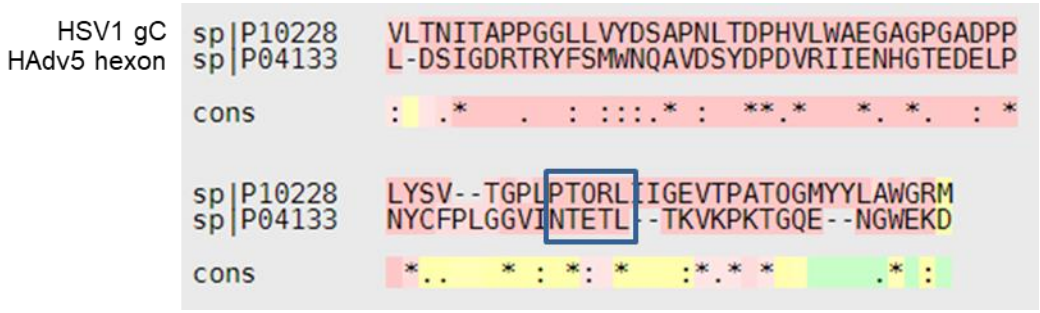

Figure 50. Sequence homology between HSV1 gC and HAdv5 hexon FX-binding region

Alignment of the HSV1 gC and HADv5 hexon sequences was performed with T-Coffee (Proteomics identifications database code P10228 and P04133, respectively). The blue box highlights the Thr423-Glu424-Thr425 of human adenovirus serotype 5 (HAdv5) hexon protein was demonstrated to be crucial for FX binding. Amino acid residues that are identical (*), conserved with strongly similar properties (:) or weakly similar (.) are note in the consensus row (cons). The color in the consensus is the Transitive Consistency Score (TCS) that describes the reliability of the alignment and if they are structurally correct: red is high, yellow is moderate, green is low.

5.1.2 gC sequence similarity to FVIIa binding proteins

The ability of gC to bind to FVIIa is particularly interesting as it enhanced its proteolytic activity. Sequence alignment using T-Coffee of the extracellular domains of gC and TF (Figure 51) demonstrated 9/27 sequence identity of residues known to be implicated in FVIIa interaction. The majority of these homologous residues are found in the C-terminal ectodomain (Figure 52). The 33-123 region of gC contains one identical and one conserved match to TF interacting residues with FVIIa. Insights to the interaction between gC and FVIIa can also be obtained by comparing gC to EPCR as EPCR can bind to FVIIa and affect its function [97,399].

Comparison of the extracellular domains of gC and EPCR showed three identical amino acid residues and one conserved amino acid residues (Figure 53) that interact with the Gla domain or co-ordinate with calcium bound to the Gla domain of Protein C (Figure 54) [400]. Activated Protein C binding to and FVIIa binding to soluble EPCR are similar [399]. In the case of FX, the Gla domain of FX lack similarity to the EPCR binding moieties of Protein C [399]. Thus, gC binding to FVIIa may include interaction(s) with the Gla domain but may not interact with the Gla domain of FX. This is supported by the observation that the loss of the 33-123 amino acid residues of gC inhibited FX interaction. This region does not overlap with the Gla domain interacting region of EPCR (Figure 53).

Crystal structures of gC have remained elusive but the structure could potentially be solved using cryo-EM. The inclusion of a phospholipid membrane, TF, FVIIa and/or FX may stabilize a complex for which a structure can be solved. This would give more insight to the interacting regions and may benefit procoagulant therapeutics or vaccine development.

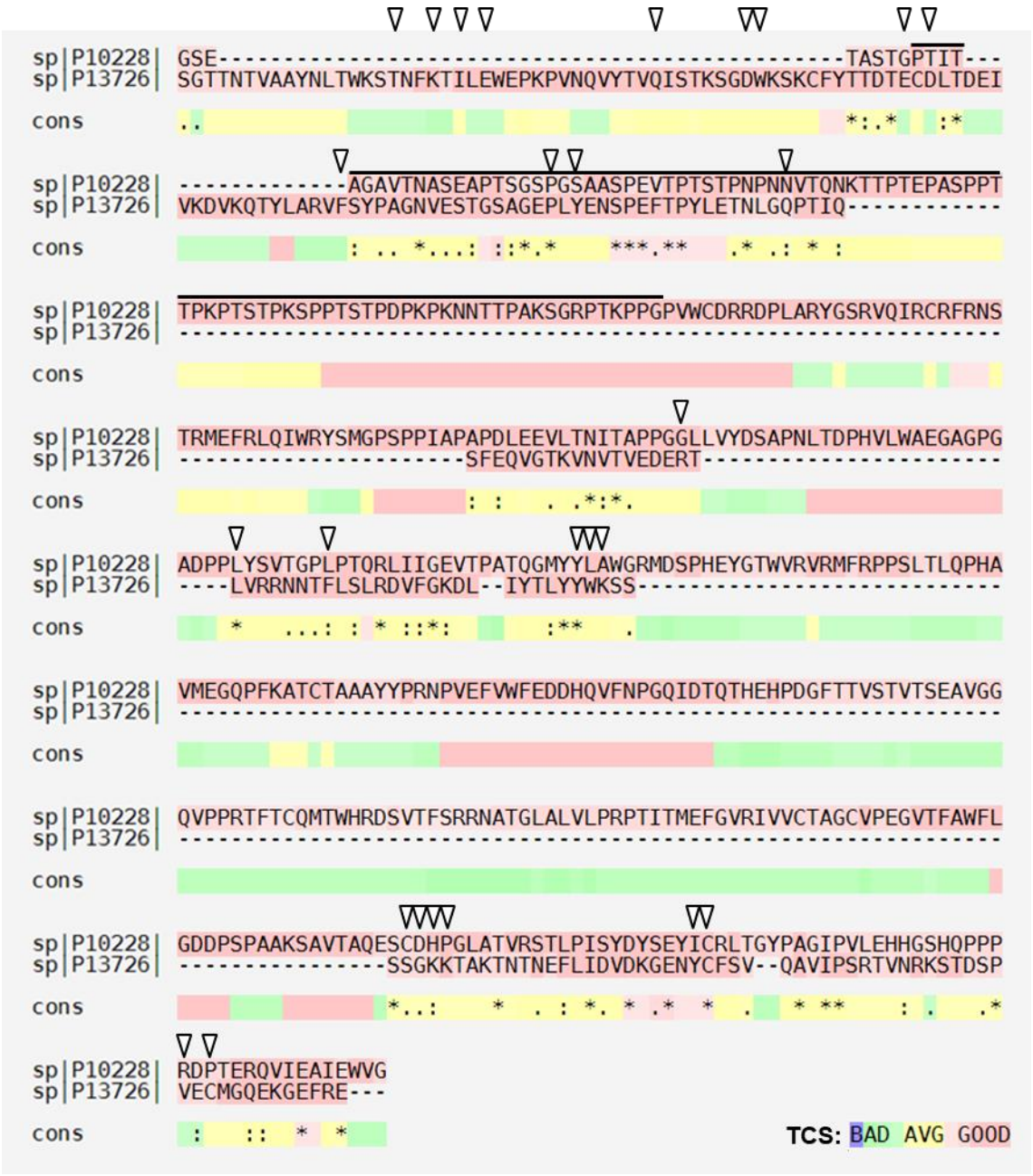

Figure 51. gC sequence comparison to TF.

Sequence alignment of the extracellular domain of gC and the extracellular domain of TF was performed with T-Coffee (Proteomics identifications database code P10228 and P13726, respectively). The 33-123 region of gC known to interact with FX is overlined in black. TF amino acid residues that have been implicated in FVIIa interaction are marked (arrow heads). Amino acid residues that are identical (*), conserved with strongly similar properties (:) or weakly similar (.) are note in the consensus row (cons). The TCS legend is color coded from low to high confidence (bottom right).

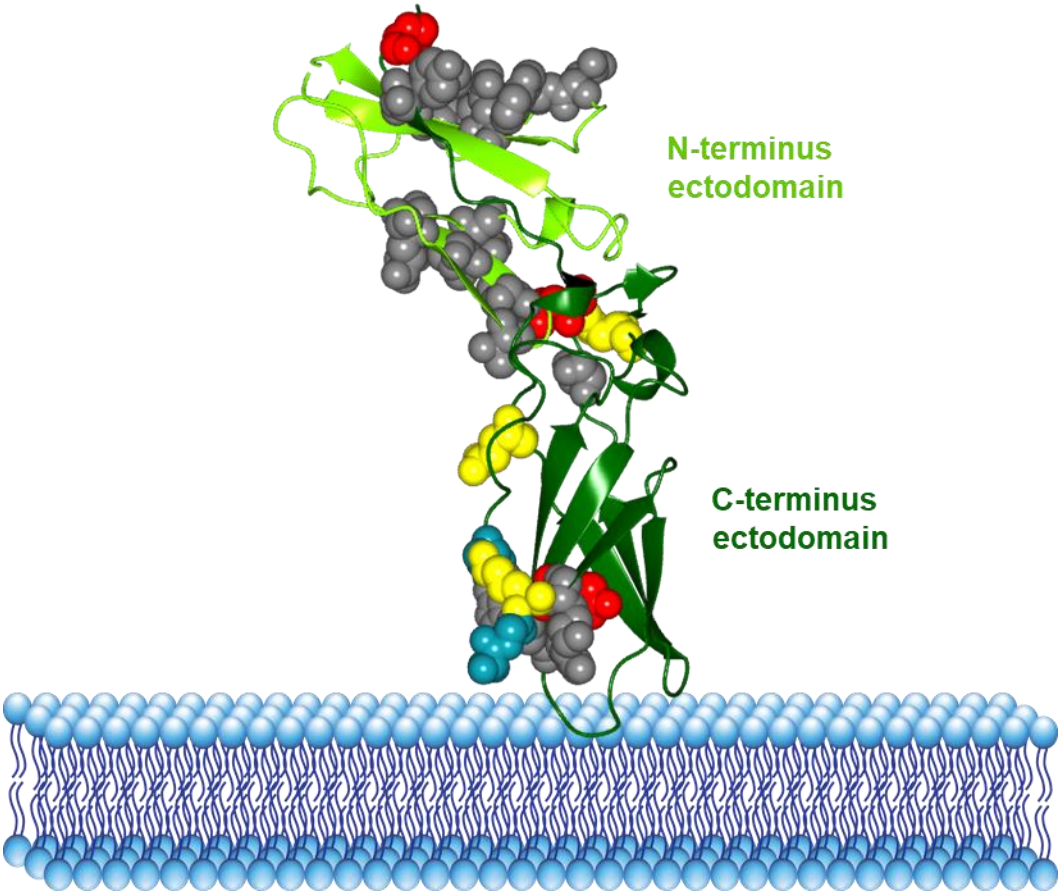

Figure 52. Model of gC homology with the conserved sequence of TF interaction with FVIIa.

The crystal structure of the N-terminus and C-terminus ectodomains of soluble TF (light green and dark green, respectively) was obtained from PDB code 1DAN. Residues of identical matches, conserved matches, weak similarity and no homology to gC from sequence comparison are depicted as balls (red, yellow, teal and gray, respectively). A phospholipid bilayer is depicted for orientation.

Figure 53. gC sequence comparison to EPCR.

Sequence alignment of the extracellular domain of gC and the extracellular domain of EPCR was performed with T-Coffee (Proteomics identifications database code P10228 and Q9UNN8, respectively) [398]. The 33-123 region of gC known to interact with FX is overlined in black. EPCR interacting amino acid residues with the Gla domain of Protein C are marked (arrow heads). Amino acid residues that are identical (*), conserved with strongly similar properties (:) or weakly similar (.) are note in the consensus row (cons). The TCS legend is color coded from low to high confidence (bottom right).

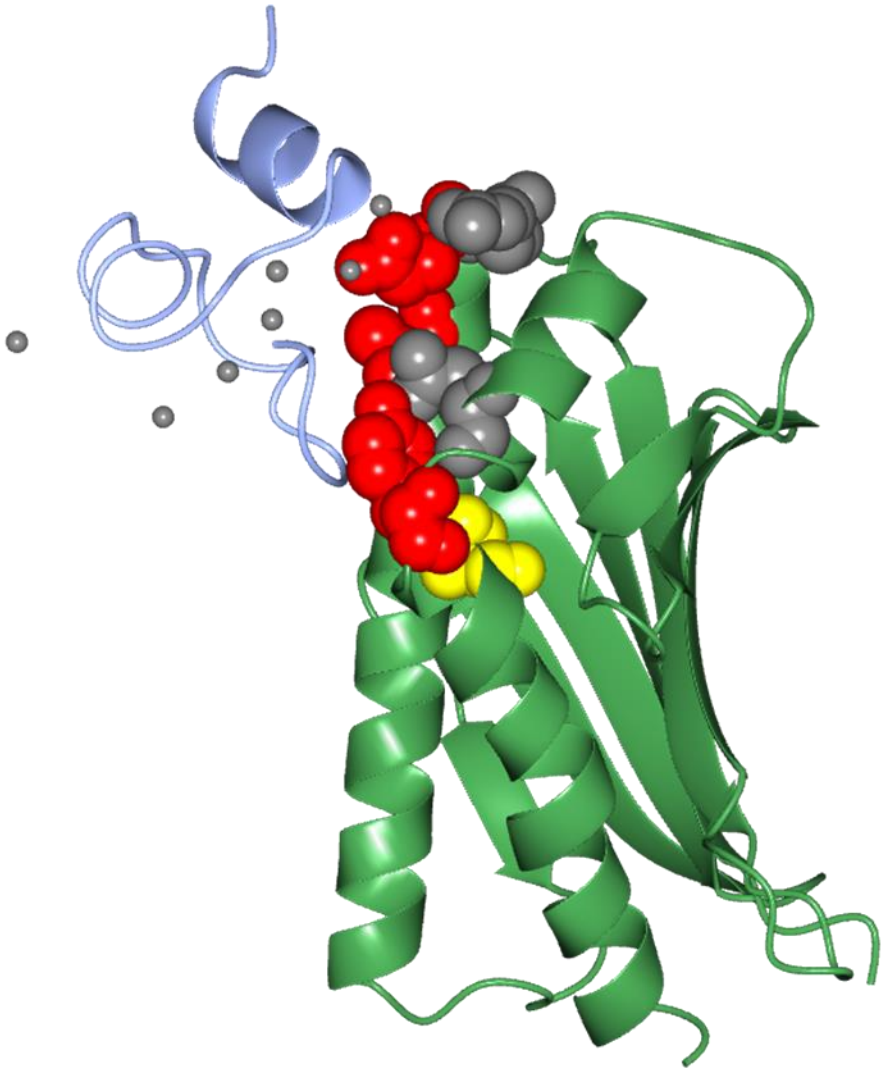

Figure 54. Model of gC homology with the structure of EPCR interaction with Protein C.

The crystal structure of the interaction between the Gla domain of Protein C (blue) and the extracellular domain of EPCR (green) was obtained from PDB code 1LQV. Residues of identical matches, conserved matches and no homology to gC from sequence comparison are depicted as balls (red, yellow and gray, respectively). Calcium is shown as small gray spheres.

5.2 Host TF-deriving enveloped viruses

The presence of TF on DENV, HIV and HCV in addition to the previously established herpesviruses [2] supported the hypothesis that many enveloped viruses can obtain TF. This is observed in HIV and HCV patients, thus providing a clinical link to hypercoagulability. As a common antigen is found on these viruses, it raises the question on why and how these viruses have evolved to obtain TF.

5.2.1 HIV and HCV TF procoagulant activity

HIV and HCV obtain TF antigen from the host, but whether these TF-expressing virus particles also express TF procoagulant function is not known. One could speculate that it is probable that HIV expresses TF procoagulant function based off of a previous study with TF-expressing microparticles in HIV patients. However, to demonstrate that the TF-expressing HIV particles are functional, differentiation from microparticles is necessary. This could be achieved through density centrifugation [401,402]. Subsequent testing of TF procoagulant function can be assessed with FX chromogenic assays and/or plasma clotting assays. The question then remains, why do these viruses incorporate TF into its envelope?

5.2.2 Functional advantage of TF expression

It has been shown that HIV can utilize PAR-1 and PAR-2 signaling to upregulate the HIV-1 coreceptor CCR5 in oral keratinocytes [403]. It has also been demonstrated that HIV-1 increases PAR-1 expression in astrocytes and may contribute to inflammation leading to neurodegeneration in HIV encephalitis [404]. As TF is known to be expressed by astrocytes [65], one would wonder whether PAR-1 and/or PAR-2 activation is mediated directly or indirectly by TF function (via

FVIIa or FX activation). *In vitro* studies, similar to previous work on HSV1 and TF-mediated PAR activation leading to enhanced infection [12], could be performed to investigate the effect of TF-expressing HIV on cell infection via PARs.

If TF is functional and contributes to virus infection, could this common antigen be used as a pan-specific antiviral target? *In vivo* studies have demonstrated that anticoagulants targeted toward TF and FXa could reduce HSV1 infection [13]. In particular, apixaban and NAPc2 diminished the presence of infectious virus in all tested tissues. NAPc2 has also been evidenced to decrease morbidity and increase survival times in Ebola-infected rhesus macaques [405]. As a consequence of treating the disease progression with NAPc2, viral load was lowered in treated rhesus macaques. Anti-TF antibodies that inhibited TF/FVIIa activation of proteases resulted in diminished HSV1 infection [13]. One method of adapting this knowledge could be the creation of bivalent antibodies [406] to TF and a virus antigen to selectively inhibit TF function on the virus but not physiological TF function. Bivalent antibodies may also serve to better neutralize these pathogenic viruses [406]. TF can serve as a pan-specific antiviral as TF is a common surface antigen and viral expression of TF antigen and/or function can be targeted to reduce infection and disease progression.

References

1 Lozano R, Naghavi M, Foreman K, Lim S, Shibuya K, Aboyans V, Abraham J, Adair T, Aggarwal R, Ahn SY, Alvarado M, Anderson HR, Anderson LM, Andrews KG, Atkinson C, Baddour LM, Barker-Collo S, Bartels DH, Bell ML, Benjamin EJ, et al. Global and regional mortality from 235 causes of death for 20 age groups in 1990 and 2010: a systematic analysis for the Global Burden of Disease Study 2010. *Lancet* England; 2012; **380**: 2095–128.

2 Sutherland MR, Raynor CM, Leenknegt H, Wright JF, Pryzdial EL. Coagulation initiated on herpesviruses. *Proc Natl Acad Sci U S A* United States; 1997; **94**: 13510–4.

3 Wendelboe AM, Raskob GE. Global Burden of Thrombosis: Epidemiologic Aspects. *Circ Res* United States; 2016; **118**: 1340–7.

4 Lindsberg PJ, Grau AJ. Inflammation and infections as risk factors for ischemic stroke. *Stroke* United States; 2003; **34**: 2518–32.

5 Sacco RL. Risk factors and outcomes for ischemic stroke. *Neurology* 1995; **45**: S10—4.

6 Alikhan R, Cohen AT, Combe S, Samama MM, Desjardins L, Eldor A, Janbon C, Leizorovicz A, Olsson C-G, Turpie AGG. Risk factors for venous thromboembolism in hospitalized patients with acute medical illness: analysis of the MEDENOX Study. *Arch Intern Med* United States; 2004; **164**: 963–8.

7 Anderson FAJ, Spencer FA. Risk factors for venous thromboembolism. *Circulation* United States; 2003; **107**: I9-16.

8 Allain J-P, Stramer SL, Carneiro-Proietti ABF, Martins ML, da Silva SNL, Ribeiro M, Proietti FA, Reesink HW. Transfusion-transmitted infectious diseases. *Biologicals* 2009; **37**: 71–7.

9 World Health Organization. Global Report for Research on Infectious Diseases of Poverty. Geneva, Switzerland; 2012.

10 Delvaeye M, Conway EM. Coagulation and innate immune responses: can we view them separately? *Blood* United States; 2009; **114**: 2367–74.

11 Verhamme P, Hoylaerts MF. Hemostasis and inflammation: two of a kind? *Thromb J* England; 2009; **7**: 15.

12 Sutherland MR, Ruf W, Pryzdial ELG. Tissue factor and glycoprotein C on herpes simplex virus type 1 are protease-activated receptor 2 cofactors that enhance infection. *Blood* United States; 2012; **119**: 3638–45.

13 Sutherland MR, Simon AY, Shanina I, Horwitz MS, Ruf W, Pryzdial ELG. Virus envelope tissue factor promotes infection in mice. *J Thromb Haemost* England; 2019; **17**: 482–91.

14 Kamikubo Y, Mendolicchio GL, Zampolli A, Marchese P, Rothmeier AS, Orje JN, Gale AJ, Krishnaswamy S, Gruber A, Østergaard H, Petersen LC, Ruf W, Ruggeri ZM. Selective factor VIII activation by the tissue factor-factor VIIa-factor Xa complex. *Blood* American Society of Hematology; 2017; **130**: 1661–70.

15 Kane WH, Davie EW. Blood coagulation factors V and VIII: structural and functional similarities and their relationship to hemorrhagic and thrombotic disorders. *Blood* United States; 1988; **71**: 539–55.

16 Schuijt TJ, Bakhtiari K, Daffre S, Deponte K, Wielders SJH, Marquart JA, Hovius JW, van der Poll T, Fikrig E, Bunce MW, Camire RM, Nicolaes GAF, Meijers JCM, van ’t Veer C. Factor Xa activation of factor V is of paramount importance in initiating the coagulation system: lessons from a tick salivary protein. *Circulation* United States; 2013;

128: 254–66.

17 von dem Borne PA, Meijers JC, Bouma BN. Feedback activation of factor XI by thrombin in plasma results in additional formation of thrombin that protects fibrin clots from fibrinolysis. *Blood* United States; 1995; **86**: 3035–42.

18 Gershom ES, Sutherland MR, Lollar P, Pryzdial ELG. Involvement of the contact phase and intrinsic pathway in herpes simplex virus-initiated plasma coagulation. *J Thromb Haemost* England; 2010; **8**: 1037–43.

19 Bach R, Nemerson Y, Konigsberg W. Purification and characterization of bovine tissue factor. *J Biol Chem* United States; 1981; **256**: 8324–31.

20 Spicer EK, Horton R, Bloem L, Bach R, Williams KR, Guha A, Kraus J, Lin TC, Nemerson Y, Konigsberg WH. Isolation of cDNA clones coding for human tissue factor: primary structure of the protein and cDNA. *Proc Natl Acad Sci U S A* United States; 1987; **84**: 5148–52.

21 Harlos K, Martin DM, O'Brien DP, Jones EY, Stuart DI, Polikarpov I, Miller A, Tuddenham EG, Boys CW. Crystal structure of the extracellular region of human tissue factor. *Nature* England; 1994; **370**: 662–6.

22 Morrissey JH, Fakhrai H, Edgington TS. Molecular cloning of the cDNA for tissue factor, the cellular receptor for the initiation of the coagulation protease cascade. *Cell* Elsevier; 1987; **50**: 129–35.

23 Muller YA, Ultsch MH, de Vos AM. The crystal structure of the extracellular domain of human tissue factor refined to 1.7 A resolution. *J Mol Biol* England; 1996; **256**: 144–59.

24 Rehemtulla A, Ruf W, Edgington TS. The integrity of the cysteine 186-cysteine 209 bond of the second disulfide loop of tissue factor is required for binding of factor VII. *J Biol*

Chem United States; 1991; **266**: 10294–9.

25 Bazan JF. Structural design and molecular evolution of a cytokine receptor superfamily. *Proc Natl Acad Sci U S A* United States; 1990; **87**: 6934–8.

26 Versteeg HH. Tissue factor as an evolutionary conserved cytokine receptor: Implications for inflammation and signal transduction. *Semin Hematol* United States; 2004; **41**: 168–72.

27 Carmeliet P, Mackman N, Moons L, Luther T, Gressens P, Van Vlaenderen I, Demunck H, Kasper M, Breier G, Evrard P, Muller M, Risau W, Edgington T, Collen D. Role of tissue factor in embryonic blood vessel development. *Nature* England; 1996; **383**: 73–5.

28 Bugge TH, Xiao Q, Kombrinck KW, Flick MJ, Holmback K, Danton MJ, Colbert MC, Witte DP, Fujikawa K, Davie EW, Degen JL. Fatal embryonic bleeding events in mice lacking tissue factor, the cell-associated initiator of blood coagulation. *Proc Natl Acad Sci U S A* United States; 1996; **93**: 6258–63.

29 Toomey JR, Kratzer KE, Lasky NM, Stanton JJ, Broze GJJ. Targeted disruption of the murine tissue factor gene results in embryonic lethality. *Blood* United States; 1996; **88**: 1583–7.

30 Ke K, Yuan J, Morrissey JH. Tissue factor residues that putatively interact with membrane phospholipids. *PLoS One* United States; 2014; **9**: e88675.

31 Roy S, Hass PE, Bourell JH, Henzel WJ, Vehar GA. Lysine residues 165 and 166 are essential for the cofactor function of tissue factor. *J Biol Chem* 1991; **266**: 22063–6.

32 Huang Q, Neuenschwander PF, Rezaie AR, Morrissey JH. Substrate recognition by tissue factor-factor VIIa. Evidence for interaction of residues Lys165 and Lys166 of tissue factor with the 4-carboxyglutamate-rich domain of factor X. *J Biol Chem* United States; 1996;

271: 21752–7.

33 Banner DW. The crystal structure of the complex of blood coagulation factor VIIa with soluble tissue factor. *Nat* Macmillan Journals Ltd., etc; 1996; **380**: 41–6.

34 Kirchhofer D, Eigenbrot C, Lipari MT, Moran P, Peek M, Kelley RF. The tissue factor region that interacts with factor Xa in the activation of factor VII. *Biochemistry* United States; 2001; **40**: 675–82.

35 Ruf W, Rehemtulla A, Morrissey JH, Edgington TS. Phospholipid-independent and -dependent interactions required for tissue factor receptor and cofactor function. *J Biol Chem* 1991; **266**: 2158—2166.

36 Hoffman M. The Tissue Factor Pathway and Wound Healing. *Semin Thromb Hemost* United States; 2018; **44**: 142–50.

37 Chen J, Kasper M, Heck T, Nakagawa K, Humpert PM, Bai L, Wu G, Zhang Y, Luther T, Andrassy M, Schiekofer S, Hamann A, Morcos M, Chen B, Stern DM, Nawroth PP, Bierhaus A. Tissue factor as a link between wounding and tissue repair. *Diabetes* United States; 2005; **54**: 2143–54.

38 Brem H, Tomic-Canic M. Cellular and molecular basis of wound healing in diabetes. *J Clin Invest* United States; 2007; **117**: 1219–22.

39 Rosenberg CS. Wound healing in the patient with diabetes mellitus. *Nurs Clin North Am* United States; 1990; **25**: 247–61.

40 Belting M, Dorrell MI, Sandgren S, Aguilar E, Ahamed J, Dorfleutner A, Carmeliet P, Mueller BM, Friedlander M, Ruf W. Regulation of angiogenesis by tissue factor cytoplasmic domain signaling. *Nat Med* 2004; **10**: 502–9.

41 Collier MEW, Ettelaie C. Regulation of the incorporation of tissue factor into

microparticles by serine phosphorylation of the cytoplasmic domain of tissue factor. *J Biol Chem* United States; 2011; **286**: 11977–84.

42 Siegbahn A, Johnell M, Sorensen BB, Petersen LC, Heldin C-H. Regulation of chemotaxis by the cytoplasmic domain of tissue factor. *Thromb Haemost* Germany; 2005; **93**: 27–34.

43 Ahamed J, Ruf W. Protease-activated receptor 2-dependent phosphorylation of the tissue factor cytoplasmic domain. *J Biol Chem* United States; 2004; **279**: 23038–44.

44 van den Berg YW, van den Hengel LG, Myers HR, Ayachi O, Jordanova E, Ruf W, Spek CA, Reitsma PH, Bogdanov VY, Versteeg HH. Alternatively spliced tissue factor induces angiogenesis through integrin ligation. *Proc Natl Acad Sci* 2009; **106**: 19497 LP – 19502.

45 Coughlin SR. Protease-activated receptors in vascular biology. *Thromb Haemost* Germany; 2001; **86**: 298–307.

46 Rao LVM, Pendurthi UR. Tissue factor-factor VIIa signaling. *Arterioscler Thromb Vasc Biol* 2005; **25**: 47–56.

47 ElKeeb AM, Collier MEW, Maraveyas A, Ettelaie C. Accumulation of tissue factor in endothelial cells induces cell apoptosis, mediated through p38 and p53 activation. *Thromb Haemost* Germany; 2015; **114**: 364–78.

48 Greeno EW, Bach RR, Moldow CF. Apoptosis is associated with increased cell surface tissue factor procoagulant activity. *Lab Invest* United States; 1996; **75**: 281–9.

49 Mueller BM, Reisfeld RA, Edgington TS, Ruf W. Expression of tissue factor by melanoma cells promotes efficient hematogenous metastasis. *Proc Natl Acad Sci* National Academy of Sciences; 1992; **89**: 11832–6.

50 Belting M, Dorrell MI, Sandgren S, Aguilar E, Ahamed J, Dorfleutner A, Carmeliet P,

Mueller BM, Friedlander M, Ruf W. Regulation of angiogenesis by tissue factor cytoplasmic domain signaling. *Nat Med* Nature Publishing Group; 2004; **10**: 502.

51 Liu Y, Mueller BM. Protease-activated receptor-2 regulates vascular endothelial growth factor expression in MDA-MB-231 cells via MAPK pathways. *Biochem Biophys Res Commun* United States; 2006; **344**: 1263–70.

52 Hjortoe GM, Petersen LC, Albrektsen T, Sorensen BB, Norby PL, Mandal SK, Pendurthi UR, Rao LVM. Tissue factor-factor VIIa-specific up-regulation of IL-8 expression in MDA-MB-231 cells is mediated by PAR-2 and results in increased cell migration. *Blood* United States; 2004; **103**: 3029–37.

53 Rong Y, Belozerov VE, Tucker-Burden C, Chen G, Durden DL, Olson JJ, Van Meir EG, Mackman N, Brat DJ. Epidermal growth factor receptor and PTEN modulate tissue factor expression in glioblastoma through JunD/activator protein-1 transcriptional activity. *Cancer Res* United States; 2009; **69**: 2540–9.

54 Yu JL, May L, Lhotak V, Shahrzad S, Shirasawa S, Weitz JI, Coomber BL, Mackman N, Rak JW. Oncogenic events regulate tissue factor expression in colorectal cancer cells: implications for tumor progression and angiogenesis. *Blood* United States; 2005; **105**: 1734–41.

55 Dorfleutner A, Hintermann E, Tarui T, Takada Y, Ruf W. Cross-talk of integrin alpha3beta1 and tissue factor in cell migration. *Mol Biol Cell* The American Society for Cell Biology; 2004; **15**: 4416–25.

56 Geddings JE, Mackman N. Tumor-derived tissue factor-positive microparticles and venous thrombosis in cancer patients. *Blood* American Society of Hematology; 2013; **122**: 1873–80.

57 Versteeg HH, Schaffner F, Kerver M, Petersen HH, Ahamed J, Felding-Habermann B, Takada Y, Mueller BM, Ruf W. Inhibition of tissue factor signaling suppresses tumor growth. *Blood* United States; 2008; **111**: 190–9.

58 Schaffner F, Versteeg HH, Schillert A, Yokota N, Petersen LC, Mueller BM, Ruf W. Cooperation of tissue factor cytoplasmic domain and PAR2 signaling in breast cancer development. *Blood* United States; 2010; **116**: 6106–13.

59 Yang YH, Hall P, Milenkovski G, Sharma L, Hutchinson P, Melis E, Carmeliet P, Tipping P, Morand E. Reduction in arthritis severity and modulation of immune function in tissue factor cytoplasmic domain mutant mice. *Am J Pathol* United States; 2004; **164**: 109–17.

60 He H-L, Zhang J-B, Li Q. Clinical significance of expression of tissue factor and tissue factor pathway inhibitor in ulcerative colitis. *World J Gastroenterol* 2014; **20**: 7461.

61 Wang S. Astrocyte tissue factor controls CNS hemostasis and autoimmune inflammation. *Thromb Res* Elsevier; 5AD; **141**: S65–7.

62 Drake TA, Morrissey JH, Edgington TS. Selective cellular expression of tissue factor in human tissues. Implications for disorders of hemostasis and thrombosis. *Am J Pathol* United States; 1989; **134**: 1087–97.

63 Pawlinski R, Tencati M, Holscher T, Pedersen B, Voet T, Tilley RE, Marynen P, Mackman N. Role of cardiac myocyte tissue factor in heart hemostasis. *J Thromb Haemost* England; 2007; **5**: 1693–700.

64 Fleck RA, Rao L V, Rapaport SI, Varki N. Localization of human tissue factor antigen by immunostaining with monospecific, polyclonal anti-human tissue factor antibody. *Thromb Res* United States; 1990; **59**: 421–37.

65 Eddleston M, de la Torre JC, Oldstone MB, Loskutoff DJ, Edgington TS, Mackman N.

Astrocytes are the primary source of tissue factor in the murine central nervous system. A role for astrocytes in cerebral hemostasis. *J Clin Invest* United States; 1993; **92**: 349–58.

66 Hoffman M, Colina CM, McDonald AG, Arepally GM, Pedersen L, Monroe DM. Tissue factor around dermal vessels has bound factor VII in the absence of injury. *J Thromb Haemost* England; 2007; **5**: 1403–8.

67 Klomsiri C, Karplus PA, Poole LB. Cysteine-based redox switches in enzymes. *Antioxid Redox Signal* 2011; **14**: 1065–77.

68 Ahamed J, Versteeg HH, Kerver M, Chen VM, Mueller BM, Hogg PJ, Ruf W. Disulfide isomerization switches tissue factor from coagulation to cell signaling. *Proc Natl Acad Sci U S A* United States; 2006; **103**: 13932–7.

69 Chen F, Zhao Z, Zhou J, Lu Y, Essex DW, Wu Y. Protein disulfide isomerase enhances tissue factor-dependent thrombin generation. *Biochem Biophys Res Commun* Academic Press; 2018; **501**: 172–7.

70 Wood JP, Ellery PER, Maroney SA, Mast AE. Biology of tissue factor pathway inhibitor. *Blood* American Society of Hematology; 2014; **123**: 2934–43.

71 Baugh RJ, Broze GJJ, Krishnaswamy S. Regulation of extrinsic pathway factor Xa formation by tissue factor pathway inhibitor. *J Biol Chem* United States; 1998; **273**: 4378–86.

72 Girard TJ, Warren LA, Novotny WF, Likert KM, Brown SG, Miletich JP, Broze GJJ. Functional significance of the Kunitz-type inhibitory domains of lipoprotein-associated coagulation inhibitor. *Nature* England; 1989; **338**: 518–20.

73 Herbert JM, Savi P, Laplace MC, Lale A. IL-4 inhibits LPS-, IL-1 beta- and TNF alpha-induced expression of tissue factor in endothelial cells and monocytes. *FEBS Lett*

England; 1992; **310**: 31–3.

74 Wharram BL, Fitting K, Kunkel SL, Remick DG, Merritt SE, Wiggins RC. Tissue factor expression in endothelial cell/monocyte cocultures stimulated by lipopolysaccharide and/or aggregated IgG. Mechanisms of cell:cell communication. *J Immunol* United States; 1991; **146**: 1437–45.

75 Cermak J, Key NS, Bach RR, Balla J, Jacob HS, Vercellotti GM. C-reactive protein induces human peripheral blood monocytes to synthesize tissue factor. *Blood* United States; 1993; **82**: 513–20.

76 van den Berg YW, Osanto S, Reitsma PH, Versteeg HH. The relationship between tissue factor and cancer progression: insights from bench and bedside. *Blood* United States; 2012; **119**: 924–32.

77 Milsom CC, Yu JL, Mackman N, Micallef J, Anderson GM, Guha A, Rak JW. Tissue factor regulation by epidermal growth factor receptor and epithelial-to-mesenchymal transitions: effect on tumor initiation and angiogenesis. *Cancer Res* United States; 2008; **68**: 10068–76.

78 Vrana JA, Stang MT, Grande JP, Getz MJ. Expression of tissue factor in tumor stroma correlates with progression to invasive human breast cancer: paracrine regulation by carcinoma cell-derived members of the transforming growth factor beta family. *Cancer Res* United States; 1996; **56**: 5063–70.

79 Rong Y, Hu F, Huang R, Mackman N, Horowitz JM, Jensen RL, Durden DL, Van Meir EG, Brat DJ. Early growth response gene-1 regulates hypoxia-induced expression of tissue factor in glioblastoma multiforme through hypoxia-inducible factor-1-independent mechanisms. *Cancer Res* United States; 2006; **66**: 7067–74.

80 Nakagaki T, Foster DC, Berkner KL, Kisiel W. Initiation of the extrinsic pathway of blood coagulation: evidence for the tissue factor dependent autoactivation of human coagulation factor VII. *Biochemistry* United States; 1991; **30**: 10819–24.

81 Rao L V, Bajaj SP, Rapaport SI. Activation of human factor VII during clotting in vitro. *Blood* United States; 1985; **65**: 218–26.

82 Butenas S, Mann KG. Kinetics of human factor VII activation. *Biochemistry* United States; 1996; **35**: 1904–10.

83 Neuenschwander PF, Fiore MM, Morrissey JH. Factor VII autoactivation proceeds via interaction of distinct protease-cofactor and zymogen-cofactor complexes. Implications of a two-dimensional enzyme kinetic mechanism. *J Biol Chem* United States; 1993; **268**: 21489–92.

84 Higashi S, Matsumoto N, Iwanaga S. Molecular mechanism of tissue factor-mediated acceleration of factor VIIa activity. *J Biol Chem* United States; 1996; **271**: 26569–74.

85 Tavoosi N, Smith SA, Davis-Harrison RL, Morrissey JH. Factor VII and protein C are phosphatidic acid-binding proteins. *Biochemistry* United States; 2013; **52**: 5545–52.

86 Bajaj SP, Schmidt AE, Agah S, Bajaj MS, Padmanabhan K. High resolution structures of p-aminobenzamidine- and benzamidine-VIIa/soluble tissue factor: unpredicted conformation of the 192-193 peptide bond and mapping of Ca2+, Mg2+, Na+, and Zn2+ sites in factor VIIa. *J Biol Chem* United States; 2006; **281**: 24873–88.

87 Pike AC, Brzozowski AM, Roberts SM, Olsen OH, Persson E. Structure of human factor VIIa and its implications for the triggering of blood coagulation. *Proc Natl Acad Sci U S A* 1999; **96**: 8925–30.

88 Bode W, Brandstetter H, Mather T, Stubbs MT. Comparative analysis of haemostatic

proteinases: structural aspects of thrombin, factor Xa, factor IXa and protein C. *Thromb Haemost* Germany; 1997; **78**: 501–11.

89 Tuddenham EG, Pemberton S, Cooper DN. Inherited factor VII deficiency: genetics and molecular pathology. *Thromb Haemost* Germany; 1995; **74**: 313–21.

90 Rosen ED, Xu H, Liang Z, Martin JA, Suckow M, Castellino FJ. Generation of genetically-altered mice producing very low levels of coagulation factorVII. *Thromb Haemost* Germany; 2005; **94**: 493–7.

91 Mariani G, Bernardi F. Factor VII deficiency. *Semin Thromb Hemost* 2009; **35**: 400–6.

92 Krishnaswamy S. Exosite-driven substrate specificity and function in coagulation. *J Thromb Haemost* England; 2005; **3**: 54–67.

93 Baugh RJ, Dickinson CD, Ruf W, Krishnaswamy S. Exosite interactions determine the affinity of factor X for the extrinsic Xase complex. *J Biol Chem* United States; 2000; **275**: 28826–33.

94 Neuenschwander PF, Morrissey JH. Roles of the membrane-interactive regions of factor VIIa and tissue factor. The factor VIIa Gla domain is dispensable for binding to tissue factor but important for activation of factor X. *J Biol Chem* United States; 1994; **269**: 8007–13.

95 Vadivel K, Agah S, Messer AS, Cascio D, Bajaj MS, Krishnaswamy S, Esmon CT, Padmanabhan K, Bajaj SP. Structural and functional studies of γ-carboxyglutamic acid domains of factor VIIa and activated Protein C: role of magnesium at physiological calcium. *J Mol Biol* 2013; **425**: 1961–81.

96 Rao L V, Ruf W. Tissue factor residues Lys165 and Lys166 are essential for rapid formation of the quaternary complex of tissue factor.VIIa with Xa.tissue factor pathway

inhibitor. *Biochemistry* United States; 1995; **34**: 10867–71.

97 Kondreddy V, Wang J, Keshava S, Esmon CT, Rao LVM, Pendurthi UR. Factor VIIa induces anti-inflammatory signaling via EPCR and PAR1. *Blood* United States; 2018; **131**: 2379–92.

98 Logan AC, Yank V, Stafford RS. Off-label use of recombinant factor VIIa in U.S. hospitals: analysis of hospital records. *Ann Intern Med* 2011; **154**: 516–22.

99 Witmer CM, Huang Y-S, Lynch K, Raffini LJ, Shah SS. Off-label recombinant factor VIIa use and thrombosis in children: a multi-center cohort study. *J Pediatr* 2011; **158**: 820-825.e1.

100 Morrissey JH, Macik BG, Neuenschwander PF, Comp PC. Quantitation of activated factor VII levels in plasma using a tissue factor mutant selectively deficient in promoting factor VII activation. *Blood* United States; 1993; **81**: 734–44.

101 Fair DS. Quantitation of factor VII in the plasma of normal and warfarin-treated individuals by radioimmunoassay. *Blood* United States; 1983; **62**: 784–91.

102 LOELIGER EA, ESCH van der, ter HAAR C, WACHTER R, BOOIJ HL. Factor VII; its turnover rate and its possible role in thrombogenesis. *Thromb Diath Haemorrh* Germany; 1960; **4**: 196–200.

103 Erhardtsen E. Pharmacokinetics of recombinant activated factor VII (rFVIIa). *Semin Thromb Hemost* United States; 2000; **26**: 385–91.

104 Seligsohn U, Kasper CK, Osterud B, Rapaport SI. Activated factor VII: presence in factor IX concentrates and persistence in the circulation after infusion. *Blood* United States; 1979; **53**: 828–37.

105 Hjortoe G, Sorensen BB, Petersen LC, Rao LVM. Factor VIIa binding and internalization

in hepatocytes. *J Thromb Haemost* 2005; **3**: 2264–73.

106 Lawson JH, Butenas S, Ribarik N, Mann KG. Complex-dependent inhibition of factor VIIa by antithrombin III and heparin. *J Biol Chem* United States; 1993; **268**: 767–70.

107 Kamata K, Kawamoto H, Honma T, Iwama T, Kim S-H. Structural basis for chemical inhibition of human blood coagulation factor Xa. *Proc Natl Acad Sci* National Academy of Sciences; 1998; **95**: 6630–5.

108 Faure G, Gowda VT, Maroun RC. Characterization of a human coagulation factor Xa-binding site on Viperidae snake venom phospholipases A2 by affinity binding studies and molecular bioinformatics. *BMC Struct Biol* England; 2007; **7**: 82.

109 Fung MR, Campbell RM, MacGillivray RTA. Blood coagulation factor X mRNA encodes a single polypeptide chain containing a prepro leader sequence. *Nucleic Acids Res* 1984; **12**: 4481–92.

110 Venkateswarlu D, Perera L, Darden T, Pedersen LG. Structure and dynamics of zymogen human blood coagulation factor X. *Biophys J* United States; 2002; **82**: 1190–206.

111 Krupiczojc MA, Scotton CJ, Chambers RC. Coagulation signalling following tissue injury: focus on the role of factor Xa. *Int J Biochem Cell Biol* Netherlands; 2008; **40**: 1228–37.

112 Nelsestuen GL, Kisiel W, Di Scipio RG. Interaction of vitamin K dependent proteins with membranes. *Biochemistry* American Chemical Society; 1978; **17**: 2134–8.

113 Venkateswarlu D, Duke RE, Perera L, Darden TA, Pedersen LG. An all-atom solution-equilibrated model for human extrinsic blood coagulation complex (sTF-VIIa-Xa): a protein-protein docking and molecular dynamics refinement study. *J Thromb Haemost* England; 2003; **1**: 2577–88.

114 Norledge B V, Petrovan RJ, Ruf W, Olson AJ. The tissue factor/factor VIIa/factor Xa complex: a model built by docking and site-directed mutagenesis. *Proteins* United States; 2003; **53**: 640–8.

115 Lee CJ, Chandrasekaran V, Wu S, Duke RE, Pedersen LG. Recent estimates of the structure of the factor VIIa (FVIIa)/tissue factor (TF) and factor Xa (FXa) ternary complex. *Thromb Res* United States; 2010; **125 Suppl**: S7–10.

116 Mizuno H, Fujimoto Z, Atoda H, Morita T. Crystal structure of an anticoagulant protein in complex with the Gla domain of factor X. *Proc Natl Acad Sci* National Academy of Sciences; 2001; **98**: 7230–4.

117 Di Scipio RG, Hermodson MA, Yates SG, Davie EW. A comparison of human prothrombin, factor IX (Christmas factor), factor X (Stuart factor), and protein S. *Biochemistry* United States; 1977; **16**: 698–706.

118 Mann KG, Jenny RJ, Krishnaswamy S. Cofactor proteins in the assembly and expression of blood clotting enzyme complexes. *Annu Rev Biochem* United States; 1988; **57**: 915–56.

119 Stavenuiter F, Dienava-Verdoold I, Boon-Spijker MG, Brinkman HJM, Meijer AB, Mertens K. Factor seven activating protease (FSAP): does it activate factor VII? *J Thromb Haemost* England; 2012; **10**: 859–66.

120 Neuenschwander PF, Jesty J. Thrombin-activated and factor Xa-activated human factor VIII: Differences in cofactor activity and decay rate. *Arch Biochem Biophys* 1992; **296**: 426–34.

121 Carter RLR, Talbot K, Hur WS, Meixner SC, Van Der Gugten JG, Holmes DT, Cote HCF, Kastrup CJ, Smith TW, Lee AYY, Pryzdial ELG. Rivaroxaban and apixaban induce clotting factor Xa fibrinolytic activity. *J Thromb Haemost* England; 2018; **16**: 2276–88.

122 Talbot K, Meixner SC, Pryzdial ELG. Enhanced fibrinolysis by proteolysed coagulation factor Xa. *Biochim Biophys Acta* Netherlands; 2010; **1804**: 723–30.

123 Pryzdial EL, Lavigne N, Dupuis N, Kessler GE. Plasmin converts factor X from coagulation zymogen to fibrinolysis cofactor. *J Biol Chem* United States; 1999; **274**: 8500–5.

124 Schuepbach RA, Riewald M. Coagulation factor Xa cleaves protease-activated receptor-1 and mediates signaling dependent on binding to the endothelial protein C receptor. *J Thromb Haemost* England; 2010; **8**: 379–88.

125 Camerer E, Huang W, Coughlin SR. Tissue factor- and factor X-dependent activation of protease-activated receptor 2 by factor VIIa. *Proc Natl Acad Sci* National Academy of Sciences; 2000; **97**: 5255–60.

126 Blanc-Brude OP, Archer F, Leoni P, Derian C, Bolsover S, Laurent GJ, Chambers RC. Factor Xa stimulates fibroblast procollagen production, proliferation, and calcium signaling via PAR1 activation. *Exp Cell Res* United States; 2005; **304**: 16–27.

127 Koo BH, Chung KH, Hwang KC, Kim DS. Factor Xa induces mitogenesis of coronary artery smooth muscle cell via activation of PAR-2. *FEBS Lett* England; 2002; **523**: 85–9.

128 Rauch BH, Millette E, Kenagy RD, Daum G, Clowes AW. Thrombin- and factor Xa-induced DNA synthesis is mediated by transactivation of fibroblast growth factor receptor-1 in human vascular smooth muscle cells. *Circ Res* United States; 2004; **94**: 340–5.

129 Borensztajn K, Stiekema J, Nijmeijer S, Reitsma PH, Peppelenbosch MP, Spek CA. Factor Xa stimulates proinflammatory and profibrotic responses in fibroblasts via protease-activated receptor-2 activation. *Am J Pathol* United States; 2008; **172**: 309–20.

130 Disse J, Petersen HH, Larsen KS, Persson E, Esmon N, Esmon CT, Teyton L, Petersen LC, Ruf W. The endothelial protein C receptor supports tissue factor ternary coagulation initiation complex signaling through protease-activated receptors. *J Biol Chem* United States; 2011; **286**: 5756–67.

131 Kovacs B, Bereczky Z, Olah Z, Gindele R, Kerenyi A, Selmeczi A, Boda Z, Muszbek L. The superiority of anti-FXa assay over anti-FIIa assay in detecting heparin-binding site antithrombin deficiency. *Am J Clin Pathol* England; 2013; **140**: 675–9.

132 Jordan RE, Oosta GM, Gardner WT, Rosenberg RD. The kinetics of hemostatic enzyme-antithrombin interactions in the presence of low molecular weight heparin. *J Biol Chem* United States; 1980; **255**: 10081–90.

133 Ho G, Toomey JR, Broze GJJ, Schwartz AL. Receptor-mediated endocytosis of coagulation factor Xa requires cell surface-bound tissue factor pathway inhibitor. *J Biol Chem* United States; 1996; **271**: 9497–502.

134 Narita M, Rudolph AE, Miletich JP, Schwartz AL. The low-density lipoprotein receptor-related protein (LRP) mediates clearance of coagulation factor Xa in vivo. *Blood* United States; 1998; **91**: 555–60.

135 Kalafatis M, Rand MD, Mann KG. The mechanism of inactivation of human factor V and human factor Va by activated protein C. *J Biol Chem* United States; 1994; **269**: 31869–80.

136 Esmon CT. The protein C pathway. *Chest* United States; 2003; **124**: 26S-32S.

137 Cesarman-Maus G, Hajjar KA. Molecular mechanisms of fibrinolysis. *Br J Haematol* England; 2005; **129**: 307–21.

138 McCarthy M, Norenberg MD, Norenberg LO, Dix RD. Herpes simplex virus type 1

infection of rat astrocytes in primary culture: effects of dibutyryl cyclic AMP. *J Neuropathol Exp Neurol* England; 1990; **49**: 3–20.

139 Ramos C, SÁNchez G, Pando RH, Baquera J, HernÁNdez D, Mota J, Ramos J, Flores A, LlausÁS E. Dengue virus in the brain of a fatal case of hemorrhagic dengue fever. *J Neurovirol* Taylor & Francis; 1998; **4**: 465–8.

140 Eugenin EA, Clements JE, Zink MC, Berman JW. Human immunodeficiency virus infection of human astrocytes disrupts blood-brain barrier integrity by a gap junction-dependent mechanism. *J Neurosci* 2011; **31**: 9456–65.

141 Shrivastava S, Ma L, Tham E-L, H McVey J, Chen D, Dorling A. Protease-activated receptor-2 signalling by tissue factor on dendritic cells suppresses antigen-specific CD4+ T-cell priming. *Immunology* 2013; **139**: 219–26.

142 Kruse M, Rosorius O, Krätzer F, Stelz G, Kuhnt C, Schuler G, Hauber J, Steinkasserer A. Mature dendritic cells infected with herpes simplex virus type 1 exhibit inhibited T-cell stimulatory capacity. *J Virol* 2000; **74**: 7127–36.

143 Wu SJ, Grouard-Vogel G, Sun W, Mascola JR, Brachtel E, Putvatana R, Louder MK, Filgueira L, Marovich MA, Wong HK, Blauvelt A, Murphy GS, Robb ML, Innes BL, Birx DL, Hayes CG, Frankel SS. Human skin Langerhans cells are targets of dengue virus infection. *Nat Med* United States; 2000; **6**: 816–20.

144 Sun P, Fernandez S, Marovich MA, Palmer DR, Celluzzi CM, Boonnak K, Liang Z, Subramanian H, Porter KR, Sun W, Burgess TH. Functional characterization of ex vivo blood myeloid and plasmacytoid dendritic cells after infection with dengue virus. *Virology* United States; 2009; **383**: 207–15.

145 Ader DB, Celluzzi C, Bisbing J, Gilmore L, Gunther V, Peachman KK, Rao M, Barvir D,

Sun W, Palmer DR. Modulation of dengue virus infection of dendritic cells by Aedes aegypti saliva. *Viral Immunol* United States; 2004; **17**: 252–65.

146 Hladik F, Sakchalathorn P, Ballweber L, Lentz G, Fialkow M, Eschenbach D, McElrath MJ. Initial events in establishing vaginal entry and infection by human immunodeficiency virus type-1. *Immunity* United States; 2007; **26**: 257–70.

147 Frankel SS, Tenner-Racz K, Racz P, Wenig BM, Hansen CH, Heffner D, Nelson AM, Pope M, Steinman RM. Active replication of HIV-1 at the lymphoepithelial surface of the tonsil. *Am J Pathol* United States; 1997; **151**: 89–96.

148 Frankel SS, Wenig BM, Burke AP, Mannan P, Thompson LD, Abbondanzo SL, Nelson AM, Pope M, Steinman RM. Replication of HIV-1 in dendritic cell-derived syncytia at the mucosal surface of the adenoid. *Science* United States; 1996; **272**: 115–7.

149 Pachiadakis I, Pollara G, Chain BM, Naoumov N V. Is hepatitis C virus infection of dendritic cells a mechanism facilitating viral persistence? *Lancet Infect Dis* Elsevier; 2005; **5**: 296–304.

150 Goutagny N, Fatmi A, De Ledinghen V, Penin F, Couzigou P, Inchauspe G, Bain C. Evidence of viral replication in circulating dendritic cells during hepatitis C virus infection. *J Infect Dis* United States; 2003; **187**: 1951–8.

151 Bain C, Fatmi A, Zoulim F, Zarski JP, Trepo C, Inchauspe G. Impaired allostimulatory function of dendritic cells in chronic hepatitis C infection. *Gastroenterology* United States; 2001; **120**: 512–24.

152 Chen Z, Sager R. Differential expression of human tissue factor in normal mammary epithelial cells and in carcinomas. *Mol Med* 1995; **1**: 153–60.

153 Shetty S, Bhandary YP, Shetty SK, Velusamy T, Shetty P, Bdeir K, Gyetko MR, Cines

DB, Idell S, Neuenschwander PF, Ruppert C, Guenther A, Abraham E, Shetty RS. Induction of Tissue Factor by Urokinase in Lung Epithelial Cells and in the Lungs. *Am J Respir Crit Care Med* 2010; **181**: 1355–66.

154 Agelidis AM, Shukla D. Cell entry mechanisms of HSV: what we have learned in recent years. *Future Virol* 2015; **10**: 1145–54.

155 Shah A, Farooq A V, Tiwari V, Kim M-J, Shukla D. HSV-1 infection of human corneal epithelial cells: receptor-mediated entry and trends of re-infection. *Mol Vis* 2010; **16**: 2476–86.

156 Martinez-Betancur V, Marin-Villa M, Martinez-Gutierrez M. Infection of epithelial cells with dengue virus promotes the expression of proteins favoring the replication of certain viral strains. *J Med Virol* United States; 2014; **86**: 1448–58.

157 Liu R, Huang L, Li J, Zhou X, Zhang H, Zhang T, Lei Y, Wang K, Xie N, Zheng Y, Wang F, Nice EC, Rong L, Huang C, Wei Y. HIV Infection in gastric epithelial cells. *J Infect Dis* United States; 2013; **208**: 1221–30.

158 Deforges S, Evlashev A, Perret M, Sodoyer M, Pouzol S, Scoazec J-Y, Bonnaud B, Diaz O, Paranhos-Baccalà G, Lotteau V, André P. Expression of hepatitis C virus proteins in epithelial intestinal cells in vivo. *J Gen Virol* 2004; **85**: 2515–23.

159 De Vita S, Sansonno D, Dolcetti R, Ferraccioli G, Carbone A, Cornacchiulo V, Santini G, Crovatto M, Gloghini A, Dammacco F, Boiocchi M. Hepatitis C virus within a malignant lymphoma lesion in the course of type II mixed cryoglobulinemia. *Blood* United States; 1995; **86**: 1887–92.

160 Arrieta JJ, Rodriguez-Inigo E, Casqueiro M, Bartolome J, Manzarbeitia F, Herrero M, Pardo M, Carreno V. Detection of hepatitis C virus replication by In situ hybridization in

epithelial cells of anti-hepatitis C virus-positive patients with and without oral lichen planus. *Hepatology* United States; 2000; **32**: 97–103.

161 Morrissey JH, Drake TA. Procoagulant Response of the Endothelium and Monocytes. In: Schlag G, Redl H, editors. *Pathophysiology of Shock, Sepsis, and Organ Failure*. Berlin, Heidelberg: Springer Berlin Heidelberg; 1993. p. 564–74.

162 Parry GC, Mackman N. Transcriptional regulation of tissue factor expression in human endothelial cells. *Arterioscler Thromb Vasc Biol* United States; 1995; **15**: 612–21.

163 Andoh K, Pettersen KS, Filion-Myklebust C, Prydz H. Observations on the cell biology of tissue factor in endothelial cells. *Thromb Haemost* Germany; 1990; **63**: 298–302.

164 Contrino J, Hair G, Kreutzer DL, Rickles FR. In situ detection of tissue factor in vascular endothelial cells: Correlation with the malignant phenotype of human breast disease. *Nat Med* 1996; **2**: 209–15.

165 Key NS, Vercellotti GM, Winkelmann JC, Moldow CF, Goodman JL, Esmon NL, Esmon CT, Jacob HS. Infection of vascular endothelial cells with herpes simplex virus enhances tissue factor activity and reduces thrombomodulin expression. *Proc Natl Acad Sci* United States; 1990; **87**: 7095–9.

166 Sugioka K, Drake JD, Fukuda M, Shimomura Y, Hwang DG. Susceptibility of human corneal endothelial cells to HSV-1 infection. *Curr Eye Res* England; 2005; **30**: 863–9.

167 Smiley ML, Hoxie JA, Friedman HM. Herpes simplex virus type 1 infection of endothelial, epithelial, and fibroblast cells induces a receptor for C3b. *J Immunol* United States; 1985; **134**: 2673–8.

168 Scheglovitova ON, Romanov YA, Maksianina E V, Svintsitskaya VA, Pronin AG. Herpes simplex type I virus infected human vascular endothelial cells induce the production of

anti-viral and proinflammatory factors by peripheral blood leukocytes in vitro. *Russ J Immunol* Russia (Federation); 2002; **7**: 115–22.

169 Sutherland MR, Friedman HM, Pryzdial EL. Herpes Simplex Virus Infection of Endothelial Cells Is Enhanced by Thrombin. *Blood* American Society of Hematology; 2004; **104**: 1926.

170 Arevalo MT, Simpson-Haidaris PJ, Kou Z, Schlesinger JJ, Jin X. Primary human endothelial cells support direct but not antibody-dependent enhancement of dengue viral infection. *J Med Virol* United States; 2009; **81**: 519–28.

171 AbuBakar S, Shu M-H, Johari J, Wong P-F. Senescence affects endothelial cells susceptibility to dengue virus infection. *Int J Med Sci* Australia; 2014; **11**: 538–44.

172 Diamond MS, Edgil D, Roberts TG, Lu B, Harris E. Infection of human cells by dengue virus is modulated by different cell types and viral strains. *J Virol* United States; 2000; **74**: 7814–23.

173 Bagasra O, Lavi E, Bobroski L, Khalili K, Pestaner JP, Tawadros R, Pomerantz RJ. Cellular reservoirs of HIV-1 in the central nervous system of infected individuals: identification by the combination of in situ polymerase chain reaction and immunohistochemistry. *AIDS* England; 1996; **10**: 573–85.

174 Ades EW, Hierholzer JC, George V, Black J, Candal F. Viral susceptibility of an immortalized human microvascular endothelial cell line. *J Virol Methods* Netherlands; 1992; **39**: 83–90.

175 Fletcher NF, Wilson GK, Murray J, Hu K, Lewis A, Reynolds GM, Stamataki Z, Meredith LW, Rowe IA, Luo G, Lopez-Ramirez MA, Baumert TF, Weksler B, Couraud P-O, Kim KS, Romero IA, Jopling C, Morgello S, Balfe P, McKeating JA. Hepatitis C virus infects

the endothelial cells of the blood-brain barrier. *Gastroenterology* United States; 2012; **142**: 634-643.e6.

176 Stephenne X, Vosters O, Najimi M, Beuneu C, Dung KN, Wijns W, Goldman M, Sokal EM. Tissue factor-dependent procoagulant activity of isolated human hepatocytes: relevance to liver cell transplantation. *Liver Transplant Off Publ Am Assoc Study Liver Dis Int Liver Transplant Soc* United States; 2007; **13**: 599–606.

177 Sullivan BP, Kopec AK, Joshi N, Cline H, Brown JA, Bishop SC, Kassel KM, Rockwell C, Mackman N, Luyendyk JP. Hepatocyte tissue factor activates the coagulation cascade in mice. *Blood* United States; 2013; **121**: 1868–74.

178 Dienes HP, Ramadori G, Falke D, Thoenes W. Electron microscopic observations on primary hepatocyte cultures infected with herpes simplex virus Types I and II. *Virchows Arch B* 1984; **46**: 321.

179 Kaufman B, Gandhi SA, Louie E, Rizzi R, Illei P. Herpes simplex virus hepatitis: case report and review. *Clin Infect Dis* United States; 1997; **24**: 334–8.

180 Lang J, Vera D, Cheng Y, Tang H. Modeling Dengue Virus-Hepatic Cell Interactions Using Human Pluripotent Stem Cell-Derived Hepatocyte-like Cells. *Stem cell reports* 2016; **7**: 341–54.

181 Suksanpaisan L, Cabrera-Hernandez A, Smith DR. Infection of human primary hepatocytes with dengue virus serotype 2. *J Med Virol* United States; 2007; **79**: 300–7.

182 Kong L, Cardona Maya W, Moreno-Fernandez ME, Ma G, Shata MT, Sherman KE, Chougnet C, Blackard JT. Low-level HIV infection of hepatocytes. *Virol J* England; 2012; **9**: 157.

183 Farquhar MJ, McKeating JA. Primary hepatocytes as targets for hepatitis C virus

replication. *J Viral Hepat* 2008; **15**: 849–54.

184 Brambilla M, Facchinetti L, Canzano P, Rossetti L, Ferri N, Balduini A, Abbonante V, Boselli D, De Marco L, Di Minno MND, Toschi V, Corsini A, Tremoli E, Camera M. Human megakaryocytes confer tissue factor to a subset of shed platelets to stimulate thrombin generation. *Thromb Haemost* Germany; 2015; **114**: 579–92.

185 Soslau G, Pastorino MB, Morgan DA, Brodsky I, Howett MK. Herpes simplex virus replication and protein synthesis in a human blood-derived cell line. *J Gen Virol* England; 1987; **68 (Pt 8)**: 2079–92.

186 Clark KB, Hsiao H-M, Bassit L, Crowe JEJ, Schinazi RF, Perng GC, Villinger F. Characterization of dengue virus 2 growth in megakaryocyte-erythrocyte progenitor cells. *Virology* 2016; **493**: 162–72.

187 Nakao S, Lai CJ, Young NS. Dengue virus, a flavivirus, propagates in human bone marrow progenitors and hematopoietic cell lines. *Blood* United States; 1989; **74**: 1235–40.

188 Clark KB, Noisakran S, Onlamoon N, Hsiao H-M, Roback J, Villinger F, Ansari AA, Perng GC. Multiploid CD61+ cells are the pre-dominant cell lineage infected during acute dengue virus infection in bone marrow. *PLoS One* United States; 2012; **7**: e52902.

189 Basu A, Jain P, Gangodkar S V, Shetty S, Ghosh K. Dengue 2 virus inhibits in vitro megakaryocytic colony formation and induces apoptosis in thrombopoietin-inducible megakaryocytic differentiation from cord blood CD34+ cells. *FEMS Immunol Med Microbiol* England; 2008; **53**: 46–51.

190 Gibellini D, Clò A, Morini S, Miserocchi A, Ponti C, Re MC. Effects of human immunodeficiency virus on the erythrocyte and megakaryocyte lineages. *World J Virol* 2013; **2**: 91–101.

191 Sakaguchi M, Sato T, Groopman JE. Human immunodeficiency virus infection of megakaryocytic cells. *Blood* United States; 1991; **77**: 481–5.

192 Li X, Jeffers LJ, Garon C, Fischer ER, Scheffel J, Moore B, Reddy KR, Demedina M, Schiff ER. Persistence of hepatitis C virus in a human megakaryoblastic leukaemia cell line. *J Viral Hepat* England; 1999; **6**: 107–14.

193 Franco RF, de Jonge E, Dekkers PE, Timmerman JJ, Spek CA, van Deventer SJ, van Deursen P, van Kerkhoff L, van Gemen B, ten Cate H, van der Poll T, Reitsma PH. The in vivo kinetics of tissue factor messenger RNA expression during human endotoxemia: relationship with activation of coagulation. *Blood* United States; 2000; **96**: 554–9.

194 Shivkumar M, Lawler C, Milho R, Stevenson PG. Herpes Simplex Virus 1 Interaction with Myeloid Cells In Vivo. *J Virol* American Society for Microbiology; 2016; **90**: 8661–72.

195 Bruun T, Kristoffersen AK, Rollag H, Degre M. Interaction of herpes simplex virus with mononuclear phagocytes is dependent on the differentiation stage of the cells. *APMIS* Denmark; 1998; **106**: 305–14.

196 Lee DH, Ghiasi H. Roles of M1 and M2 Macrophages in Herpes Simplex Virus 1 Infectivity. *J Virol* American Society for Microbiology; 2017; **91**: e00578-17.

197 Daughaday CC, Brandt WE, McCown JM, Russell PK. Evidence for two mechanisms of dengue virus infection of adherent human monocytes: trypsin-sensitive virus receptors and trypsin-resistant immune complex receptors. *Infect Immun* United States; 1981; **32**: 469–73.

198 Stevenson M. HIV-1 pathogenesis. *Nat Med* United States; 2003; **9**: 853–60.

199 Bouffard P, Hayashi PH, Acevedo R, Levy N, Zeldis JB. Hepatitis C virus is detected in a

monocyte/macrophage subpopulation of peripheral blood mononuclear cells of infected patients. *J Infect Dis* United States; 1992; **166**: 1276–80.

200 Lerat H, Rumin S, Habersetzer F, Berby F, Trabaud MA, Trepo C, Inchauspe G. In vivo tropism of hepatitis C virus genomic sequences in hematopoietic cells: influence of viral load, viral genotype, and cell phenotype. *Blood* United States; 1998; **91**: 3841–9.

201 Sansonno D, Iacobelli AR, Cornacchiulo V, Iodice G, Dammacco F. Detection of hepatitis C virus (HCV) proteins by immunofluorescence and HCV RNA genomic sequences by non-isotopic in situ hybridization in bone marrow and peripheral blood mononuclear cells of chronically HCV-infected patients. *Clin Exp Immunol* England; 1996; **103**: 414–21.

202 De Palma R, Cirillo P, Ciccarelli G, Barra G, Conte S, Pellegrino G, Pasquale G, Nassa G, Pacifico F, Leonardi A, Insabato L, Cali G, Golino P, Cimmino G. Expression of functional tissue factor in activated T-lymphocytes in vitro and in vivo: A possible contribution of immunity to thrombosis? *Int J Cardiol* Netherlands; 2016; **218**: 188–95.

203 Kirchner H, Kleinicke C, Northoff H. Replication of Herpes Simplex Virus in Human Peripheral T Lymphocytes. *J Gen Virol* 1977; **37**: 647–9.

204 JAHMIAS AJ, KIBRICK S, ROSAN RC. VIRAL LEUKOCYTE INTERRELATIONSHIPS. I. MULTIPLICATION OF A DNA VIRUS--HERPES SIMPLEX--IN HUMAN LEUKOCYTE CULTURES. *J Immunol* United States; 1964; **93**: 69–74.

205 Raftery MJ, Behrens CK, Müller A, Krammer PH, Walczak H, Schönrich G. Herpes simplex virus type 1 infection of activated cytotoxic T cells: Induction of fratricide as a mechanism of viral immune evasion. *J Exp Med* 1999; **190**: 1103–14.

206 Silveira GF, Wowk PF, Cataneo AHD, Dos Santos PF, Delgobo M, Stimamiglio MA, Lo

Sarzi M, Thomazelli APFS, Conchon-Costa I, Pavanelli WR, Antonelli LR V, Bafica A, Mansur DS, Dos Santos CND, Bordignon J. Human T Lymphocytes Are Permissive for Dengue Virus Replication. *J Virol* United States; 2018; **92**.

207 Grivel JC, Penn ML, Eckstein DA, Schramm B, Speck RF, Abbey NW, Herndier B, Margolis L, Goldsmith MA. Human immunodeficiency virus type 1 coreceptor preferences determine target T-cell depletion and cellular tropism in human lymphoid tissue. *J Virol* United States; 2000; **74**: 5347–51.

208 Brenchley JM, Hill BJ, Ambrozak DR, Price DA, Guenaga FJ, Casazza JP, Kuruppu J, Yazdani J, Migueles SA, Connors M, Roederer M, Douek DC, Koup RA. T-Cell Subsets That Harbor Human Immunodeficiency Virus (HIV) In Vivo: Implications for HIV Pathogenesis. *J Virol* American Society for Microbiology Journals; 2004; **78**: 1160–8.

209 Klatzmann D, Barre-Sinoussi F, Nugeyre MT, Danquet C, Vilmer E, Griscelli C, Brun-Veziret F, Rouzioux C, Gluckman JC, Chermann JC. Selective tropism of lymphadenopathy associated virus (LAV) for helper-inducer T lymphocytes. *Science* United States; 1984; **225**: 59–63.

210 Sarhan MA, Pham TNQ, Chen AY, Michalak TI. Hepatitis C Virus Infection of Human T Lymphocytes Is Mediated by CD5. *J Virol* American Society for Microbiology Journals; 2012; **86**: 3723–35.

211 Navas S, Mart\'\in J, Quiroga JA, Castillo I, Carreño V. Genetic Diversity and Tissue Compartmentalization of the Hepatitis C Virus Genome in Blood Mononuclear Cells, Liver, and Serum from Chronic Hepatitis C Patients. *J Virol* American Society for Microbiology Journals; 1998; **72**: 1640–6.

212 Laskus T, Radkowski M, Piasek A, Nowicki M, Horban A, Cianciara J, Rakela J.

Hepatitis C virus in lymphoid cells of patients coinfected with human immunodeficiency virus type 1: evidence of active replication in monocytes/macrophages and lymphocytes. *J Infect Dis* United States; 2000; **181**: 442–8.

213 Morissette G, Flamand L. Herpesviruses and chromosomal integration. *J Virol* United States; 2010; **84**: 12100–9.

214 Grinde B. Herpesviruses: latency and reactivation - viral strategies and host response. *J Oral Microbiol* United States; 2013; **5**.

215 Garceau R, Leblanc D, Thibault L, Girouard G, Mallet M. Herpes simplex virus type 1 is the leading cause of genital herpes in New Brunswick. *Can J Infect Dis Med Microbiol = J Can des Mal Infect la Microbiol medicale* Egypt; 2012; **23**: 15–8.

216 Farooq A V, Shukla D. Herpes simplex epithelial and stromal keratitis: an epidemiologic update. *Surv Ophthalmol* United States; 2012; **57**: 448–62.

217 Roberts S. Herpes simplex virus: incidence of neonatal herpes simplex virus, maternal screening, management during pregnancy, and HIV. *Curr Opin Obstet Gynecol* England; 2009; **21**: 124–30.

218 Tyler KL. Acute Viral Encephalitis. *N Engl J Med* United States; 2018; **379**: 557–66.

219 Spear PG, Longnecker R. Herpesvirus entry: an update. *J Virol* 2003; **77**: 10179–85.

220 Akhtar J, Tiwari V, Oh M-J, Kovacs M, Jani A, Kovacs SK, Valyi-Nagy T, Shukla D. HVEM and nectin-1 are the major mediators of herpes simplex virus 1 (HSV-1) entry into human conjunctival epithelium. *Invest Ophthalmol Vis Sci* United States; 2008; **49**: 4026–35.

221 Clement C, Tiwari V, Scanlan PM, Valyi-Nagy T, Yue BYJT, Shukla D. A novel role for phagocytosis-like uptake in herpes simplex virus entry. *J Cell Biol* United States; 2006;

174: 1009–21.

222 Nicola A V, Straus SE. Cellular and viral requirements for rapid endocytic entry of herpes simplex virus. *J Virol* United States; 2004; **78**: 7508–17.

223 Atanasiu D, Saw WT, Cohen GH, Eisenberg RJ. Cascade of events governing cell-cell fusion induced by herpes simplex virus glycoproteins gD, gH/gL, and gB. *J Virol* United States; 2010; **84**: 12292–9.

224 Dingwell KS, Johnson DC. The herpes simplex virus gE-gI complex facilitates cell-to-cell spread and binds to components of cell junctions. *J Virol* United States; 1998; **72**: 8933–42.

225 Karasneh GA, Shukla D. Herpes simplex virus infects most cell types in vitro: clues to its success. *Virol J* 2011; **8**: 481.

226 Loret S, Guay G, Lippé R. Comprehensive Characterization of Extracellular Herpes Simplex Virus Type 1 Virions. *J Virol* 2008; **82**: 8605 LP – 8618.

227 Benditt EP, Barrett T, McDougall JK. Viruses in the etiology of atherosclerosis. *Proc Natl Acad Sci U S A* United States; 1983; **80**: 6386–9.

228 Vercellotti GM. Effects of viral activation of the vessel wall on inflammation and thrombosis. *Blood Coagul Fibrinolysis* England; 1998; **9 Suppl 2**: S3-6.

229 Span AH, van Dam-Mieras MC, Mullers W, Endert J, Muller AD, Bruggeman CA. The effect of virus infection on the adherence of leukocytes or platelets to endothelial cells. *Eur J Clin Invest* England; 1991; **21**: 331–8.

230 Etingin OR, Hajjar DP. Evidence for cytokine regulation of cholesterol metabolism in herpesvirus-infected arterial cells by the lipoxygenase pathway. *J Lipid Res* United States; 1990; **31**: 299–305.

231 Görek A, Akçay Ş, Ibiş OA, Atar I, Eyüboğlu FÖ. Herpes simplex virus infection, massive pulmonary thromboembolism, and right atrial thrombi in a single patient: Case report. *Hear Lung J Acute Crit Care* 2007; **36**: 148–53.

232 Al-Ghamdi A. Role of herpes simplex virus-1, cytomegalovirus and Epstein-Barr virus in atherosclerosis. *Pak J Pharm Sci* Pakistan; 2012; **25**: 89–97.

233 Ibrahim AI, Obeid MT, Jouma MJ, Moasis GA, Al-Richane WL, Kindermann I, Boehm M, Roemer K, Mueller-Lantzsch N, Gartner BC. Detection of herpes simplex virus, cytomegalovirus and Epstein-Barr virus DNA in atherosclerotic plaques and in unaffected bypass grafts. *J Clin Virol* Netherlands; 2005; **32**: 29–32.

234 Wu YP, Sun DD, Wang Y, Liu W, Yang J. Herpes Simplex Virus Type 1 and Type 2 Infection Increases Atherosclerosis Risk: Evidence Based on a Meta-Analysis. *Biomed Res Int* Hindawi Publishing Corporation; 2016; **2016**.

235 European Medicines Agency. Imlygic. 2016.

236 Leite J, Ribeiro A, Goncalves D, Sargento-Freitas J, Trindade L, Duque V. Cerebral Venous Thrombosis as Rare Presentation of Herpes Simplex Virus Encephalitis. *Case reports in infectious diseases*. Egypt; 2019. p. 7835420.

237 Gorek A, Akcay S, Ibis OA, Atar I, Eyuboglu FO. Herpes simplex virus infection, massive pulmonary thromboembolism, and right atrial thrombi in a single patient: case report. *Heart Lung* United States; 2007; **36**: 148–53.

238 Singh TD, Fugate JE, Hocker S, Wijdicks EFM, Aksamit AJ, Rabinstein AA. Predictors of outcome in HSV encephalitis. *J Neurol* 2016; **263**: 277–89.

239 Li JZ, Sax PE. HSV-1 encephalitis complicated by cerebral hemorrhage in an HIV-positive person. *AIDS Read* United States; 2009; **19**: 153–5.

240 Etingin OR, Silverstein RL, Friedman HM, Hajjar DP. Viral activation of the coagulation cascade: molecular interactions at the surface of infected endothelial cells. *Cell* United States; 1990; **61**: 657–62.

241 Livingston JR, Sutherland MR, Friedman HM, Pryzdial ELG. Herpes simplex virus type 1-encoded glycoprotein C contributes to direct coagulation factor X-virus binding. *Biochem J* England; 2006; **393**: 529–35.

242 Fitzpatrick DR, Babiuk LA, Zamb TJ. Nucleotide sequence of bovine herpesvirus type 1 glycoprotein gIII, a structural model for gIII as a new member of the immunoglobulin superfamily, and implications for the homologous glycoproteins of other herpesviruses. *Virology* United States; 1989; **173**: 46–57.

243 Olofsson S, Sjoblom I, Lundstrom M, Jeansson S, Lycke E. Glycoprotein C of herpes simplex virus type 1: characterization of O-linked oligosaccharides. *J Gen Virol* England; 1983; **64 (Pt 12**: 2735–47.

244 Aasrum M, Prydz H. Gene targeting of tissue factor, factor X, and factor VII in mice: their involvement in embryonic development. *Biochemistry (Mosc)* United States; 2002; **67**: 25–32.

245 Rux AH, Moore WT, Lambris JD, Abrams WR, Peng C, Friedman HM, Cohen GH, Eisenberg RJ. Disulfide bond structure determination and biochemical analysis of glycoprotein C from herpes simplex virus. *J Virol* United States; 1996; **70**: 5455–65.

246 Altgärde N, Eriksson C, Peerboom N, Phan-xuan T, Moeller S, Schnabelrauch M, Svedhem S, Trybala E, Bergstro T, Bally M, Altgarde N, Eriksson C, Peerboom N, Phan-xuan T, Moeller S, Schnabelrauch M, Svedhem S, Trybala E, Bergstrom T, Bally M. Mucin-like Region of Herpes Simplex Virus Type 1 Attachment Protein Glycoprotein C

(gC) Modulates the Virus-Glycosaminoglycan Interaction. *J Biol Chem* United States; 2015; **290**: 21473–85.

247 Mardberg K, Trybala E, Tufaro F, Bergstrom T. Herpes simplex virus type 1 glycoprotein C is necessary for efficient infection of chondroitin sulfate-expressing gro2C cells. *J Gen Virol* England; 2002; **83**: 291–300.

248 Rux AH, Lou H, Lambris JD, Friedman HM, Eisenberg RJ, Cohen GH. Kinetic Analysis of Glycoprotein C of Herpes Simplex Virus Types 1 and 2 Binding to Heparin , Heparan Sulfate , and Complement Component C3b. *Virology* 2002; **332**: 324–32.

249 Mardberg K, Trybala E, Glorioso JC, Bergstrom T. Mutational analysis of the major heparan sulfate-binding domain of herpes simplex virus type 1 glycoprotein C. *J Gen Virol* England; 2001; **82**: 1941–50.

250 Trybala E, Olofsson S, Mårdberg K, Svennerholm B, Umemoto K, Glorioso JC, Bergström T. Structural and functional features of the polycationic peptide required for inhibition of herpes simplex virus invasion of cells. *Antiviral Res* 2004; **62**: 125–34.

251 MacLeod DT, Nakatsuji T, Yamasaki K, Kobzik L, Gallo RL. HSV-1 exploits the innate immune scavenger receptor MARCO to enhance epithelial adsorption and infection. *Nat Commun* England; 2013; **4**: 1963.

252 Herold BC, WuDunn D, Soltys N, Spear PG. Glycoprotein C of herpes simplex virus type 1 plays a principal role in the adsorption of virus to cells and in infectivity. *J Virol* 1991; **65**: 1090–8.

253 Lubinski JM, Wang L, Soulika AM, Burger R, Wetsel RA, Colten H, Cohen GH, Eisenberg RJ, Lambris JD, Friedman HM. Herpes Simplex Virus Type 1 Glycoprotein gC Mediates Immune Evasion In Vivo. *J Virol* American Society for Microbiology Journals;

1998; **72**: 8257–63.

254 Friedman HM, Cohen GH, Eisenberg RJ, Seidel CA, Cines DB. Glycoprotein C of herpes simplex virus 1 acts as a receptor for the C3b complement component on infected cells. *Nature* England; 1984; **309**: 633–5.

255 Hung SL, Peng C, Kostavasili I, Friedman HM, Lambris JD, Eisenberg RJ, Cohen GH. The interaction of glycoprotein C of herpes simplex virus types 1 and 2 with the alternative complement pathway. *Virology* United States; 1994; **203**: 299–312.

256 Noris M, Remuzzi G. Overview of complement activation and regulation. *Semin Nephrol* W.B. Saunders; 2013; **33**: 479–92.

257 Lubinski J, Wang L, Mastellos D, Sahu A, Lambris JD, Friedman HM. In vivo role of complement-interacting domains of herpes simplex virus type 1 glycoprotein gC. *J Exp Med* 1999; **190**: 1637–46.

258 Sutherland MR, Friedman HM, Pryzdial ELG. Herpes simplex virus type 1-encoded glycoprotein C enhances coagulation factor VIIa activity on the virus. *Thromb Haemost* Germany; 2004; **92**: 947–55.

259 Bhatt S, Gething PW, Brady OJ, Messina JP, Farlow AW, Moyes CL, Drake JM, Brownstein JS, Hoen AG, Sankoh O, Myers MF, George DB, Jaenisch T, Wint GRW, Simmons CP, Scott TW, Farrar JJ, Hay SI. The global distribution and burden of dengue. *Nature* England; 2013; **496**: 504–7.

260 Mustafa MS, Rasotgi V, Jain S, Gupta V. Discovery of fifth serotype of dengue virus (DENV-5): A new public health dilemma in dengue control. *Med journal, Armed Forces India* Elsevier; 2015; **71**: 67–70.

261 Crill WD, Chang G-JJ. Localization and characterization of flavivirus envelope

glycoprotein cross-reactive epitopes. *J Virol* United States; 2004; **78**: 13975–86.

262 Aubry M, Richard V, Green J, Broult J, Musso D. Inactivation of Zika virus in plasma with amotosalen and ultraviolet A illumination. *Transfusion* United States; 2016; **56**: 33–40.

263 Guzman MG, Alvarez M, Halstead SB. Secondary infection as a risk factor for dengue hemorrhagic fever/dengue shock syndrome: an historical perspective and role of antibody-dependent enhancement of infection. *Arch Virol* Austria; 2013; **158**: 1445–59.

264 Halstead SB. In vivo enhancement of dengue virus infection in rhesus monkeys by passively transferred antibody. *J Infect Dis* United States; 1979; **140**: 527–33.

265 Martina BEE, Koraka P, Osterhaus ADME. Dengue Virus Pathogenesis: an Integrated View. *Clin Microbiol Rev* 2009; **22**: 564 LP – 581.

266 Srichaikul T, Nimmannitya S. Haematology in dengue and dengue haemorrhagic fever. *Baillieres Best Pract Res Clin Haematol* England; 2000; **13**: 261–76.

267 Funahara Y, Sumarmo, Wirawan R. Features of DIC in dengue hemorrhagic fever. *Bibl Haematol* Switzerland; 1983; : 201–11.

268 Chuansumrit A, Chaiyaratana W. Hemostatic derangement in dengue hemorrhagic fever. *Thromb Res* Elsevier; 2014; **133**: 10–6.

269 Roy A, Chaudhuri J, Chakraborty S. Deep vein thrombosis associated with dengue fever. *Indian Pediatr* India; 2013; **50**: 1053–4.

270 da Costa PSG, Ribeiro GM, Junior CS, da Costa Campos L. Severe thrombotic events associated with dengue fever, Brazil. *Am J Trop Med Hyg* 2012; **87**: 741–2.

271 Agarwal A, Sharma S, Airun M. Life-Threatening Thrombo-embolic Events in a Case of Dengue Hemorrhagic Fever. *The Journal of the Association of Physicians of India*. India;

2016. p. 87–9.

272 Samarasekara K, Munasinghe J. Dengue shock syndrome complicated with acute liver failure and kidney injury, infective endocarditis, and deep vein thrombosis: a case report. *J Med Case Rep* 2018; **12**: 321.

273 Bhargava V, Gupta P, Kauntia R, Bajpai G. Dengue Fever-induced Thrombotic Microangiopathy: An Unusual Cause of Renal Failure. *Indian J Nephrol* India; 2017; **27**: 321–3.

274 Srikiatkhachorn A, Kelley JF. Endothelial cells in dengue hemorrhagic fever. *Antiviral Res* 2014; **109**: 160–70.

275 Sosothikul D, Seksarn P, Pongsewalak S, Thisyakorn U, Lusher J. Activation of endothelial cells, coagulation and fibrinolysis in children with Dengue virus infection. *Thromb Haemost* Germany; 2007; **97**: 627–34.

276 Jiang Z, Tang X, Xiao R, Jiang L, Chen X. Dengue virus regulates the expression of hemostasis-related molecules in human vein endothelial cells. *J Infect* England; 2007; **55**: e23-8.

277 Frueh J, Maimari N, Homma T, Bovens SM, Pedrigi RM, Towhidi L, Krams R. Systems biology of the functional and dysfunctional endothelium. *Cardiovasc Res* England; 2013; **99**: 334–41.

278 Friedl J, Puhlmann M, Bartlett DL, Libutti SK, Turner EN, Gnant MFX, Alexander HR. Induction of permeability across endothelial cell monolayers by tumor necrosis factor (TNF) occurs via a tissue factor-dependent mechanism: relationship between the procoagulant and permeability effects of TNF. *Blood* United States; 2002; **100**: 1334–9.

279 El-Serag HB. Epidemiology of viral hepatitis and hepatocellular carcinoma.

Gastroenterology United States; 2012; **142**: 1264-1273.e1.

280 Perz JF, Armstrong GL, Farrington LA, Hutin YJF, Bell BP. The contributions of hepatitis B virus and hepatitis C virus infections to cirrhosis and primary liver cancer worldwide. *J Hepatol* Netherlands; 2006; **45**: 529–38.

281 Westbrook RH, Dusheiko G. Natural history of hepatitis C. *J Hepatol* Netherlands; 2014; **61**: S58-68.

282 Brown RS. Hepatitis C and liver transplantation. *Nature* England; 2005; **436**: 973–8.

283 Ploss A, Evans MJ. Hepatitis C virus host cell entry. *Curr Opin Virol* 2012; **2**: 14–9.

284 Martin NK, Vickerman P, Dore GJ, Grebely J, Miners A, Cairns J, Foster GR, Hutchinson SJ, Goldberg DJ, Martin TCS, Ramsay M, Hickman M. Prioritization of HCV treatment in the direct-acting antiviral era: An economic evaluation. *J Hepatol* Netherlands; 2016; **65**: 17–25.

285 Nielsen NS, Jespersen S, Gaardbo JC, Arnbjerg CJ, Clausen MR, Kjær M, Gerstoft J, Ballegaard V, Ostrowski SR, Nielsen SD. Impaired Platelet Aggregation and Rebalanced Hemostasis in Patients with Chronic Hepatitis C Virus Infection. *Int J Mol Sci* MDPI; 2017; **18**: 1016.

286 Lisman T, Kwaan HC. Hemostatic Dysfunction in Liver Diseases. *Semin Thromb Hemost* United States; 2015; **41**: 445–6.

287 Lisman T, Porte RJ. Rebalanced hemostasis in patients with liver disease: evidence and clinical consequences. *Blood* United States; 2010; **116**: 878–85.

288 Kiefer EM, Shi Q, Hoover DR, Kaplan R, Tracy R, Augenbraun M, Liu C, Nowicki M, Tien PC, Cohen M, Golub ET, Anastos K. Association of hepatitis C with markers of hemostasis in HIV-infected and uninfected women in the women's interagency HIV study

(WIHS). *J Acquir Immune Defic Syndr* 2013; **62**: 301–10.

289 Antonova T V, Romanova MA, Lymar' I V. [Markers of endothelial dysfunction (VCAM-1 and vWF) in chronic hepatitis C]. *Ter Arkh* Russia (Federation); 2013; **85**: 86–9.

290 Feys HB, Canciani MT, Peyvandi F, Deckmyn H, Vanhoorelbeke K, Mannucci PM. ADAMTS13 activity to antigen ratio in physiological and pathological conditions associated with an increased risk of thrombosis. *Br J Haematol* England; 2007; **138**: 534–40.

291 Kamphuisen PW, Eikenboom JC, Bertina RM. Elevated factor VIII levels and the risk of thrombosis. *Arterioscler Thromb Vasc Biol* 2001; **21**: 731–8.

292 Schreiber ZA, Brau N. Acquired factor VIII inhibitor in patients with hepatitis C virus infection and the role of interferon-alpha: a case report. *Am J Hematol* United States; 2005; **80**: 295–8.

293 Dentale N, Fulgaro C, Guerra L, Fasulo G, Mazzetti M, Fabbri C. Acquisition of factor VIII inhibitor after acute hepatitis C virus infection. *Blood* United States; 1997; **90**: 3233–4.

294 Zeichner SB, Harris A, Turner G, Francavilla M, Lutzky J. An Acquired Factor VIII Inhibitor in a Patient with HIV and HCV: A Case Presentation and Literature Review. *Case Rep Hematol* United States; 2013; **2013**: 628513.

295 Mauser-Bunschoten EP, Damen M, Reesink HW, Roosendaal G, Chamuleau RA, van den Berg HM. Formation of antibodies to factor VIII in patients with hemophilia A who are treated with interferon for chronic hepatitis C. *Ann Intern Med* United States; 1996; **125**: 297–9.

296 Shredi A, Elberson BW, El Nawaa S, Ismail A. Acquired factor VIII inhibitor associated with chronic untreated hepatitis C. *Southwest Respir Crit Care Chronicles; Vol 6, No 23 Southwest Respir Crit Care Chronicles* 2018; .

297 Dhar A, Tschotazis E, Brown R, Manousou P, Millson C, Aldersley M, Forbes S, Aggarwal K, Gera A, Cramp M, Holt A, Mutimer D, McPherson S, Burroughs A, Anstee Q, Goldin R, Thursz MR. LP11 : Warfarin anticoagulation for liver fibrosis in patients transplanted for hepatitis C (WAFT-C): results at one year. *J Hepatol* Elsevier; 2015; **62**: S268–9.

298 Enger C, Forssen UM, Bennett D, Theodore D, Shantakumar S, McAfee A. Thromboembolic Events Among Patients with Hepatitis C Virus Infection and Cirrhosis: A Matched-Cohort Study. *Adv Ther* 2014; : 891–903.

299 Violi F, Ferro D, Basili S, Artini M, Valesini G, Levrero M, Cordova C. Increased rate of thrombin generation in hepatitis C virus cirrhotic patients. Relationship to venous thrombosis. *J Investig Med* England; 1995; **43**: 550–4.

300 Ambrosino P, Tarantino L, Criscuolo L, Nasto A, Celentano A, Di Minno MND. The risk of venous thromboembolism in patients with hepatitis C. A systematic review and meta-analysis. *Thromb Haemost* Germany; 2016; **116**: 958–66.

301 Saliola M, Lorenzet R, Ferro D, Basili S, Caroselli C, Di Santo A, Sallese M, Violi F. Enhanced expression of monocyte tissue factor in patients with liver cirrhosis. *Gut* BMJ Publishing Group; 1998; **43**: 428–32.

302 Kräusslich HG. Morphogenesis and Maturation of Retroviruses. Springer Berlin Heidelberg; 2012.

303 Griffiths DJ. Endogenous retroviruses in the human genome sequence. *Genome Biol* 2001;

2: REVIEWS1017.

304 Kurian KM, Watson CJ, Wyllie AH. Retroviral vectors. *Mol Pathol* 2000; **53**: 173–6.

305 Lucic B, Lusic M. Connecting HIV-1 integration and transcription: a step toward new treatments. *FEBS Lett* 2016; **590**: 1927–39.

306 Doms RW, Moore JP. HIV-1 membrane fusion: targets of opportunity. *J Cell Biol* 2000; **151**: F9-14.

307 Cohen MS, Hellmann N, Levy JA, DeCock K, Lange J. The spread, treatment, and prevention of HIV-1: evolution of a global pandemic. *J Clin Invest* The American Society for Clinical Investigation; 2008; **118**: 1244–54.

308 Garlassi E, Carli F, Orlando G, Guaraldi G, Menozzi M, Zona S, Berti A, Rossi E, Roverato A, Palella F. Premature Age-Related Comorbidities Among HIV-Infected Persons Compared With the General Population. *Clin Infect Dis* 2011; **53**: 1120–6.

309 Bibas M, Biava G, Antinori A. HIV-Associated Venous Thromboembolism. *Mediterr J Hematol Infect Dis* Università Cattolica del Sacro Cuore; 2011; **3**: e2011030–e2011030.

310 Funderburg NT, Mayne E, Sieg SF, Asaad R, Jiang W, Kalinowska M, Luciano AA, Stevens W, Rodriguez B, Brenchley JM, Douek DC, Lederman MM. Increased tissue factor expression on circulating monocytes in chronic HIV infection: relationship to in vivo coagulation and immune activation. *Blood* United States; 2010; **115**: 161–7.

311 Funderburg NT, Zidar DA, Shive C, Lioi A, Mudd J, Musselwhite LW, Simon DI, Costa MA, Rodriguez B, Sieg SF, Lederman MM. Shared monocyte subset phenotypes in HIV-1 infection and in uninfected subjects with acute coronary syndrome. *Blood* United States; 2012; **120**: 4599–608.

312 Baker J V, Huppler Hullsiek K, Bradford RL, Prosser R, Tracy RP, Key NS. Circulating

levels of tissue factor microparticle procoagulant activity are reduced with antiretroviral therapy and are associated with persistent inflammation and coagulation activation among HIV-positive patients. *J Acquir Immune Defic Syndr* United States; 2013; **63**: 367–71.

313 Ronsholt FF, Gerstoft J, Ullum H, Johansson PI, Katzenstein TL, Ostrowski SR. Thromboelastography on plasma reveals delayed clot formation and accelerated clot lyses in HIV-1 infected persons compared with healthy controls. *BMC Infect Dis* England; 2015; **15**: 388.

314 Thulasi Raman R, Manimaran D, Rachakatla P, Bharathi K, Afroz T, Sagar R. Study of Basic Coagulation Parameters among HIV Patients in Correlation to CD4 Counts and ART Status. *J Clin Diagn Res* India; 2016; **10**: EC04-6.

315 Omoregie R, Osakue SI, Ihemeje V, Omokaro EU, Ogeferet HO. Correlation of CD4 count with platelet count, prothrombin time and activated partial thromboplastin time among HIV patients in Benin City, Nigeria. *West Indian Med J* Jamaica; 2009; **58**: 437–40.

316 Camire RM, Larson PJ, Stafford DW, High KA. Enhanced γ-Carboxylation of Recombinant Factor X Using a Chimeric Construct Containing the Prothrombin Propeptide. *Biochemistry* American Chemical Society; 2000; **39**: 14322–9.

317 Aronson DL, Mustafa AJ, Mushinski JF. Purification of human factor X and comparison of peptide maps of human factor X and prothrombin. *Biochim Biophys Acta - Protein Struct* 1969; **188**: 25–30.

318 Waters EK, Morrissey JH. Restoring full biological activity to the isolated ectodomain of an integral membrane protein. *Biochemistry* United States; 2006; **45**: 3769–74.

319 Willis SH, Peng C, Leon MP, Nicola A V, Rux AH, Cohen GH, Eisenberg RJ. Expression

and Purification of Secreted Forms of HSV Glycoproteins from Baculovirus-Infected Insect Cells. *Methods Mol Med* United States; 1998; **10**: 131–56.

320 Tal-Singer R, Peng C, Ponce De Leon M, Abrams WR, Banfield BW, Tufaro F, Cohen GH, Eisenberg RJ. Interaction of herpes simplex virus glycoprotein gC with mammalian cell surface molecules. *J Virol* United States; 1995; **69**: 4471–83.

321 Morrissey JH, Fair DS, Edgington TS. Monoclonal antibody analysis of purified and cell-associated tissue factor. *Thromb Res* United States; 1988; **52**: 247–61.

322 Ruf W, Edgington TS. An anti-tissue factor monoclonal antibody which inhibits TF.VIIa complex is a potent anticoagulant in plasma. *Thromb Haemost* Germany; 1991; **66**: 529–33.

323 Verkley AJ, Leunissen JLM. Immunogold Labeling in Cell Biology. Boca Raton, Florida, USA: CRC Press; 1989.

324 Higgins DL, Mann KG. The interaction of bovine factor V and factor V-derived peptides with phospholipid vesicles. *J Biol Chem* United States; 1983; **258**: 6503–8.

325 Morrissey JH, Waters EK. Procoagulants based on metal-chelating lipids. 2006. p. 17.

326 Laue M, Bannert N. Detection limit of negative staining electron microscopy for the diagnosis of bioterrorism-related micro-organisms. *J Appl Microbiol* England; 2010; **109**: 1159–68.

327 Hsu AY-H, Wu S-R, Tsai J-J, Chen P-L, Chen Y-P, Chen T-Y, Lo Y-C, Ho T-C, Lee M, Chen M-T, Chiu Y-C, Perng GC. Infectious dengue vesicles derived from CD61+ cells in acute patient plasma exhibited a diaphanous appearance. *Sci Rep* Nature Publishing Group; 2015; **5**: 17990.

328 Fiore MM, Neuenschwander PF, Morrissey JH. The biochemical basis for the apparent

defect of soluble mutant tissue factor in enhancing the proteolytic activities of factor VIIa. *J Biol Chem* United States; 1994; **269**: 143–9.

329 Krishnaswamy S. The interaction of human factor VIIa with tissue factor. *J Biol Chem* United States; 1992; **267**: 23696–706.

330 Rand MD, Lock JB, van't Veer C, Gaffney DP, Mann KG. Blood clotting in minimally altered whole blood. *Blood* United States; 1996; **88**: 3432–45.

331 Ratnoff OD, Moneme V. Inhibition of ellagic acid-activated Hageman factor (factor XII) and Hageman factor fragments by popcorn inhibitor. *Proc Soc Exp Biol Med* United States; 1981; **166**: 297–9.

332 Rodger G, Boname J, Bell S, Minson T. Assembly and organization of glycoproteins B, C, D, and H in herpes simplex virus type 1 particles lacking individual glycoproteins: No evidence for the formation of a complex of these molecules. *J Virol* United States; 2001; **75**: 710–6.

333 Jerabek-Willemsen M, André T, Wanner R, Roth HM, Duhr S, Baaske P, Breitsprecher D. MicroScale Thermophoresis: Interaction analysis and beyond. *J Mol Struct* Elsevier; 2014; **1077**: 101–13.

334 Andreev YA, Kozlov SA, Vassilevski AA, Grishin E V. Cyanogen bromide cleavage of proteins in salt and buffer solutions. *Anal Biochem* 2010; **407**: 144—146.

335 Stone MJ, Ruf W, Miles DJ, Edgington TS, Wright PE. Recombinant soluble human tissue factor secreted by Saccharomyces cerevisiae and refolded from Escherichia coli inclusion bodies: glycosylation of mutants, activity and physical characterization. *Biochem J* 1995; **310**: 605 LP – 614.

336 Pryzdial EL, Wright JF. Prothrombinase assembly on an enveloped virus: evidence that

the cytomegalovirus surface contains procoagulant phospholipid. *Blood* United States; 1994; **84**: 3749–57.

337 Cairns TM, Huang Z-Y, Gallagher JR, Lin Y, Lou H, Whitbeck JC, Wald A, Cohen GH, Eisenberg RJ. Patient-Specific Neutralizing Antibody Responses to Herpes Simplex Virus Are Attributed to Epitopes on gD, gB, or Both and Can Be Type Specific. *J Virol* American Society for Microbiology; 2015; **89**: 9213–31.

338 Para MF, Baucke RB, Spear PG. Immunoglobulin G(Fc)-binding receptors on virions of herpes simplex virus type 1 and transfer of these receptors to the cell surface by infection. *J Virol* United States; 1980; **34**: 512–20.

339 Dubin G, Frank I, Friedman HM. Herpes simplex virus type 1 encodes two Fc receptors which have different binding characteristics for monomeric immunoglobulin G (IgG) and IgG complexes. *J Virol* United States; 1990; **64**: 2725–31.

340 Berman EJ, Hill JM. Spontaneous ocular shedding of HSV-1 in latently infected rabbits. *Invest Ophthalmol Vis Sci* United States; 1985; **26**: 587–90.

341 Sen P, Neuenschwander PF, Pendurthi UR, Rao LVM. Analysis of factor VIIa binding to relipidated tissue factor by surface plasmon resonance. *Blood Coagul fibrinolysis an Int J Haemost Thromb* 2010; **21**: 376–9.

342 Delguste M, Peerboom N, Le Brun G, Trybala E, Olofsson S, Bergström T, Alsteens D, Bally M. Regulatory Mechanisms of the Mucin-Like Region on Herpes Simplex Virus during Cellular Attachment. *ACS Chem Biol* American Chemical Society; 2019; **14**: 534–42.

343 Paborsky LR, Harris RJ. Post-translational modifications of recombinant human tissue factor. *Thromb Res* United States; 1990; **60**: 367–76.

344 Kothari H, Rao LVM, Pendurthi UR. Glycosylation of tissue factor is not essential for its transport or functions. *J Thromb Haemost* England; 2011; **9**: 1511–20.

345 Smith SA, Morrissey JH. Heparin is procoagulant in the absence of antithrombin. *Thromb Haemost* 2008; **100**: 160–2.

346 Varki A, Cummings RD, Esko JD, Stanley P, Hart GW, Aebi M, Darvill AG, Kinoshita T, Packer NH, Prestegard JH, Schnaar RL, Seeberger PH. Glycosaminoglycan-binding Proteins. *Essentials of Glycobiology*. New York: Cold Spring Harbor Laboratory Press; 1999.

347 Martinez-Martinez I, Ordonez A, Pedersen S, de la Morena-Barrio ME, Navarro-Fernandez J, Kristensen SR, Minano A, Padilla J, Vicente V, Corral J. Heparin affinity of factor VIIa: implications on the physiological inhibition by antithrombin and clearance of recombinant factor VIIa. *Thromb Res* United States; 2011; **127**: 154–60.

348 Nogami K, Freas J, Manithody C, Wakabayashi H, Rezaie AR, Fay PJ. Mechanisms of interactions of factor X and factor Xa with the acidic region in the factor VIII A1 domain. *J Biol Chem* United States; 2004; **279**: 33104–13.

349 Lata S, Reichel A, Brock R, Tampe R, Piehler J. High-affinity adaptors for switchable recognition of histidine-tagged proteins. *J Am Chem Soc* United States; 2005; **127**: 10205–15.

350 Petersen LC, Albrektsen T, Hjorto GM, Kjalke M, Bjorn SE, Sorensen BB. Factor VIIa/tissue factor-dependent gene regulation and pro-coagulant activity: effect of factor VIIa concentration. *Thromb Haemost* Germany; 2007; **98**: 909–11.

351 Waxman E, Ross JB, Laue TM, Guha A, Thiruvikraman S V, Lin TC, Konigsberg WH, Nemerson Y. Tissue factor and its extracellular soluble domain: the relationship between

intermolecular association with factor VIIa and enzymatic activity of the complex. *Biochemistry* United States; 1992; **31**: 3998–4003.

352 Meng ZH, Wolberg AS, Monroe DM 3rd, Hoffman M. The effect of temperature and pH on the activity of factor VIIa: implications for the efficacy of high-dose factor VIIa in hypothermic and acidotic patients. *J Trauma* United States; 2003; **55**: 886–91.

353 Longstaff C, Thelwell C, Williams SC, Silva MMCG, Szabó L, Kolev K. The interplay between tissue plasminogen activator domains and fibrin structures in the regulation of fibrinolysis: kinetic and microscopic studies. *Blood* 2011; **117**: 661–8.

354 McCallum CD, Hapak RC, Neuenschwander PF, Morrissey JH, Johnson AE. The location of the active site of blood coagulation factor VIIa above the membrane surface and its reorientation upon association with tissue factor. A fluorescence energy transfer study. *J Biol Chem* United States; 1996; **271**: 28168–75.

355 Neuenschwander PF, Morrissey JH. Deletion of the membrane anchoring region of tissue factor abolishes autoactivation of factor VII but not cofactor function. Analysis of a mutant with a selective deficiency in activity. *J Biol Chem* United States; 1992; **267**: 14477–82.

356 Sedlackova L, Perkins KD, Lengyel J, Strain AK, van Santen VL, Rice SA. Herpes simplex virus type 1 ICP27 regulates expression of a variant, secreted form of glycoprotein C by an intron retention mechanism. *J Virol* United States; 2008; **82**: 7443–55.

357 Roosterman D, Schmidlin F, Bunnett NW. Rab5a and rab11a mediate agonist-induced trafficking of protease-activated receptor 2. *Am J Physiol Cell Physiol* United States; 2003; **284**: C1319-29.

358 Stegen C, Yakova Y, Henaff D, Nadjar J, Duron J, Lippe R. Analysis of virion-incorporated host proteins required for herpes simplex virus type 1 infection through a RNA interference screen. *PLoS One* United States; 2013; **8**: e53276.

359 Hollinshead M, Johns HL, Sayers CL, Gonzalez-Lopez C, Smith GL, Elliott G. Endocytic tubules regulated by Rab GTPases 5 and 11 are used for envelopment of herpes simplex virus. *EMBO J* England; 2012; **31**: 4204–20.

360 Harris SL, Frank I, Yee A, Cohen GH, Eisenberg RJ, Friedman HM. Glycoprotein C of herpes simplex virus type 1 prevents complement- mediated cell lysis and virus neutralization. *J Infect Dis* 1990; **162**: 331–7.

361 Friedman HM, Wang L, Fishman NO, Lambris JD, Eisenberg RJ, Cohen GH, Lubinski J. Immune evasion properties of herpes simplex virus type 1 glycoprotein gC. *J Virol* 1996; **70**: 4253–60.

362 Leta S, Beyene TJ, De Clercq EM, Amenu K, Kraemer MUG, Revie CW. Global risk mapping for major diseases transmitted by Aedes aegypti and Aedes albopictus. *Int J Infect Dis* 2018; **67**: 25–35.

363 Giordano B V, Gasparotto A, Hunter FF. A checklist of the 67 mosquito species of Ontario, Canada. *J Am Mosq Control Assoc* United States; 2015; **31**: 101–3.

364 Windsor-Essex County Health Unit. Aedes albopictus mosquito: 2018 adult mosquito survillance - Ae. albopictus mosquitoes identified. 2018.

365 Ng V, Rees E, Lindsay L, Drebot M, Brownstone T, T S, Khan S. Could exotic mosquito-borne diseases emerge in Canada with climate change? *Can Commun Dis Rep* 2019; **45**: 98–107.

366 Kilpatrick AM, Kramer LD, Jones MJ, Marra PP, Daszak P. West Nile virus epidemics in

North America are driven by shifts in mosquito feeding behavior. *PLoS Biol* United States; 2006; **4**: e82.

367 Giordano B V, Kaur S, Hunter FF. West Nile virus in Ontario, Canada: A twelve-year analysis of human case prevalence, mosquito surveillance, and climate data. *PLoS One* Public Library of Science; 2017; **12**: e0183568.

368 Zheng H, Drebot MA, Coulthart MB. West Nile virus in Canada: ever-changing, but here to stay. *Can Commun Dis Rep* Canada; 2014; **40**: 173–7.

369 Butenas S, Bouchard BA, Brummel-Ziedins KE, Parhami-Seren B, Mann KG. Tissue factor activity in whole blood. *Blood* United States; 2005; **105**: 2764–70.

370 Burke DS, van Panhuis WG, Endy TP, Rothman AL, Srikiatkhachorn A, Cummings DAT, Nisalak A, Gibbons R V. Inferring the Serotype Associated with Dengue Virus Infections on the Basis of Pre- and Postinfection Neutralizing Antibody Titers. *J Infect Dis* 2010; **202**: 1002–10.

371 Del Moral-Hernández O, Martínez-Hernández NE, Mosso-Pani MA, Hernández-Sotelo D, Illades-Aguiar B, Flores-Alfaro E, Antonio-Vejar V, Leyva-Vázquez MA. Association DENV1 and DENV2 infection with high serum levels of soluble thrombomodulin and VEGF in patients with dengue fever and dengue hemorrhagic fever. *Int J Clin Exp Med* 2014; **7**: 370–8.

372 Sasmono RT, Taurel A-F, Prayitno A, Sitompul H, Yohan B, Hayati RF, Bouckenooghe A, Hadinegoro SR, Nealon J. Dengue virus serotype distribution based on serological evidence in pediatric urban population in Indonesia. *PLoS Negl Trop Dis* 2018; **12**: e0006616.

373 Murakami MT, Rios-Steiner J, Weaver SE, Tulinsky A, Geiger JH, Arni RK.

Intermolecular Interactions and Characterization of the Novel Factor Xa Exosite Involved in Macromolecular Recognition and Inhibition: Crystal Structure of Human Gla-domainless Factor Xa Complexed with the Anticoagulant Protein NAPc2 from the Hematophagou. *J Mol Biol* 2007; **366**: 602–10.

374 Zhang Q, Hunke C, Yau YH, Seow V, Lee S, Tanner LB, Guan XL, Wenk MR, Fibriansah G, Chew PL, Kukkaro P, Biukovic G, Shi P-Y, Shochat SG, Gruber G, Lok S-M. The stem region of premembrane protein plays an important role in the virus surface protein rearrangement during dengue maturation. *J Biol Chem* United States; 2012; **287**: 40525–34.

375 Callahan MK, Popernack PM, Tsutsui S, Truong L, Schlegel RA, Henderson AJ. Phosphatidylserine on HIV Envelope Is a Cofactor for Infection of Monocytic Cells. *J Immunol* 2003; **170**: 4840 LP – 4845.

376 Merz A, Long G, Hiet M-S, Brügger B, Chlanda P, Andre P, Wieland F, Krijnse-Locker J, Bartenschlager R. Biochemical and morphological properties of hepatitis C virus particles and determination of their lipidome. *J Biol Chem* American Society for Biochemistry and Molecular Biology; 2011; **286**: 3018–32.

377 Stefas I, Tigrett S, Dubois G, Kaiser M, Lucarz E, Gobby D, Bray D, Ellerbrok H, Zarski JP, Veas F. Interactions between Hepatitis C Virus and the Human Apolipoprotein H Acute Phase Protein: A Tool for a Sensitive Detection of the Virus. *PLoS One* Public Library of Science; 2015; **10**: e0140900.

378 Briggs JAG, Wilk T, Welker R, Kräusslich H-G, Fuller SD. Structural organization of authentic, mature HIV-1 virions and cores. *EMBO J* Oxford University Press; 2003; **22**: 1707–15.

379 Faivre-Moskalenko C, Bernaud J, Thomas A, Tartour K, Beck Y, Iazykov M, Danial J, Lourdin M, Muriaux D, Castelnovo M. RNA Control of HIV-1 Particle Size Polydispersity. *PLoS One* Public Library of Science; 2014; **9**: e83874.

380 Zhu P, Chertova E, Bess JJ, Lifson JD, Arthur LO, Liu J, Taylor KA, Roux KH. Electron tomography analysis of envelope glycoprotein trimers on HIV and simian immunodeficiency virus virions. *Proc Natl Acad Sci U S A* United States; 2003; **100**: 15812–7.

381 Muriel L, Anne G, Jean D. HCV Glycoproteins: Assembly of a Functional E1–E2 Heterodimer. In: SL T, editor. *Hepatitis C Viruses: Genomes and Molecular Biology*. Norfolk, UK: Horizon Bioscience; 2006.

382 Ralston R, Thudium K, Berger K, Kuo C, Gervase B, Hall J, Selby M, Kuo G, Houghton M, Choo QL. Characterization of hepatitis C virus envelope glycoprotein complexes expressed by recombinant vaccinia viruses. *J Virol* American Society for Microbiology Journals; 1993; **67**: 6753–61.

383 Drummer HE, Maerz A, Poumbourios P. Cell surface expression of functional hepatitis C virus E1 and E2 glycoproteins. *FEBS Lett* England; 2003; **546**: 385–90.

384 Catanese MT, Uryu K, Kopp M, Edwards TJ, Andrus L, Rice WJ, Silvestry M, Kuhn RJ, Rice CM. Ultrastructural analysis of hepatitis C virus particles. *Proc Natl Acad Sci U S A* United States; 2013; **110**: 9505–10.

385 Piver E, Boyer A, Gaillard J, Bull A, Beaumont E, Roingeard P, Meunier J-C. Ultrastructural organisation of HCV from the bloodstream of infected patients revealed by electron microscopy after specific immunocapture. *Gut* BMJ Publishing Group; 2017; **66**: 1487–95.

386 Owens AP 3rd, Mackman N. Microparticles in hemostasis and thrombosis. *Circ Res* 2011; **108**: 1284–97.

387 Germi R, Crance J-M, Garin D, Guimet J, Lortat-Jacob H, Ruigrok RWH, Zarski J-P, Drouet E. Heparan Sulfate-Mediated Binding of Infectious Dengue Virus Type 2 and Yellow Fever Virus. *Virology* 2002; **292**: 162–8.

388 Pereira EMA, Dario AF, França RFO, Fonseca BAL, Petri DFS. Binding of Dengue Virus Particles and Dengue Proteins onto Solid Surfaces. *ACS Appl Mater Interfaces* American Chemical Society; 2010; **2**: 2602–10.

389 Raghav SK, Gupta B, Agrawal C, Saroha A, Das RH, Chaturvedi VP, Das HR. Altered expression and glycosylation of plasma proteins in rheumatoid arthritis. *Glycoconj J* United States; 2006; **23**: 167–73.

390 Shen W-F, Galula JU, Chang G-JJ, Wu H-C, King C-C, Chao D-Y. Improving dengue viral antigens detection in dengue patient serum specimens using a low pH glycine buffer treatment. *J Microbiol Immunol Infect* 2017; **50**: 167–74.

391 Lippe R. Flow Virometry: a Powerful Tool To Functionally Characterize Viruses. *J Virol* United States; 2018; **92**.

392 Dowbenko DJ, Lasky LA. Extensive homology between the herpes simplex virus type 2 glycoprotein F gene and the herpes simplex virus type 1 glycoprotein C gene. *J Virol* 1984; **52**: 154–63.

393 Hook LM, Lubinski JM, Jiang M, Pangburn MK, Friedman HM. Herpes simplex virus type 1 and 2 glycoprotein C prevents complement-mediated neutralization induced by natural immunoglobulin M antibody. *J Virol* 2006; **80**: 4038–46.

394 Jarosinski KW, Osterrieder N. Marek's disease virus expresses multiple UL44 (gC)

variants through mRNA splicing that are all required for efficient horizontal transmission. *J Virol* 2012; **86**: 7896–906.

395 Irons EE, Flatt JW, Doronin K, Fox TL, Acchione M, Stewart PL, Shayakhmetov DM. Coagulation factor binding orientation and dimerization may influence infectivity of adenovirus-coagulation factor complexes. *J Virol* United States; 2013; **87**: 9610–9.

396 Parker AL, Waddington SN, Nicol CG, Shayakhmetov DM, Buckley SM, Denby L, Kemball-Cook G, Ni S, Lieber A, McVey JH, Nicklin SA, Baker AH. Multiple vitamin K-dependent coagulation zymogens promote adenovirus-mediated gene delivery to hepatocytes. *Blood* United States; 2006; **108**: 2554–61.

397 Doronin K, Flatt JW, Di Paolo NC, Khare R, Kalyuzhniy O, Acchione M, Sumida JP, Ohto U, Shimizu T, Akashi-Takamura S, Miyake K, MacDonald JW, Bammler TK, Beyer RP, Farin FM, Stewart PL, Shayakhmetov DM. Coagulation factor X activates innate immunity to human species C adenovirus. *Science* United States; 2012; **338**: 795–8.

398 Notredame C, Higgins DG, Heringa J. T-Coffee: A novel method for fast and accurate multiple sequence alignment. *J Mol Biol* England; 2000; **302**: 205–17.

399 Ghosh S, Pendurthi UR, Steinoe A, Esmon CT, Rao LVM. Endothelial cell protein C receptor acts as a cellular receptor for factor VIIa on endothelium. *J Biol Chem* United States; 2007; **282**: 11849–57.

400 Oganesyan V, Oganesyan N, Terzyan S, Qu D, Dauter Z, Esmon NL, Esmon CT. The crystal structure of the endothelial protein C receptor and a bound phospholipid. *J Biol Chem* United States; 2002; **277**: 24851–4.

401 Kutner RH, Zhang X-Y, Reiser J. Production, concentration and titration of pseudotyped HIV-1-based lentiviral vectors. *Nat Protoc* England; 2009; **4**: 495–505.

402 Dettenhofer M, Yu X-F. Highly Purified Human Immunodeficiency Virus Type 1 Reveals a Virtual Absence of Vif in Virions. *J Virol* American Society for Microbiology Journals; 1999; **73**: 1460–7.

403 Giacaman RA, Nobbs AH, Ross KF, Herzberg MC. Porphyromonas gingivalis Selectively Up-Regulates the HIV-1 Coreceptor CCR5 in Oral Keratinocytes. *J Immunol* American Association of Immunologists; 2007; **179**: 2542–50.

404 Boven LA, Vergnolle N, Henry SD, Silva C, Imai Y, Holden J, Warren K, Hollenberg MD, Power C. Up-Regulation of Proteinase-Activated Receptor 1 Expression in Astrocytes During HIV Encephalitis. *J Immunol* American Association of Immunologists; 2003; **170**: 2638–46.

405 Geisbert TW, Hensley LE, Jahrling PB, Larsen T, Geisbert JB, Paragas J, Young HA, Fredeking TM, Rote WE, Vlasuk GP. Treatment of Ebola virus infection with a recombinant inhibitor of factor VIIa/tissue factor: a study in rhesus monkeys. *Lancet* England; 2003; **362**: 1953–8.

406 Wang P, Yang X. Neutralization Efficiency Is Greatly Enhanced by Bivalent Binding of an Antibody to Epitopes in the V4 Region and the Membrane-Proximal External Region within One Trimer of Human Immunodeficiency Virus Type 1 Glycoproteins. *J Virol* American Society for Microbiology Journals; 2010; **84**: 7114–23.

407 Jesty J. The determination of enzyme-cofactor dissociation constants by kinetic methods: a correction. *Thromb Res* United States; 1988; **50**: 745–6.

Appendices

Appendix A

A.1 Derivation of quadratic binding isotherm

The quadratic binding isotherm is used to determine the apparent dissociation constant for the FVIIa and cofactor (lipid and/or protein). Please refer to Figure 20. Schematic of non-enzymatic and enzymatic reactions involved in FVIIa-mediated FX activation. The following equations are derived from the schematic:

$[E]_0 = [E] + [EC] + [ES] + [ECS]$ (Equation 1)

$[C]_0 = [C] + [EC] + [ECS]$ (Equation 2)

$[E] \cdot [C] = K_d \cdot [EC]$ (Equation 3)

$[ES] \cdot [C] = K_d' \cdot [ESC]$ (Equation 4)

$[EC] \cdot [S] = K_s \cdot [ECS]$ (Equation 5)

$[E] \cdot [S] = K_s' \cdot [ES]$ (Equation 6)

$[C_L] \cdot [C_P] = K_c \cdot [C]$ (Equation 7)

Using equations 1-4, E_0 can be expressed as: (brackets denoting concentration are removed for improved clarity)

$$E_0 = \frac{K_d \cdot EC}{C_0 - EC - ECS} + EC + \frac{K_d' \cdot ECS}{C_0 - EC - ECS} + ECS$$

Substituting equation 5 for EC obtains:

$$E_0 = \frac{K_d \cdot \frac{K_s \cdot ECS}{S} + K_d' \cdot ECS}{C_0 - \frac{K_s \cdot ECS}{S} - ECS} + \frac{K_s \cdot ECS}{S} + ECS$$

$$E_0 = \frac{K_d \cdot \frac{K_s \cdot ECS}{S} + K_d' \cdot ECS}{C_0 - \frac{K_s \cdot ECS}{S} - ECS} + \frac{ECS(K_s + S)}{S}$$

Multiplying both sides by $C_0 - \frac{K_s \cdot ECS}{S} - ECS$ and S results in:

$$E_0 \cdot C_0 \cdot S - E_0 \cdot K_s \cdot ECS - E_0 \cdot ECS \cdot S = S \cdot (K_d \cdot \frac{K_s \cdot ECS}{S} + K'_d \cdot ECS) + ECS(K_s + S)(C_0 - \frac{K_s \cdot ECS}{S} - ECS)$$

Dividing both sides by $(K_s + S)$ with rearranging:

$$\frac{E_0 \cdot C_0 \cdot S - E_0 \cdot K_s \cdot ECS - E_0 \cdot ECS \cdot S}{K_s + S} = \frac{K_d \cdot K_s \cdot ECS + S \cdot K'_d \cdot ECS}{K_s + S} + ECS \cdot C_0 - \frac{K_s \cdot ECS^2}{S} - ECS^2$$

Rearranging to the left side results in:

$$ECS^2 + \frac{K_s \cdot ECS^2}{S} - ECS \cdot C_0 + \frac{E_0 \cdot C_0 \cdot S - E_0 \cdot K_s \cdot ECS - E_0 \cdot ECS \cdot S - K_d \cdot K_s \cdot ECS - S \cdot K'_d \cdot ECS}{K_s + S} = 0$$

$$ECS^2 \left(\frac{K_s + S}{S}\right) - ECS \cdot C_0 + \frac{E_0 \cdot C_0 \cdot S - E_0 \cdot K_s \cdot ECS - E_0 \cdot ECS \cdot S - K_d \cdot K_s \cdot ECS - S \cdot K'_d \cdot ECS}{K_s + S} = 0$$

Substitution of $-E_0 \cdot K_s \cdot ECS - E_0 \cdot ECS \cdot S$ for $-(K_s + S)(E_0 ECS)$ yields:

$$ECS^2 \left(\frac{K_s + S}{S}\right) - ECS \cdot C_0 + \frac{E_0 \cdot C_0 \cdot S - (K_s + S)(E_0 ECS) - K_d \cdot K_s \cdot ECS - S \cdot K'_d \cdot ECS}{K_s + S} = 0$$

Some rearrangements:

$$ECS^2 \left(\frac{K_s + S}{S}\right) - ECS \cdot C_0 - E_0 ECS + \frac{-K_d \cdot K_s \cdot ECS - S \cdot K'_d \cdot ECS}{K_s + S} + \frac{E_0 \cdot C_0 \cdot S}{K_s + S} = 0$$

$$ECS^2 \left(\frac{K_s + S}{S}\right) - ECS \cdot (C_0 + E_0) - \frac{K_d \cdot K_s \cdot ECS + K'_d \cdot S \cdot ECS}{K_s + S} + \frac{E_0 \cdot C_0 \cdot S}{K_s + S} = 0$$

$$ECS^2 \left(\frac{K_s + S}{S}\right) - ECS \left(\frac{K_d \cdot K_s + K'_d \cdot S}{K_s + S} + E_0 + C_0\right) + \frac{E_0 \cdot C_0 \cdot S}{K_s + S} = 0 \qquad \text{(Equation 8)}$$

For the given activity of the reaction, $v = k_{cat} \cdot ECS + k_{cat}{}' \cdot ES$. As $k_{cat}{}'$ was experimentally determined to be must less than k_{cat}, the equation becomes: $v \approx k_{cat} \cdot ECS$. Substituting $k_{cat} = \frac{V_{max}}{E_0}$, the equation becomes $v = V_{max} \cdot \frac{ECS}{E_0}$. By using the quadratic equation to solve for ECS from equation 8, one can solve for v:

$ECS = \frac{-b \pm \sqrt{b^2-4ac}}{2a}$ where $a = \frac{(K_s+S)}{S}$, $b = \frac{K_d \cdot K_s + K'_d \cdot S}{K_s+S} + E_0 + C_0$, and $c = \frac{E_0 \cdot C_0 \cdot S}{K_s+S}$,

$$v = \frac{V_{max} \cdot S}{2 \cdot E_0 (K_s+S)} \left(E_0 + C_0 + \frac{K_d \cdot K_s + K'_d \cdot S}{K_s+S} \pm \sqrt{\left(E_0 + C_0 + \frac{K_d \cdot K_s + K'_d \cdot S}{K_s+S} \right)^2 - 4 \cdot E_0 \cdot C_0} \right) \quad \text{(Equation 9)}$$

Based on previous works [94,407], the quadratic isotherm is similar to equation 9 with

$K_{d,app} = \frac{K_d \cdot K_s + K'_d \cdot S}{K_s+S}$

$K_d \cdot K_s = K'_d \cdot K'_s$ is predicted based on symmetry (Figure 20). This allows the following rearrangement after substitution of K'_d:

$K_{d,app} = K_d \frac{K_s + K_s \cdot S / K'_s}{K_s+S}$

K_d can thus be solved if K_s and K'_s are known. Furthermore, if $K_s = K'_s$, then $K_{d,app} = K_d$.

As described by Equation 7, Ni-chelating lipids affect the available membrane-bound cofactor. The complexity of the added effect of phospholipid was ablated with the assumption that the dissociation value of cofactor to FVIIa is much larger than that of cofactor/lipid to FVIIa. This allows a minor change to the quadratic binding isotherm to:

$$v = \frac{V_{max} \cdot S}{2 \cdot E_0 (K_s + S)} \left(E_0 + C_0 - C_L + \frac{K_d \cdot K_s + K'_d \cdot S + C_L}{K_s + S} \pm \sqrt{\left(E_0 + C_0 - C_L + \frac{K_d \cdot K_s + K'_d \cdot S + C_L}{K_s + S} \right)^2 - 4 \cdot E_0 \cdot C_0} \right)$$

Where $K_{d,app} = \frac{K_d \cdot K_s + K'_d \cdot S + C_L}{K_s+S}$.

A.2 FVIIa-R retains most of its FVIIa function

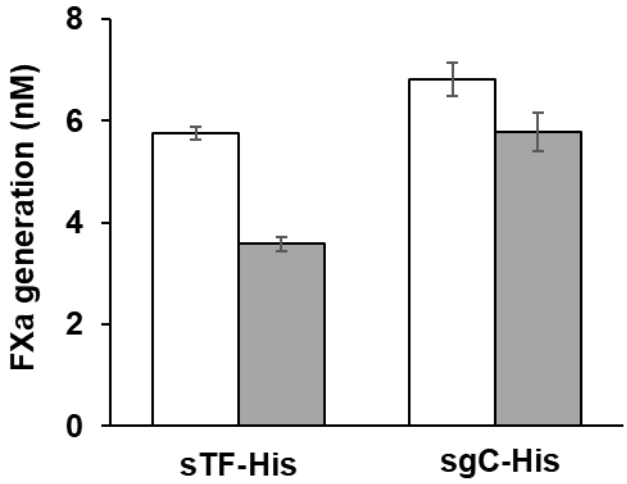

Figure 55. FVIIa-R retains its function when bound to sTF-His or sgC-His.

FVIIa-R FX-activating ability was assessed by FX chromogenic assay. 5 pM of FVIIa (white bar) or FVIIa-R (gray bar) was incubated with 50 μM NiPCPS, 5 mM Ca^{2+} and 400 pM sTF-His or 400 nM sgC-His. FX was added to initiate the reaction and the mixture was incubated for 20 min at 37 °C prior to stopping the reaction with EDTA and measuring FX activation with chromogenic substrate.

A.3 Comparison of fits for MST-derived FVIIa-R interactions

Table A5. Comparison of fits for MST-derived FVIIa-R interactions

		Simple binding fit			
		No FX		With FX	
Ligand	Lipid	K_d (μM) (95% CI)	r2	K_d (μM) (95% CI)	r2
sTF-His	NiPCPS	8.2×10^{-4} (8.6×10^{-5} – 1.5×10^{-3})	0.93	3.0×10^{-5} (0.8×10^{-5} – 5.2×10^{-5})	0.9468
sgC-His	NiPC	2.0 (1.3 – 2.8)	0.896	0.9 (0.7 – 1.0)	0.98
sgC-His	NiPCPS	1.3 (0.8 – 1.7)	0.935	0.6 (0.2 – 0.9)	0.963
sgC-His	PCPS	No fit	-	2.2 (0.9 – 3.5)	0.822
sgC-His	None	No fit	-	2.9 (1.5 – 4.2)	0.994

		Hill equation fit			
		No FX		With FX	
Ligand	Lipid	EC_{50} (μM) (95% CI)	r^2	EC_{50} (μM) (95% CI)	r^2
sTF-His	NiPCPS	1.0×10^{-3} (4.3×10^{-4} – 2.4×10^{-3})	0.927	3.2×10^{-5} (1.8×10^{-5} – 5.6×10^{-5})	0.957
sgC-His	NiPC	1.6 (0.7 – 3.7)	0.925	1.0 (0.8 – 1.1)	0.992
sgC-His	NiPCPS	0.8 (0.5 – 1.3)	0.943	0.4 (0.3 – 0.6)	0.974
sgC-His	PCPS	>13.0 (-)	-	2.7 (1.3 – 5.3)	0.812
sgC-His	None	>12.0 (-)	-	2.9 (1.6 – 4.2)	0.994

A.4 Immunogold centrifugation of HSV1

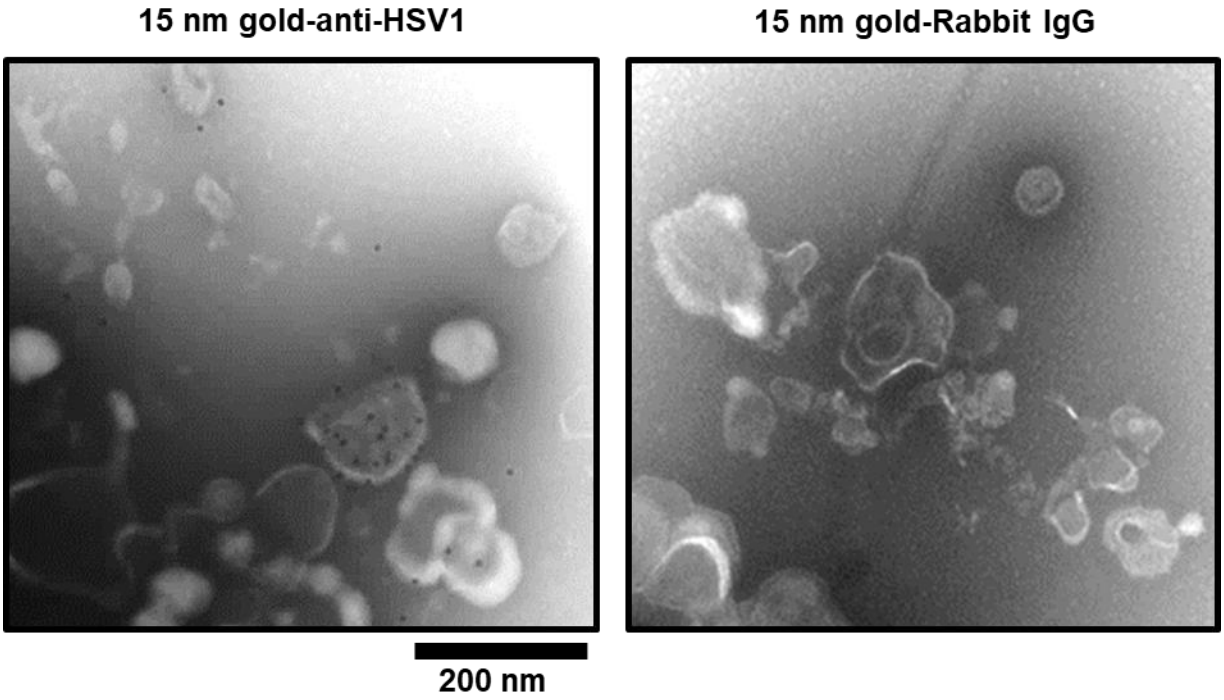

Figure 56. Immunogold differential centrifugation of HSV1.

HSV1/TF+/gC+ (10^8 vp/mL) was incubated with 15 nm gold-conjugated anti-HSV1 gC polyclonal rabbit antibodies (1:100) or 15 nm gold-conjugated rabbit IgG isotype control for 2 h at 37 °C. The virus-gold mixture was pelleted at 10,000 x g for 25 min, washed with HBS + 0.1% BSA-c and pelleted again. The washed pellet was resuspended in 20 µL HBS and loaded onto an EM grid. Grids were negatively stained with 2% PTA before visualization by transmission EM.